JUN KINASES IN HEMATOPOIESIS, AND VASCULAR DEVELOPMENT AND FUNCTION

A Dissertation Presented

By

Kasmir Ramo

Submitted to the Faculty of

the University of Massachusetts Graduate School of Biomedical Sciences, Worcester

in partial fulfillment of the requirements for the degree of

DOCTOR OF PHILOSOPHY

July 6, 2015

MD/PHD PROGRAM

JUN KINASES IN HEMATOPOIESIS, AND VASCULAR DEVELOPMENT AND FUNCTION

A Dissertation Presented By

Kasmir Ramo

The signatures of the Dissertation Defense Committee
signify completion and approval as to style and content of the Dissertation.

_____
Roger J. Davis, Ph.D., Thesis Advisor

_____
Michael Brehm, Ph.D., Member of Committee

_____
Lucio Castilla, Ph.D., Member of Committee

_____
John F. Keaney, M.D., Member of Committee

_____
Joseph Loscalzo, M.D., PhD., Member of Committee

The signature of the Chair of the Committee signifies that
the written dissertation meets the requirements of the Dissertation Committee.

_____
Gregory Pazour, Ph.D., Chair of Committee

The signature of the Dean of the Graduate School of Biomedical Sciences
signifies that the student has met all graduation requirements of the school.

_____
Anthony Carruthers, Ph.D.
Dean of the Graduate School of Biomedical Sciences

MD/PHD PROGRAM
July 6, 2015

© Copyright by
Kasmir Ramo
2015

Acknowledgements

I would first like to thank my advisor, Dr. Roger J. Davis for giving me the opportunity to explore diverse areas of biology in his laboratory and for providing scientific guidance and support during my PhD studies presented in this dissertation.

I would also like to thank past and present members of our lab for useful discussions and great friendship; particularly my bench mate, good friend and fierce table tennis competitor, Santiago Vernia.

Tammy Barrett, Julie Cavanagh and Kathy Gemme provided much helpful technical and administrative assistance, and I am greatly appreciative.

I would like to thank the members of my Thesis Research Advisory Committee, Drs. Michael Brehm, Lucio Castilla, John Keaney and Gregory Pazour for their advice and suggestions. I would also like to express my gratitude to Dr. Joseph Loscalzo for his time and willingness to participate as my outside examiner.

I would like to particularly acknowledge Dr. John Keaney and members of his lab for embarking with us on an exciting project that has lead to the identification of important aspects of vascular biology.

My mother, father and brother provide unwavering support in anything I do. My parents interrupted their lives in Albania to bring my brother and I to the land of opportunity. I can only hope that my endeavors do justice to their sacrifices. I would also like to thank my uncle and his family for making our transition to the US, easy, and for their continued support. My beautiful and smart girlfriend Sharanya Iyengar has the ability to make everything better. Thank you all so much!

Abstract

Arterial occlusive diseases are major causes of morbidity and mortality in industrialized countries and represent a huge economic burden. The extent of the native collateral circulation is an important determinant of blood perfusion restoration and therefore the severity of tissue damage and functional impairment that ensues following arterial occlusion. Understanding the mechanisms responsible for collateral artery development may provide avenues for therapeutic intervention. Here, we identify a critical requirement for mixed lineage kinase (MLK) – cJun-NH_2-terminal kinase (JNK) signaling in vascular morphogenesis and native collateral artery development. We demonstrate that *Mlk2*$^{-/-}$*Mlk3*$^{-/-}$ mice or mice with compound JNK-deficiency in the vascular endothelium display abnormal collateral arteries, which are unable to restore blood perfusion following arterial occlusion, leading to severe tissue necrosis in animal models of femoral and coronary artery occlusion. Employing constitutive and inducible conditional deletion strategies, we demonstrate that endothelial JNK acts during the embryonic development of collateral arteries to ensure proper patterning and maturation, but is dispensable for angiogenic and arteriogenic responses in adult mice. During developmental vascular morphogenesis, MLK – JNK signaling is required for suppression of excessive sprouting angiogenesis likely via JNK-dependent regulation of Dll4 expression and Notch signaling. This function of JNK may underlie its critical requirement for native collateral artery formation. Thus, this study introduces MLK – JNK

signaling as a major regulator of vascular development.

In contrast, we find that JNK in hematopoietic cells, which are thought to share a common mesodermally-derived precursor with endothelial cells, is cell-autonomously dispensable for normal hematopoietic development and hematopoietic stem cell self-renewal, illustrating the highly context dependent function of JNK.

Table of Contents

Title Page		i
Signature Page		ii
Copyright Page		iii
Acknowledgements		iv
Abstract		v
Table of Contents		vii
List of Figures		ix
List of Abbreviations		xii
Preface		xv
Publications		xvi
Chapter I	**Introduction**	1
	cJun NH_2-Terminal Kinases	2
	The Vascular System	11
	Hematopoiesis	40
	Rationale and Objectives	47
Chapter II	**Endothelial MLK – JNK Signaling Regulates Vascular Morphogenesis and is Critically Required for Native Collateral Artery Development**	61
	Abstract	62
	Introduction	63
	Results	67

	Discussion	86
	Experimental Procedures	93
Chapter III	**JNK is Cell-Autonomously Dispensable for Hematopoietic Development and Hematopoietic Stem Cell Self-Renewal**	156
	Abstract	157
	Introduction	158
	Results	160
	Discussion	168
	Experimental Procedures	171
Chapter IV	**Discussion & Future Directions**	197
	Discussion	198
	Future Directions	204
References		208

List of Figures

Chapter I

Figure I.1 MAP kinase signal transduction.

Figure I.2 JNK isoforms.

Figure I.3 Early postnatal development of the retinal vasculature as a model for studying sprouting angiogenesis.

Figure I.4 Notch signaling.

Figure I.5 Collateral arteries.

Figure I.6 The hematopoietic hierarchy.

Chapter II

Figure II.1 Enhanced blood perfusion blockade and severe ischemic injury in endothelial JNK-deficient mice upon arterial occlusion.

Figure II.2 Endothelial JNK-deficient mice display abnormal native collateral arteries.

Figure II.3 Abnormal native collateral arteries, and enhanced blood perfusion blockade and ischemic injury in *Mlk2*$^{-/-}$*Mlk3*$^{-/-}$ mice upon arterial occlusion.

Figure II.4 Endothelial JNK is dispensable for arteriogenic responses in adult mice.

Figure II.5 Endothelial JNK deficiency results in altered collateral artery patterning during ontogeny

Figure II.6 *Mlk2*$^{-/-}$*Mlk3*$^{-/-}$ mice phenocopy the defects in native collateral artery formation of endothelial JNK deficient mice at P6

Figure II.7 Abnormal retinal vascular development marked by excessive sprouting in endothelial JNK-deficient mice

Figure II.8 Abnormal retinal vascular development marked by excessive sprouting in *Mlk2*$^{-/-}$*Mlk3*$^{-/-}$ mice

Figure II.9 RNA-Seq analysis of genes differentially regulated between control and JNK-deficient endothelial cells

Figure II.10 Reduced Dll4 – Notch signaling in the JNK-deficient vascular endothelium

Figure II.11 Diagram illustrating the functional importance of collateral arteries during arterial occlusion, and the collateral artery patterning / maturation defects and functional impairment in mice with disrupted MLK – JNK signaling.

Supplementary Figure II.1 Characterization of endothelial JNK-deficient mice and lung endothelial cells.

Supplementary Figure II.2 Endothelial JNK-deficient mice have no major perturbations in the hematopoietic system.

Supplementary Figure II.3 Endothelial JNK is dispensable for proliferation, migration and angiogenic responses *in vitro*.

Supplementary Figure II.4 Endothelial JNK is dispensable for *in vivo* pathologic angiogenesis.

Supplementary Figure II.5 Normal hypoxia responses and VEGF signaling in JNK-deficient endothelial cells.

Supplementary Figure II.6 Compound endothelial deficiency of JNK1 plus JNK2 leads to enhanced blood perfusion blockade in models of arterial occlusion.

Supplementary Figure II.7 JNK deficient mice show no perturbations in overall cardiovascular function.

Supplementary Figure II.8 Gene expression analysis in adductor and calf muscles of E^{3KO} and control mice.

Supplementary Figure II.9 Abnormal retinal vascular development marked by excessive sprouting in E^{2KO} mice.

Supplementary Figure II.10 No major perturbations in $NG2^{+}$ pericyte coverage in the E^{2KO} retinal vasculature at P6.

Supplementary Figure II.11 Intimate association of gracilis collaterals and

peripheral nerves in adductor muscles.

Chapter III

Figure III.1 *Jnk1*$^{-/-}$ and *Jnk2*$^{-/-}$ mice have normal HSC and progenitor cell composition in the bone marrow.

Figure III.2 Bone marrow cells from *Jnk1*$^{-/-}$ and *Jnk2*$^{-/-}$ mice display normal multilineage reconstitution potential in serial competitive transplantation experiments

Figure III.3 HSC and progenitor analysis 20 weeks post-transplantation in the bone marrow of primary recipients from the experiment in Figure III.2

Figure III.4 Compound ablation of both *Jnk1* plus *Jnk2* genes in hematopoietic cells of adult mice does not perturb hematopoiesis or BM cell homing and engraftment following transplantation.

Figure III.5 Compound ablation of both *Jnk1* plus *Jnk2* genes in hematopoietic cells starting in embryonic life does not perturb HSC and progenitor cell development.

Figure III.6 Compound ablation of both *Jnk1* plus *Jnk2* genes in hematopoietic cells starting in embryonic life does not perturb HSC and progenitor function upon transplantation

Figure III.7 Sensitivity to 5-fluorouracil (5-FU) is not altered in H^{2KO} mice.

Supplementary Figure III.1 Gating strategy and fluorescence minus one (FMO) controls used for the identification of HSC and progenitor cell populations.

Supplementary Figure III.2 Normal body mass and blood cell indices in H^{2KO} mice.

List of Abbreviations

ADAM	a disintegrin and metalloprotease
AGM	aorta-gonad mesonephros
AP	activator protein
ASK	apoptosis stimulating kinase
ATF	activating transcription factor
BAD	BCL2-associated agonist of cell death
BCL-2	B-cell CLL/lymphoma 2
bFGP	basic fibroblast growth factor
BHLH	basic helix-loop-helix
BID	BH_3-interacting domain death agonist
BIM	BCL-2-interacting mediator of cell death
BMF	BCL-2-modifying factor
BMP	bone morphogenetic protein
CLP	common lymphoid progenitor
CMP	common myeloid progenitor
CNV	choroidal neovascularization
dHSC	definitive hematopoietic stem cell
DiI	Tetramethylindocarbocyanine Perchlorate
Dll	Delta-like
dpc	days post coitus
Dpp	Decapentaplegic
DSL	Delta and Serrate/Lag2
EC	endothelial cells
EEA	early endosome antigen
EGF	epidermal growth factor
ERK	extracellular regulated kinases
Esm	endothelial cell-specific molecule
FA	femoral artery
FAL	femoral artery ligation
FLK	fetal liver kinase
FPKM	Fragments Per Kilobase of exon per Million fragments mapped
GMP	granulocyte/macrophage progenitor
GSK	glycogen synthase kinase
HC	hematopoietic cell
HES	Hairy/Enhancer of Split
HEY	Hes-related proteins
HSC	hematopoietic stem cell

IFN	Interferon
Jag	Jagged
JIP	JNK-interacting protein
JNK	cJun-NH_2-terminal kinase
KDR	kinase insert domain receptor
LFNG	Lunatic Fringe
LPS	lipopolysaccharide
LSK	Lineage$^-$, Sca1$^+$, cKit$^+$,
Maml	Mastermind-like
MAPK	mitogen activated protein kinase
MAPKK	mitogen activated protein kinase kinase
MCL	myeloid cell leukemia
MEF	mouse embryonic fibroblasts
MEP	megakaryocyte/erythrocyte progenitor
MFNG	Maniac Fringe
Mib	Mind bomb
MKP	MAPK phosphatase
MLK	mixed lineage kinase
MPP	multipotent progenitor
mRNA	messenger RNA
NECD	Notch extracellular domain
NEDD	Neural precursor cell expressed, developmentally down-regulated
Neurl	Neuralized
NF	nuclear factor
NICD	Notch intracellular domain
PA	popliteal artery
PCFA	proximal caudal femoral artery
PCP	planar cell polarity
PCR	polymerase chain reaction
PDGF	platelet-derived growth factor
PLGF	placenta growth factor
POFUT	Protein O-fucosyl transferase
PTP	phosphotyrosine phosphatase
Puc	Puckered
RFNG	Radical Fringe
ROP	retinopathy of prematurity
ROS	reactive oxygen species
SA	saphenous artery
SAPK	stress-activated protein kinases

SDF	stromal cell-derived factor
SR-A	scavenger receptor A
ST-HSC	short-term hematopoietic stem cell
Su(dx)]	Suppressor of deltex tumor progression locus
TAK	transforming growth factor (TGF)-β-activated kinase
T_H	T helper
TNF	tumor necrosis factor
TPL	tumor progression locus
TSP	thromobospondin
UV	ultraviolet light
VEGFR	vascular endothelial growth factor receptor
μCT	micro-computed tomography

Preface

The work presented in Chapter II was done in collaboration with Dr. John F. Keaney's laboratory. The following individuals contributed:

Xiaoyun Huang – Performed femoral artery ligation (FAL) surgeries and laser Doppler scanning.

Koichi Sugamura – Performed heart rate and blood pressure measurements contributed to the aortic contraction and relaxation experiments and helped with initial coordination and transport of mice for FAL surgery.

Siobhan Craige – Helped with scheduling of FAL surgeries and provided instructions on how to perform the contraction and relaxation assay on aortic segments.

We also utilized the expertise of a bioinformatician and core facilities.

Yvonne Edwards – Helped with a portion of the RNA sequencing analysis.

μCT imaging and flow cytometry was done at the Musculoskeletal Imaging Core (grant S10RR023540) and the Flow Cytometry Core respectively at the University of Massachusetts Medical School.

The coronary artery ligation model and echocardiographic analysis was done at the Partners Cardiovascular Physiology Core at Brigham and Women's Hospital.

Publications

Kasmir Ramo, Koichi Sugamura, Siobhan Craige, John F. Keaney and Roger J. Davis.
Suppression of ischemia in arterial occlusive disease by JNK-promoted native collateral artery development. *Submitted.*

Kasmir Ramo, and Roger J. Davis.
JNK is cell-autonomously dispensable for hematopoietic development and hematopoietic stem cell self-renewal. *In preparation*.

Kasmir Ramo, and Roger J. Davis.
Wnt - β-catenin pathway regulation by Jun kinases. *In preparation*.

Chapter I

Introduction

cJUN NH_2-TERMINAL KINASES (JNK)

JNK belongs to the group of stress and mitogen activated protein kinases (MAPK) that mediate pleiotropic cellular responses to diverse environmental stimuli.[1]

MAPK Signal Transduction

Cells respond to environmental stimuli by activating diverse signal transduction cascades that sense, process and relay outside information into the cell in order to generate appropriate biological responses. Among the many signaling pathways that cooperate in this process, the family of mitogen activated protein kinases (MAPK) encompasses groups of signal transduction pathways that are highly conserved and play important pleiotropic roles in many biological processes.[1-3] These signaling pathways are regulated through three-tiered kinase signaling cascades whereby a MAPK is activated through phosphorylation by a MAPK kinase (MAPKK, MKK or MAP2K), which is, in turn, activated through phosphorylation by a MAPKK kinase (MAPKKK or MAP3K; Figure I.1).[1] In mammals, three groups of MAPK have been identified and include the extracellular regulated kinases (ERK), the p38 kinases and the cJun NH_2-terminal kinases (JNK), also known as stress-activated protein kinases (SAPK). Each MAPK is activated by dual phosphorylation of a tripeptide motif (Thr-Glu-Tyr for ERK, Thr-Gly-Tyr for p38 and Thr-Pro-Tyr for JNK).[1,4] The specific MAP2K that phosphorylate each MAPK have been well characterized. Thus,

MKK1, 2 and 5 phosphorylate ERK, MKK3 and 6 phosphorylate p38 (with some contribution from MKK4) and MKK4 and MKK7 phosphorylate JNK.[1,2] However, the situation is much more complex with regard to the specific MAP3K that participate in the activation of different MAPK pathways in specific contexts *in vivo*. Particularly for p38 and JNK, the MAP3K that have been implicated in their activation include over a dozen members from heterogeneous families. For example, the MEK kinases (MEKK 1-4), the transforming growth factor (TGF)-β-activated kinase 1 (TAK1), the tumor progression locus-2 (TPL-2), the apoptosis stimulating kinases (ASK1 and 2) and the mixed-lineage kinase group (MLK1-4, DLK and LZK) have all been shown to activate JNK or its upstream activators MKK4 and/or MKK7 in overexpression or *in vitro* kinase assays.[1,2] However, the relevance of these MAP3K as physiologic regulators of the JNK pathway has only been established for a few members.

One example is illustrated by the MAP3K, MLK2 and MLK3, for which biochemical and genetic data in primary cells and mice has confirmed their physiologically important role for JNK activation by tumor necrosis factor (TNF) as well as JNK activation mediated by saturated fatty acids.[5,6] In contrast, MLK3 was found to be dispensable for JNK activation by some stress stimuli, including ultraviolet light (UV), Anisomycin or Ceramide and by some growth factors such as platelet-derived growth factor (PDGF) or epidermal growth factor (EGF).[7] These studies illustrate two important points regarding MAP3K. First, they demonstrate that there is functional redundancy between different MAP3K family

members. Thus, combined disruption of both *Mlk2* plus *Mlk3* results in greater defects in JNK activation by TNF than disruption of *Mlk3* alone.[5] Second, they demonstrate the existence of some degree of specificity of particular MAP3K members for certain stimuli. These characteristics of MAP3K may provide avenues for targeted modulation of the MAPK signaling pathways for therapeutic benefit.

JNK structure, regulation and function

In mammals, the JNK group of MAPK includes proteins encoded by three separate genes.[1] *Jnk1* and *Jnk2* are ubiquitously expressed, whereas *Jnk3* displays a much more restricted pattern of expression confined largely to the brain, heart and testis.[1] Alternative splicing of the messenger RNA (mRNA) transcripts from the three *Jnk* genes generates ten different *Jnk* isoforms (Figure I.2).[3] One alternative splicing site involves selection of one of two alternative exons that encode part of the kinase domain. This splice site is restricted to *Jnk1* and *Jnk2*, and gives rise to JNK isoforms with different substrate binding specificities. The second splice site at the COOH-terminus of the protein results in proteins that differ by 42 or 43 amino acids.[3]

Although functional differences between different *Jnk* isoforms from the same gene transcript have not yet been characterized, significant functional redundancy exists between *Jnk* isoforms from different gene transcripts. This is illustrated by the analysis of mice with genetic ablation of different *Jnk* genes.

Thus, mice with disruption of single *Jnk* genes are viable and appear morphologically normal, however combined disruption of both *Jnk1* plus *Jnk2* results in embryonic lethality at midgestation due to neural tube closure defects.[8] Tissue specific roles for the ubiquitously expressed *Jnk1* and *Jnk2* genes have also been reported,[9] but this may reflect the particular isoform distribution profile from each gene transcript rather than bona fide differences between *Jnk1* and *Jnk2* isoforms.

As described above, JNK is fully activated through phosphorylation by the upstream MAP2 kinases MKK4 and MKK7. Both kinases can activate JNK by dual phosphorylation on Thr and Tyr residues, however some degree of specificity is conferred via activation of MKK4 or MKK7 by MAP3K in different contexts. For example, stimulation by various cytokines preferentially activates MKK7, whereas some environmental stress stimuli primarily activate MKK4.[10]

Additional layers of regulation of the JNK signaling pathway are afforded by Ser/Thr phosphatases, Tyr phosphatases or dual specificity phosphatases that can dephosphorylate and inactivate JNK.[1] Furthermore, scaffold proteins including JNK-interacting protein (JIP1, 2 and 3) have been identified that organize MAPK modules incorporating a MAP3K, a MAP2K and a MAPK, thus facilitating their interaction leading to modulation of MAPK activity.[1]

Upon activation, JNK phosphorylates Ser/Thr-Pro motifs on numerous proteins that include transcription factors and cytoplasmic proteins. JNK phosphorylates several members of the activator protein 1 (AP-1) transcription factor complex, including cJun, JunB and activating transcription factor 2 (ATF2).[1] Indeed, JNK1 was molecularly cloned as a protein kinase, activated by UV and Ha-Ras, that binds and phosphorylates the activation domain of cJun.[11] JNK-mediated phosphorylation of cJun on Ser-63 and Ser-73 promotes the transcriptional activity of the AP-1 transcription complex resulting in gene expression changes that often underlie the multitude of biological processes that are regulated by JNK, including its role in cancer and metabolism.[12,13] In addition, JNK has been reported to phosphorylate a number of cytoplasmic targets. These include p53, cMyc, and Itch, several B-cell CLL/lymphoma 2 (BCL-2)-family members, including the anti-apoptotic factors BCL-2, BCL-$_{XL}$ and myeloid cell leukemia (MCL-1), and the pro-apoptotic factors BCL-2-interacting mediator of cell death (BIM), BCL-2-modifying factor (BMF), BH$_3$-interacting domain death agonist (BID) and BCL2-associated agonist of cell death (BAD), among other cytoplasmic proteins.[1,12] Thus, through its effects on gene transcription and direct phosphorylation of cytoplasmic proteins, JNK affects many biological processes from apoptosis and cell survival to embryonic development, inflammation, metabolism and cancer.

Role of JNK in cell death and survival

The role of JNK in cell death and survival is complex and highly context dependent. The time course of JNK activation appears to have a significant impact.[14] Thus, in mouse embryonic fibroblasts (MEF), sustained JNK activation by TNF, particularly in the context of nuclear factor (NF)-κB inhibition can induce apoptosis, whereas transient JNK activation is required for cell survival.[14] Treatment of cells with TNF causes a biphasic JNK activation response. The early phase of JNK activation is robust and appears to signal a JunD-dependent survival response that also requires cooperation with the NF-κB and AKT pathways.[14,15] This response is thought to involve AP-1-mediated enhancement of anti-apoptotic gene expression by NF-κB and AKT signaling.[2] The late phase of JNK activation appears to contribute to cell death when pro-survival signaling by NF-κB is inhibited.[16] This role of JNK may be mediated by its ability to promote TNF-induced production of reactive oxygen species (ROS).[17,18]

In hepatocytes, another mechanism proposed for a JNK1-dependent TNF-induced increase in cell death is the ability of JNK1 to phosphorylate and activate the E3 ubiquitin ligase Itch.[19] This was shown to promote apoptosis via Itch-mediated ubiquitination and proteasomal degradation of the NF-κB-induced anti-apoptotic protein c-FLIP, an inhibitor of caspase-8. Because Itch phosphorylation is reversible, the authors proposed that sustained JNK activity was required to maintain pro-apoptotic signaling in this context.[19]

JNK may also promote cell death by mediating induction of the mitochondrial apoptotic pathway.[1,12] Indeed, compound deficiency of *Jnk1* plus *Jnk2* or *Mkk4* plus *Mkk7* in MEF causes defects in the stress-induced apoptosis response in these cells.[10,20] This may be due to alterations in the release of mitochondrial pro-apoptotic factors, including cytochrome c, that have been attributed to the ability of JNK to phosphorylate and either inhibit or activate the function of various BCL-2 family members.[1,12]

MCL-1 is one such pro-survival factor that may function by binding to and sequestering the pro-apoptotic factor BAK in an inactive complex.[21] JNK phosphorylates MCL-1 priming it for phosphorylation by glycogen synthase kinase 3 (GSK3), an event that promotes stress-induced MCL-1 proteasomal degradation.[22] Thus, JNK-mediated MCL-1 degradation may allow the pro-apoptotic function of BAK to proceed unhindered. JNK may also promote the function of other pro-apoptotic BCL-2 family members, including BIM and BMF by direct phosphorylation.[1,12]

As the above discussion illustrates, stress-induced JNK activity, in general, has been associated with promotion of apoptosis and cell death with the exception that early transient JNK activation may contribute to cell survival.[14] Additional evidence exists implicating JNK in survival responses. This role of JNK is

supported by studies showing that survival signals transduced by integrin engagement in fibroblasts following growth factor removal are mediated by a Ras/Rac1/PAK1/MKK4/JNK signaling pathway.[23] Furthermore, survival signals during *in vitro* or *in vivo* BCR-ABL transformation of B lymphoblasts may be mediated by JNK1-dependent *Bcl2* expression as defective transformation of *Jnk1*$^{-/-}$ lymphoblasts was associated with reduced *Bcl2* expression, and transgenic restoration of *Bcl2* levels rescued the defective transformation of *Jnk1*$^{-/-}$ lymphoblasts.[24] Perhaps the most compelling evidence supporting a role for JNK in cell survival comes form the analysis of compound mutant *Jnk1*$^{-/-}$*Jnk2*$^{-/-}$ embryos, which exhibit defects in apoptosis in certain regions of the hindbrain during embryonic development.[8] Interestingly, regions of the forebrain showed increased apoptosis.[8] Thus, JNK may mediate both pro-survival and pro-apoptotic responses during embryonic development depending on the specific cell types and likely developmental timing.

Role of JNK during embryonic development

The essential function of JNK during embryogenesis is underscored by the early embryonic death of compound mutant *Jnk1*$^{-/-}$*Jnk2*$^{-/-}$ mouse embryos.[8] This is likely in part due to the aforementioned perturbations in apoptotic responses in the developing brain that contribute to defective nervous system morphogenesis and exencephaly.[8] In addition to its role in cell death and survival, JNK has important functions in cell and tissue morphogenesis via its effects on the actin cytoskeleton, cell polarity and cell migration. Some of the functions of JNK in cell

and tissue morphogenesis are evolutionarily conserved. In *Drosophila melanogaster,* JNK is required for dorsal closure, a major morphogenetic process whereby lateral epithelia from the two sides of the embryo come together to seal a dorsal hole.[25] This process depends on actin cytoskeleton rearrangements that drive epithelial sheet movements and has many parallels with the neural tube closure process in vertebrates.[25] In the absence of JNK, dorsal closure does not proceed normally resulting in a dorsal open phenotype. Two transcriptional targets of JNK, the TGF-β-related factor and BMP4 ortholog, Decapentaplegic (Dpp), and the dual specificity phosphatase, Puckered (Puc), whose expression is absent in JNK mutants, are required for proper dorsal closure morphogenesis.[25] JNK also regulates convergent extension movements during gastrulation both in *Drosophila* and *Xenopus*.[26] The process of convergence extension involves a series of highly coordinated movements that contribute to the formation of the body axis.[26] JNK regulates this process through its involvement in the non-canonical Wnt/planar cell polarity (PCP) pathway.[26,27]

Furthermore, in mice, in addition to its role in neural tube closure, JNK is also important for a number of other morphogenetic processes. The presence of one allele of *Jnk2* in *Jnk1*$^{-/-}$*Jnk2*$^{+/-}$ mice overcomes the embryonic death of *Jnk1*$^{-/-}$ *Jnk2*$^{-/-}$ mice and allows the study of additional processes during mouse embryonic development.[28,29] *Jnk1*$^{-/-}$*Jnk2*$^{+/-}$ mice display defects in epithelial development in the skin, intestines and lung as well as optic fissure and eyelid

closure defects.[28,29] Perturbations in epidermal growth factor (EGF) expression and EGF receptor function may underlie the eyelid closure defects in *Jnk1*$^{-/-}$ *Jnk2*$^{+/-}$ mice,[28] while the optic fissure closure defects were attributed to a JNK-dependent decrease in bone morphogenetic protein 4 (BMP4, an ortholog of Drosophila Dpp) expression in the retina.[29] Thus, JNK intersects with a number of signaling pathways to regulate developmental processes important for morphogenesis and maturation of various tissues and organs.

THE VASCULAR SYSTEM

Evolutionary History of the Blood Circulatory System

The rise of multicellular organisms required a system that would overcome the time-distance constraints of diffusion and allow efficient gas exchange, distribution of necessary factors and removal of metabolic waste products from all cells of the organism. In all, but the most primitive metazoans, these vital tasks are facilitated by the circulatory system, an interconnected network of chambers and channels that permeates virtually all tissues bringing necessary factors within a few microns from all cells in organisms as small as mites and as large as whales.[30]

Circulatory systems can be classified as open, found in arthropods (e.g. insects and crustaceans) and non-cephalopod mollusks (e.g. snails, slugs and clams) or closed, present in all other metazoans.[30] Open circulatory systems consist of a

contractile heart and major vessels that open into the body cavity (or hemocoel), which is lined by the basal surface of tissue cells. Blood (called hemolymph) empties from the major supply vessels and heart into the hemocoel, where it bathes all organs. In this case, there is no physical separation and thus no distinction between hemolymph and interstitial/extracellular fluid. By contrast, in closed circulatory systems, blood remains inside channels and chambers and is physically separated from the interstitial fluid and tissue cells. Exchange of gases, nutrients and other factors between blood, the interstitium and tissue cells in this case occurs in capillary plexi, specialized, thin walled regions of the circulatory system network that facilitate diffusion.[30]

The closed circulatory system of invertebrates consists of channels that are lined by the extracellular matrix of basement membranes of tissue epithelia. Vertebrates, on the other hand, have blood vessels that are lined by endothelium, a specialized monolayer of mesodermally derived cells with apico-basal polarity. Intercellular junctions define the boundary between the apical side facing the lumen of vessels from the basolateral side which rests on a basement membrane surrounding all vessels.

Development of the Circulatory System

The cardiovascular system is essential for the development and survival of the organism and is the first system that forms during organogenesis.[31] In vertebrates, vascular development starts with the emergence of angioblasts from

the primitive streak, which in mice occurs around embryonic day (E) 7.5. Angioblasts are fetal liver kinase 1 [FLK-1, also known as kinase insert domain receptor (KDR) or vascular endothelial growth factor receptor (VEGFR)-2, the major receptor for VEGF-A] positive, Brachyury positive mesodermal precursors that migrate to the extra embryonic yolk sac, where they coalesce to form a network that includes clusters known as blood islands.[31-33] The inner cells within blood islands will give rise to primitive hematopoietic precursors that initiate erythropoiesis. The outer cells of blood islands are endothelial cells that form the extra embryonic vasculature. Concurrently, in the embryo proper, angioblasts aggregate to form primitive vascular cords and plexi, a process known as vasculogenesis. These primitive vascular structures will subsequently lumenize and form the dorsal aorta and cardinal vein, which join the primitive heart tube creating the basis for the future circulatory system.[31-33]

Following formation of primary plexi via vasculogenesis in the yolk sac and embryo, the vasculature continues to expand via sprouting of new vessels from these preexisting plexi, a process known as angiogenesis. Thus, while initial vessels form via direct differentiation of precursors into endothelial cells, most of the embryonic vasculature expands via sprouting, migration, and proliferation of existing endothelial cells.[34]

The retinal vasculature as a model for studying sprouting angiogenesis

Many of the detailed aspects of the angiogenic sprouting process have been studied during the postnatal development of the retinal vasculature in mice.[35] This system offers unique advantages for exploring the intricate cellular and often molecular mechanisms of vascular development as it allows detailed analysis of sprouting angiogenesis in a relatively easily accessible tissue that is avascular at birth. Vascularization of the retina in mice occurs in the first few weeks of postnatal life. Extension of the retinal vascular plexus proceeds initially (P0 to ~P9) on the inner surface of the retina in a highly stereotypic fashion from the center of the retina towards the periphery in two dimensions (Figure I.3) This enables high-resolution analysis of many cellular and molecular aspects of sprouting angiogenesis, including tip/stalk cell specification, extension of filopodia and formation of endothelial cell-to-cell junctions as well as vascular progression, branching morphogenesis, and maturation processes such as vascular pruning and mural cell recruitment.[36]

Sprouting angiogenesis – an interplay of tips and stalks

Angiogenesis starts when endothelial cells within the wall of existing vessels receive the appropriate signals from the extracellular environment, acquire high migratory ability and emerge (or sprout) away from the main body of a vessel while maintaining contact with other endothelial cells lining the vessel. Sprouting endothelial cells are called tip cells. They are highly motile cells with low

proliferative capacity that elaborate numerous filopodia and guide the extension of the newly forming vascular plexus. Endothelial cells trailing tip cells are referred to as stalk cells. They have fewer filopodia and low migratory, but high proliferative capacity and form the stalk (or body) of the growing nascent vessel.[37-39]

At the growing edge of the vascular plexus, filopodia and other protrusions of tip cells in close proximity often encounter each other and appear to fuse together, forming a bridge-like structure that may represent the beginning of the formation of a new tubule that will subsequently incorporate endothelial cell bodies, lumenize and become a new addition to the developing plexus. The emergence of new endothelial cell sprouts from the body of the nascent tubule will result in a new round of sprouting, fusion, bridge formation and tubulogenesis, ensuring further extension of the developing plexus. Thus, the formation of an initial immature vascular network involves multiple rounds of sprouting and tubulogenesis. VEGF signaling is at the core of this angiogenic sprouting processes.[37-39]

VEGF – VEGFR signaling

VEGF-VEGFR signaling is critical for many aspects of the angiogenic sprouting process. In mammals, three VEGFRs (VEGFR1 [also known as fms-related tyrosine kinase 1 (FLT1), VEGFR2 and VEGFR3 [also known as FLT4]) and five VEGFR ligands, VEGF-A, B, C, D and placenta growth factor (PLGF) have been

identified.[40] Further complexity in this signaling system is added by the existence of multiple splice variants of the different receptors and ligands. These ligands and receptors, and the ligand-receptor complexes that they form have been demonstrated to display both common and unique signaling properties that affect a multitude of processes during vascular development.[40] This is accomplished via the interaction of activated VEGFRs with numerous components of a variety of other signaling pathways, leading to the modulation of their signaling output, and thus, the regulation of various processes, including endothelial cell proliferation, survival and migration as well as regulation of cell-to-(cell or extracellular matrix) adhesion and vascular permeability. VEGFRs belong to the superfamily of receptor tyrosine kinases. Upon binding VEGF ligands, VEGFRs undergo homo or heterodimerization and autophosphorylation at various tyrosine (Y) residues that facilitate interaction with a variety of proteins resulting in activation of signaling pathways including PI3K / AKT and PI3K / Rac1, and Ras / MEK / ERK, among others.[40] In contrast to VEGFR2, which has high kinase activity, VEGFR1 displays strong binding to VEGF ligands, but has low kinase activity and is thought to antagonize the function of VEGFR2 by competing for VEGF ligands. Soluble forms of VEGFR1 have also been identified and act as a sink for VEGF, contributing to the regulation of VEGF bioavailability.[40] The most studied and best understood of the VEGF–VEGFR signaling interactions is that between VEGF-A and VEGFR2.

VEGF – VEGFR signaling drives sprouting angiogenesis

In the retina, VEGF-A is produced in part by an astrocytic network in the initially avascular retina and forms a chemoatractive gradient that guides the extension of the developing vascular plexus, while ensuring endothelial cell survival, proliferation and migration.[37-39] Specifically, VEGF-A signaling via VEGR2 guides the migration of endothelial tip cells into a new sprout and stimulates extension of filopodia from these cells without stimulating proliferation.[41] VEGF-A – VEGFR2 signaling in stalk cells, however, stimulates their proliferation. This response is dependent on the concentration of VEGF-A. Thus, VEGF-A – VEGFR2 signaling mediates different cellular responses in distinct endothelial cell populations within the developing vascular plexus.[41] How does the same VEGF signaling pathway specify distinct cell fates and responses in endothelial cells that are in physical contact and interacting with each other? These distinct responses in neighboring endothelial cells are largely defined by VEGF-mediated regulation of Notch signaling.

Notch signaling

(Refer to Figure I.4)

In mammals, four receptors (Notch1-4) that interact with five canonical Notch ligands, namely Delta-like1 (Dll1), Delta-like3 (Dll3), Delta-like4 (Dll4), Jagged1 (Jag1) and Jagged2 (Jag2) collectively referred to as DSL (after the invertebrate Delta and Serrate/Lag2 proteins) have been identified.[37-39] Notch receptors and

their DSL ligands are transmembrane proteins that contain extracellular domains with numerous epidermal growth factor (EGF) repeats.[37-39] Therefore, canonical Notch signaling requires direct physical contact between the cell expressing the ligand and that expressing the receptor.

Notch receptors are synthesized as single polypeptide precursors, which following fucosylation by the enzyme Protein O-fucosyl transferase (POFUT1), undergo cleavage by the protease Furin in the trans-Golgi network generating the non-covalently linked Notch extracellular and intracellular domains (NECD and NICD, respectively). Upon ligand binding, Notch receptors undergo two additional proteolytic cleavage events. First, the NECD is cleaved at the juxta-membrane region by a member of the a disintegrin and metalloprotease (ADAM) family and trans-endocytosed coupled to the ligand. Second, due to NECD cleavage and/or protein conformational changes imparted by NECD endocytosis into the ligand-presenting cell, the remaining Notch subunit becomes susceptible and is cleaved by γ-secretase within the transmembrane region, thus, releasing the NICD from the membrane. NICD translocates into the nucleus where it interacts with the transcription factor RBP-J (also known as CSL, named after mammalian CBF1, Drosophila Su(H), and Caenorhabditis elegans LAG1), displaces corepressors and forms a transcription complex that includes the coactivator Mastermind-like (Maml) and histone acetyltransferases (e.g. P300) driving transcription of Notch target genes such as the basic helix-loop-helix

(bHLH) proteins *Hairy/Enhancer of Split* (*Hes*) and *Hes-related proteins* (*Hey*).[37-39]

In addition to POFUT1-mediated fucosylation and sequential cleavage events, this pathway is regulated by a number of other receptor and ligand modifications. Thus, Notch receptors can be further glycosylated on several EGF repeats by Fringe glycosyltransferases (3 in mammals, Lunatic Fringe [LFNG], Manic Fringe [MFNG] and Radical Fringe [RFNG]), a modification that potentiates pathway activation by Delta-like ligands. Furthermore, the NICD can be ubiquitinated by the HECT domain E3 ligases Suppressor of deltex [Su(dx)] and Neural precursor cell expressed, developmentally down-regulated 4 (NEDD4) leading to Notch degradation and inhibition of signaling. In contrast, ubiquitination by the ring finger E3 ligase Deltex can antagonize Su(dx) and lead to either enhanced or decreased Notch signaling depending on the organism and cell type.[37-39]

Largely via unknown mechanisms, ubiquitination of DSL ligands by the E3 ligases Neuralized (Neurl) and Mind bomb (Mib) is important for ligand activation, and interaction with the ubiquitin-binding protein Epsin is required for full Notch pathway activity.[37-39]

Collectively, these multiple and diverse layers of regulation ensure tight control of Notch signaling output as both decreased and enhanced pathway activity can

have dramatic consequences on cell fate specification, tissue morphogenesis and organismal survival.

VEGF and Dll4 – Notch signaling interactions specify tip/stalk cell selection and vascular morphogeneis

In the vascular endothelium, Notch signaling is crucial for tip/stalk cell specification, vascular morphogenesis and arterial identity. Endothelial cells express Notch receptors 1, 2 and 4, and the ligands Dll1, Dll4 and Jag1.[37-39] During sprouting angiogenesis, hypoxia and VEGF signaling upregulate Dll4 expression in tip cells leading to increased Notch signaling in adjacent cells.[37-39] Enhanced Notch signaling in endothelial cells results in downregulation of VEGFR2[42,43] and VEGFR3[44] (and reportedly upregulation of VEGFR1),[43] and thus, reduced VEGF responsiveness and suppression of sprouting activity, including decreased migration capacity and reduced numbers of filopodia; effectively defining them as stalk cells. In addition to VEGF signaling, Dll4 expression is also positively controlled by Notch signaling.[37,45] This suggests that the identity of endothelial cells as tips and stalks is not static, but highly dynamic. Indeed, it is thought that endothelial cells constantly compete for the tip cell position through the interaction of VEGF and Notch signaling.[45] A balance between formation of new tip cells that guide the extension of the vascular plexus and stalk cells that proliferate and enable the growth of the tubular network must be established in order to maintain normal vascular patterning.

Perturbations in Notch signaling in endothelial cells result in dramatically altered vascular morphogenesis. Specifically, loss of Dll4,[46] Notch1,[46] LFNG,[47] RBP-J[48,49] or chemical inhibition of γ-secretase with N-[N-(3,5–Difluorophenacetyl- L-alanyl)]-S-phenylglycine t-butyl ester (DAPT)[46] leads to reduced Notch signaling in endothelial cells and results in excessive sprouting angiogenesis, increased branching and density, and abnormal vascular patterning. In contrast, transgenic NICD overexpression[50] or loss of Jag1[47] (which has weak signaling capacity, competes with Dll4 for Notch receptors and has pro-angiogenic functions)[47] results in decreased sprouting, branching and vascular density.

Sprouting angiogenic processes driven by VEGF and Notch signaling initially result in formation of immature vascular networks lined only by endothelium. These pathways and their interaction with many others, including the ephrin-Eph receptor pathway, the transforming growth factor (TGF)-β pathway, the Wnt – β-catenin pathway, the Slit – roundabout (Robo) pathway and the angiopoietin (Ang) – TIE pathway also play important roles in the continued patterning, remodeling and maturation of the vasculature.[51-56] These processes include stabilization of intercellular junctions, branching, tubulogenesis, pruning of excess vessels and recruitment of supporting mural cells including pericytes and smooth muscle cells resulting in the formation of mature hierarchical networks; and upon further specialization, the formation of distinct arteries, veins and capillaries that have unique structural and functional characteristics.[51-56]

General Characteristics of the Circulatory System

Vessels are tubular structures with walls composed of layers (or tunics). The luminal side of all vessels is lined by a monolayer of endothelial cells that is supported on the basal side by the basement membrane, an extracellular matrix layer consisting mostly of collagen and laminin. Capillary walls are lined only by endothelium, the basement membrane and interspersed pericytes that are located on the abluminal side. Arteries and veins have a more complex structure encompassing three distinct tunics. The endothelial/basement membrane layer constitutes the tunica intima. Encircling the tunica intima are several concentric layers of smooth muscle cells and elastic fibers that make up the tunica media. The media varies in thickness between arteries and veins as well as the size of the vessel. Arteries have thicker tunica medias with more smooth muscle and elastic fibers compared to veins. A third layer, the tunica externa, surrounds the media and is composed of fibroblasts interspersed within a matrix of connective tissue.

By definition, arteries are vessels that take blood away from the heart and distribute it to peripheral tissues; in contrast, veins bring blood back to the heart. Thus, the arterial system is a high-pressure system as it is immediately downstream of the pumping action of the heart, and hence has evolved structural characteristics that allow it to not only withstand high pressures, but also regulate arterial pressure by altering lumen diameter via selective contraction and dilation

of the vascular wall. As large arteries travel towards peripheral tissues, they branch extensively into smaller caliber arteries and arterioles, progressively losing smooth muscle cell coverage. Small arterioles continue into capillary beds, where exchange of gas, nutrients, numerous other factors and metabolic waste products between blood and the extracellular fluid occurs. Capillaries merge to form postcapillary venules, which join larger venules that start to reacquire smooth muscle cell coverage. Venules join larger veins that eventually return blood to the heart, completing the systemic circulatory loop.

In addition to the typical arrangement (artery>arteriole>capillary>venule>vein) described above, many, if not all tissues and organs, including skeletal muscle, heart, brain, skin and intestine display an alternative arrangement of arteries and arterioles consisting of direct artery-to-artery or arteriole-to-arteriole interconnection without an intervening capillary bed. These vessels are called collaterals.[57,58]

Importance of the Collateral Circulation

Collateral arteries interconnect adjacent arterial trees (Figure I.5). Normally, there is little blood flowing through collateral arteries due to the lack of a pressure gradient between the two ends of the vessel and their relatively narrow lumen.[58] The function of collateral vessels under normal physiological conditions remains unclear, however, their vital importance during vasoocclusive disease, including

myocardial infarction, stroke and peripheral artery disease has been demonstrated in numerous human studies and experimental animal models.[59-63] During certain pathological states, atherosclerotic and/or thromboembolic events can result in partial or complete occlusion of one or more arteries. The ensuing ischemia and hypoxia in tissues supplied by the occluded artery can have major detrimental consequences on the health and function of the affected tissue or organ. If blood flow, and therefore nutrients and oxygen are not restored within a short period of time, irreversible necrotic damage will ensue. In these circumstances, the native (pre-existing) collateral circulation can provide an alternative route for blood flow restoration to the affected region from an adjacent artery (Figure I.5), thus reestablishing tissue homeostasis and limiting ischemic damage.[58]

Native Collateral Artery Development

Few studies, almost exclusively from the Faber group, have traced the formation of native collateral arteries during ontogeny. These studies have focused on the development of leptomeningeal (or pial) collaterals that interconnect the medial, anterior and posterior cerebral artery trees in the brain and have provided evidence that these collaterals form during embryonic development starting ~E13.5 as sprout-like extensions of endothelial cells from arterioles of existing cerebral artery trees.[61] These nascent vessels appear to course above the pial capillary plexus and fuse with an arteriole from an adjacent arterial tree.[61] By

E15.5 a portion of these collaterals have acquired expression of the arterial marker EphrinB2.[64] Pial collateral density peaks ~E18.5 and is followed by extensive remodeling, maturation and pruning that continues postnatally, achieving adult form and density by P21.[64] The process of collateral artery formation during embryonic development has been termed collaterogenesis.[57,65]

There is extensive variability in the extent (i.e., number and size) of the native collateral circulation both in humans[66-73] and between different mouse strains[74-76], which correlates negatively with the magnitude of tissue damage following arterial occlusion. For example, the C57BL/6 is a strain that displays large collaterals and high collateral artery density; in contrast the BALB/c strain has fewer, smaller collaterals.[74-76] In models of arterial occlusion, including femoral artery (FA)[74,75] and medial cerebral artery (MCA)[76] ligation, C57BL/6 mice show lower reductions in blood flow, faster and higher blood flow restoration and therefore milder ischemic sequelae compared to the BALB/c strain. Both genetic and environmental factors are thought to contribute to the variability in the extent of the collateral circulation, and some of the specific genetic determinants that influence native collateral artery development are beginning to be uncovered.

Early clues regarding one of these genetic factors came from differential gene expression analysis between the C57BL/6 and BALB/c strains of mice.[64,74] The higher number and size of pial collaterals in C57BL/6 mice correlated with higher

expression of VEGF-A in the collateral zone of this strain compared to that of the low collateral BALB/c strain.[64,74] Subsequent studies utilizing $VEGF^{lo/+}$, $VEGF^{hi/+}$, $VEGFR1^{+/-}$ and $VEGFR2^{+/-}$ mice provided further evidence of the intimate involvement of the VEGF signaling pathway in native collateral artery development.[61,77]

Several other studies have identified additional proteins that affect formation of the native collateral circulation including, endothelial nitric oxide synthase (eNOS),[62] prolyl hydroxylase domain-containing protein 2 (PHD2),[78] chloride intracellular channel 4 (CLIC4),[65] platelet-endothelial cell adhesion molecule 1 (PECAM1),[79] gap junction protein connexin37 (Cx37),[80,81] and the Notch ligand Dll4.[82] Furthermore, genetic linkage analysis of F2 progeny from C57BL/6 x BALB/c crosses has identified quantitative trait loci (QTL) for collateral density and diameter.[83-85] One QTL on chromosome 7 in mice appears to account for the majority of the collateral differences between these two strains.[83,85] This QTL, originally named Candq1, has recently been refined from 27 to 0.737 Mb with full retention of the effect and is now designated as determinant of collateral extent 1 (Dce1).[85] Introgression of Dce1 into BALB/c restores collateral extent and rescues blood perfusion in models of FA and MCA occlusion in this low collateral strain to levels approaching those present in C57BL/6 mice.[85] Interestingly, Dce1 introgression into BALB/c restores pial collateral extent more efficiently (85% of C57BL/6) than muscle collaterals (55% of C57BL/6)[85] suggesting that collateral

formation in different tissues is regulated by both common and distinct mechanisms. Clearly, much remains to be uncovered about the factors, signaling pathways and mechanisms that determine native collateral artery formation.

Arteriogenesis

In contrast to the paucity of studies on the mechanisms that drive native collateral artery development, arteriogenesis, the process of outward remodeling of narrow preexisting collaterals into functional conduits upon vascular occlusion, is a much more scrutinized process. This is in part likely due to smaller technical challenges, but most importantly propelled by the realization that enhancing arteriogenesis may provide better therapeutic benefit in vascular occlusive diseases compared to enhancing angiogenesis, which has been the goal of numerous failed clinical trials.[86]

Angiogenesis is driven largely by ischemia and hypoxia, leading to stabilization of hypoxia inducible factors that drive expression of numerous hypoxia responsive genes including VEGF. As described above, VEGF binding to its receptors VEGFR1 and 2 on endothelial cells stimulates migration and proliferation of these cells from existing vessels initiating the formation of new capillary networks.[85,87] While angiogenesis may provide some improvement in blood flow distribution, it cannot functionally replace an occluded artery because the

addition of small high resistance vessels increases the overall resistance of the vascular bed distal to the occluded artery limiting blood flow restoration.[88] Thus, in the setting of vascular occlusion, only muscular collateral arteries are able to supply sufficient blood flow to prevent severe ischemia and its consequences.[89] Unlike angiogenesis, arteriogenesis does not require ischemia or hypoxia and can occur spatially and temporally dissociated from them.[89,90] Following vascular stenosis or occlusion, preexisting collateral arteries undergo extensive growth and remodeling that harnesses their full potential at restoring blood perfusion downstream of an occlusion.[91] Some of the mechanisms that mediate arteriogenic remodeling of collateral arteries will be discussed next.

Flow-mediated biomechanical forces initiate arteriogenesis

Arteriogenesis in the setting of vascular occlusion is thought to be initiated by biomechanical forces[91-93] and requires the coordinated interaction of several cell types including endothelial cells, smooth muscle cells (SMC), monocyte/macrophages, neurons and likely other cell types.[78,94,95] Vascular occlusion redirects blood flow to preexisting collaterals resulting in increased fluid shear stress (FSS) over the endothelial surface, as well as in increased longitudinal, circumferential and radial wall stress due to the elevated pressure within the collateral network.[89,91] The endothelium and SMCs can sense these

physical changes and undergo molecular and morphological alterations that underlie collateral artery remodeling.

Substantial evidence exists implicating FSS as an important early trigger for arteriogenesis.[91,96] Increases in FSS stimulate the activity of endothelial nitric oxide synthase (eNOS) resulting in enhanced generation of nitric oxide (NO) that mediates smooth muscle cell relaxation and vascular dilation in an attempt to accommodate the increase in blood flow. Vascular dilation causes increased circumferential wall stress that, along with NO, directly contributes to smooth muscle cell proliferation and hypertrophy resulting in increased thickness of the tunica media, which is one of the most important aspects of the arteriogenic remodeling process. The critical importance of NO in arterial remodeling has been demonstrated by several studies utilizing eNOS-deficient mice that show markedly reduced arteriogenesis and increased collateral artery rarefaction.[62,94,97] Inducible nitric oxide (iNOS) synthase has also been implicated in the arteriogenic process,[98] although its role is much less well understood.

Furthermore, the endothelium responds to increased FSS by acquiring an activated phenotype that involves cytoskeletal changes, but perhaps most significantly, up-regulation of numerous chemoattractants and cell surface adhesion molecules.[91,99] Monocyte chemoattractant protein 1 (MCP-1, encoded by *Ccl2*) is one of the most important factors that has been shown to play a major

role during arteriogenesis following vascular occlusion.[100,101] Both activated endothelial cells as well as SMCs produce and secrete MCP-1 setting up a strong chemoattractive gradient for monocytes. These adhere to the endothelial surface via interaction with selectins and adhesion molecules including intercellular adhesion molecule (ICAM-1 and 2) as well as vascular cell adhesion molecule 1 (VCAM-1) on the endothelial surface. Upon migration to the perivascular region, recruited monocytes differentiate into macrophages that secrete various matrix metalloproteases, which orchestrate extracellular matrix degradation that facilitates the arterial remodeling process. In addition, monocytes/macrophages produce numerous cytokines and growth factors that stimulate proliferation and migration of both endothelial and smooth muscle cells.[89,102]

Role of macrophages in arteriogenesis

Numerous lines of evidence support the crucial importance of the role of monocyte/macrophages and their secreted factors in arteriogenesis. Both blood monocyte levels and their recruitment to growing collaterals have been shown to affect collateral artery growth.[63,103] Thus, chemically modulating blood monocyte levels correlates with the extent of collateral growth[103] and impaired monocyte recruitment in *Ccr2*$^{-/-}$ mice results in decreased arteriogenesis.[63] In contrast,

MCP-1 administration to the region of growing collaterals augments monocyte recruitment and enhances arteriogenesis.[101,104]

The specific macrophage differentiation state appears to be particularly important as wound-healing/pro-angiogenic “M2-like” macrophages characterized by their higher expression of M2-type genes including *Tie2, Arg1, Cxcr4, Ccr2, Hgf, Pdgfb, Nrp1, Mmp2, Cxcl12* (also known as *Sdf1*) and *Tgfb* appear to promote enhanced collateral artery remodeling not only in models of arterial occlusion, but also developmentally.[78] Thus, *Phd2* haplodeficiency in myeloid cells results in an overabundance of M2-like macrophages in pericollateral regions that is associated with increased collateral artery number and size at baseline and enhanced collateral artery growth in models of arterial occlusion.[78] This was attributed to increased NF-κB activity in *Phd2*$^{+/-}$ macrophages that was hypothesized to drive a pro-arteriogenic transcriptional program including upregulation of *Pdgfb* and *Sdf1*. These were in turn shown to promote SMC migration and growth *in vitro*.[78] A subsequent study from the same group linked *Phd2* downregulation in macrophages to increased expression of the angiopoietin (ANG) receptor TIE2.[105] They reported a feed-forward loop whereby increased ANG1 in the setting of vascular occlusion acts via TIE2 to downregulate *Phd2*, allowing enhanced NF-κB signaling and increased *Tie2* expression in macrophages, which was shown to be required for macrophage skewing to the proarteriogenic phenotype. Using a *Herpes Simplex* virus

thymidine kinase-gancyclovir cell suicide system, they demonstrated that TIE2-expressing monocyte/macrophages (TEM) were indeed required for collateral artery growth. These data were complemented by a translational study that demonstrated increased numbers of TEM in the blood of patients with critical limb ischemia.[106] TEM abundance was reduced following revascularization or amputation. These studies support the possibility that TEM may be relevant to collateral artery remodeling in humans as well as in mice.

Role of growth factors in arteriogenesis

As mentioned above, macrophages promote arteriogenesis, in part, via production of various chemokines and growth factors. These factors contribute to collateral artery remodeling via either one or both of the following mechanisms: (1) providing a feed forward stimulus for recruitment, survival and activation of additional monocytes; (2) by directly acting on endothelial and smooth muscle cells altering their migratory and proliferative capacity.

GM-CSF and G-CSF

Granulocyte/monocyte colony stimulating factor (GM-CSF) and G-CSF promote myeloid cell recruitment, proliferation and survival. Following promising results in augmenting arteriogenesis and blood perfusion in animal models of vascular occlusion,[107,108] GM-CSF and G-CSF were tested in clinical trials in patients with

coronary artery or peripheral artery disease, however their beneficial effects in humans have been modest and equivocal.[59,109-111] The differences in response between animal models and humans may be due to intrinsic biological differences between humans and other animals or due to factor doses selected, treatment regimens, patient selection, outcome measures and sensitivity of techniques used to measure response. Additional, better-designed studies may be required to definitively determine the therapeutic potential of these factors.[86]

Fibroblast growth factors

Other growth factors including different members of the fibroblast growth factor (FGF) family as well as placental growth factor (PlGF), platelet derived growth factor B (PDGFB) and VEGF have been shown to participate in the growth and remodeling of collateral arteries in the experimental setting.[112,113]

Initial studies suggested that macrophage secreted FGFs may augment arteriogenesis and improve collateral artery flow[114-116] likely via their ability to stimulate both endothelial and SMC migration and proliferation.[117] FGFs may also act via cooperation with other growth factor systems by upregulating expression or promoting the action of VEGF, PDGFB, hepatocyte growth factor and MCP-1.[113] The story is, however, quite complex as *Fgf1*$^{-/-}$, *Fgf2*$^{-/-}$ or double *Fgf1* plus *Fgf2* knockout mice show little phenotypic vascular defects.[118-120] Additionally, clinical trials aimed at therapeutic angiogenesis in patients with

ischemic disease have shown little therapeutic efficacy of any single growth factor delivery from this family,[121] pointing to the significant redundancy in the FGF system and indicating the need for combinatorial strategies with factors from the same family or combination of growth factors from different families. Thus, understanding the intricate details and differences in the action of various growth factors may lead to better therapeutic strategies.

VEGF-A

In this respect, despite the disappointing outcome of clinical trials utilizing VEGF at improving therapeutic angiogenesis in ischemic diseases,[122] much research has continued to focus on understanding the arteriogenic potential of the VEGF/VEGFR signaling pathway.[94] Numerous experimental studies in mice support an important role for this pathway in arteriogenesis in the setting of vascular occlusion.[77,94,123,124] However, given this pathway's unquestionable pleiotropic functions during developmental angiogenesis, specification of arterial identity and arterial branching morphogenesis[94,125] as well as in formation of native collateral arteries,[61,77] it is often difficult to separate whether the results obtained in genetically modified mice with perturbation of this pathway are due to developmentally-derived differences in the formation of the vasculature or whether VEGF signaling indeed plays a role during remodeling of collateral arteries in adult animals in the setting of vascular occlusion. This distinction may be important for the design of therapeutic modalities as well as for the

interpretation of the outcome of clinical trials aimed at modulating this pathway in patients with vaso-occlusive disease.

Studies have reported the involvement of VEGF signaling during both developmental and adult arteriogenesis. A recent study demonstrated the existence of a chemokine-coupled β_2 integrin-induced Rac2-Myosin 9 (Myh9) interaction that leads to nuclear-to-cytosolic translocation of the RNA-binding protein HuR and VEGF-A mRNA stabilization.[123] Thus, mice with myeloid-specific disruption of Myh9 show reduced VEGF-A expression in macrophages and have blunted arteriogenic responses in adulthood following femoral artery occlusion, but do not display measurable defects in developmental angiogenesis, arteriogenesis or collateral artery formation.[123] These are surprising, but interesting findings that may truly reflect intrinsic biological differences between developmental and adult vascular biology. However, as the authors point out, these observations could be due to the timing of deletion of Myh9. Additionally, these findings may reflect differences in vascular development in different tissues since developmental vascular processes in this study were examined in the retina, kidney and brain, whereas adult arteriogenesis was analyzed in hindlimb skeletal muscle.

Other studies have analyzed the mechanisms of VEGF-VEGFR2 signaling in endothelial cells and its importance in arteriogenesis. A critical outcome of this

signaling is phosphorylation and activation of the mitogen-activated protein kinases ERK1 and 2, which mediate endothelial cell proliferation, migration and tube formation and are required for vascular development and arterial branching morphogenesis.[94] In arterial endothelial cells, VEGF-VEGFR2 mediated ERK phosphorylation requires VEGFR2 endocytosis and trafficking through the endosomal compartment, a process that is regulated in part by the VEGF and semaphorin non-tyrosine kinase receptor Neuropilin 1 (Nrp1) and its interaction with synectin and myosin-VI.[124,126,127] Thus, VEGF-A binding to VEGFR2 leads to receptor dimerization and autophosphorylation at Y^{1175}, an event that is required for subsequent ERK phosphorylation.[128] Following VEGF-A binding, dimerization and autophosphorylation, VEGFR2 undergoes clathrin-dependent endocytosis in a complex that includes Nrp1, synectin and myosin-VI.[94] In this complex the function of Nrp1, which contains a PDZ-binding domain is to facilitate interaction with the PDZ domain-containing protein synectin. This, in turn, interacts with the actin-based molecular motor myosin-VI to promote trafficking of the VEGFR2 receptor complex from clathrin-coated pits to early endosome antigen 1+ (EEA1+) endosomes.[94,129] Delayed trafficking of the VEGFR2 receptor complex in synectin or myosin-VI knockout mice[126] or in knockin mice, in which Nrp1 lacks the cytoplasmic PDZ-binding domain[124] results in reduced ERK phosphorylation and decreased developmental and reportedly adult arteriogenesis; although formal demonstration of the effects on adult arteriogenesis would require disruption of these components using inducible systems in adult mice. The

decreased ERK phosphorylation, when VEGFR2 trafficking to EEA1+ endosomes is delayed, has been attributed to phosphotyrosine phosphatase 1b (PTP1b)-mediated dephosphorylation of VEGFR2 at Y^{1175},[94,130] which serves as a binding site for PLCγ and subsequent activation of Raf1/MEK/ERK signaling.[128,131] Indeed, ERK phosphorylation is enhanced in PTP1b-deficient endothelial cells, and endothelial specific conditional deletion of *Ptpn1* (encoding PTP1b) in adult mice results in enhanced arteriogenesis and improved blood perfusion restoration in a model of femoral artery occlusion.[130]

Role of JNK in the vasculature

JNK has been implicated in angiogenic responses and other aspects of vascular biology. Studies have reported that treatment of human endothelial cells in culture with VEGF causes JNK activation that may be important for tube formation *in vitro*.[132,133] Using siRNA knockdown approaches in bovine aortic endothelial cells, one study reported that the chemokine stromal cell-derived factor-1α (SDF-1α, also known as CXCL12) causes selective phosphorylation of JNK3, but not JNK1 or JNK2, and that JNK3 was important for cell migration and tube formation *in vitro*.[134] Induction of JNK3 phosphorylation by SDF-1α was attributed to SDF-1α-stimulated endothelial nitric oxide synthase (eNOS) activation leading to nitric oxide-mediated nitrosylation and inactivation of MAPK phosphatase 7 (MKP7).[134]

Two *in vivo* studies employing whole body *Jnk1*$^{-/-}$ mice or chemical inhibition of JNK have reported a positive regulatory role for JNK in pathological ocular neovascularization in a model of retinopathy of prematurity (ROP)[135] and in a model of laser-induced choroidal neovascularization (CNV).[136] One study showed that hypoxia activates JNK in macrophages *in vitro* leading to JNK-dependent positive regulation of VEGF expression in these cells.[135] *Jnk1*$^{-/-}$ mice exhibited decreased VEGF expression in retinas during the development of retinopathy and this was proposed to contribute to decreased retinal neovascularization in the ROP model.[135] In the second study, decreased apoptosis in the choroid of *Jnk1*$^{-/-}$ mice following laser-induced injury was reported to lead to decreased macrophage recruitment, decreased VEGF secretion in choroidal tissues and decreased CNV size.[136]

Two other studies have reported results that appear contradictory to those above. An earlier study reported a negative regulatory role for JNK1 in angiogenesis.[137] This study showed that treatment of human endothelial cells with the potent natural angiogenesis inhibitor Thromobospondin-1 (TSP-1) activates JNK in a CD36 (a TSP-1 receptor)-dependent manner. JNK1 was then shown to mediate the antiangiogenic action of TSP-1 by demonstrating that TSP-1 inhibition of basic FGF-induced corneal neovascularization *in vivo* or VEGF-induced angiogenic sprouting in a corneal assay *in vitro* was impaired in corneas from *Jnk1*$^{-/-}$ mice.[137] A recent study showed that increased JNK3 expression in

endothelial cells expressing a mutant form of EphrinB2 (lacking tyrosine residues important for signaling) mediates increased endothelial cell death.[138] Consequently, this study reported that *Jnk3*$^{-/-}$ mice display reduced regression and thus, increased branching and density of the hyaloid vasculature (a vascular network in the eye that in mice is present at birth and regresses in the early postnatal period).[138]

Furthermore, numerous studies have implicated JNK in the response of endothelial cells to flow and flow-induced shear stress.[139-144] Thus, acute exposure of endothelial cells to disturbed flow causes JNK activation that promotes endothelial cell inflammatory responses, including NF-κB activation, that have important roles in promoting regional development of atherosclerosis in the arterial vasculature.[139,140] In contrast, exposure of the arterial endothelium to sustained laminar shear stress results in gene expression changes, including upregulation of the transcription factor KLF2, that lead to inhibition of JNK signaling, decreased expression of adhesion molecules on the endothelial surface, and decreased endothelial inflammation leading to endothelial normalization and protection from atherosclerosis.[139,141,144] The role of JNK in transducing flow-induced shear stress responses during arteriogenesis has not, however, been explored.

HEMATOPOIESIS

Hematopoiesis is the process of blood cell production.[145] During embryogenesis, hematopoiesis occurs spatially and temporally in intimate association with vascular development. Indeed, hematopoietic and endothelial cells are thought to arise from a common precursor.[33]

Hematopoietic and Vascular Endothelial Cells Share Common Origins

Although still somewhat controversial, the existence of the hemangioblast, a common mesodermally-derived progenitor that gives rise to both hematopoietic and endothelial cells has been reported by several studies.[33] Hematopoietic cells first appear within the blood islands of the extra-embryonic yolk sac in close apposition to endothelial cells.[31,33] This association as well as the sharing of various markers between hematopoietic and endothelial cells and the impairment of both the hematopoietic and vascular systems in mutants, such as the *Flk-1*$^{-/-}$ mice,[146] has lead to the hypothesis of the hemangioblast. Lineage tracing studies have provided support for a common origin between hematopoietic and endothelial cells, yet, definitive direct evidence that a single cell divides asymmetrically to form an endothelial and a blood cell *in vivo* is lacking.[33]

Hematopoietic stem cell emergence

During development, blood production occurs at several different sites. These include the yolk sac, a region surrounding the aorta called aorta-gonad

mesonephros (AGM), the placenta, the fetal liver and ultimately the bone marrow.[33] In mammals, the first wave of hematopoiesis occurs in the yolk sac, is termed “primitive” and generates erythroid cells that are necessary for oxygenation of the rapidly developing embryo.[33] Cells with myeloid characteristics are also generated at this stage.[147] However, whether hematopoietic stem cells (HSCs) are present in the yolk sac remains controversial.[148] HSCs are defined functionally as cells that are capable of generating all blood cells and that undergo self-renewing divisions, whereby a single cell generates daughter cells with the same characteristics and potential as the original cell.[33] Definitive HSCs (dHSCs) with engrafting potential are first detected in the AGM ~E10.5 and are thought to bud off from specialized endothelial cells lining the aorta termed hemogenic endothelial cells.[149] The placenta has also been shown to contain dHSCs, although it is unclear whether these arise *de novo* or colonize the placenta via the circulation.[150,151] By E11.5 HSCs have colonized the fetal liver and subsequently, the thymus, spleen and ultimately the bone marrow, which is the primary site of adult hematopoiesis.[33]

The hematopoietic hierarchy

HSCs stand at the top of the hematopoietic hierarchy (Figure I.6).[145] They have definitive replication potential and are maintained in a quiescent state with a small number of HSCs cycling at any one time. Theoretically, HSCs can undergo three types of cell divisions: (1) symmetrical, giving rise to two daughter HSCs with the same characteristics and potential of the original cell; (2) asymmetrical

division, generating a daughter HSC plus a more differentiated cell with reduced self-renewal potential (often termed short-term HSC [ST-HSC]); and (3) symmetrical division resulting in the production of two ST-HSCs.[33,152] ST-HSCs proceed down the differentiation hierarchy to successively generate more differentiated progenitors that will ultimately produce mature blood cells. Thus, ST-HSCs give rise to multipotent progenitors (MPPs) that retain multilineage differentiation potential, but lack self-renewal capacity. MPPs can produce both common myeloid progenitors (CMPs) and common lymphoid progenitors (CLPs). CLPs are the source of committed precursors that will generate B and T cells, whereas CMPs give rise to megakaryocyte/erythrocyte progenitors (MEPs) and granulocyte/macrophage progenitors (GMPs). Neutrophils, eosinophils, basophils, mast cells, dendritic cells and monocyte/macrophages arise from GMP-derived precursors.[33]

Methods of stem and progenitor cell identification and functional characterization

Immunolabeling of surface markers coupled with multicolor flow cytometry approaches affords the identification and isolation of stem, progenitor and mature hematopoietic cell populations with high purity.[153] In adult mice, all HSC activity is contained within the Lineage$^{-/low}$, Sca1^{+}, cKit^{+} (LSK) population of bone marrow cells.[153] This population is highly heterogeneous, and more specific stem and progenitor cell populations can be further defined by the utilization of additional cell surface markers.[153] Indeed current methods allow identification of bone

marrow cell populations in which one out of two cells is a functionally confirmed HSC (i.e., engrafts and gives long term multilineage reconstitution in lethally irradiated mice).[154] This is remarkable given that HSCs comprise only < 0.01% of bone marrow cells.[153] *In vivo* functional characterization of stem and progenitor populations involves their transplantation into irradiated mice and analysis of blood production in recipient mice over time.[155] HSCs are the only cells capable of conferring long term (> 4 months) multilineage reconstitution when transplanted into lethally irradiated mice, yet HSCs have definitive replication potential. The competitive serial bone marrow transplantation assay remains the most rigorous test for determining HSC function and self-renewal capacity. In this assay, as HSCs are transferred from one recipient to the next, they are repeatedly forced to cycle in order to repopulate the BM niches of the new recipient and maintain hematopoiesis. During this process, HSCs with lower self-renewal potential will be lost earlier than HSCs with higher self-renewal potential, thus maintenance of multilineage blood production in recipient mice over long periods in multiple recipient mice can be used to infer HSC self-renewal capacity.[155-157]

Role of JNK in hematopoietic cells

JNK has been implicated in hematopoietic cell development and function in various contexts. JNK is activated by exposure of cells to various cytokines as

well as antigen or ligand binding to immune cell receptors, including T and B cell receptors, and toll like receptors.[158] Studies employing single *Jnk1*$^{-/-}$ or *Jnk2*$^{-/-}$ mice or transgenic mice expressing a dominant negative JNK1 protein have demonstrated that JNK is not required for lymphocyte development, but may play a role during negative selection of thymocytes by mediating apoptotic responses to T cell receptor engagement.[158-160] JNK has also been reported to affect differentiation, activation and proliferation of mature T cells. Thus, JNK1 appears to be required for appropriate effector T cell differentiation.[161] $CD4^+$ precursor cells undergo differentiation into type 1 or type 2 T helper (T_H) cells that mediate differential immune responses. *Jnk1*$^{-/-}$ T cells exhibit enhanced production of T_H2 cytokines, undergo hyperproliferation and differentiate preferentially into T_H2 cells.[161] Additionally, *Jnk2*$^{-/-}$ mice display defects in differentiation of $CD4^+$ precursor cells into T_H1, but not T_H2 cells. Defective T_H1 differentiation in *Jnk2*$^{-/-}$ mice has been attributed to impaired production of interferon (IFN)-γ production during the early stages of differentiation and can be rescued by exogenous IFN-γ.[162] In contrast to T cells, neither JNK1 nor JNK2 has been reported to contribute to normal B cell function including proliferation/survival or antibody production, despite JNK activation in B cells by various stimuli, including B cell receptor ligation.[158] However, a positive regulatory role for JNK1 in B lymphoblast survival in the context of BCR-ABL transformation has been reported.[24]

JNK is activated in macrophages by inflammatory cytokines, lipopolysaccharide (LPS) and other stimuli.[5,163,164] An important function of JNK2, but not JNK1, in the uptake and degradation of modified lipoproteins and foam cell formation has been reported and explains the protection of *Jnk2*$^{-/-}$*ApoE*$^{-/-}$ from atherosclerosis.[165] Mechanistically, it was demonstrated that JNK2 in macrophages phosphorylates scavenger receptor A (SR-A), an event that is required for receptor/lipoprotein complex internalization and formation of foam cells,[165] which are critical mediators of the atherosclerotic process.[166] JNK in macrophages has also been reported to be important for IFN-γ or LPS-induced pro-inflammatory cytokine expression *in vitro* and high fat diet-induced pro-inflammatory macrophage polarization and inflammation *in vivo*.[163]

In addition to its role in immune cell differentiation and function, the JNK signaling pathway has also been implicated in normal hematopoietic cell survival. Thus, the MAP3K, TAK1, which can mediate JNK activation by inflammatory cytokines, is critical for hematopoietic cell survival.[167] *Tak1*$^{-/-}$ mice die during embryogenesis.[168,169] Inducible conditional deletion of *Tak1* in adult mice using a *Mx1-Cre* system results in lethality within 10 days of polyI:C administration due to bone marrow and liver failure resulting from massive apoptotic death of hematopoietic cells and hepatocytes.[167] Apoptosis was confirmed in hematopoietic stem/progenitor cells (LSK cells), and the cell-autonomous requirement of TAK1 for hematopoietic cell survival was demonstrated in

transplantation experiments.[167] A recent study investigated the role of JNK in hematopoietic stem and progenitor cell development in whole body JNK knockout mice and reported that *Jnk2*$^{-/-}$ and *Jnk1*$^{+/-}$*Jnk2*$^{-/-}$ but not *Jnk1*$^{-/-}$ mice exhibited increased progenitor cell apoptosis and decreased numbers of HSCs and progenitors in the bone marrow.[170] Thus, JNK may have important functions in hematopoietic development.

RATIONALE AND OBJECTIVES

As illustrated above, in response to diverse extracellular stimuli, JNK phosphorylates numerous transcription factors and cytoplasmic proteins altering gene expression programs and regulating a multitude of biological processes that affect cellular, tissue and organismal physiology. JNK is ubiquitously expressed and exists in multiple isoforms, which may have distinct roles or may contribute to functional diversity via cell or tissue specific distribution profiles. However, often, JNK isoforms display high functional redundancy requiring careful interpretation of results from studies that employ disruption of distinct JNK isoform subsets. Standard whole body knockout mouse models disrupting individual or combinations of JNK genes have provided important insight into the pleiotropic functions of JNK in mammalian physiology. However, these studies have been limited by the early embryonic death of compound *Jnk1*$^{-/-}$*Jnk2*$^{-/-}$ mice. The generation of conditional JNK alleles, combined with tissue specific constitutive and inducible *Cre* technology, now, affords more intimate dissection of tissue specific functions of JNK in mice with compound disruption of multiple or all JNK isoforms.

Although JNK has been implicated in vascular and, more specifically, endothelial cell biology, both pro and anti-angiogenic functions have been reported. These results may stem from differential functions of specific JNK isoforms or JNK isoform profiles in different tissues that may affect the same biological process

differently. Furthermore, these studies have been focused specifically on the role of JNK in pathological angiogenesis or *in vitro* systems, which have some benefits, but also significant limitations. Therefore, studies that utilize multiple model systems that dissect different aspects of vascular biology and employ genetically modified mice with compound disruption of multiple or all JNK isoforms in specific cell types are required to definitively characterize the function of JNK in vascular biology. The purpose of the study presented in Chapter II was to provide critical and conclusive insights into the role of JNK in endothelial cell-mediated vascular development and function.

Additionally, given the intimate relationship both developmentally and physically between endothelial and hematopoietic cells as well as the numerous lines of evidence linking JNK to the regulation of immune cell gene expression, cytokine production, and hematopoietic cell survival and function, we aimed to generate and utilize previously uncharacterized mouse models with compound hematopoietic cell specific disruption of JNK in order to analyze its function in normal hematopoietic development and HSC self-renewal. These data are presented in Chapter III.

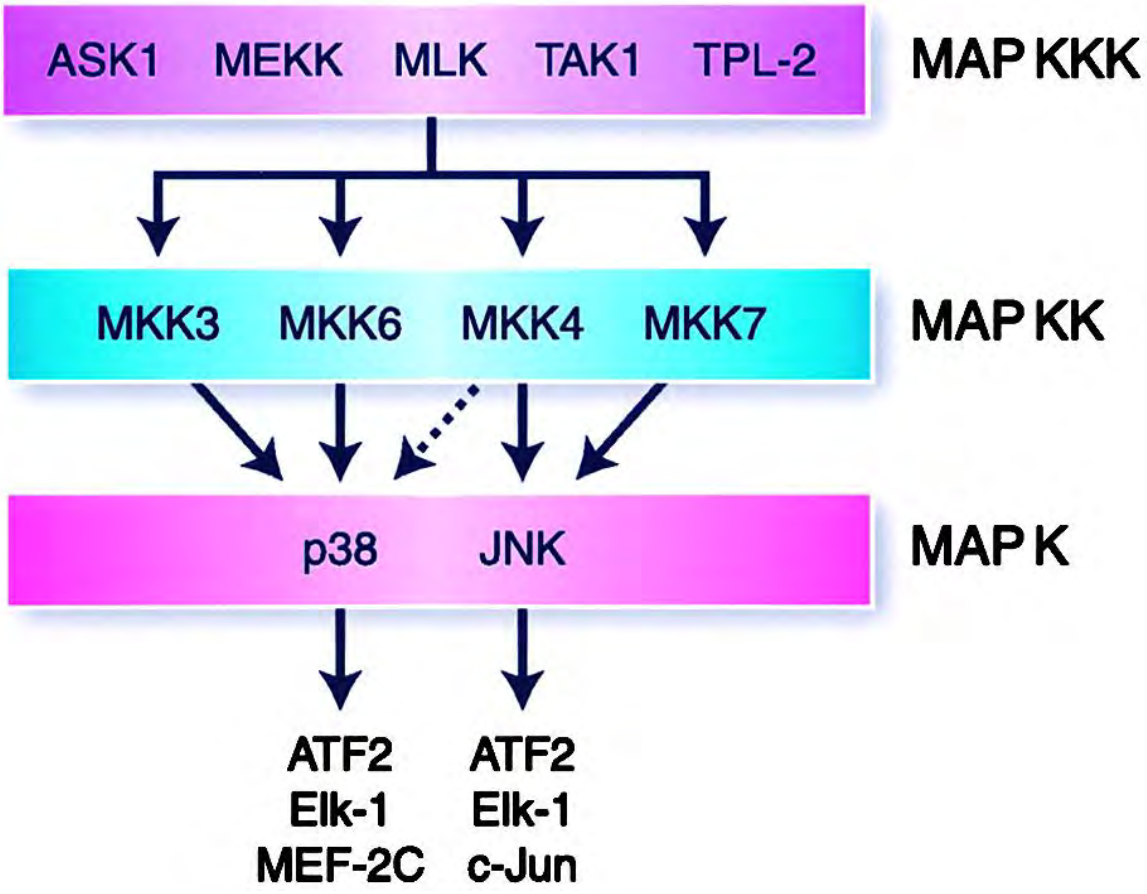
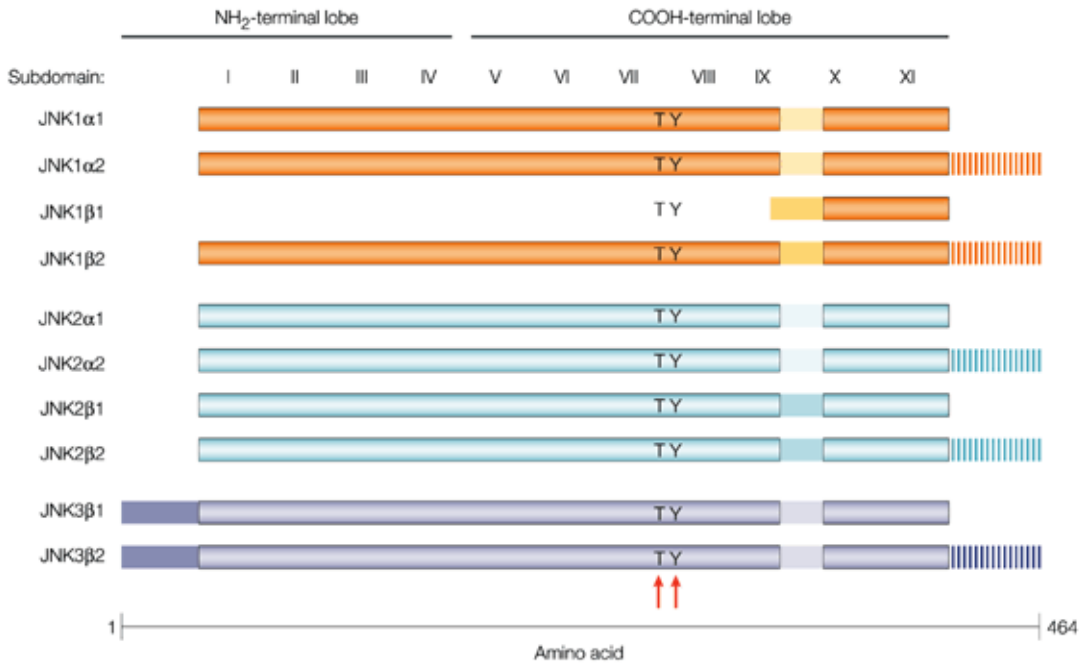

ASK1 MEKK MLK TAK1 TPL-2
MAP KKK
MKK3 MKK6 MKK4 MKK7
MAP KK
p38 JNK
MAP K
ATF2
Elk-1
MEF-2C
ATF2
Elk-1
c-Jun

Figure I.1 MAP kinase signal transduction.

Numerous mitogen activated protein kinase kinase kinases (MAP KKK) have been identified. Upon activation by a multitude of stimuli, MAP KKK phosphorylate and activate MAP kinase kinases (MAP KK). Four MAP KK are shown that mediate phosphorylation and activation of the MAP kinases, p38 and JNK. MKK4 and MKK7 mediate activation of JNK, while MKK3 and MKK6 activate p38. MKK4 may also activate p38. Similar signaling cascades lead to activation of the ERK group of MAP kinases (not depicted). Upon activation, MAP K phosphorylate numerous substrates.

Image taken from Davis, R.J. Signal transduction by the JNK group of MAP kinases. *Cell* **103**, 239-252 (2000).



Nature Reviews | Drug Discovery

Figure I.2 JNK isoforms.

The c-Jun NH_2-terminal kinase (JNK) is a serine / threonine kinase containing 11 kinase subdomains (I-XI). JNK is fully activated upon phosphorylation of two critical residues (threonine (T) 183 and tyrosine (Y) 185) indicated by red arrows. Ten total JNK isoforms are generated by alternative splicing of the three *Jnk* genes (*Jnk1, Jnk2* and *Jnk3*). One alternative splicing site located between subdomains IX and X (indicated by the shaded regions) involves selection of one of two alternative exons that encode part of the kinase domain. This splice site is restricted to *Jnk1* and *Jnk2*, and gives rise to JNK isoforms with different substrate binding specificities. The second splice site at the COOH-terminus of the protein results in proteins that differ by 42 or 43 amino acids, indicated by the hatched regions. The functional role of these isoforms is not known.

Image taken from Manning, AM and Davis, RJ. Nat Rev Drug Discov. 2003;2(7):554-65.

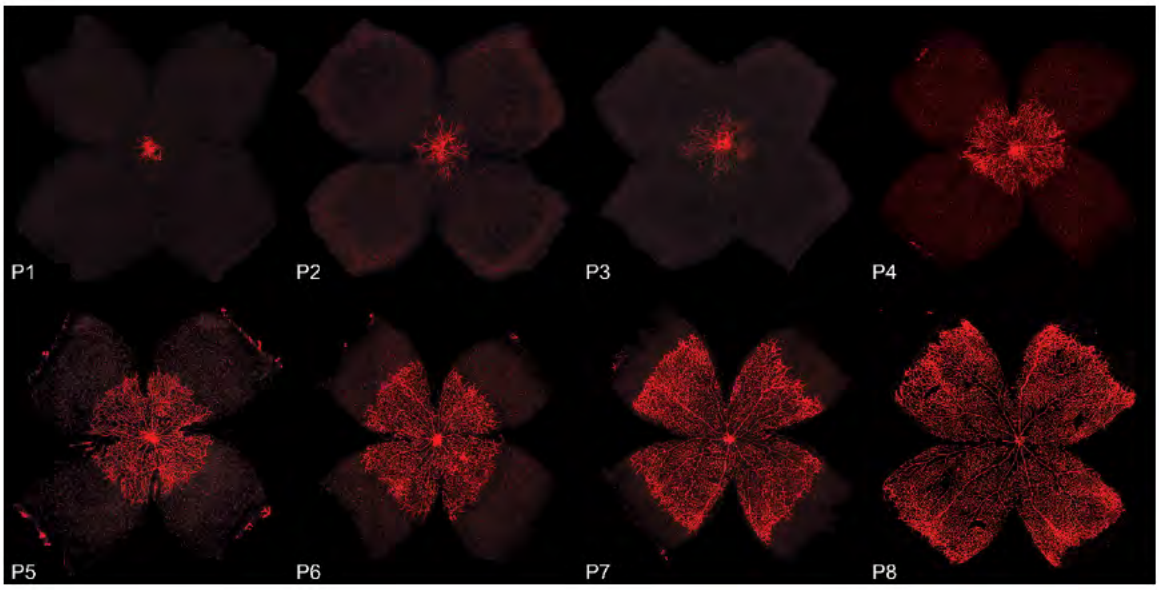

P1
P2
P3
P4
P5
P6
P7
P8

Figure I.3 Early postnatal development of the retinal vasculature as a model for studying sprouting angiogenesis.

At birth (postnatal day [P] 0) the retina is avascular. Formation of the superficial retinal vascular plexus occurs in the first few days of postnatal life from the center of the retina towards the periphery. This highly stereotypic process initially occurs in two dimensions on the inner surface of the retina, which can be flatmounted as shown and allows for detailed microscopic analysis of many aspects of the sprouting angiogenic process.

Image taken from Stahl, A., Connor, K.M., Sapieha, P., Chen, J., Dennison, R.J., Krah, N.M., Seaward, M.R., Willett, K.L., Aderman, C.M., Guerin, K.I., Hua, J., Lofqvist, C., Hellstrom, A. & Smith, L.E. The mouse retina as an angiogenesis model. *Invest Ophthalmol Vis Sci* **51**, 2813-2826 (2010).

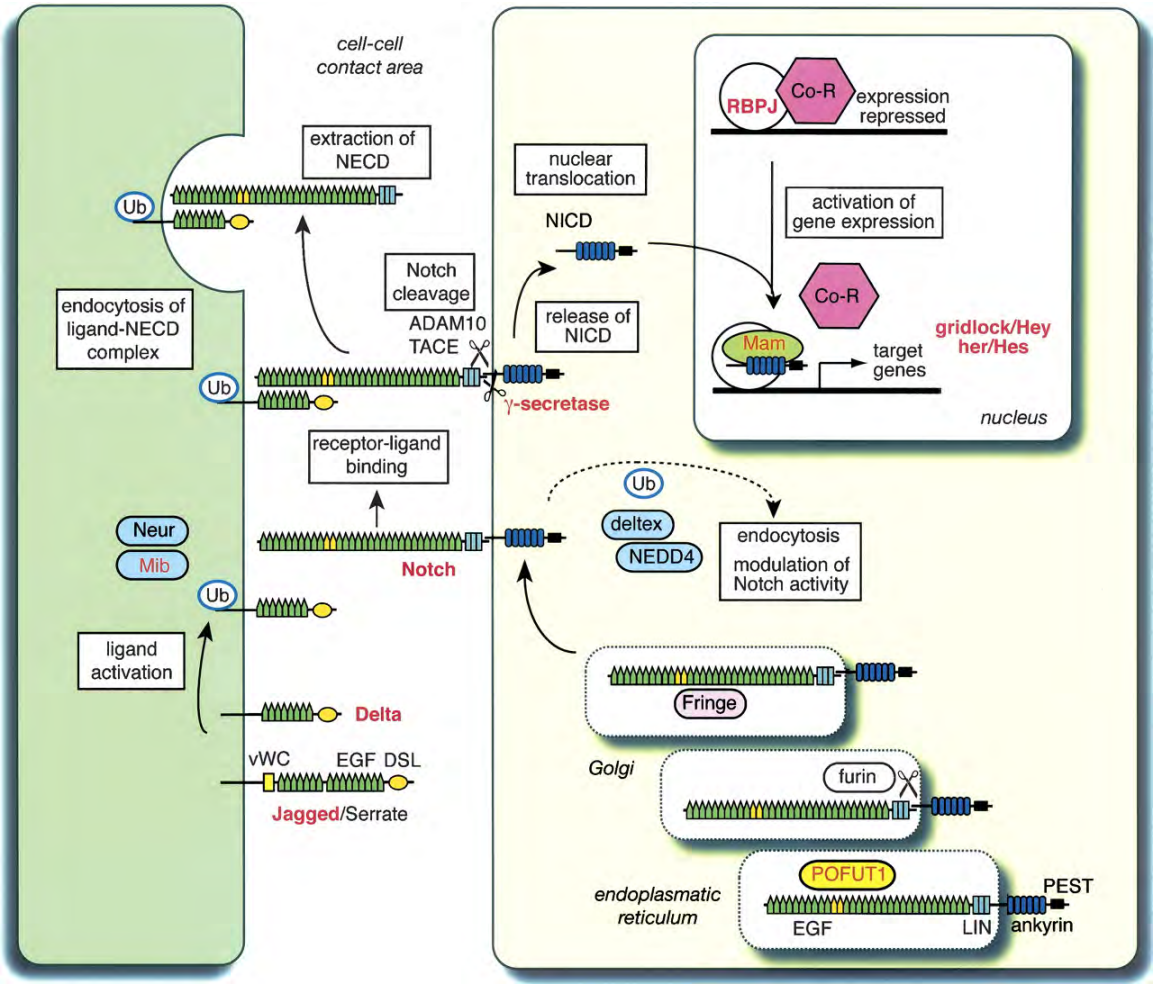

cell-cell
contact area
extraction of
NECD
Ub
endocytosis of
ligand-NECD
complex
Notch
cleavage
ADAM10
TACE
γ-secretase
nuclear
translocation
NICD
release of
NICD
RBPJ
Co-R
expression
repressed
activation of
gene expression
Co-R
Mam
target
genes
gridlock/Hey
her/Hes
nucleus
receptor-ligand
binding
Ub
deltex
NEDD4
endocytosis
modulation of
Notch activity
Neur
Mib
Notch
Ub
ligand
activation
Fringe
Golgi
furin
Delta
vWC
EGF DSL
Jagged/Serrate
endoplasmatic
reticulum
POFUT1
EGF
LIN
PEST
ankyrin

Figure I.4 Notch signaling.

Refer to the Notch Signaling section of the introduction for a detailed description of the pathway.

Image taken from Roca, C. & Adams, R.H. Regulation of vascular morphogenesis by Notch signaling. *Genes Dev* **21**, 2511-2524 (2007).

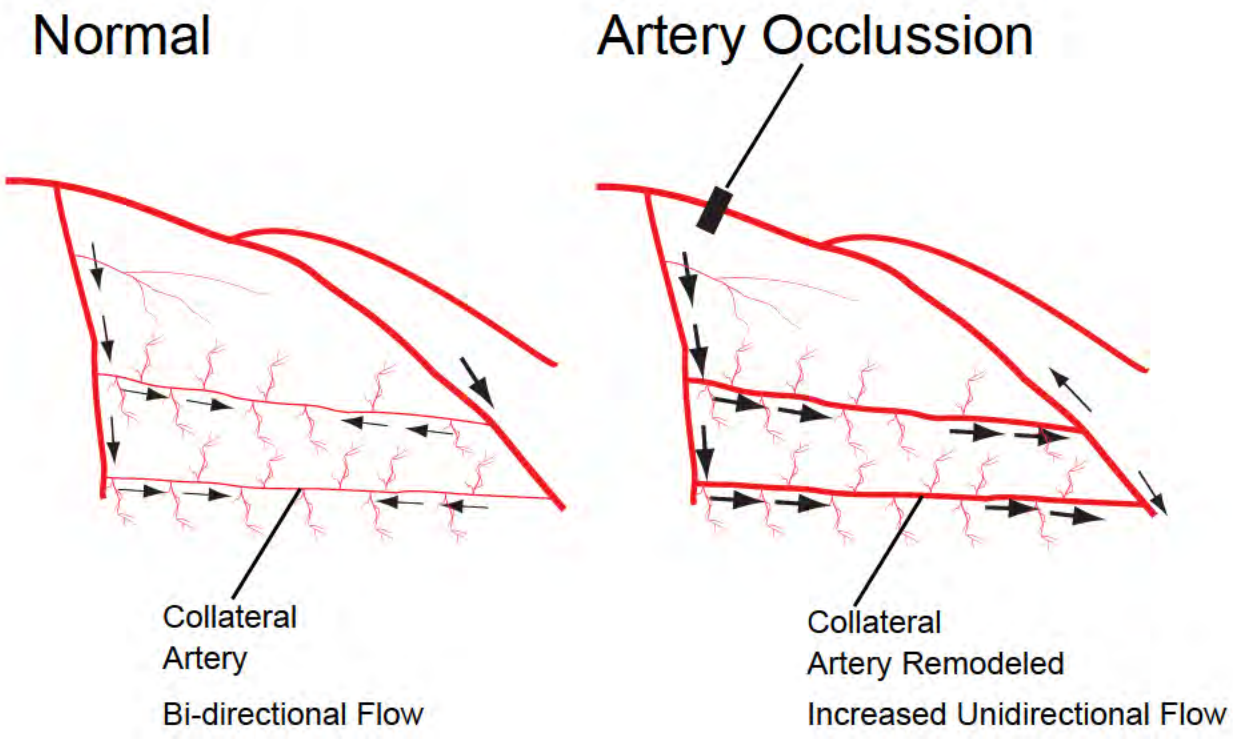

Normal
Artery Occlusion
Collateral
Artery
Bi-directional Flow
Collateral
Artery Remodeled
Increased Unidirectional Flow

Figure I.5 Collateral arteries.

Collateral arteries interconnect adjacent arterial trees. Collaterals have narrow lumens and experience bi-directional flow. Following arterial occlusion more blood flow is redirected through these alternative routes. Increased proximal and decreased distal pressure results in unidirectional flow through collaterals in the setting of arterial occlusion. Collateral arteries remodel outwardly increasing in diameter.

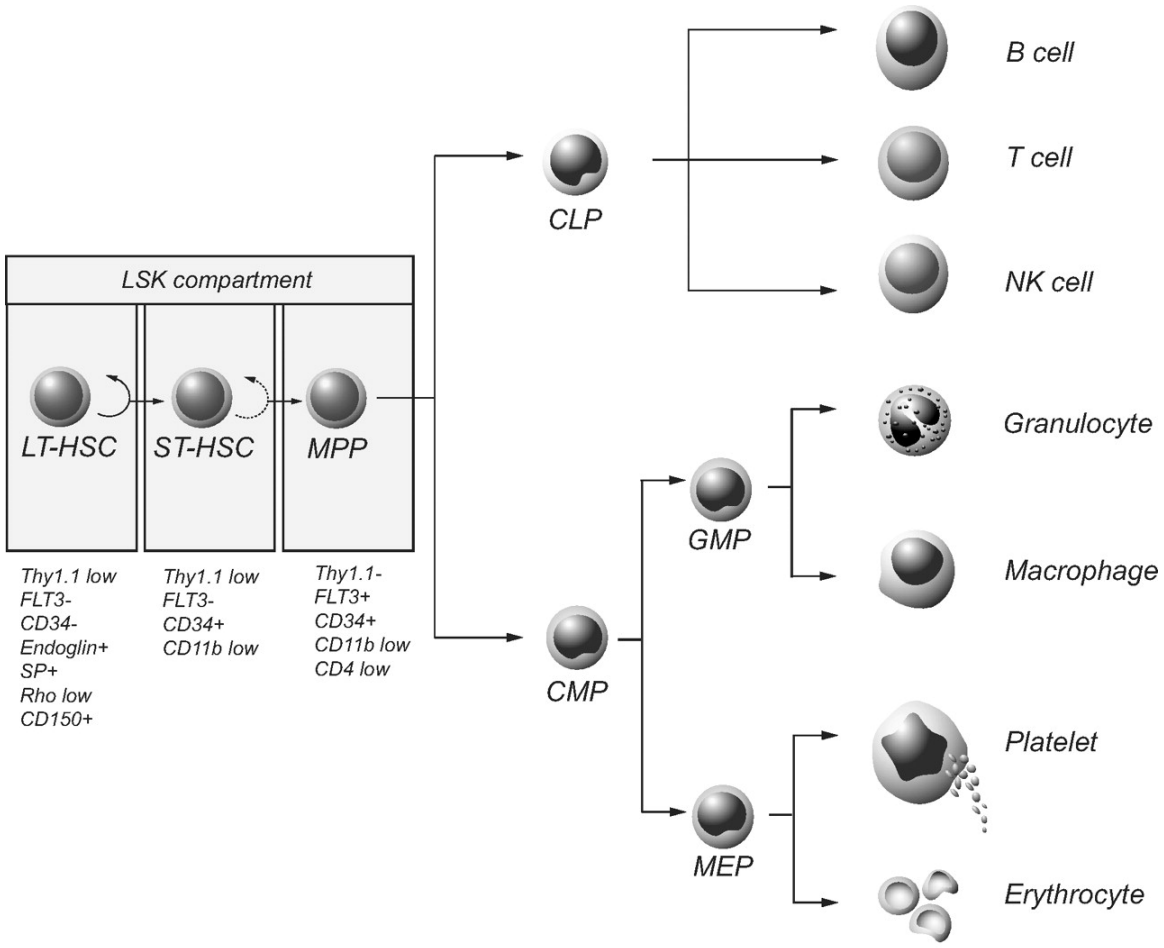

LSK compartment
LT-HSC
ST-HSC
MPP
Thy1.1 low
FLT3-
CD34-
Endoglin+
SP+
Rho low
CD150+
Thy1.1 low
FLT3-
CD34+
CD11b low
Thy1.1-
FLT3+
CD34+
CD11b low
CD4 low
CLP
CMP
GMP
MEP
B cell
T cell
NK cell
Granulocyte
Macrophage
Platelet
Erythrocyte

Figure I.6 The hematopoietic hierarchy.

Hematopoietic stem cells (HSC) stand at the top of the hematopoietic hierarchy and give rise to all blood cells. The lineage$^-$, Sca-1$^+$, cKit$^+$ (LSK) population of bone marrow cells is enriched in long-term (LT)-HSC, short-term (ST)-HSC and multipotent progenitors. LT-HSCs and ST-HSCs can undergo self-renewing divisions or can give rise to more differentiated progenitors, which will produce lineage specific progenitors such as the common lymphoid progenitors (CLP) that will lead to the generation of precursors for B, T and natural killer (NK) cells. Common myeloid progenitors (CMP) give rise to granulocyte/macrophage progenitors (GMP) and megakaryocyte/erythrocyte progenitors. GMPs generate granulocytes and macrophages, while MEPs generate platelets and erythrocytes.

Image taken from Blank, U., Karlsson, G. & Karlsson, S. Signaling pathways governing stem-cell fate. *Blood* **111**, 492-503 (2008).

Chapter II

Endothelial MLK – JNK Signaling Regulates Vascular Morphogenesis and is Critically Required for Native Collateral Artery Development

Abstract

Arterial occlusive diseases are major causes of morbidity and mortality. Blood flow to the affected tissue must be restored quickly if viability and function are to be preserved. Collaterals are artery-to-artery or arteriole-to-arteriole interconnections that can bypass an occlusion by providing an alternative route for blood flow to the affected tissue. The increased flow and shear stress initiate processes that result in the remodeling (arteriogenesis) of these vessels into efficient conductance arteries. Here we report that the mixed-lineage kinase (MLK) pathway activates cJun NH_2-terminal kinase (JNK) in endothelial cells. Disruption of *Mlk2/3* or *Jnk1/2* genes caused severe blockade of blood flow and failure to recover in the femoral artery ligation model of hindlimb ischemia because of abnormal collateral arteries. We show that the MLK-JNK pathway is essential for patterning and maturation of collateral arteries during development, but this pathway is not required for angiogenesis or arteriogenesis in adults. JNK in endothelial cells promotes Delta-like 4-induced Notch signaling and suppresses excessive sprouting angiogenesis during development. This function of the MLK-JNK pathway contributes to normal formation of native collateral arteries. The MLK-JNK pathway is therefore a key regulatory mechanism for vascular development. These data highlight the crucial importance of the collateral circulation in the response to arterial occlusive diseases.

Introduction

Arterial occlusion, the common denominator in ischemic stroke, myocardial infarction and peripheral artery disease, blocks blood flow and can result in severe tissue ischemia and necrosis. To prevent loss of tissue viability and function, blood flow to the affected tissue must be restored quickly. Collaterals are natural artery-to-artery or arteriole-to-arteriole interconnections that can bypass an occlusion by providing an alternative route for blood flow to the affected tissue, thus, restoring tissue homeostasis and limiting tissue damage.[57,58,60,94,171,172] Indeed, clinical outcome in patients with arterial occlusion depends on the presence of an adequate collateral circulation[68,172] and animal models of arterial occlusion provide strong evidence for the critical importance of the extent of the native (pre-existing) collateral circulation in restoring blood perfusion and limiting ischemic sequelae following arterial occlusion.[65,75,101,104,173]

Important characteristics of the collateral circulation include collateral artery number and size,[60,76,174] but also collateral artery connectivity patterns and functional adaptation to changes in blood flow.[82] Furthermore, collateral artery structural adaptations are also essential for adequate blood flow restoration. Following arterial occlusion more blood flow is diverted to the collateral circulation and the increased flow and shear stress in collateral arteries initiates a number of processes that result in the outward remodeling (arteriogenesis) of

these vessels into efficient conductance arteries that allow increased blood flow. Collateral artery remodeling includes endothelial cell activation and proliferation, monocyte/macrophage recruitment and smooth muscle cell proliferation, all of which contribute to increased collateral artery diameter, including increased thickness of the tunica media. These structural and functional adaptations are, however, likely to depend heavily on the presence of an adequate native collateral circulation prior to vascular occlusion.[58,88,89,91,94]

Little is known about the cellular and morphogenetic processes, or about the molecular factors and mechanisms that contribute to native collateral artery formation. A small number of studies, largely focused on the formation of the leptomenengial (or pial) collateral arteries in the brain, have provided significant insight.[61,64,77,84] In mice, pial collaterals are established during embryonic development with some remodeling and maturation continuing postnatally.[61,64] The process of native collateral artery formation during embryogenesis has been termed collaterogenesis. The molecular factors or signaling pathways that have been reported to contribute to native collateral artery formation include, platelet-endothelial cell adhesion molecule 1 (PECAM1),[79] gap junction protein, connexin37 (Cx37),[80,81] prolyl hydroxylase domain-containing protein 2 (PHD2),[78] endothelial nitric oxide synthase (eNOS),[62] chloride intracellular channel 4 (CLIC4),[65] Synectin[95], NF-κB signaling,[175] VEGF signaling,[61,74] and Dll4 – Notch signaling.[82] In addition to affecting native collateral artery formation, many of

these factors are known modulators of developmental angiogenesis (i.e., the process of new vessel formation from existing vasculature) and vascular morphogenesis, suggesting that the patterning of initial vascular networks may affect their subsequent remodeling and maturation, and formation of native collateral arteries. VEGF and Dll4 – Notch signaling play critical roles in endothelial cell survival, proliferation and migration, and therefore, regulate developmental sprouting angiogenesis and vascular morphogenesis.[37,54,125] They are also critical for formation of the native collateral circulation.[82]

cJun-NH_2 terminal kinases (JNK) are members of the stress and mitogen activated protein kinase (MAPK) family that are activated by diverse environmental stimuli, including cytokines, growth factors and flow-mediated shear stress.[1,12,139-144] Three *Jnk* genes encode for transcripts that are alternatively spliced, generating 10 different JNK isoforms with high functional redundancy.[1,3] JNK1 and JNK2 isoforms are ubiquitously expressed, whereas expression of JNK3 isoforms is restricted to brain, heart, testes[1,3] and possibly endothelial cells.[134] Signaling cascades involving one (or more) of a dozen MAPK kinase kinases (MAP3K) and one of two (or both) MAPK kinases (MAP2K) mediate JNK phosphorylation and activation. JNK phosphorylates numerous substrates, some of which are components of the activator protein complex 1 (AP-1) that regulates expression of many genes. In this manner, JNK regulates various gene expression programs and mediates diverse cellular responses in

different cell types.[1]

JNK has been implicated in both pro and anti-angiogenic responses in vivo.[136,137] These studies have used whole body *Jnk1*$^{-/-}$ mice in pathologic models of angiogenesis and thus have significant limitations. The role of other JNK isoforms and the specific cell types in which JNK is important for vascular biology as well as the role of JNK in physiologic vascular development and function remain outstanding questions.

Here, we employ compound mutant mice with constituitive and inducible endothelial-specific disruption of all JNK isoforms in combination with various model systems to explore the role of endothelial JNK in various aspects of vascular biology. We find that JNK regulates Dll4 – Notch signaling in endothelial cells and identify a critical role for mixed lineage kinase (MLK) – JNK signaling in vascular morphogenesis and native collateral artery development.

Results

Generation and initial characterization of mice with targeted ablation of all JNK isoforms in the vascular endothelium

To examine the role of endothelial JNK in vascular development and function, we crossed mice with conditional alleles of *Jnk* to mice expressing a constitutively active cre recombinase (Cre) driven by the vascular endothelium cadherin (also known as *Cdh5*) promoter[176] to generate mice with vascular endothelium specific compound deficiency of JNK1 plus JNK2 (E^{2KO}, *Cdh5Cre*$^{+}$ *Jnk1*$^{LoxP/LoxP}$ *Jnk2*$^{LoxP/LoxP}$) or JNK1 plus JNK2 plus JNK3 (E^{3KO}, *Cdh5-Cre*$^{+}$ *Jnk1*$^{LoxP/LoxP}$ *Jnk2*$^{LoxP/LoxP}$ *Jnk3*$^{-/-}$). Control mice included *Cre*$^{+}$ (E^{WT}, *Cdh5-Cre*$^{+}$ *Jnk1*$^{+/+}$ *Jnk2*$^{+/+}$ and E^{Ctrl}, *Cdh5-Cre*$^{+}$ *Jnk1*$^{+/+}$ *Jnk2*$^{+/+}$ *Jnk3*$^{-/-}$ respectively) mice as well as respective *Cre*$^{-}$ littermates (E^{fCtrl}, *Cdh5-Cre*$^{-}$ *Jnk1*$^{LoxP/LoxP}$ *Jnk2*$^{LoxP/LoxP}$ and *Cdh5-Cre*$^{-}$ *Jnk1*$^{LoxP/LoxP}$ *Jnk2*$^{LoxP/LoxP}$ *Jnk3*$^{-/-}$). Immunoblot analysis of lysates from purified (Supplementary Figure II.1D and E) lung endothelial cells from E^{3KO} mice revealed a robust reduction in JNK protein levels in these cells (Figure II.1A). E^{2KO} and E^{3KO} mice used in this study developed normally and were healthy and fertile (see also the Methods section). We found no differences in body weight at birth and postnatal (P) day 6 (Supplementary Figure II.1A). Adult E^{2KO} and E^{3KO} mice were slightly smaller than control mice, but continued to gain weight indistinguishably from control mice (Supplementary Figure II.1B and C).

Endothelial (EC) and hematopoietic (HC) cells are thought to share a common precursor, the hemangioblast,[33] and it has been reported that the *Cdh5* promoter is active in a subset of HC.[176] Indeed, polymerase chain reaction (PCR) analysis of bone marrow, spleen or blood from E^{3KO} mice detected a low level of recombination of *Jnk* alleles (Supplementary Figure II.2B). However, importantly, immunoblot analysis showed no detectable reduction in JNK protein levels in any of the hematopoietic tissues from E^{3KO} mice (Supplementary Figure II.2A). Furthermore, complete blood cell analysis of E^{3KO} mice showed no major perturbation of any of the indices measured (Supplementary Figure II.2C). Flow cytometry analysis demonstrated no significant differences in the frequency of myeloid, B, T cells or T cell subsets in the blood of E^{3KO} mice (Supplementary Figure II.2D). Finally, competitive bone marrow transplantation experiments indicated no significant differences in the number and function of hematopoietic stem/progenitor cells from E^{3KO} mice (Supplementary Figure II.2E). These experiments indicate that E^{3KO} mice have a normal hematopoietic system. Collectively, these data indicate that E^{3KO} mice represent an appropriate model for studying the function of JNK in the vascular endothelium.

<u>JNK in the vascular endothelium is dispensable for angiogenic responses in adult mice</u>

JNK1 has recently been reported to be an important mediator of pathologic angiogenesis in a laser-induced model of choroidal neovascularization (CNV),[136]

however the cell type(s) in which JNK activity is responsible for this effect remain unknown. We examined how JNK in vascular EC affects angiogenic responses. JNK deficient EC formed cord like structures comparably to control EC in a tube formation assay in matrigel (Supplementary Figure II.3A). Additionally, collagen embedded and VEGF stimulated aortic ring explants from E^{2KO} or E^{3KO} mice produced similar numbers of microvessels compared to aortic rings from control mice (Supplementary Figure II.3B). Consistent with these findings, we found no differences in the number of EC incorporating 5-ethynyl-2-deoxyuridine (Edu) or staining for the proliferation marker Ki-67 (Supplementary Figure II.3C and D) demonstrating that proliferation is not altered in JNK deficient EC. Furthermore, JNK deficient EC showed no defects in migration in an *in vitro* wound closure assay (Supplementary Figure II.3E).

To assess the role of endothelial JNK *in vivo*, we examined two models of angiogenesis. First, we employed a laser-induced CNV mouse model in which laser-induced injury in the back of the eye initiates an inflammatory, pro-angiogenic cascade that stimulates sprouting of new vessels from the choroid. Confocal imaging and quantification of CNV size in whole mount preparations revealed no significant differences between E^{3KO} and control mice (Supplementary Figure II.4A and B). Second, we examined tumor angiogenesis. Subcutaneous injection of B16F10 melanoma cells into the flanks of E^{2KO} or E^{3KO} mice produced tumors comparable to those in control mice (Supplementary

Figure II.4C and D). Quantification of vascular density within tumors revealed only minor non-significant differences between tumors from E^{3KO} and control mice (Supplementary Figure II.4E and F). In agreement with these data, JNK in endothelial cells was not activated by either hypoxia or VEGF (Supplementary Figure II.5A and B), and hypoxia responses and VEGF signaling were unimpaired in JNK-deficient endothelial cells (Supplementary Figure II.5C-E). Thus, JNK in the vascular endothelium is, dispensable for hypoxia and VEGF-driven angiogenic responses in adult mice.

Endothelial JNK deficiency results in enhanced blockade of blood perfusion and severe ischemic injury in models of arterial occlusion

To examine the role of JNK in other aspects of vascular biology and function, we turned to a model of experimental arterial occlusion. Femoral artery ligation (FAL) causes hypoxia in the calf muscles stimulating angiogenesis; whereas the proximal adductor muscles experience little or no decrease in oxygen and nutrient supply due to an abundance of preexisting collateral arteries[90] (Figure II.1B)

We ligated the femoral artery (FA) between the proximal caudal femoral artery (PCFA) and the popliteal artery (PA, Figure II.1B),[177] a very mild version of this model. Following occlusion, laser Doppler imaging revealed an ~80% decrease in blood perfusion in the ligated limbs of control mice and blood perfusion was

restored to ~60% of the contralateral limbs by day 3 (Figure II.1C and D). In striking contrast, even in this mild version of the model, most E^{3KO} mice showed complete blockade of blood flow to the limbs following occlusion (Figure II.1C and D) leading to severe necrosis of the paws (Figure II.1E) with over 70% of mice developing "autoamputation" of the ligated limb (Figure II.1F and G). Control mice showed almost no signs of ischemia and only minor movement impairments (Figure II.1E-G). Ligation of the FA more proximally at its origin gave the same result (Supplementary Figure II.6A and B). It is worth noting that, to our knowledge, the severity of the blood perfusion defect in E^{3KO} mice appears to be more profound than that of any other genetically modified mouse reported thus far.

A similar model of coronary artery occlusion in the heart resulted in significantly higher mortality of E^{3KO} mice compared to control mice (Supplementary Figure II.6C and D), suggesting that the vascular defects resulting in enhanced blood perfusion blockade upon arterial occlusion are not confined to the hindlimb.

Following FAL, blood perfusion blockade and restoration in single *Jnk1*$^{-/-}$ or *Jnk2*$^{-/-}$ mice was comparable to WT mice (Supplementary Figure II.6E) indicating that JNK1 isoforms and JNK2 isoforms are functionally redundant for the process(es) that govern blood perfusion blockade/restoration following FAL. E^{2KO} mice, which lack both JNK1 plus JNK2 in the endothelium, performed

similarly to E^{3KO} mice (Supplementary Figure II.6F), ruling out a required role for JNK3 in the severe phenotype observed in E^{3KO} mice. Of note, we do not detect *Jnk3* mRNA expression in lung endothelial cells from WT or E^{2KO} mice under conditions in which *Jnk3* expression is readily detectable in brain tissues. Together, these data demonstrate that JNK1 plus JNK2 in the vascular endothelium are critically required for the process(es) that determine the extent of blood perfusion blockade and/or restoration following occlusion of a major artery.

In contrast, JNK in hematopoietic or skeletal muscle cells was dispensable for these process(es) because compound JNK1 plus JNK2 deficiency in all hematopoietic (*Vav1-Cre*, H^{2KO}), myeloid (*Lyz2-Cre*, Φ^{2KO}) or skeletal muscle (*Ckm-Cre*, M^{2KO}) cells had no effect on blood perfusion blockade/restoration or ischemic damage following FAL (Figure II.1H-J).

<u>JNK in the vascular endothelium is necessary for proper patterning and connectivity of collateral arteries</u>

Analysis of functional cardiovascular parameters, including blood pressure and heart rate in *Jnk1*$^{-/-}$, *Jnk2*$^{-/-}$ or E^{3KO} mice revealed no major JNK-dependent perturbations (Supplementary Figure II.7A and B). Echocardiographic analysis showed normal cardiac function in E^{3KO} mice (Supplementary Figure II.7C). Furthermore, contraction and endothelium-dependent relaxation responses in

aortic explants from E^{3KO} mice were comparable to control mice (Supplementary Figure II.7D). These data indicated that the severe defect in blood perfusion in E^{3KO} mice following FAL is unlikely to be due to overall cardiovascular dysfunction or defective vasodilatory responses in these mice.

Much of the blood supply to the limb, particularly in the first few days following FAL, is provided by preexisting collateral arteries in the adductor muscles. The early and severe blood perfusion blockade in E^{3KO} mice following FAL indicated a defect in these arteries and prompted their analysis. While multiple collateral arteries course through the adductor muscles at various depths, two highly stereotypic arteries (gracilis collaterals) stretch along the gracilis muscle in the medial aspect of the thigh (Figure II.1B). Their superficial location affords reliable visualization on wholemount preparations following intravascular Microfil perfusion and tissue clearing.

In the unligated limbs of control mice, gracilis collaterals were easily identified as two lumenized continuous arteries that connected the PCFA to the saphenous artery (SA) (Figure II.2A, Unligated). Gracilis collaterals expanded radially by day 4 following FAL (Figure II.2A, Ligated). In contrast, these arteries were highly abnormal in the unligated limbs of E^{3KO} mice. In these mice, arteries emerged from both the PCFA and the SA (Figure II.2A), but they were thinner than in control mice (Figure II.2A-C) and branched off into multiple smaller vessels

forming a disorganized network instead of the continuous larger and very distinct collateral arteries that were observed in control mice (Figure II.2A-C). Micro-computed tomography (μCT) analysis following intravascular contrast injection confirmed reduced collateral artery size and continuity in the limbs of E^{3KO} mice (Figure II.2D).

The mRNA abundance of endothelial cell specific markers *Cdh5* and *Pecam1* was not altered in the adductor muscles and was significantly higher in the calf muscles of the unligated limbs of E^{3KO} mice compared to control mice (Figure II.2E and Supplementary Figure II.8A) indicating that overall muscle vascularization was not reduced in E^{3KO} mice. Following FAL, the mRNA abundance of endothelial cell specific markers was further increased in the muscles of E^{3KO} mice compared to control mice (Figure II.2E and Supplementary Figure II.8A) likely due to enhanced angiogenesis resulting from higher levels of hypoxia. Indeed, expression of the hypoxia responsive gene, *Glut1*, was induced significantly higher in the adductor and calf muscles of E^{3KO} mice compared to control mice (Figure II.2F).

We also found no significant differences in the mRNA abundance of the macrophage marker *Emr1* in the hindlimb muscles of E^{3KO} mice compared to control mice (Supplementary Figure II.8B), suggesting no impairment in monocyte recruitment in E^{3KO} mice.

Thus, although endothelial JNK appears to be dispensable for angiogenic responses in adult mice, it is critically required for proper patterning, connectivity and/or maturation of the collateral circulation. E^{3KO} mice have highly abnormal collateral arteries that fail to provide an adequate alternative route for blood flow upon FAL, resulting in severe blood perfusion blockade that leads to extensive necrosis of the occluded limbs.

The MLK group of MAP3Ks contributes to endothelial JNK activity and is important for proper native collateral artery development

We explored additional molecular components within the MAPK signaling network that may mediate JNK activation during vascular development. The MAP2Ks, MKK4 and MKK7, have been clearly defined to directly phosphorylate and activate JNK.[1] However, the role of individual MAP3Ks in mediating JNK activation in particular contexts *in vivo* is unclear. The MLK group of MAP3Ks has been shown to mediate TNF-induced JNK activation in a Rac1/Cdc42-dependent manner.[5,178] Given the crucial role of Rac1/Cdc42 Rho family GTPases in endothelial cell cytoskeletal rearrangement and vascular development, we explored whether MLKs might mediate JNK activation important for vascular development *in vivo*.

Of the four members of the MLK group of kinases,[179] *Mlk2* and *Mlk3* were the two most highly expressed in endothelial cells (Figure II.3A). $Mlk2^{-/-}Mlk3^{-/-}$ endothelial

cells displayed reduced bFGF-induced JNK activity as demonstrated by decreased cJun phosphorylation levels compared to WT endothelial cells (Figure II.3B). Therefore, we subjected *Mlk2*$^{-/-}$*Mlk3*$^{-/-}$ double knockout mice to FAL to test if they would phenocopy the defects observed in endothelial JNK-deficient mice.

Indeed, upon FAL, *Mlk2*$^{-/-}$*Mlk3*$^{-/-}$ mice showed significantly more pronounced blood perfusion reduction compared to WT mice and almost no blood perfusion restoration by day 3 post FAL (Figure II.3C and D). Similarly to E^{2KO} and E^{3KO} mice, all *Mlk2*$^{-/-}$*Ml3*$^{-/-}$ mice showed necrotic damage of the toes and paws of the ligated limb (Figure II.3E-G). Microphil perfusion analysis revealed abnormal gracilis collateral artery patterning in *Mlk2*$^{-/-}$*Mlk3*$^{-/-}$ mice (Figure II.3H). Thus, these data strongly support the existence of an *in vivo* MLK/JNK signaling axis that is crucial for proper native collateral artery development.

<u>JNK in the vascular endothelium is dispensable for arteriogenic responses in adult mice</u>

The severe defect in preexisting collateral arteries in *Mlk2*$^{-/-}$*Mlk3*$^{-/-}$ and E^{3KO} mice prevented analysis of the role of endothelial JNK signaling in arteriogenesis in adult mice. We, therefore, employed the *Cdh5(PAC)-CreERT2* driver line[180] to generate mice, iE^{3KO} (*Cdh5(PAC)-CreERT2 Jnk1*$^{LoxP/LoxP}$*Jnk2*$^{LoxP/LoxP}$*Jnk3*$^{-/-}$) in which disruption of floxed alleles of JNK could be specifically induced in the vascular endothelium by tamoxifen administration at a desired time. We

administered tamoxifen to these mice as well as to appropriate *Cre*$^{+}$ control (iE^{Ctrl}, *Cdh5(PAC)-CreERT2 Jnk1*$^{+/+}$*Jnk2*$^{+/+}$*Jnk3*$^{-/-}$) and *Cre*$^{-}$ (E^{fCtrl}, *Jnk1*$^{LoxP/LoxP}$*Jnk2*$^{LoxP/LoxP}$*Jnk3*$^{-/-}$) littermate mice at 6-8 weeks of age (a time when the native collateral circulation has been fully established) and following a recovery period, subjected them to FAL (Figure II.4A). JNK protein levels in purified endothelial cells from iE^{3KO} mice were robustly diminished (Figure II.4B), however, in contrast to E^{3KO} mice, blood perfusion blockade in iE^{3KO} mice following FAL was similar to control mice, and there were no significant differences in blood perfusion recovery over 28 days (Figure II.4C). Intravascular Microfil perfusion analysis revealed a normal collateral circulation in the unligated limbs of iE^{3KO} mice and these arteries remodeled similarly to those of control mice following FAL (Figure II.4D). These data, together with those from constitutive E^{3KO} mice, demonstrate that endothelial JNK is dispensable for arteriogenic responses in adult mice, but is required for the proper formation of collateral arteries at an early time during development. Indeed, iE^{3KO} mice in which recombination of floxed alleles of JNK was induced early during embryonic development by administering tamoxifen to pregnant females at 12.5 days post coitus (dpc) (Figure II.4E) and materials and methods) displayed significantly more severe blood perfusion reduction following FAL compared to littermate control mice (Figure II.4F). The severity of the blood perfusion blockade in this case was not as pronounced as that in constitutive E^{3KO} mice because of highly variable recombination efficiency as demonstrated by analysis of *Cdh5(PAC)-*

CreERT2, *Rosa26-mT/mG* (E^{mTmG}) double transgenic reporter mice that were subjected to the same tamoxifen treatment protocol (Figure II.4G).

Endothelial MLK/JNK signaling is critically required for muscle collaterogenesis during embryonic development

Prior studies have described the development of the pial collateral circulation, which interconnects the distal branches of the middle cerebral and the anterior cerebral arteries. However, a detailed analysis of the formation of collateral arteries in muscle during ontogeny has not been reported. We, therefore, developed several immunofluorescence and 1,1'-Dioctadecyl-3,3,3',3'-Tetramethylindocarbocyanine Perchlorate (Dil) perfusion protocols and generated genetic reporter mice to label the vasculature in order to trace the development of muscle collaterals at various stages of development in whole-mount preparations of adductor muscles.

At P6 and P0 in control mice, gracilis collaterals appeared fully formed connecting the PCFA to the SA (Figure II.5A and B). They were lumenized as evidenced by Dil perfusion analysis (Figure II.5A and B) and were fully covered by smooth muscle cells at P6 (Figure II.5A, SMA), but not P0 (Figure II.5B, SMA). In contrast, gracilis collaterals in E^{3KO} mice had not properly formed at either P6 or P0 (Figure II.5A and B). Individual vessels did emerge from both the PCFA and the SA, but instead of interconnecting to form true collaterals,

these vessels branched off into multiple smaller caliber vessels (Figure II.5A and B, DiI Perfusion) that lacked smooth muscle coverage even at P6 (Figure II.5A, SMA) and appeared to enter the capillary circulation (Figure II.5A and B, DiI Perfusion). Similarly, analysis of the abdominal muscle arterial circulation in P0 pups revealed numerous arteriolar arcades (direct arteriole-to-arteriole interconnections) in control mice (Figure II.5C), but this type of arterial arrangement was almost entirely absent in E^{3KO} mice. Instead, E^{3KO} mice displayed a tree like arterial pattern with very few direct artery-to-artery interconnections (Figure II.5C).

Analysis of gracilis collaterals in adductor muscles and arteriolar arcades in abdominal muscles from P6 *Mlk2*$^{-/-}$*Mlk3*$^{-/-}$ mice revealed defects similar to those observed in E^{3KO} mice supporting a MLK/JNK signaling axis crucial for collateral artery formation (Figure II.6A and B).

To understand how the defects in collateral artery patterning/maturation in E^{3KO} mice may have arisen, we analyzed the vasculature in whole mount preparations of adductor muscles during embryonic life. In control mice at embryonic day (E)16.5, large caliber vessels including the FA/SA and PCFA were established in their typical positions (Figure II.5D and E) as observed in postnatal mice. However, distinct vessels directly interconnecting the PCFA to the SA had not been fully established at this time and the gracilis muscle region where collateral

arteries are present in postnatal mice was, for the most part, covered by a capillary plexus (Figure II.5D and E). Larger, more prominent vessels staining more intensely for iB4 could be distinguished to emerge from the PCFA and the SA (Figure II.5E, arrowheads), but instead of running the entire course of the gracilis muscle length as distinct collaterals, they branched off and entered the capillary plexus (Figure II.5E). Thus, it appears that gracilis collateral arteries form through a plexus intermediate, whereby certain vessels within the plexus undergo extensive remodeling and maturation into distinct arteries that interconnect the PCFA to the SA. This process of maturation appears to start at the two distal ends, where the future gracilis collaterals emerge from the PCFA and the SA and continues toward the middle of the muscle - a pattern of remodeling that likely reflects and is driven by the blood flow characteristics through these vessels.

Large caliber vessels in E16.5 E^{3KO} adductor muscles were similar to those in control mice, however, the capillary network between the PCFA and the SA displayed a hyperbranched and more disorganized arrangement of vessels with more pronounced thickness variation and that appeared to elaborate more filopodia (Figure II.5D and E). These observations suggested that the pronounced defects in collateral artery patterning/maturation in E^{3KO} mice may arise due to defective sprouting angiogenesis that initially generates a hyperbranched, denser and more chaotically organized plexus that later fails to

remodel properly.

Endothelial JNK deficiency results in abnormal sprouting angiogenesis during retinal vascular development

To explore the role of endothelial JNK in sprouting angiogenesis in more detail, we analyzed retinal vascular development during the early postnatal period as this represents a well-characterized system that allows high-resolution analysis of sprouting angiogenesis in a developing vascular plexus that initially extends from the center towards the periphery of the retina in two dimensions.[35,38] Analysis of retinal flatmounts from P6 E^{3KO} and E^{2KO} mice revealed significantly reduced radial extension of the vascular plexus toward the periphery of the retina (Figure II.7A-C, L and Supplementary Figure II.9A-C and L). Closer examination showed higher vascular density in the region of the growing angiogenic front of E^{3KO} and E^{2KO} retinas compared to retinas from respective littermate control mice (Figure II.7D-G, H, J, M and Supplementary Figure II.9D-G, H, J, M). Regions of higher vascular density were particularly prominent adjacent to veins. Vascular extension in the retina occurs through the coordinated interaction, migration and proliferation of endothelial tip and stalk cells as well as non-endothelial cells including pericytes that help stabilize the vascular plexus.[37] We found no differences in vessel pericyte coverage (Supplementary Figure II.10), however the E^{3KO} and E^{2KO} angiogenic front displayed significantly more tip cells (Figure II.7H, J yellow asterisks, N and Supplementary Figure II.9H, J yellow asterisks,

N). Additionally, JNK deficient tip cells exhibited more filopodia (Figure II.7I, K red dots, O and Supplementary Figure II.9I, K red dots, O). All retinal vascular defects observed in E^{3KO} and E^{2KO} mice were phenocopied in *Mlk2*$^{-/-}$*Mlk3*$^{-/-}$ mice (Figure II.8) confirming a MLK/JNK signaling axis critical for restraining excessive endothelial cell sprouting during developmental angiogenesis.

Reduced DLL4 – Notch signaling may contribute to the vascular morphogenetic defects of endothelial JNK deficient mice

Endothelial cell hypersprouting in the absence of MLK/JNK signaling provides a basis for the defective cellular process that likely underlies abnormal patterning and maturation of collateral arteries in E^{3KO} and *Mlk2*$^{-/-}$*Mlk3*$^{-/-}$ mice. To begin to understand the molecular mechanisms that contribute to these cellular defects, we analyzed gene expression in isolated primary endothelial cells from control and E^{3KO} mice by RNA sequencing (RNA Seq). JNK-deficient endothelial cells displayed altered gene expression compared to control cells. Of the ~$1x10^4$ genes that were expressed (Fragments Per Kilobase of exon per Million fragments mapped [FPKM] >2) in endothelial cells, 781 genes were significantly differentially expressed (log_2 fold change ≤ -0.5 or ≥ +0.5; $q \leq 0.05$) in E^{3KO} vs. E^{Ctrl} and E^{fCtrl} endothelial cells. Approximately similar numbers of genes were upregulated or downregulated (Figure II.9A). Gene ontology analysis of the group of differentially expressed genes identified significant enrichment in genes involved in several biological processes including mitosis/cell division/cell cycle,

and vascular development and morphogenesis (Figure II.9B).

Differentially expressed genes related to mitosis/cell division/cell cycle identified by the gene ontology analysis are presented as a heat map in Figure II.9C; however, because we have not detected alterations in proliferation of JNK-deficient endothelial cells (Supplementary Figure II.3C and D), these changes may not be biologically relevant.

We additionally surveyed ~200 genes with known or putative roles in vascular development and function and identified 64 significantly differentially expressed genes in E^{3KO} vs. E^{Ctrl} and E^{fCtrl} endothelial cells, including those revealed by the gene ontology analysis. These genes, grouped in several categories, are presented as a heatmap in Figure II.9D. Several of these gene expression changes could contribute to the vascular defects observed in the absence of endothelial JNK signaling and the potential relevance of some is further considered in Chapter IV below.

RNA Seq analysis revealed significant perturbations in Notch pathway gene expression, including downregulation of the Notch ligand and target gene *Dll4* as well as the glycosyltransferase *Lunatic Fringe* (*Lfng*) and the Notch target gene *Hey1* (Figure II.9D). We focused on Notch signaling as this represents a pathway that plays major roles during developmental angiogenesis, in particular tip/stalk

cell specification and endothelial cell sprouting.[37] Indeed, the hypersprouting defects observed in E^{3KO} and *Mlk2*$^{-/-}$*Mlk3*$^{-/-}$ mice appear to closely resemble those previously reported in mice with reduced Dll4/Notch signaling,[43,46,47] including *Lfng*$^{-/-}$ mice.[47] Additionally, *Dll4*$^{+/-}$ mice display perturbations in collateral artery formation[82] and along with *Notch1*$^{+/-}$ mice[181] show reduced recovery of blood perfusion in models of vascular occlusion.

We confirmed decreased expression of *Dll4* and other Notch pathway genes by quantitative RT-PCR analysis of mRNA from independent preparations of E^{3KO} and control endothelial cells (Figure II.10A). Additionally, we verified reduced Dll4 protein expression in E^{3KO} endothelial cells compared to control cells by immunofluorescence analysis (Figure II.10B). VEGF stimulation is known to induce Dll4 expression and Notch signaling. Treatment of endothelial cell cultures with VEGF-A lead to increased abundance of Dll4 protein and Notch1 intracellular domain (NICD) in control cells and reduced levels of both in E^{3KO} cells (Figure II.10C). We also found that, similar to VEGF-A, basic fibroblast growth factor (bFGF) treatment caused increased Dll4 and NICD levels in endothelial cells (Figure II.10D). This response was suppressed in E^{3KO} cells (Figure II.10D). Interestingly, in contrast to VEGF-A, bFGF induced marked JNK activation and cJun phosphorylation in endothelial cells (Figure II.10D). Thus, multiple stimuli may regulate Dll4 levels and Notch signaling *in vivo* during sprouting angiogenesis and some of these intersect with JNK signaling.

To provide *in vivo* evidence for the Dll4-Notch signaling perturbations detected in E^{3KO} endothelial cells, we performed immunofluorescence analysis for Dll4 on P6 retinas. This analysis revealed significantly reduced Dll4 immunostaining at the angiogenic front of retinas from E^{3KO} mice compared to retinas from littermate control mice (Figure II.10E), suggesting that reduced Dll4-Notch signaling in the endothelium of E^{3KO} mice may contribute to the endothelial cell hypersprouting observed in these mice.

Thus, JNK may modulate Notch signaling in endothelial cells *in vivo* by regulating Dll4 expression leading to suppression of excessive sprouting angiogenesis and ensuring normal vascular morphogenesis. This function of JNK may be important for its critical role in ensuring proper formation and maturation of native collateral arteries and suppression of ischemic damage following arterial occlusion (Figure II.11).

Discussion

Formation of properly organized vascular networks is essential for function and requires the coordinated interaction of numerous factors and signaling pathways that regulate diverse cellular processes. VEGF signaling promotes endothelial cell survival, proliferation and motility, while Dll4–Notch signaling suppresses some of the effects of VEGF in part by regulating VEGFR expression.[34,37,39,41,45,46] Thus, the cooperation of VEGF and Notch signaling specifies unique endothelial cell phenotypes including highly motile tip cells that extend numerous filopodia and trailing stalk cells with low motility that form the lumen of nascent tubules. The proper specification and interplay of tip and stalk cells is essential for the orchestration of sprouting angiogenesis that mediates expansion of vascular networks.[34,37,39,41,45,46] This study identifies a MLK – JNK signaling pathway that regulates tip cell identity, and filopodia dynamics, in part, likely via JNK-dependent regulation of Dll4 expression. Thus, *Mlk2*$^{-/-}$*Mlk3*$^{-/-}$ mice or mice with compound endothelial-specific JNK-deficiency display excessive sprouting angiogenesis in the retina that is marked by an increased number of tips and filopodia, and increased vascular density and is associated with decreased Dll4 expression at the angiogenic front of endothelial JNK-deficient mice (Figure II.11).

The hypersprouting defects during developmental sprouting angiogenesis in the absence of MLK – JNK signaling may underlie the critical requirement of this

signaling pathway for native collateral artery formation. This is supported by our analysis of adductor muscle vasculature in *Mlk2*$^{-/-}$*Mlk3*$^{-/-}$ and endothelial-specific JNK-deficient mice at various stages of development.

Analysis of muscle collateral artery formation during ontogeny has been hampered by technical difficulties. We have generated reporter mice in conjunction with compound endothelial-specific conditional deletion of JNK isoforms and have adapted and optimized DiI perfusion and immunofluorescence protocols that have allowed us to visualize several aspects of the vascular morphogenetic processes involved in collateral artery formation during ontogeny as well as their perturbations in mice that lack JNK signaling in the endothelium. The observations from this analysis lead us to propose a model of collateral artery formation in hindlimb adductor muscles that may have features that are distinctly different from those described for pial collateral artery formation in the brain.[61] Thus, our analysis suggests that gracilis collaterals are not formed in isolation as distinct sprouts from existing arteries, but may arise through selection and maturation of vessels within a pre-formed capillary network that separates adjacent arteries. Preliminary analysis suggests that the sites where these collaterals form may be dictated by the presence of nerve fibers coursing through the gracilis muscle (Supplementary Figure II.11). Presumably, factors secreted from these fibers may guide the selection and maturation of vessels in close proximity. Additionally, our observation that the maturation of gracilis collaterals

appears to start where these vessels emerge from the parent arteries and continues towards the middle of the collateral vessels suggests that the maturation of gracilis collaterals may also be driven by the blood flow characteristics through these vessels.[182]

At E16.5 when collaterals in control mice have not fully formed, the capillary plexus between adjacent arteries in mice with endothelial JNK deficiency appears denser and more chaotically organized than that in control mice. High variation in vessel thickness and increased numbers of filopodia are also evident in the JNK-deficient vasculature. These perturbations appear to mirror those seen in the retinal vasculature of *Mlk2*$^{-/-}$*Mlk3*$^{-/-}$ and E^{3KO} mice suggesting that similar mechanisms are involved. These morphogenetic defects are likely to contribute to the defective maturation of collateral arteries that are observed at later developmental timepoints in mice with disrupted MLK – JNK signaling.

At P6 we observed that collateral vessels in control mice were invested with smooth muscle cells throughout their length effectively defining them as collateral arteries. In contrast, the analogous vessels in the gracilis muscle of *Mlk2*$^{-/-}$*Mlk3*$^{-/-}$ and E^{3KO} mice lacked continuous smooth muscle cell coverage suggesting that smooth muscle cell recruitment might be defective in these mice. However, at P0, smooth muscle cell coverage was absent in control mice, yet continuous and distinct gracilis collateral vessels interconnecting the PCFA to the SA were fully

formed. In contrast, the analogous vessels in the gracilis muscle of E^{3KO} mice were also defective (branching extensively into smaller vessels that entered the capillary circulation) at P0, indicating that defective smooth muscle coverage is not likely to be a primary defect in these mice, but may occur subsequent to defective primary plexus formation.

Our data indicate that the morphogenetic defects in the JNK-deficient capillary network arise due to excessive endothelial cell sprouting and that reduced Dll4 – Notch signaling may be a significant contributor. This idea is supported by prior studies that have investigated the function of Dll4 – Notch signaling during sprouting angiogenesis and collateral artery formation. Thus, various Notch loss of function mouse models, including loss of Dll4,[46] Notch1,[46] Lfng,[47] RBP-J[48,49] or chemical inhibition of γ-secretase with N-[N-(3,5–Difluorophenacetyl- L-alanyl)]-S-phenylglycine t-butyl ester (DAPT)[46], exhibit excessive endothelial cell sprouting during the postnatal development of the retinal vasculature. Furthermore, *Dll4*$^{+/-}$ mice show increased pial collateral artery branching that is not associated with decreased infarct size following medial cerebral artery occlusion, suggesting that these vessels, although more numerous, are functionally defective and do not result in improved blood perfusion.[82] *Dll4*$^{+/-}$ mice also display defects in blood perfusion restoration following FAL,[82] however collateral arteries were not specifically analyzed in the hindlimb adductor muscles in that study. Micro-CT angiography of the occluded hindlimb vasculature revealed significantly

decreased arteriolar numbers in the calf muscles of *Dll4*$^{+/-}$ mice compared to control mice,[82] but this could have resulted from impaired contrast perfusion due to defective collateral artery patterning in the adductor muscles. A more direct analysis of the native collateral arteries in the adductors of *Dll4*$^{+/-}$ mice using methods similar to those employed in our study would help clarify the role of Dll4 in native collateral artery formation.

The collateral artery defects observed in *Mlk2*$^{-/-}$*Mlk3*$^{-/-}$ and E^{3KO} mice in the early postnatal period continue into adulthood and underlie the severe blood perfusion blockade and exuberant necrosis that follows shortly after FAL in these mice (Figure II.11). The severity of the blood perfusion defect and limb necrosis in *Mlk2*$^{-/-}$*Mlk3*$^{-/-}$ and E^{3KO} is remarkable and unprecedented, particularly because we performed very mild versions of the FAL model that involved only ligation of the femoral artery without excision. Despite this, all *Mlk2*$^{-/-}$*Mlk3*$^{-/-}$ and E^{3KO} mice develop paw necrosis and over 70% of E^{3KO} mice undergo complete autoamputation of the paw on the ligated limb highlighting the critical importance of MLK – JNK signaling in native collateral artery development and the essential role of pre-existing collaterals in restoring blood perfusion following arterial occlusion.

In contrast to its critical function in native collateral artery formation during embryonic development, we find that endothelial JNK is dispensable for

arteriogenic remodeling in adult mice in the setting of arterial occlusion (at least in our mild version of the model). We were able to uncouple the role of JNK in these two processes by employing an inducible conditional deletion strategy that allowed us to induce JNK ablation from the endothelium in adult mice at a time when native collateral arteries are fully established. Indeed, endothelial JNK disruption in adult mice had no effect on collateral artery remodeling or blood perfusion restoration following FAL. This is consistent with the lack of perturbations in the proliferation capacity of JNK-deficient endothelial cells, the absence of endothelial cell-dependent recruitment of monocyte/macrophages in E^{3KO} mice and the absence of major defects in angiogenic responses in adult E^{3KO} mice. Remarkably, though not unexpectedly, inducing deletion of JNK during embryogenesis by administering tamoxifen to pregnant mothers at 12.5 dpc lead to significantly enhanced blood perfusion reduction following arterial occlusion compared to control mice, once again pointing to an essential role for endothelial JNK in developmental vascular morphogenesis and native collateral formation, but not in adult angiogenic and arteriogenic responses in models of pathological vascularization.

Although not precise due to differences in ligation protocols, comparison of the blood perfusion reduction, the ischemic damage and functional impairment following FAL in *Mlk2*$^{-/-}$*Mlk3*$^{-/-}$ and E^{3KO} mice with those reported in Notch loss of function mice indicates that loss of MLK – JNK signaling results in more severe

defects suggesting that mechanism(s) in addition to reduced Dll4 – Notch signaling may be contributing to the collateral artery defects in E^{3KO} mice. Indeed, RNA-Seq analysis revealed additional gene expression changes in E^{3KO} endothelial cells compared to control cells that may play a role.

In summary, our study provides insight into the mechanism that controls formation of muscle collateral arteries, which are critically important for the response to arterial occlusive disease. Muscle collaterals provide an alternate route for blood flow and serve to protect against ischemic tissue damage. We show that the MLK-JNK pathway is required for collateral artery development and patterning, but is not required for angiogenesis or arteriogenesis in adults. The MLK-JNK pathway plays a key role in Notch-regulated angiogenic sprouting during capillary plexus formation and remodeling that leads to the development of the muscle collateral arteries. Defects in the MLK-JNK pathway result in the loss of muscle collateral circulation, profoundly suppressing protective responses to arterial occlusion (Figure II.11).

Experimental Procedures

Mice

We have previously described *Jnk1*$^{LoxP/LoxP}$, *Jnk2*$^{LoxP/LoxP}$, *Jnk1*$^{-/-}$, *Jnk2*$^{-/-}$, *Jnk3*$^{-/-}$, Φ^{KO} mice (*Lyz2-Cre*$^{+}$ *Jnk1*$^{LoxP/LoxP}$ *Jnk2*$^{LoxP/LoxP}$), Φ^{WT} mice (*Lyz2-Cre*$^{+}$ *Jnk1*$^{+/+}$ *Jnk2*$^{+/+}$), and *Mlk2*$^{-/-}$ *Mlk3*$^{-/-}$ mice[5,161-163183,184]. C57BL/6J mice (Stock# 000664), B6.SJL-*Ptprc*^{a} *Pepc*^{b}*/BoyJ* mice (Stock# 002014), B6.FVB-Tg(Cdh5-cre)7Mlia/J mice (Stock# 006137)[176], B6.Cg-Tg(Vav1-cre)A2Kio/J mice (Stock# 008610)[185], B6.FVB(129S4)Tg(Ckmm-cre)5Khn/J mice (Stock# 006475)[186], and B6.129(Cg)-*Gt(ROSA)26Sor*$^{tm4(ACTB-tdTomato,-EGFP)Luo}$/J (also known as *Rosa26*^{mTmG}) mice (Stock# 007676)[187] were obtained from The Jackson Laboratories. *Cdh5(PAC)-CreERT2* mice[180] were provided by Prof. Ralf H. Adams. We generated the following mice:

E^{3KO} (*Cdh5-Cre*$^{+}$ *Jnk1*$^{LoxP/LoxP}$ *Jnk2*$^{LoxP/LoxP}$ *Jnk3*$^{-/-}$)

E^{fCtrl} (*Cdh5-Cre*$^{-}$ *Jnk1*$^{LoxP/LoxP}$ *Jnk2*$^{LoxP/LoxP}$ *Jnk3*$^{-/-}$)

E^{Ctrl} (*Cdh5-Cre*$^{+}$ *Jnk1*$^{+/+}$ *Jnk2*$^{+/+}$ *Jnk3*$^{-/-}$)

E^{2KO} (*Cdh5Cre*$^{+}$ *Jnk1*$^{LoxP/LoxP}$ *Jnk2*$^{LoxP/LoxP}$)

E^{LoxP} (*Cdh5-Cre*$^{-}$ *Jnk1*$^{LoxP/LoxP}$ *Jnk2*$^{LoxP/LoxP}$)

E^{WT} (*Cdh5-Cre*$^{+}$ *Jnk1*$^{+/+}$ *Jnk2*$^{+/+}$)

$E^{2KO:mTmG}$ (*Cdh5-Cre*$^{+}$ *Jnk1*$^{LoxP/LoxP}$ *Jnk2*$^{LoxP/LoxP}$ *Rosa26*^{mTmG})

E^{mTmG} (*Cdh5-Cre*$^{+}$ *Rosa26*^{mTmG})

iE^{3KO} (*Cdh5(PAC)-CreERT2*$^{+}$*Jnk1*$^{LoxP/LoxP}$ *Jnk2*$^{LoxP/LoxP}$ *Jnk3*$^{-/-}$)

iE^{fCtrl} *(Cdh5(PAC)-CreERT2^{-} Jnk1$^{LoxP/LoxP}$ Jnk2$^{LoxP/LoxP}$ Jnk3$^{-/-}$)*

iE^{Ctrl} *(Cdh5(PAC)-CreERT2^{+} Jnk1$^{+/+}$ Jnk2$^{+/+}$ Jnk3$^{-/-}$)*

$iE^{2KO:mTmG}$ *(Cdh5(PAC)-CreERT2^{+} Jnk1$^{LoxP/LoxP}$ Jnk2$^{LoxP/LoxP}$ Rosa26^{mTmG})*

$E^{LoxP:mTmG}$ *(Cdh5(PAC)-CreERT2^{-} Jnk1$^{LoxP/LoxP}$ Jnk2$^{LoxP/LoxP}$ Rosa26^{mTmG})*

iE^{mTmG} *(Cdh5(PAC)-CreERT2^{+} Jnk1$^{+/+}$ Jnk2$^{+/+}$ Rosa26^{mTmG})*

H^{2KO} *(Vav1-Cre^{+} Jnk1$^{LoxP/LoxP}$ Jnk2$^{LoxP/LoxP}$)*

H^{LoxP} *(Vav1-Cre^{-} Jnk1$^{LoxP/LoxP}$ Jnk2$^{LoxP/LoxP}$)*

H^{WT} *(Vav1-Cre^{+} Jnk1$^{+/+}$ Jnk2$^{+/+}$)*

M^{2KO} *(Ckm-Cre^{+} Jnk1$^{LoxP/LoxP}$ Jnk2$^{LoxP/LoxP}$)*

M^{WT} *(Ckm-Cre^{+} Jnk1$^{+/+}$ Jnk2$^{+/+}$)*

All mice used in this study were backcrossed (≥ ten generations) to the C57BL/6J strain. The mice were housed in a specific pathogen-free (SPF) facility accredited by the American Association for Laboratory Animal Care. The animal studies were approved by the Institutional Animal Care and Use Committees of the University of Massachusetts Medical School, Tufts University School of Medicine, and Brigham and Women's Hospital.

Some E^{2KO} and E^{3KO} mice develop tooth abnormalities. We are currently investigating this phenotype. Only mice with normal teeth were used for experiments in this study.

Genotyping

PCR assays with genomic DNA and the amplimers 5'-TTACTGACCGTACACCAAATTTGCCTGC-3' and 5'-CCTGGCAGCGATCGCTATTTTCCATGAGTG-3' were used to detect the Cre^{+} allele (450 bp). The amplimers 5'CCTCAGGAAGAAAGGGCTTATTTC-3' and 5'-GAACCACTGTTCCAATTTCCATCC-3' detected the $Jnk1^{+}$ allele (1,550 bp), the $Jnk1^{LoxP}$ allele (1,095 bp), and the $Jnk1^{\Delta}$ allele (395 bp). The amplimers 5'-GTTTTGTAAAGGGAGCCGAC-3' and 5'-CCTGACTACTGAGCCTGGTTTCTC-3' were used to detect the $Jnk2^{+}$ allele (224 bp) and the $Jnk2^{LoxP}$ allele (264 bp). The amplimers 5'-GGAATGTTTGGTCCTTTAG-3', 5'-GCTATTCAGAGTTAAGTG-3', and 5'-TTCATTCTAAGCTCAGACTC-3' were used to detect the $Jnk2^{LoxP}$ allele (560 bp) and the $Jnk2^{\Delta}$ allele (400 bp). The amplimers 5'-CCTGCTTCTCAGAAACACCCTTC-3', 5'-CGTAATCTTGTCACAGAAATCCCATAC-3' and 5'-CTCCAGACTGCCTTGGGAAAA-3' were used to detect the $Jnk3^{+}$ allele (437 bp) and the $Jnk3^{-}$ allele (250 bp). The amplimers 5'-CTCTGCTGCCTCCTGGCTTCT-3', 5'-CGAGGCGGATCACAAGCAATA-3' and 5'-TCAATGGGCGGGGGTCGTT-3' were used to detect the *mTmG* allele (250 bp) and the WT allele (330 bp). The amplimers 5'-CCTGGTTCTCACTGGGACAACAG-3', 5'-GTCACATCCACTTTCCTGGGC-3', and 5'-CGCCTTCTATCGCCTTCTTGA-3' detected the $Mlk2^{+}$ allele (500 bp) and

the *Mlk2*$^{-}$ allele (600 bp). The amplimers 5'-AGCAAACTCCGAGCAAGGGAC-3', 5'-GGCTAAACCAGAACTCAAGCGTG-3', and 5'-GTAGAAGGTGGCGCGAAGGG-3' were used to detect the *Mlk3*$^{+}$ allele (160 bp) and the *Mlk3*$^{-}$ allele (280 bp).

Tamoxifen Treatments

Tamoxifen (Sigma) was dissolved in 2% ethanol 98% sunflower seed oil (Sigma) and 1 mg/mouse was administered intraperitoneally (ip) 5 times on alternate days to 6-8 week old male mice. To induce cre activity during embryonic development pregnant females received 3 mg of tamoxifen once via oral gavage at 12.5 days post coitus (dpc). For these experiments, we used Cre^{-} females that had been crossed to Cre^{+} males to avoid induction of Cre activity and recombination in the pregnant females. Pups were delivered by C-section at ~ 19.5 dpc and transferred to foster mothers.

Femoral Artery Ligation Model and Laser Doppler Imaging

Unilateral femoral artery ligation and laser Doppler imaging was performed using 10-14 week old male mice as previously described[188,189] with the following modifications. Two ligation protocols were performed. In one protocol we ligated the femoral artery at its origin. The second protocol involved ligation of the femoral artery between the proximal caudal femoral artery and the popliteal artery as well as ligation of the superficial epigastric artery. The

second ligation schema allows for more blood flow to be diverted to the gracilis collateral circulation. Quantitative scores for ischemia and movement post-FAL were performed as described[74].

Congenic B16F10 Tumor Model

One million congenic B16F10 melanoma cells (CRL-6475, ATCC) were injected subcutaneously on both flanks of mice. Tumors were harvested 2 weeks later, weighed, imaged on a Zeiss Stereo Discovery.V12 stereomicroscope, fixed in 4% PFA overnight at 4^{o}C, dehydrated sequentially in 15% and 30% sucrose solutions, imbedded in Optical Cutting Temperature (OCT), frozen and cryosectioned at 10 µm thickness. Sections were allowed to dry at room temperature, rehydrated in PBS, blocked and permeabilized in 10% normal goat serum, 0.1% TritonX-100 in PBS for 1 hr at RT and incubated with primary antibodies, mouse anti-smooth muscle actin (1:500, Sigma) and rat anti-CD31 (1:50, BD Biosciences) in 1% BSA PBS for 2 hrs at RT. Sections were washed 3 x 5 minutes each with PBS and incubated with Alexa Fluor 546-goat anti mouse and Alexa Fluor 488-goat anti rat antibodies in 1% BSA PBS for 1 hr at RT. Following washing as above, DNA was stained with DAPI, sections mounted in FluoromountG (Southern Biotech) and imaged on a TCS SP2 Leica confocal microscope.

Laser-Induced CNV Model

Choroidal neovascularization was induced in mice using a 532 nm laser as previously described.[190] Four laser spots/eye were applied and eyes were harvested 7 days post-lasering, fixed in 4%PFA at 4^{o}C overnight and eyecups dissected and subjected to wholemount immunofluorescence.

Aortic Ring Assay

The aortic ring assay was performed in collagen as previously described.[191]

Blood Pressure and Heart Rate

Blood pressure and heart rate measurements were done on 10-14 week old male mice using a noninvasive computerized tail cuff system (BP-2000, VisiTech Systems). Mice were trained for 1 week, and then systolic and diastolic blood pressure and heart rate were recorded as the mean of at least 16 successful measurements over 1 week.

Measurement of Arterial Contraction / Relaxation Responses

Aortas were harvested from mice, flushed and cleaned of periaortic fat as described[191], cut into 2 mm long rings and equilibrated in Opti-MEM containing penicillin/streptomycin overnight at 37^{o}C. Contraction and relaxation responses were measured using a 6-mL vessel myograph (Danish Myo Technology) as previously described[188] with the following modifications. Arterial contraction in

response to increasing doses of phenylephrine (Phe) was recorded and expressed as percent of maximum contraction obtained in response to incubation in K-PSS (60 mM potassium-containing physiologic salt solution [mM: NaCl 130, KCl 4.7, $KHPO_4$ 1.18, $MgSO_4$ 1.17, $CaCl_2$ 1.6, $NaHCO_3$ 14.9, dextrose 5.5, $CaNa_2$/EDTA 0.03]). Vasorelaxation in response to increasing doses of acetylcholine was recorded following pre-contraction with Phe (10^{-6} M).

Coronary Artery Ligation Model

Myocardial infarction studies were done at the Partners Cardiovascular Physiology Core at Brigham and Women's Hospital as previously described.[192,193] Briefly, adult male mice were anesthetized by IP injection of a mixture of ketamine (40 mg/kg) and xylazine (10 mg/kg), intubated, and mechanically ventilated. Following thoracotomy, the pericardium was removed, and the proximal left coronary artery was permanently occluded with an intramural stitch.

Echocardiography

Echocardiography (Vevo 2100, VisualSonics Inc.) was performed at the Partners Cardiovascular Physiology Core at Brigham and Women's Hospital as previously described.[193] Two-dimensional and M-mode echocardiographic images were obtained from lightly sedated (1% isoflurane in oxygen) mice and recorded. M-mode images were obtained from the parasternal short-axis view at the level of

the papillary muscles and used for measurements.

Microfil and Bismuth/Gelatin Perfusions

Deeply anesthetized (100 mg/kg ketamine and 20 mg/kg xylazine) and heparinized (400 U) mice underwent thoracotomy, the right atrium was severed and mice were maximally vasodilated by infusing, via the left ventricle, 30 ml normal saline containing 1 g/l adenosine, 4 mg/l papaverine and 100 µg/ml heparin followed by 15 ml 2% formalin and ~0.5 ml uncatalyzed blue Microfil to help visualize the abdominal aorta during cannulation. Mice were then transected just below the diaphragm, the abdominal aorta was cannulated (Mc-28, Braintree Scientific) and the vasculature perfused with ~3 ml undiluted catalyzed Microfil or 10 ml of a warm 50% Bismuth (prepared as described[194])/7% gelatin in normal saline mixture with the aid of a syringe gun (IGSET-3510, Medco). The aorta and vena cava were then clamped and the perfusate allowed to polymerize for at least an hour at 4^{o}C before the hindlimbs were harvested, the skin removed and the limbs placed in 10% formalin.

µCT Analysis

Hindlimbs were scanned in air aligned axially on a Scanco µCT 40 at 70kVp, 114µA and a resolution of 10µm. The region of interest (ROI) included the entire hindlimb. To obtain the bone/vasculature overlay image, a contour around the entire ROI was utilized and segmented to include all soft and hard tissue. A

second contour of the same ROI with the bone removed was also performed and segmented. The segmentation parameters included the values 0.8 Gauss sigma, 1.0 Gauss support, and a threshold of 212-1000 (density range of 500mg of HA/cm^3). The two segmented files were overlaid using Scanco's IPL Transparency program and a false color image of the resulting file was created using the 3D Display program.

Dil Perfusions

The Dil solution was prepared as previously described[195], with addition of a filtration step through a 40 µm filter to remove large undissolved particles. P0 or P6 pups were euthanized by Isofluorane inhalation, decapitated and immediately perfused via the left ventricle with 3 or 5 ml respectively of Dil solution using a 10 ml syringe and 27 gauge needle and/or the thoracic aorta using a micro cannula (Mc-28, Braintree Scientific). Pups were then rinsed with PBS and fixed/stored in 4% paraformaldehyde (PFA) at 4^{o}C until dissected.

Dissections

Eyes were fixed in 4% PFA for 1 hr at RT or 4^{o}C overnight and retinas were dissected as previously described.[36] For immunofluorescence or to visualize GFP, decapitated E16.5 and P0 pups were rinsed in PBS, whereas P6 pups were perfused with PBS via the left ventricle and all were fixed in 4% PFA at 4^{o}C overnight. Working under a stereomicroscope, pups were transected

below the diaphragm and a midsagital incision was performed to separate the two hindlimbs and the associated abdominal musculature. The skin and associated adipose tissue was carefully removed and the abdominal muscles isolated via incisions at their attachment to the pelvis and vertebral column. The entire medial surface of the hindlimb adductor muscles was harvested en block via careful dissection 1-2 mm around the saphenous, femoral and proximal caudal femoral arteries. Muscle tissues were then either cleared sequentially (70% and 90% glycerol/PBS, at least 5 hrs each) and mounted in 90% glycerol/PBS for direct visualization of GFP or DiI or processed for immunofluorescence analysis. The medial surface of adductor muscles of fixed and dehydrated (70 and 100% ethanol) Microfil-perfused hindlimbs from adult mice was dissected similarly; muscles were cleared in methyl salicylate (Sigma) and imaged on a Zeiss Stereo Discovery.V12 stereomicroscope.

Whole Mount Tissue Lectin and Immunofluorescence Staining

Muscles were blocked and permeabilized in 1% BSA, 0.5% TritonX-100 PBS overnight at 4^{o}C. Tissues were equilibrated by washing 3 x 10 minutes each with Pblec buffer (1% Triton X-100, 1 mM $CaCl_2$, 1 mM $MgCl_2$, and 1 mM $MnCl_2$ in PBS pH 6.8) and incubated with biotinylated *Griffonia Simplifolica* isolectin B4 (iB4, 1:25, Vector Labs) in Pblec buffer. Antibodies were diluted in 1% BSA, 1% normal donkey serum (NDS), 1% TritonX-100 PBS and muscle samples were incubated in antibody solution for two days at 4^{o}C. We used the following primary

antibodies: FITC-conjugated smooth muscle actin (1:500, Sigma), goat anti-endomucin (1:100, R&D Systems) and mouse anti-Neurofilament-M (2H3; Developmental Studies Hybridoma Bank). Following primary detection, samples were washed 3 x 20 minutes each with 0.5% BSA, 0.5% TritonX-100 PBS at room temperature (RT) and incubated with Alexa Fluor-488-conjugated streptavidin (1:100) and/or Alexa Fluor-546-conjugated donkey anti-goat or donkey anti-mouse antibodies (1:200, Invitrogen) in 1% BSA, 1% NDS, 1% TritonX-100 PBS overnight at 4^{o}C. Samples were washed 3 x 20 minutes each with 0.5% BSA, 0.5% TritonX-100 PBS and once with PBS at RT and then cleared sequentially (70% and 90% glycerol/PBS, at least 5 hrs each) and mounted in 90% glycerol/PBS.

Whole mount retina[36] and (RPE/choroid/sclera)[190] staining was performed as previously described. Samples were stained with biotinylated or Alexa Fluor-488-conjugated iB4 (1:25), rabbit anti-NG2 (1:200, Millipore), or goat anti-DLL4 (1:100, R&D Systems). Fluorescence detection was performed using Alexa Fluor-488-conjugated streptavidin, Alexa Fluor-546 or 633-conjugated secondary antibodies and Alexa Fluor 546-conjugated Phalloidin (Invitrogen). DNA was stained with 1 μM 4,6'-diamidino-2-phenylindole (DAPI) or 10 μg/ml Hoechst (both from Invitrogen) in PBS for 10 minutes at RT and retinas and (RPE/choroid/sclera) were mounted in FluoromountG (Southern Biotech).

Microscopy and Image Analysis

Whole mount muscle and retinal vasculature imaging was done on a Zeiss stereomicroscope or a TCS SP2 Leica confocal microscope. Maximum projection confocal images of the adductor muscle vasculature were generated from z-stacks (30-300 µm, 1-10 µm step size depending on specimen size, staining and objective used) acquired starting at the medial surface of the adductor muscle specimens. To visualize large areas of the vasculature on the confocal microscope, a tile-scanning technique was employed whereby multiple overlapping (20-30% overlap) maximum projection images were acquired with a 10x or 20x objective and a composite image was constructed by arraying the individual images in Photoshop. Quantification of vascularized area in whole mount retinas was done from fluorescence stereomicroscopic images using ZEN software (Zeiss). Retinal angiogenic front vascular density, endothelial sprouts and filopodia were quantified using ImageJ and maximum projection confocal images acquired with a 10x, 20x and 63x objective respectively.

Histological Analysis of Muscle

Anesthetized mice were perfusion cleared and vasodilated by infusing, via the left ventricle, 20 ml normal saline containing 1 g/l adenosine, 4 mg/l papaverine and 100 µg/ml heparin followed by 10 ml 2% formalin. The skin was removed and entire hindlimbs were emersion fixed in 10% formalin for 24 hrs. Calf and adductor muscles were dissected *en block* from fixed hindlimbs, dehydrated and

embedded in paraffin. Cross sections (7 µm) were prepared and subjected to antigen retrieval using 1x antigen unmasking solution (Vector Labs). The sections were blocked and permeabilized in 10% normal goat serum, 0.1% Triton X-100 in PBS for (RT, 1 hr) and incubated with Alexa Fluor 488-conjugated IsolectinB4 (1:25, Vector Labs) and primary antibodies, mouse anti-smooth muscle actin (1:500, Sigma) and rat anti-CD31 (1:50, BD Biosciences) in 1% BSA in PBS (RT, 2 hr). Sections were washed 3 x 5 minutes each with PBS and incubated with Alexa Fluor 546-goat anti mouse and Alexa Fluor 488-goat anti rat antibodies in 1% BSA PBS for 1 hr at RT. Following washing as above, DNA was stained with DAPI, sections mounted in FluoromountG (Southern Biotech) and imaged on a TCS SP2 Leica confocal microscope.

Murine Lung Endothelial Cells (MLEC)

Lungs were harvested aseptically, rinsed in Dulbecco's modified eagle medium (DMEM), cut into small pieces and digested in collagenase 1.7 mg/ml for 1hr at 37^{o}C. Lung digests were further triturated by pipetting repeatedly through a 10 ml pipette fitted with a 1 ml pipette tip, passed through a 40 µm filter and the cell suspensions were cultured for 2 days in gelatin-coated plates in MLEC medium containing 20% fetal bovine serum, 38% DMEM 38% Ham's F-12 with 100 µg/mL endothelial cell growth supplement (ECGS, Biomedical Technologies), 4 mmol/L L-glutamine, 100 µg/mL heparin, and penicillin/streptomycin. Endothelial cells were isolated by selection with rat anti-

mouse intercellular adhesion molecule 2 (ICAM2) antibody (BD Biosciences)-coupled sheep anti-rat magnetic beads (Invitrogen), cultured for an additional 3-4 days and a second selection was done as above. Following an additional 2 days in culture, cells were used for experiments. Endothelial purity was confirmed by staining live cells with 1,1'-dioctadecyl - 3,3,3',3'-tetramethyl-indocarbocyanine perchlorate acetylated low-density lipoprotein (BT-902, Biomedical Technologies) according to the manufacturer's recommendations or anti-Cdh5 antibodies (Biolegend or BD Biosciences). For the 5-ethynyl-2'-deoxyuridine (EdU) incorporation assay, cell cultures were incubated in the presence of 10 μM EdU for 6 hours and processed for detection of EdU incorporation using the Click-iT® EdU Alexa Fluor® 488 Imaging Kit (Invitrogen) according to the manufacturers instructions. Immunofluorescence analysis was done on cells fixed with 4% PFA at RT for 15 minutes. Following 3 washes with PBS, cells were incubated in permeabilization/blocking buffer (10% normal goat serum (NGS) or NDS (depending on the species of secondary antibody used), 0.1% TritonX-100) for 1 hr at RT, then incubated with primary antibodies including PE-conjugated rat anti-Ki-67 (1:200, eBioscience), mouse anti-α-tubulin (1:500, Sigma), rat anti-Cdh5 (1:50, BD Biosciences) and goat anti-Dll4 (1:100, R&D Systems) in 1% BSA, 0.1% TritonX-100 overnight at 4^{o}C. Following 3 x 10 minute washes with PBS, cells were incubated with the appropriate Alexa Fluor- 488, 546 or 633-conjugated secondary antibodies (1:200, Invitrogen) for 2 hrs at RT. Cells were washed 3 x 10 minutes each with PBS, DNA was stained with 4,6'-diamidino-2-

phenylindole (DAPI) or Hoechst (1 µM, Invitrogen), cells were mounted in FluoromountG (Southern Biotech) and imaged on a TCS SP2 Leica confocal microscope.

Tube Formation Assay in Matrigel

Primary MLECs ($1x10^5$ cells) in 0.5% FBS DMEM/F12 were seeded in 8 well chamberslides (BD Biosciences) layered with 300 µl polymerized growth factor reduced matrigel (BD Biosciences) and incubated at 37^oC for 8 hrs. Tubular networks were imaged on a Zeiss inverted microscope.

Migration Assay

Confluent monolayers of primary MLECs in 96 well plates were simultaneously scratched using a 96-pin wound making tool (WoundMaker™, Essen Bioscience), rinsed twice with media and wound closure was monitored by automated live cell imaging on an IncuCyte ZOOM system (Essen Bioscience) using a 10x objective. The area between the edges of the wound in images taken at different time intervals was quantified using ImageJ.

Immunoblot Analysis

Cell extracts were prepared using Triton lysis buffer (20 mM Tris at pH 7.4, 1% Triton X-100, 10% glycerol, 137 mM NaCl, 2 mM EDTA, 25 mM β-glycerophosphate, 1 mM sodium orthovanadate,

1 mM phenylmethylsulfonylfluoride, 10 mg/mL of aprotinin and leupeptin). Extracts (20-50 µg of protein) were examined by protein immunoblot analysis by probing with antibodies to JNK (R&D Systems or Pharmigen), pJNK, pERK, ERK, cleaved Notch1 (Cell Signaling), Dll4 (R&D Systems), GAPDH (Santa Cruz) and αTubulin (Sigma). Immune complexes were detected using the Odyssey infrared imaging system (LI-COR Biosciences).

RNA Isolation

To isolate RNA from tissues, mice were perfusion cleared with PBS via the left ventricle. Hindlimb adductor and calf skeletal muscles were harvested en block, snap frozen in liquid nitrogen, pulverized on a cryoPREP™ impactor (Covaris), RNA extracted with TRIzol® (Life Technologies) and purified using the RNeasy kit (Qiagen). RNA from cells and other tissues homogenized in RLT buffer was isolated using the RNeasy kit.

RT-PCR

Complementary (c) DNA was prepared using The High Capacity Reverse Transcription Kit (Life Technologies). The expression of mRNA was examined by quantitative PCR analysis using a Quantstudio PCR system (Life Technologies). TaqMan® assays were used to quantify *Cdh5* (Mm00486938_m1), *Dll4* (Mm00444619_m1), *Emr1* (Mm00802529_m1), *Hes1* (Mm01342805_m1), *Hey1* (Mm00468865_m1), *Lfng* (Mm00456128_m1), *Pecam1* (Mm01242584_m1),

Slc2a1 (Mm00441480_m1) and *Vegfa* (Mm01281449_m1). The relative mRNA expression was normalized by measurement of the amount of 18S RNA in each sample using TaqMan® assays (catalog number 4308329; Life Technologies).

RNA-Sequencing

RNA was isolated using the RNeasy kit (Qiagen). RNA quality (RIN > 9) was verified using a Bioanalyzer 2100 System (Agilent Technologies). Total RNA (10µg) from independent MLEC isolations (lungs from 4 mice per isolation) was used for the preparation of each RNA-seq library by following the manufacturer's instructions (Illumina). Three independent libraries were examined for each condition. The cDNA libraries were sequenced by Illumina Hi-Seq with a paired-end 40-bp format. Reads from each sample were aligned to the mouse genome (UCSC genome browser mm10 build) using TopHat2.[196] The average number of aligned reads per library was > 20,000,000. Endothelial cell gene expression was quantitated as fragments per kilobase of exon model per million mapped fragments (FPKM) using Cufflinks.[197] Differentially expressed genes were identified using the Cufflinks tools Cuffmerge and Cuffdiff. Gene ontology was examined by Kyoto Encyclopedia of Genes and Genome (KEGG) pathway analysis[198] with the Database for Annotation, Visualization and Integrated Discovery (DAVID).[199]

Transplantations

Bone marrow (BM) was harvested by flushing tibias and femurs from at least three 10-12 week old mice with ice cold PBS. Erythrocytes were lysed by incubating the BM in ACK lysing buffer (Life Technologies). BM cells were then resuspended in PBS and passed through a 100 µm filter. Cells were counted and mixtures of test BM cells from the indicated genotypes were prepared by mixing test BM cells expressing the CD45.2 allele with competitor BM cells from *B6.SJL-Ptprc^{a}Pepc^{b}/BoyJ* mice expressing the CD45.1 allele at a 20 test:80 competitor cell ratio. 1x10^{6} total BM cells were intravenously injected via the tail vein into lethally irradiated (11 Gy) 10-12 week old CD45.1/CD45.2 heterozygous female mice. Transplanted mice were maintained on antibiotic water for the first two weeks post transplantation. Blood was harvested via the retroorbital sinus using heparinized capillary tubes and EDTA-coated vials at 5 and 20 weeks post transplantation and subjected to flow cytometry analysis.

Complete blood cell (CBC) analysis.

CBC analysis was done using a HemaTrue hematology analyzer (Heska) by the Department of Animal Medicine, University of Massachusetts Medical School

Flow Cytometry

Blood was washed in PBS, stained with live/dead fixable blue dead cell staining kit (Invitrogen), washed in PBS and blocked in 2% FBS-PBS 0.02%

sodium azide plus Fc-block (Anti-CD16/32 antibody 1:200, BD Biosciences). Surface antigens were detected by incubation for 30 min at 4^{o}C with conjugated antibodies including CD45.1-Pacific Blue, CD45.2-FITC, CD3e-APC, CD19-APC-H7, CD11b-PE (BD Biosciences) and GR1-Alexa Fluor 700 (Biolegend). Following washing with 2% FBS-PBS 0.02% sodium azide, red cells were lysed and leukocytes fixed by incubating in lyse/fix solution (BD Biosciences). Cells were washed with PBS and analyzed on an LSR-II cytometer (Becton Dickenson). Data were processed using FlowJo Software (Tree Star).

Statistical Analysis

Differences between groups were examined for statistical significance with an unpaired Student's test with equal variance or a log-rank (Mantel-Cox) test for determining significance of Kaplan-Meier survival curves.

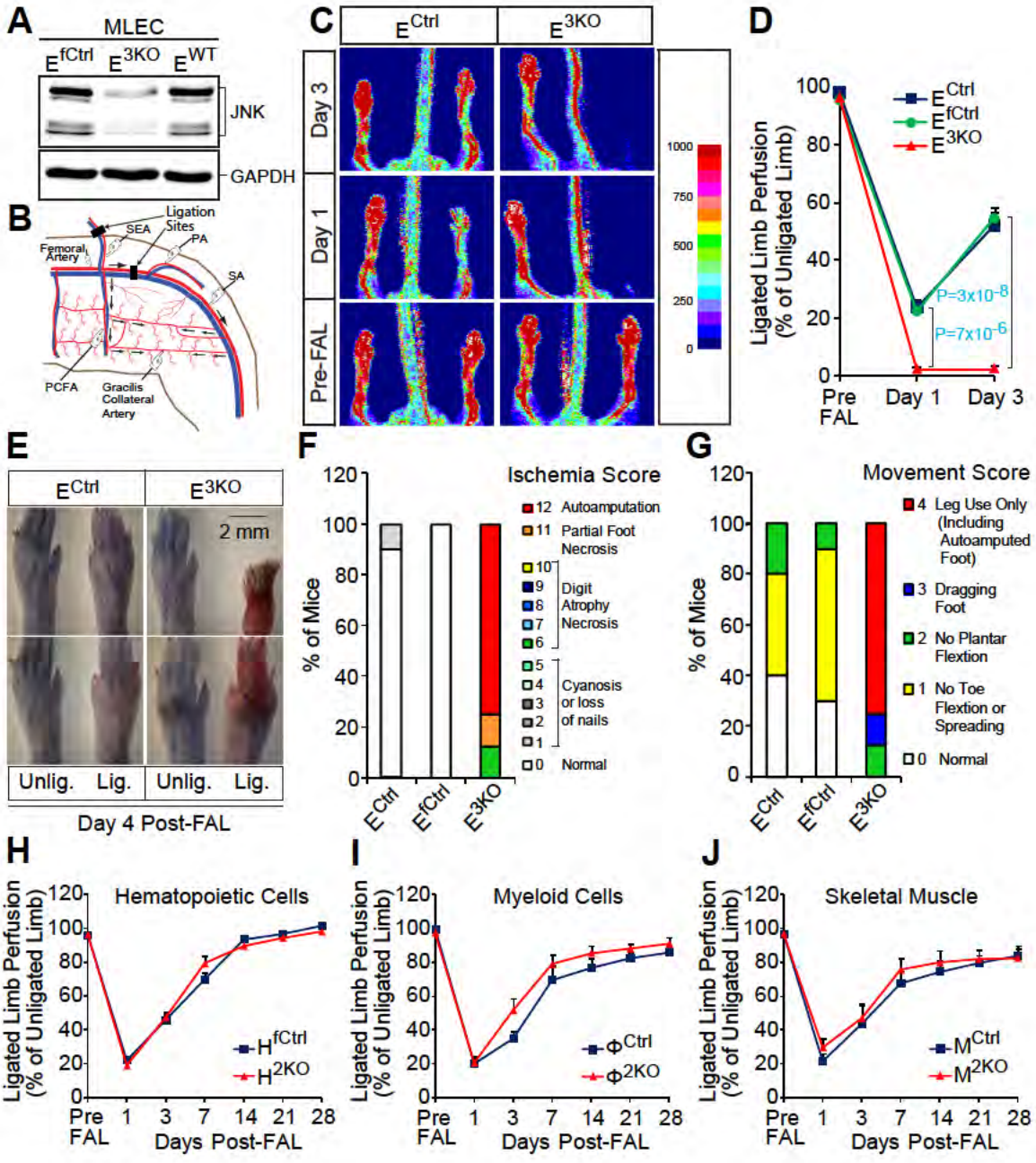

A
MLEC
E^fCtrl E^3KO E^WT
JNK
GAPDH
B
Ligation Sites
SEA
PA
SA
Femoral Artery
PCFA
Gracilis Collateral Artery
C
E^Ctrl
E^3KO
Day 3
Day 1
Pre-FAL
1000
750
500
250
0
D
Ligated Limb Perfusion (% of Unligated Limb)
E^Ctrl
E^fCtrl
E^3KO
P=3x10^-8
P=7x10^-6
Pre FAL
Day 1
Day 3
E
E^Ctrl
E^3KO
2 mm
Unlig. Lig. Unlig. Lig.
Day 4 Post-FAL
F
Ischemia Score
% of Mice
12 Autoamputation
11 Partial Foot Necrosis
10
9
8
7
6 Digit Atrophy Necrosis
5
4
3
2
1 Cyanosis or loss of nails
0 Normal
E^Ctrl
E^fCtrl
E^3KO
G
Movement Score
% of Mice
4 Leg Use Only (Including Autoamputed Foot)
3 Dragging Foot
2 No Plantar Flextion
1 No Toe Flextion or Spreading
0 Normal
E^Ctrl
E^fCtrl
E^3KO
H
Hematopoietic Cells
Ligated Limb Perfusion (% of Unligated Limb)
H^fCtrl
H^2KO
Pre FAL
Days Post-FAL
I
Myeloid Cells
Ligated Limb Perfusion (% of Unligated Limb)
Φ^Ctrl
Φ^2KO
Pre FAL
Days Post-FAL
J
Skeletal Muscle
Ligated Limb Perfusion (% of Unligated Limb)
M^Ctrl
M^2KO
Pre FAL
Days Post-FAL

Figure II.1 Enhanced blood perfusion blockade and severe ischemic injury in endothelial JNK-deficient mice upon arterial occlusion.

A) Immunoblot analysis reveals robust reduction in JNK protein abundance in purified lung endothelial cells from E^{3KO} mice. Lysates were also examined with antibodies to GAPDH.

B) Simplified diagram of the medial aspect of the mouse hindlimb skeletal muscle vasculature. The common femoral artery (FA) and its main branches (proximal caudal femoral artery [PCFA], popliteal artery [PA] and saphenous artery [SA]) supply blood to the proximal and distal hindlimb. Ligation of the FA plus the superficial epigastric artery (SEA) as indicated, leads to reduced blood flow to the distal hindlimb, while flow through the PCFA and gracillis collaterals is enhanced.

C) Representative laser Doppler images showing blood perfusion (high perfusion red, no perfusion dark blue) in the hindlimbs of control and E^{3KO} mice prior (Pre-FAL) and on days 1 and 3 post ligation.

D) Quantitation of Doppler signals shows significantly enhanced blood perfusion blockade following ligation and no recovery 3 days after ligation in E^{3KO} mice compared to control mice (mean ± SEM; n = ~7-10 mice per group).

E) E^{3KO} mice undergo severe necrosis of the paws following ligation (Lig.). Paws of ligated limbs from control mice never display necrosis. Images are representative of paws from ~7-10 mice per group. Unlig. = contralateral unligated limb.

F and **G**) All E^{3KO} mice display paw necrosis with over 70% undergoing complete autoamputation of the paw. Ligated limbs of control mice show almost no signs of ischemia (**F**) and only minor movement impairment 4 days post FAL (**G**), (~7-10 mice per group).

H - **J**) Quantification of limb blood perfusion by laser Doppler imaging showing no significant differences in blood perfusion blockade and restoration over 28 days following FAL between control mice and mice that lack JNK1 plus JNK2 in all hematopoietic cells (H^{2KO}, **H**), in myeloid cells (Φ^{2KO}, **I**) or skeletal muscle cells (M^{2KO}, **J**) (mean ± SEM; n = ~5-10 mice per group).

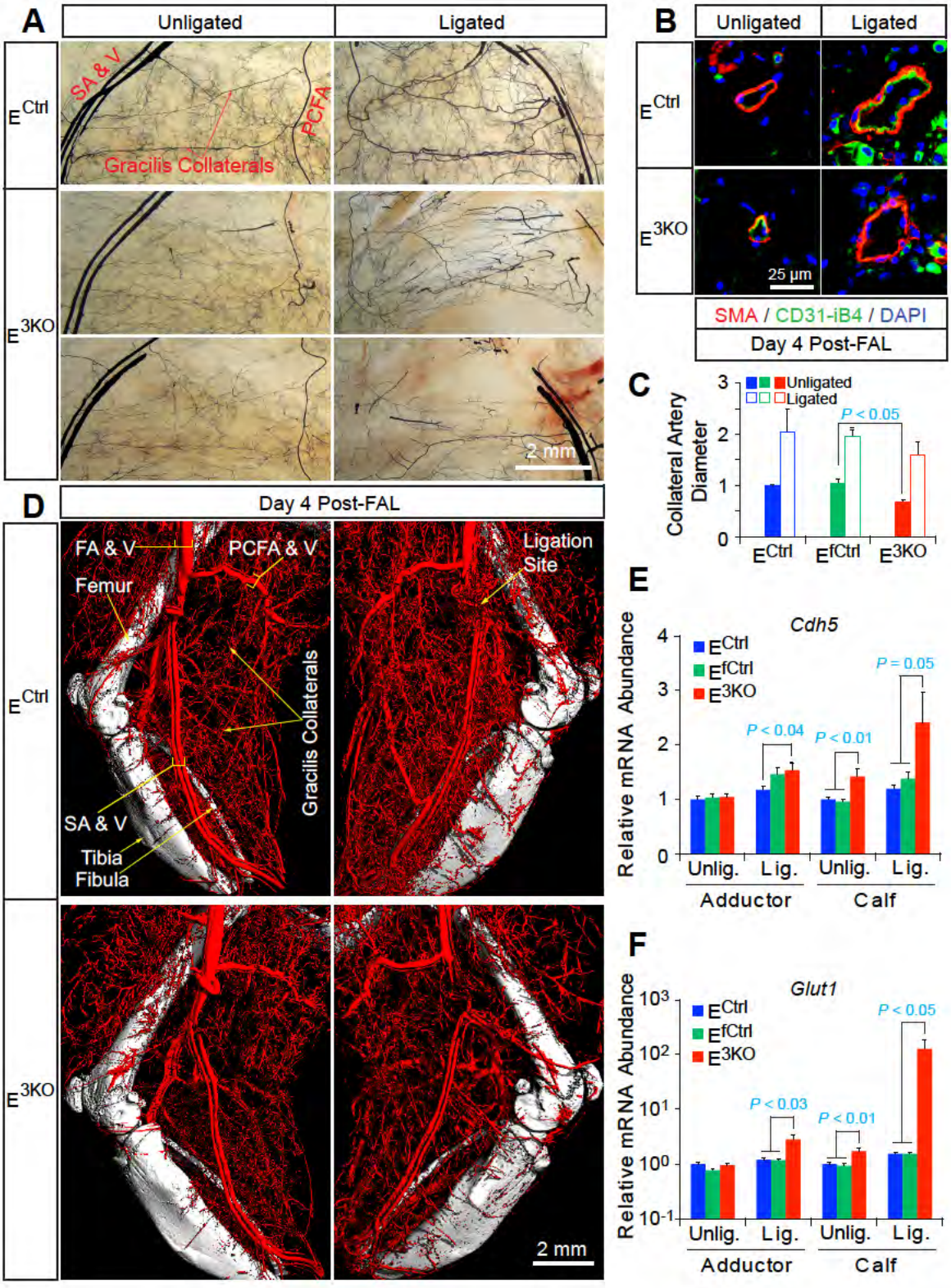

A
Unligated
Ligated
E Ctrl
E 3KO
SA & V
PCFA
Gracilis Collaterals
2 mm
B
Unligated
Ligated
E Ctrl
E 3KO
25 μm
SMA / CD31-iB4 / DAPI
Day 4 Post-FAL
C
Unligated
Ligated
P < 0.05
Collateral Artery Diameter
E Ctrl
E fCtrl
E 3KO
D
Day 4 Post-FAL
FA & V
PCFA & V
Femur
Gracilis Collaterals
SA & V
Tibia
Fibula
Ligation Site
2 mm
E
Cdh5
Relative mRNA Abundance
P < 0.04
P < 0.01
P = 0.05
Unlig.
Lig.
Adductor
Calf
F
Glut1
P < 0.03
P < 0.01
P < 0.05

Figure II.2 Endothelial JNK-deficient mice display abnormal native collateral arteries.

A) Whole mount preparations of the medial surface of Microfil filled adductor muscle vasculature from unligated and 4 days post-ligation limbs showing thin and abnormally organized gracillis collateral vessels in the unligated limbs and poor Microfil filling of the vasculature in the ligated limbs of E^{3KO} mice. Unligated limbs from control mice display distinctly thicker gracillis collateral arteries directly interconnecting the PCFA to the SA. These vessels remodel outwardly, increasing in diameter and becoming more tortuous 4 days post-ligation. Images are representative of at least 5 mice per group.

B and **C**) Immunofluorescence for smooth muscle actin (SMA) and CD31/iB4 on cross sections of adductor muscles. Quantification of artery diameter (**C**) from SMA immunofluorescence images confirms reduced size of gracillis collaterals in the unligated limbs of E^{3KO} mice (mean ± SEM; n = ~10-12 gracillis collaterals from 5 mice per group).

D) Micro-CT analysis of contrast (Bismuth/gelatin) filled hindlimb vasculature illustrates defects in artery size and connectivity in the adductor muscle region of E^{3KO} hindlimbs. Images are representative of 7-8 mice analyzed per group.

E and **F**) Taqman gene expression analysis quantitating the mRNA abundance of the endothelial cell specific marker *Cdh5* (**E**) and the hypoxia responsive gene *Slc2a1* (**F**) on day 4 post FAL (mean ± SEM; n = ~7-8 mice per group).

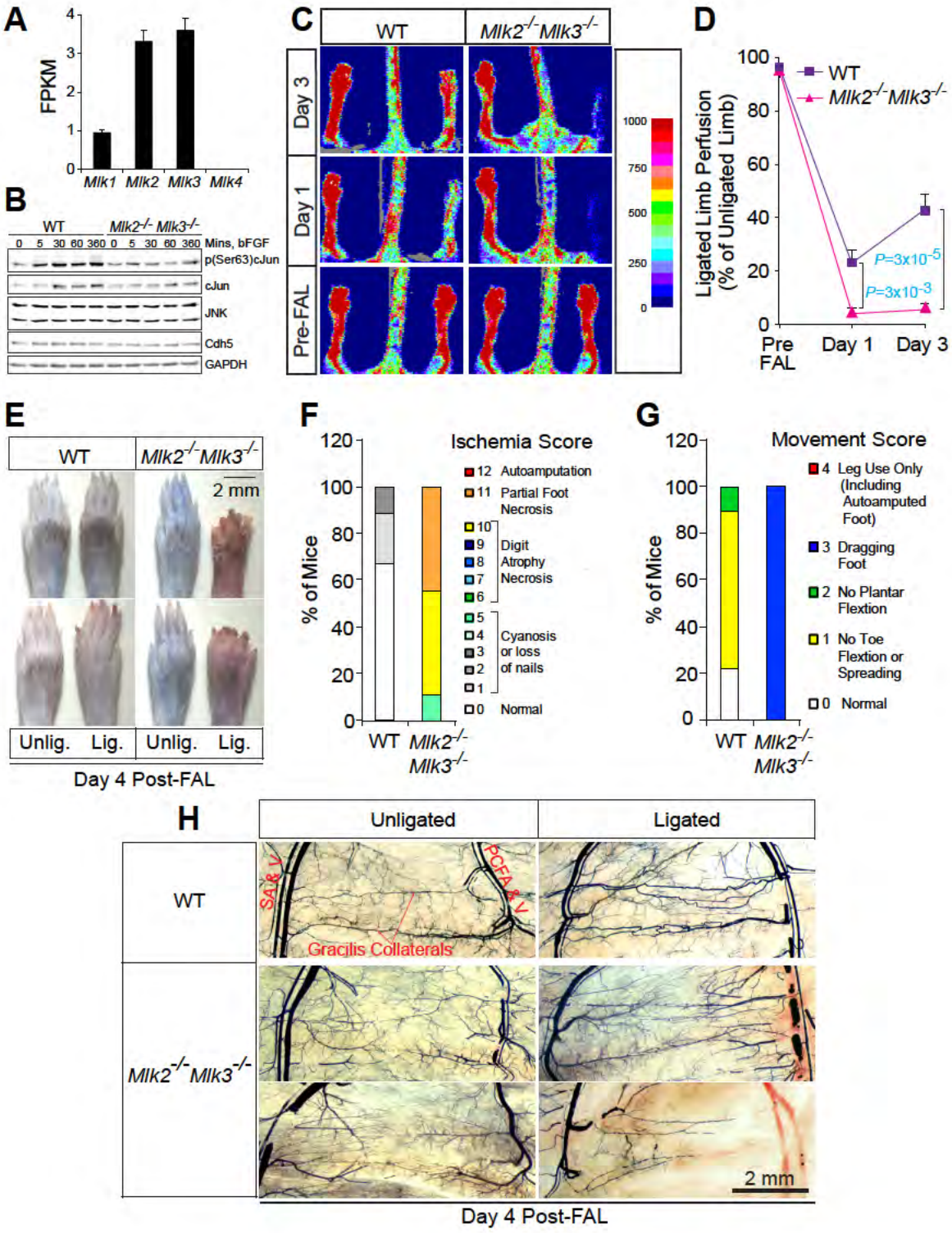

A
FPKM
Mlk1 Mlk2 Mlk3 Mlk4
B
WT
Mlk2-/- Mlk3-/-
0 5 30 60 360 0 5 30 60 360 Mins, bFGF
p(Ser63)cJun
cJun
JNK
Cdh5
GAPDH
C
WT
Mlk2-/-Mlk3-/-
Day 3
Day 1
Pre-FAL
1000
750
500
250
0
D
WT
Mlk2-/-Mlk3-/-
Ligated Limb Perfusion (% of Unligated Limb)
P=3x10-5
P=3x10-3
Pre FAL
Day 1
Day 3
E
WT
Mlk2-/-Mlk3-/-
2 mm
Unlig. Lig. Unlig. Lig.
Day 4 Post-FAL
F
Ischemia Score
% of Mice
12 Autoamputation
11 Partial Foot Necrosis
10
9 Digit Atrophy Necrosis
8
7
6
5
4 Cyanosis or loss of nails
3
2
1
0 Normal
WT
Mlk2-/-Mlk3-/-
G
Movement Score
% of Mice
4 Leg Use Only (Including Autoamputed Foot)
3 Dragging Foot
2 No Plantar Flextion
1 No Toe Flextion or Spreading
0 Normal
WT
Mlk2-/-Mlk3-/-
H
Unligated
Ligated
WT
Mlk2-/-Mlk3-/-
SAR V
PCFA & V
Gracilis Collaterals
2 mm
Day 4 Post-FAL

Figure II.3 Abnormal native collateral arteries, and enhanced blood perfusion blockade and ischemic injury in *Mlk2*$^{-/-}$*Mlk3*$^{-/-}$ mice upon arterial occlusion.

A) Gene expression analysis (from mouse endothelial cell RNA Seq analysis) of the four members of the MLK group showing highest expression of *Mlk2* and *Mlk3* in endothelial cells (mean FPKM [fragments per kilobase of transcript per million mapped reads] ± SEM; n = 6 endothelial cell libraries).

B) Immunoblot analysis reveals reduced bFGF-induced phosphorylation of the JNK substrate cJun in *Mlk2*$^{-/-}$*Mlk3*$^{-/-}$ endothelial cells compared to WT endothelial cells indicating reduced JNK activity in *Mlk2*$^{-/-}$*Mlk3*$^{-/-}$ endothelial cells. Lysates were also examined with antibodies to cJun, JNK, Cdh5 and GAPDH.

C) Representative laser Doppler images showing blood perfusion (high perfusion red, no perfusion dark blue) in the hindlimbs of WT and *Mlk2*$^{-/-}$*Mlk3*$^{-/-}$ mice prior (Pre-FAL) and on days 1 and 3 post ligation.

D) Quantitation of Doppler signals shows significantly enhanced blood perfusion blockade following ligation and no recovery 3 days after ligation in *Mlk2*$^{-/-}$*Mlk3*$^{-/-}$ mice compared to WT mice (mean ± SEM; n = 7 mice per group).

E) *Mlk2*$^{-/-}$*Mlk3*$^{-/-}$ mice undergo severe necrosis of the paws following ligation (Lig.). Paws of ligated limbs from WT mice never display necrosis. Images are representative of paws from 9 mice per group. Unlig. = contralateral unligated limb.

F and **G**) All *Mlk2*$^{-/-}$*Mlk3*$^{-/-}$ mice display digit/paw necrosis and severe movement impairment. Ligated limbs of WT mice show minor signs of ischemia (**F**) and only minor movement impairment 4 days post FAL (**G**), (9 mice per group).

H) Whole mount preparations of the medial surface of Microfil filled adductor muscle vasculature from unligated and 4 days post-ligation limbs showing thin and abnormally organized gracillis collateral vessels in the unligated limbs and poor Microfil filling of the vasculature in the ligated limbs of *Mlk2*$^{-/-}$*Mlk3*$^{-/-}$ mice. Limbs from control mice display distinctly thicker gracillis collateral arteries directly interconnecting the PCFA to the SA. These vessels remodel outwardly, increasing in diameter and becoming more tortuous 4 days post-ligation. Images are representative of at least 6 mice per group.

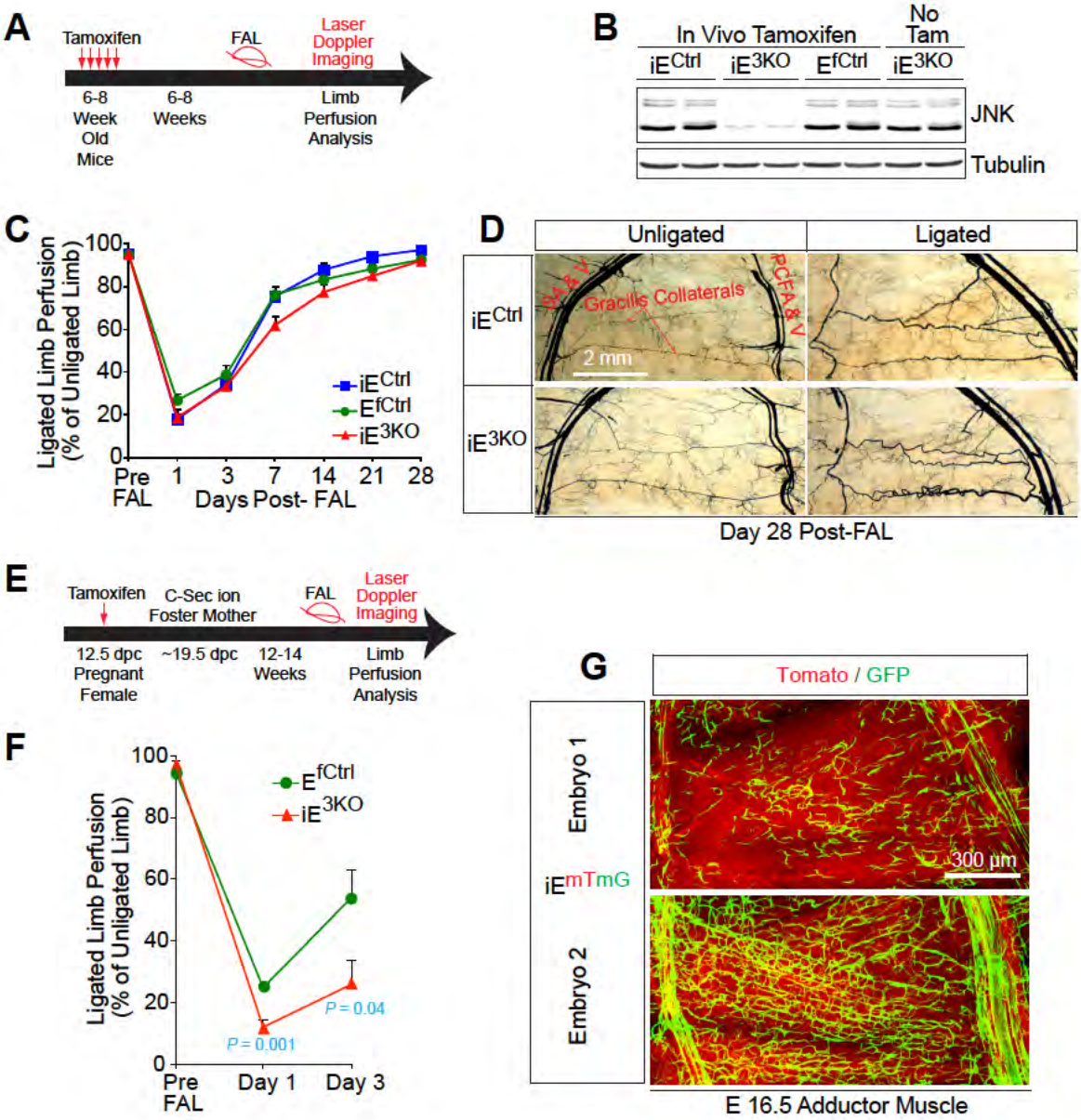

A
Tamoxifen
FAL
Laser Doppler Imaging
6-8 Week Old Mice
6-8 Weeks
Limb Perfusion Analysis
B
In Vivo Tamoxifen
No Tam
iE^Ctrl
iE^3KO
E^fCtrl
iE^3KO
JNK
Tubulin
C
Ligated Limb Perfusion (% of Unligated Limb)
Pre FAL
Days Post- FAL
iE^Ctrl
E^fCtrl
iE^3KO
D
Unligated
Ligated
iE^Ctrl
iE^3KO
Gracilis Collaterals
2 mm
Day 28 Post-FAL
E
Tamoxifen
C-Sec ion Foster Mother
FAL
Laser Doppler Imaging
12.5 dpc Pregnant Female
~19.5 dpc
12-14 Weeks
Limb Perfusion Analysis
F
Ligated Limb Perfusion (% of Unligated Limb)
E^fCtrl
iE^3KO
P = 0.04
P = 0.001
Pre FAL
Day 1
Day 3
G
Tomato / GFP
Embryo 1
iE^mTmG
Embryo 2
300 µm
E 16.5 Adductor Muscle

Figure II.4 Endothelial JNK is dispensable for arteriogenic responses in adult mice.

A) Diagram illustrating the timeline of tamoxifen administration to induce disruption of floxed *Jnk* alleles in the endothelium of adult mice. FAL was performed as described in Fig. I.1B.

B) Immunoblot analysis of lysates from purified lung endothelial cells confirming robust reduction in JNK protein abundance in cells from iE^{3KO} mice at least 8 weeks post tamoxifen administration. Lysates were also examined with antibodies to α-Tubulin. Data are representative of two independent endothelial cell isolations per group (2-3 mice used / each cell preparation).

C) Laser Doppler quantification of limb blood perfusion showing no significant differences in blood perfusion blockade and recovery over 28 days post arterial ligation in iE^{3KO} mice compared to Cre^{+} control (iE^{Ctrl}) or Cre^{-} litermate (E^{fCtrl}) mice (mean ± SEM; n = ~5-10 mice per group).

D) Microfil perfusion analysis of adductor muscle vasculature showing normal gracillis collateral arteries in the unligated limbs of iE^{3KO} mice and similar collateral artery remodeling to that in control mice 28 days post-ligation. Images are representative of ~5-8 mice per group).

E) Diagram illustrating the timeline of tamoxifen treatment to induce recombination of *Jnk* alleles during embryonic development, delivery of pups by C-section, rearing of pups by foster mothers and femoral artery ligation experiment.

F) Laser Doppler quantification of limb blood perfusion showing significantly enhanced blood perfusion reduction in iE^{3KO} adult mice in which mosaic deletion of JNK in the endothelium was induced during embryonic development (mean ± SEM; n = ~5-6 mice per group).

G) Confocal imaging of adductor muscle vasculature of three iE^{mTmG} embryos harvested from a pregnant female that was treated with tamoxifen at 12.5 dpc demonstrates highly variable mosaic recombination in the endothelium. The data presented are representative of six mice examined.

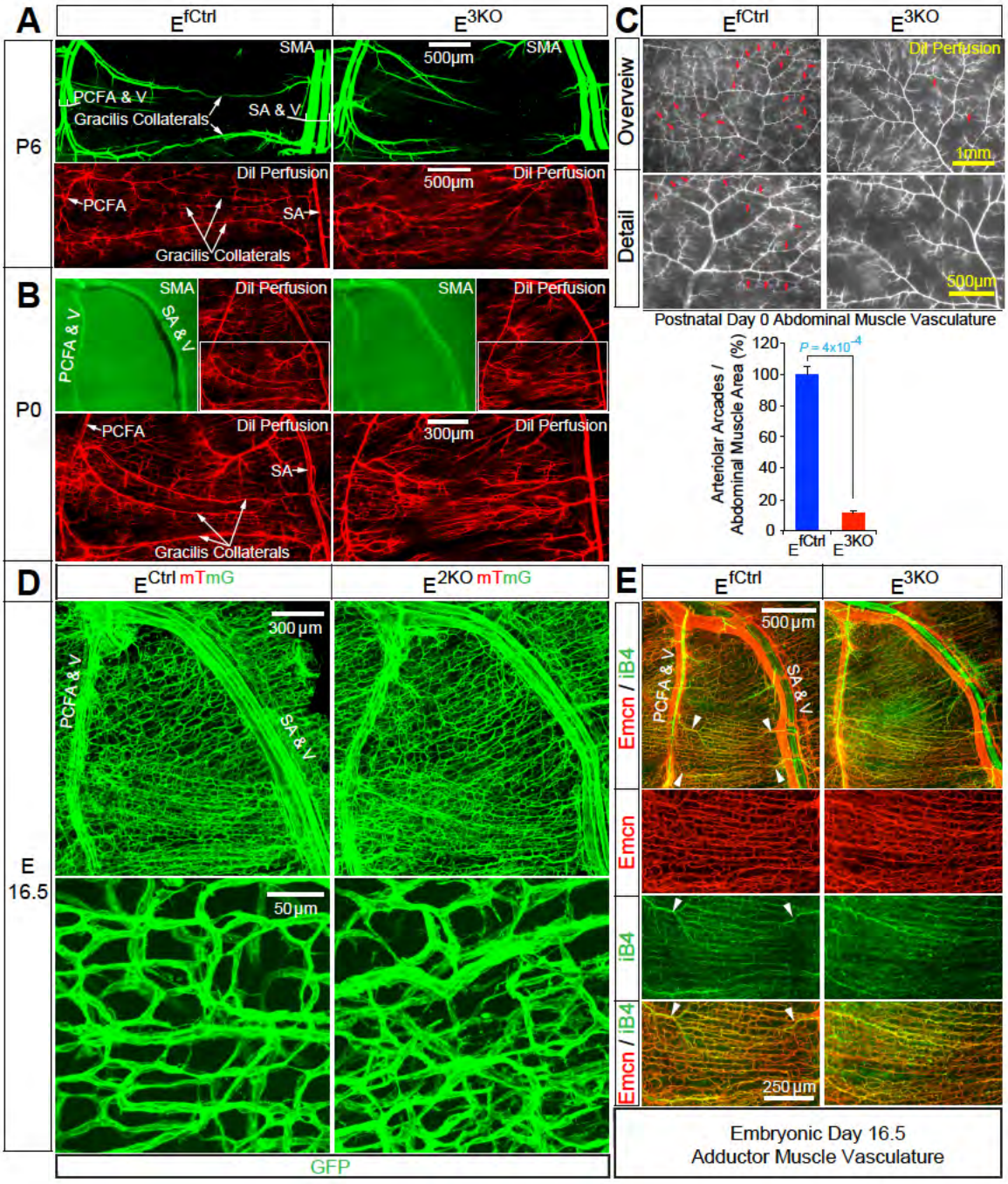

A
E^fCtrl
E^3KO
P6
SMA
500μm
PCFA & V
Gracilis Collaterals
SA & V
Dil Perfusion
PCFA
SA
B
P0
300μm
C
Overveiw
Detail
1mm
500μm
Postnatal Day 0 Abdominal Muscle Vasculature
Arteriolar Arcades / Abdominal Muscle Area (%)
P = 4x10^-4
D
E^Ctrl mTmG
E^2KO mTmG
E 16.5
300 μm
50μm
GFP
E
Emcn / iB4
Emcn
iB4
500 μm
250 μm
Embryonic Day 16.5
Adductor Muscle Vasculature

Figure II.5 Endothelial JNK deficiency results in altered collateral artery patterning during ontogeny

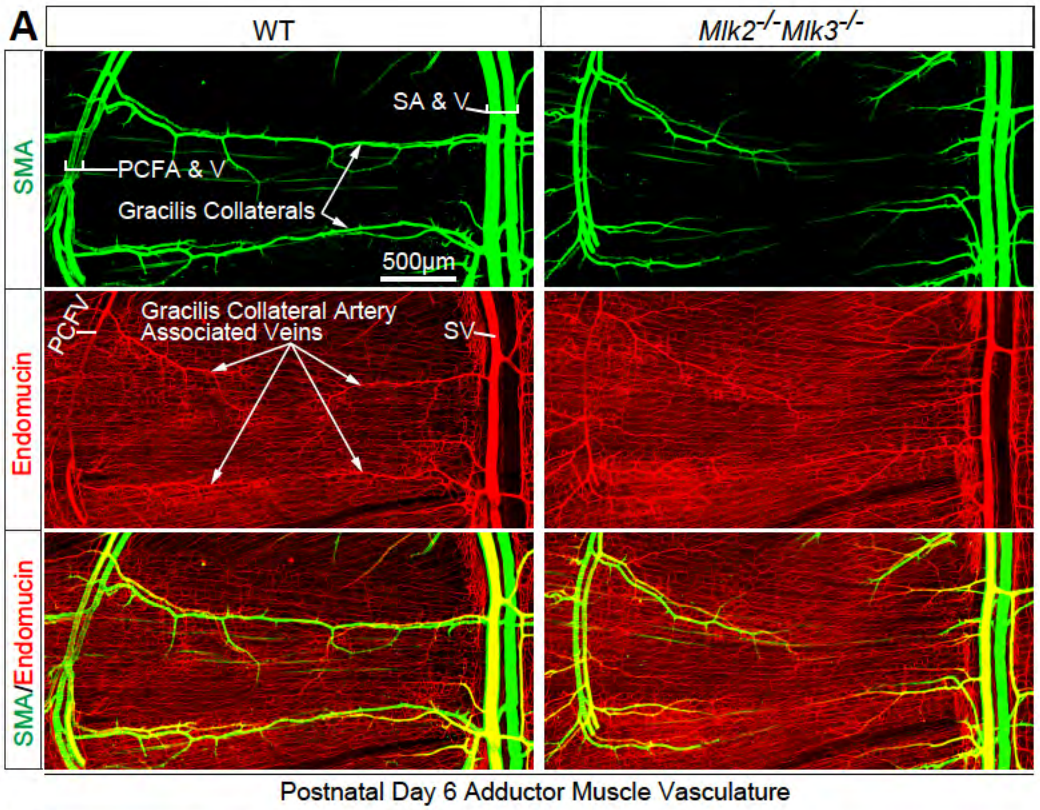
A) Confocal microscopy analysis of whole mount adductor muscle vasculature reveals distinct gracillis collateral arteries interconnecting the PCFA to the SA in P6 control mice. At this stage, gracillis collaterals are fully invested with smooth muscle cells throughout their length as demonstrated by smooth muscle acting (SMA, green) immunofluorescence. Analysis of adductor muscle vasculature in P6 E^{3KO} mice shows smooth muscle cell covered vessels emerging from both the PCFA and the SA, however continuous SMA signal interconnecting the PCFA to the SA is not observed. Adductors from at least 7 mice per group were analyzed. Intravascular DiI (red) perfusion analysis demonstrates distinct gracillis collaterals interconnecting the PCFA to the SA in control mice. Vessels emerging from the PCFA and the SA in E^{3KO} mice do not fully interconnect. Instead, they branch off into smaller vessels that appear to enter the capillary circulation. Note that DiI perfusion exclusively labels the arterial and capillary vasculature, but not veins. Adductors from at least 5 mice per group were analyzed.

B) DiI perfusion in control mice at P0 reveals gracillis collaterals as distinct vessels interconnecting the PCFA to the SA. At this stage these vessels lack extensive smooth muscle coverage. In P0 E^{3KO} mice, vessels emerging from the PCFA and the SA do not form distinct interconnecting collaterals, but branch extensively and enter the capillary circulation. Adductors from at least 5 mice per group were analyzed.

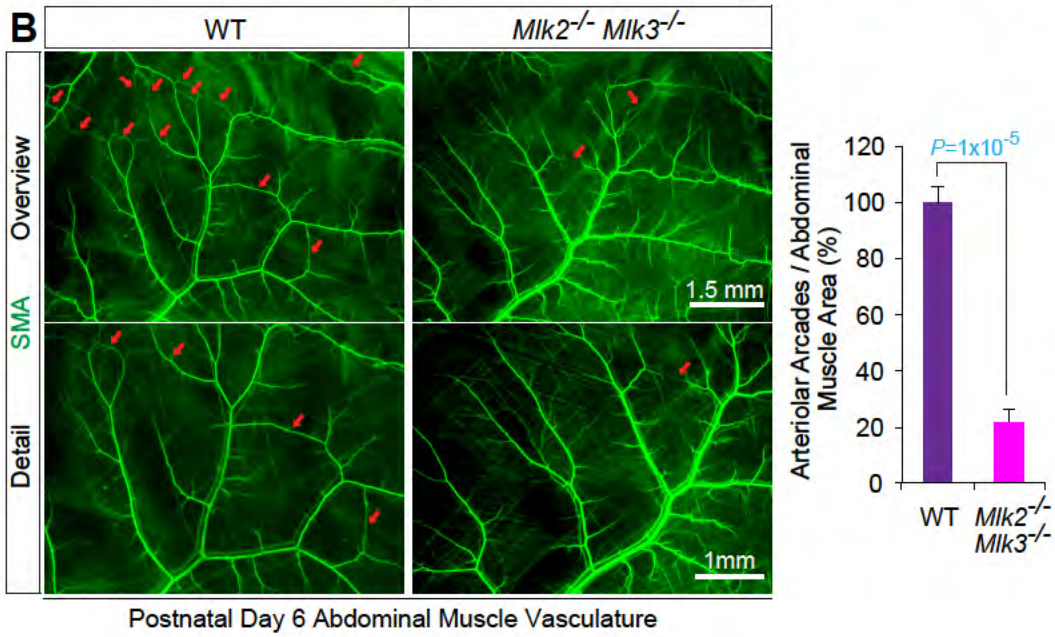
C) Stereomicroscopic imaging of DiI perfused abdominal muscle arterial vasculature at P0 reveals numerous arteriole-to-arteriole arcades in control mice (red arrows). The abdominal muscle arterial vasculature of E^{3KO} mice shows very few arteriole-to-arteriole interconnections. Quantification reveals significantly reduced arteriolar arcade numbers in E^{3KO} mice compared to littermate control mice (mean ± SEM; n = abdominal muscles from 3 mice per group).

D) Confocal imaging analysis of the vasculature by direct GFP visualization in whole mount adductor muscle preparations from control ($E^{Ctrl\ mTmG}$) and $E^{2KO\ mTmG}$ E16.5 embryos showing incomplete remodeling of collateral vessels at this stage. The gracillis muscle capillary plexus of $E^{2KO\ mTmG}$ embryos appears more chaotically organized compared to that of control embryos. High magnification images show increased branching, higher vessel thickness variation and more filopodia in the capillary plexus of $E^{2KO\ mTmG}$ embryos. Images are representative of adductors from ~3-4 mice per group.

E) Confocal imaging of E16.5 adductor muscle vasculature immunostained for Endomucin (Emcn, red) and isolectinB4 (iB4, green) reveals a denser capillary plexus with higher vessel thickness variation in the gracillis collateral region of adductors from E^{3KO} mice compared to littermate control mice. Images are representative of adductors from ~3-5 mice per group.



Postnatal Day 6 Adductor Muscle Vasculature



Postnatal Day 6 Abdominal Muscle Vasculature

Figure II.6 *Mlk2*$^{-/-}$*Mlk3*$^{-/-}$ mice phenocopy the defects in native collateral artery formation of endothelial JNK deficient mice at P6

A) Confocal microscopy analysis of wholemount adductor muscle vasculature immunostained for smooth muscle actin (SMA, green) reveals abnormal gracillis collateral arteries in *Mlk2*$^{-/-}$*Mlk3*$^{-/-}$ mice marked by absence of continuous SMA signal interconnecting the PCFA to the SA. Endomucin staining labels the capillary and venous, but not the arterial vasculature. Adductors from 5 mice per group were analyzed.

B) Stereomicroscopic imaging of SMA immunostained abdominal muscle vasculature at P6 reveals numerous arteriole-to-arteriole arcades in WT mice (red arrows). The abdominal muscle vasculature of *Mlk2*$^{-/-}$*Mlk3*$^{-/-}$ mice shows very few arteriole-to-arteriole interconnections. Quantification reveals significantly reduced arteriolar arcade numbers in *Mlk2*$^{-/-}$*Mlk3*$^{-/-}$ mice compared to WT mice (mean ± SEM; n = abdominal muscles from 5 mice per group).

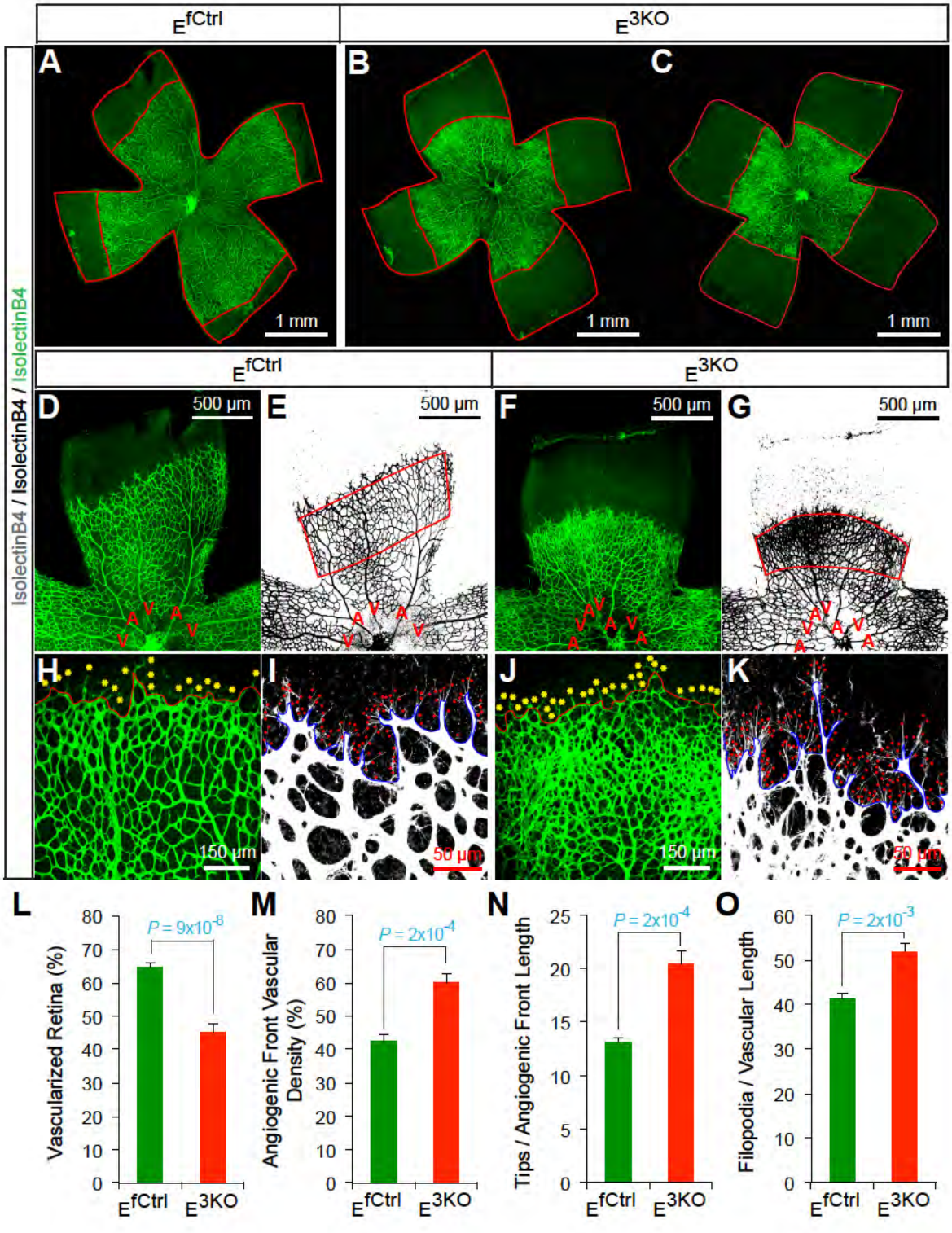

E^fCtrl
E^3KO
A
B
C
1 mm
1 mm
1 mm
IsolectinB4 / IsolectinB4 / IsolectinB4
D
E
F
G
500 µm
H
I
J
K
150 µm
50 µm
150 µm
50 µm
L
M
N
O
Vascularized Retina (%)
Angiogenic Front Vascular Density (%)
Tips / Angiogenic Front Length
Filopodia / Vascular Length
P = 9x10^-8
P = 2x10^-4
P = 2x10^-4
P = 2x10^-3
E^fCtrl
E^3KO

Figure II.7 Abnormal retinal vascular development marked by excessive sprouting in endothelial JNK-deficient mice

A-**C**) Representative examples of whole mount retina iB4 immunofluorescence showing reduced vascular extension in P6 E^{3KO} retinas (**B** and **C**) compared to littermate control retinas (**A**).

D-**K**) Closer examination reveals increased vascular density (**D**-**G** and **H** and **J**), increased tip cell numbers (yellow asterisks in **H** and **J**) and more filopodia (red dots in **I** and **K**) at the vascular front region of E^{3KO} retinas compared to littermate control retinas.

L-**O**) Quantitative analysis of vascularized retinal area (**L**), vascular density within angiogenic front regions indicated in **E** and **G** (**M**), tip cell number (**N**) and filopodia (**O**) demonstrates that differences between E^{3KO} and littermate control mice are statistically significant (mean ± SEM; n = ~17-31 retinas from at least 12 mice per group for quantification of vascular extension; n = ~6-10 retinas from at least 5 mice per group for quantification of the other parameters - multiple confocal images per retina were quantified and averaged).

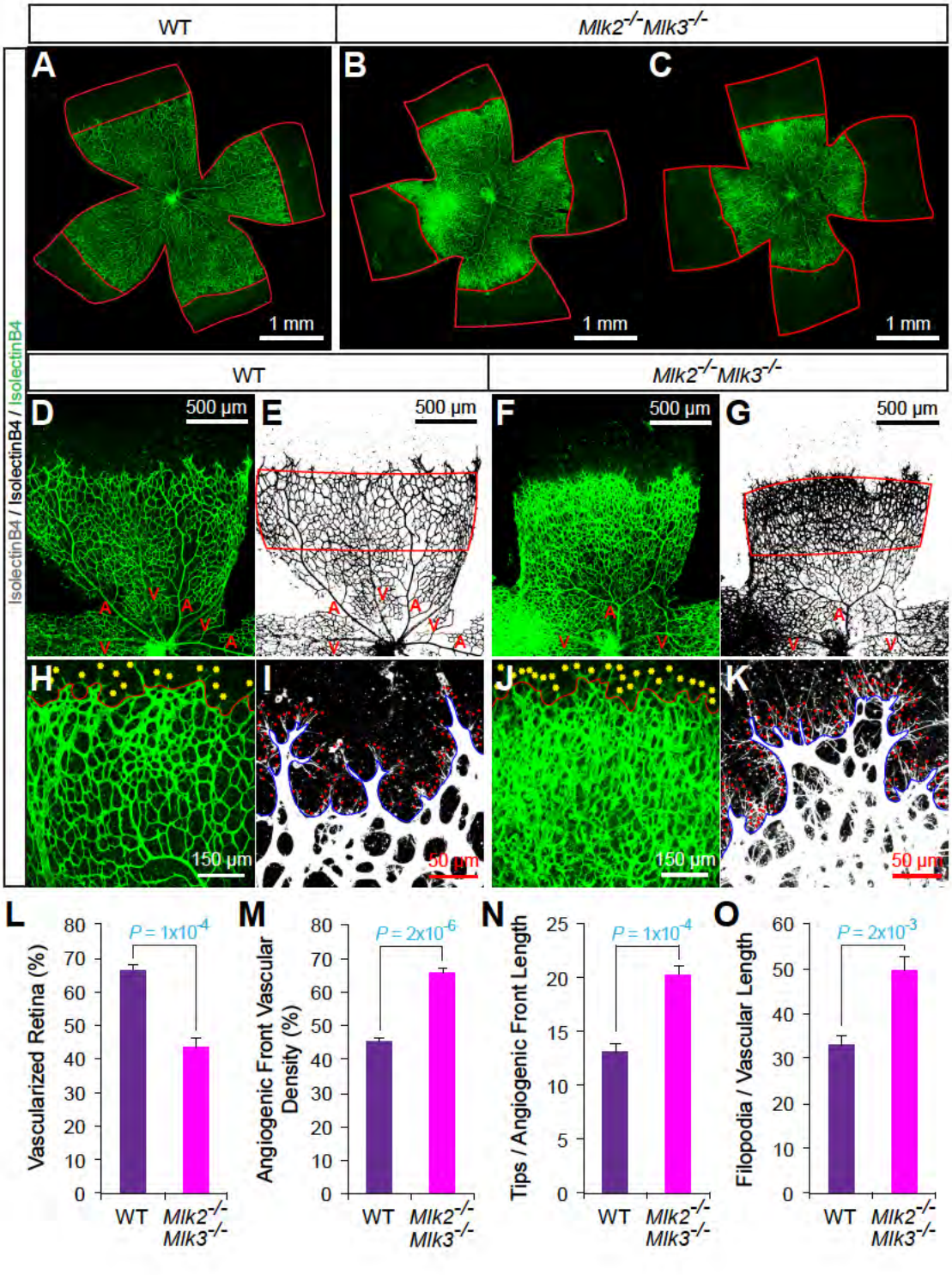

WT
Mlk2-/-Mlk3-/-
A
B
C
1 mm
1 mm
1 mm
IsolectinB4 / IsolectinB4 / IsolectinB4
WT
Mlk2-/-Mlk3-/-
D
E
F
G
500 µm
500 µm
500 µm
500 µm
A
V
H
I
J
K
150 µm
50 µm
150 µm
50 µm
L
Vascularized Retina (%)
P = 1x10-4
M
Angiogenic Front Vascular Density (%)
P = 2x10-6
N
Tips / Angiogenic Front Length
P = 1x10-4
O
Filopodia / Vascular Length
P = 2x10-3
WT
Mlk2-/-Mlk3-/-

Figure II.8 Abnormal retinal vascular development marked by excessive sprouting in *Mlk2*$^{-/-}$*Mlk3*$^{-/-}$ mice

A-**C**) Representative examples of whole mount retina iB4 immunofluorescence showing reduced vascular extension in P6 *Mlk2*$^{-/-}$*Mlk3*$^{-/-}$ retinas (**B** and **C**) compared to WT retinas (**A**).

D-**K**) Closer examination reveals increased vascular density (**D**-**G** and **H** and **J**), increased tip cell numbers (yellow asterisks in **H** and **J**) and more filopodia (red dots in **I** and **K**) at the vascular front region of *Mlk2*$^{-/-}$*Mlk3*$^{-/-}$ retinas compared to WT retinas.

L-**O**) Quantitative analysis of vascularized retinal area (**L**), vascular density within angiogenic front regions indicated in **E** and **G** (**M**), tip cell number (**N**) and filopodia (**O**) demonstrates that differences between *Mlk2*$^{-/-}$*Mlk3*$^{-/-}$ and control mice are statistically significant (mean ± SEM; n = 5 retinas from 5 mice per group - multiple confocal images per retina were quantified and averaged).

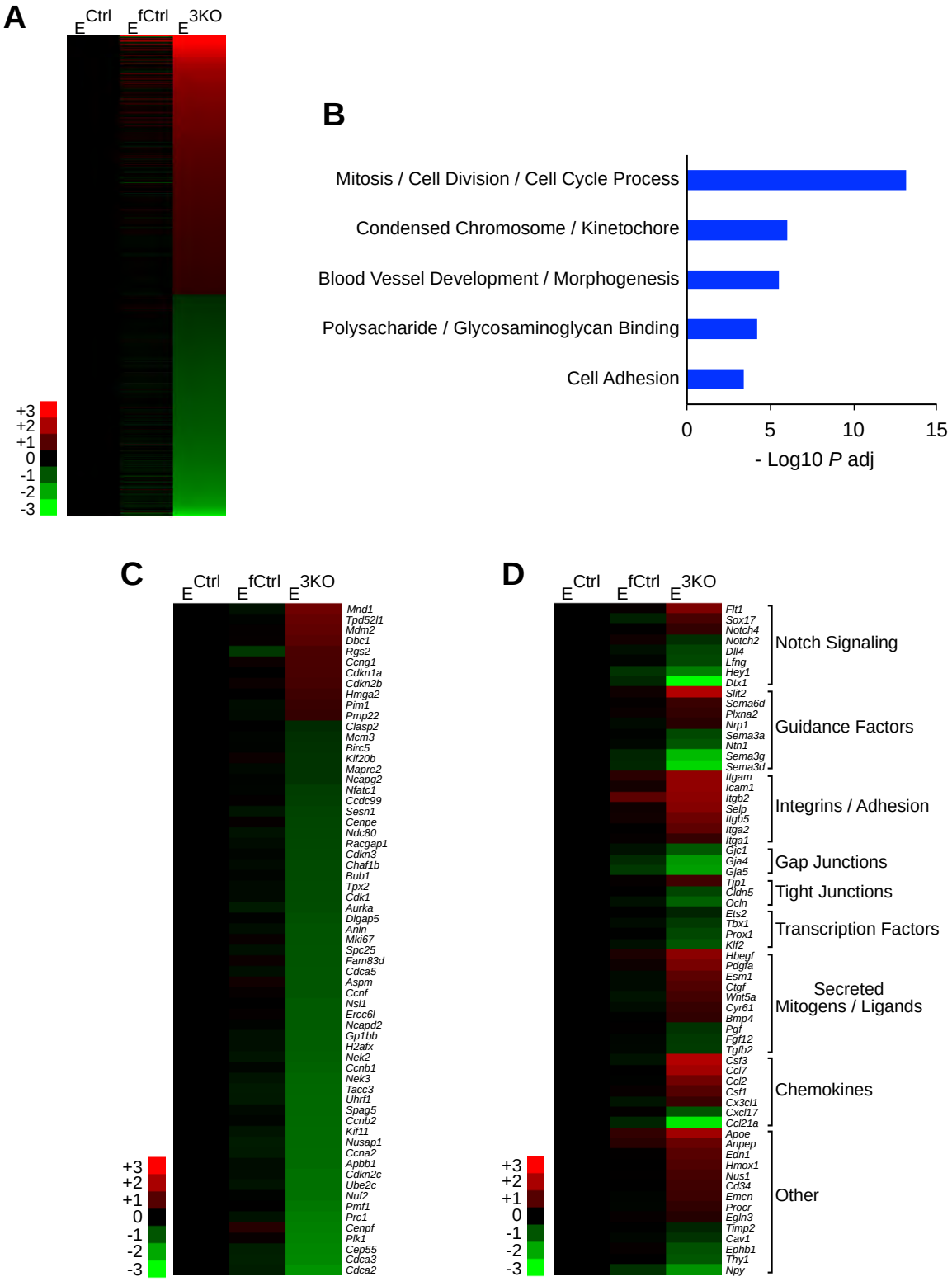

A
E Ctrl
E fCtrl
E 3KO
+3
+2
+1
0
-1
-2
-3
B
Mitosis / Cell Division / Cell Cycle Process
Condensed Chromosome / Kinetochore
Blood Vessel Development / Morphogenesis
Polysacharide / Glycosaminoglycan Binding
Cell Adhesion
0
5
10
15
- Log10 P adj
C
E Ctrl
E fCtrl
E 3KO
Mnd1
Tpd52l1
Mdm2
Dbc1
Rgs2
Ccng1
Cdkn1a
Cdkn2b
Hmga2
Pim1
Pmp22
Clasp2
Mcm3
Birc5
Kif20b
Mapre2
Ncapg2
Nfatc1
Ccdc99
Sesn1
Cenpe
Ndc80
Racgap1
Cdkn3
Chaf1b
Bub1
Tpx2
Cdk1
Aurka
Dlgap5
Anln
Mki67
Spc25
Fam83d
Cdca5
Aspm
Ccnf
Nsl1
Ercc6l
Ncapd2
Gp1bb
H2afx
Nek2
Ccnb1
Nek3
Tacc3
Uhrf1
Spag5
Ccnb2
Kif11
Nusap1
Ccna2
Apbb1
Cdkn2c
Ube2c
Nuf2
Pmf1
Prc1
Cenpf
Plk1
Cep55
Cdca3
Cdca2
+3
+2
+1
0
-1
-2
-3
D
E Ctrl
E fCtrl
E 3KO
Flt1
Sox17
Notch4
Notch2
Dll4
Lfng
Hey1
Dtx1
Notch Signaling
Slit2
Sema6d
Plxna2
Nrp1
Sema3a
Ntn1
Sema3g
Sema3d
Guidance Factors
Itgam
Icam1
Itgb2
Selp
Itgb5
Itga2
Itga1
Integrins / Adhesion
Gjc1
Gja4
Gja5
Gap Junctions
Tjp1
Cldn5
Ocln
Tight Junctions
Ets2
Tbx1
Prox1
Klf2
Transcription Factors
Hbegf
Pdgfa
Esm1
Ctgf
Wnt5a
Cyr61
Bmp4
Pgf
Fgf12
Tgfb2
Secreted
Mitogens / Ligands
Csf3
Ccl7
Ccl2
Csf1
Cx3cl1
Cxcl17
Ccl21a
Chemokines
Apoe
Anpep
Edn1
Hmox1
Nus1
Cd34
Emcn
Procr
Egln3
Timp2
Cav1
Ephb1
Thy1
Npy
Other
+3
+2
+1
0
-1
-2
-3

Figure II.9 RNA-Seq analysis of genes differentially regulated between control and JNK-deficient endothelial cells

A) Heatmap of the 781 differentially expressed genes (FPKM > 2; log_2 fold change ≤ -0.5 or ≥ +0.5; q ≤ 0.05) between E^{3KO} and control endothelial cells showing similar numbers of upregulated and downregulated genes in E^{3KO} cells (mean; n = 3 libraries per group prepared with RNA from 3 independent lung endothelial cell preparations per group. Each endothelial cell preparation included lungs from 4 mice).

B) Gene ontology analysis of the group of differentially expressed genes identifying significant enrichment in genes involved in several biological processes.

C) Genes related to mitosis/cell division/cell cycle processes that were identified by the gene ontology analysis are presented as a heatmap. Genes are displayed with highest upregulation top and highest downregulation bottom.

D) Genes related to vascular development/morphogenesis and function, including those identified by the gene ontology analysis, were grouped in several categories and are presented as a heatmap. Genes are displayed with highest upregulation top and highest downregulation bottom within each category.

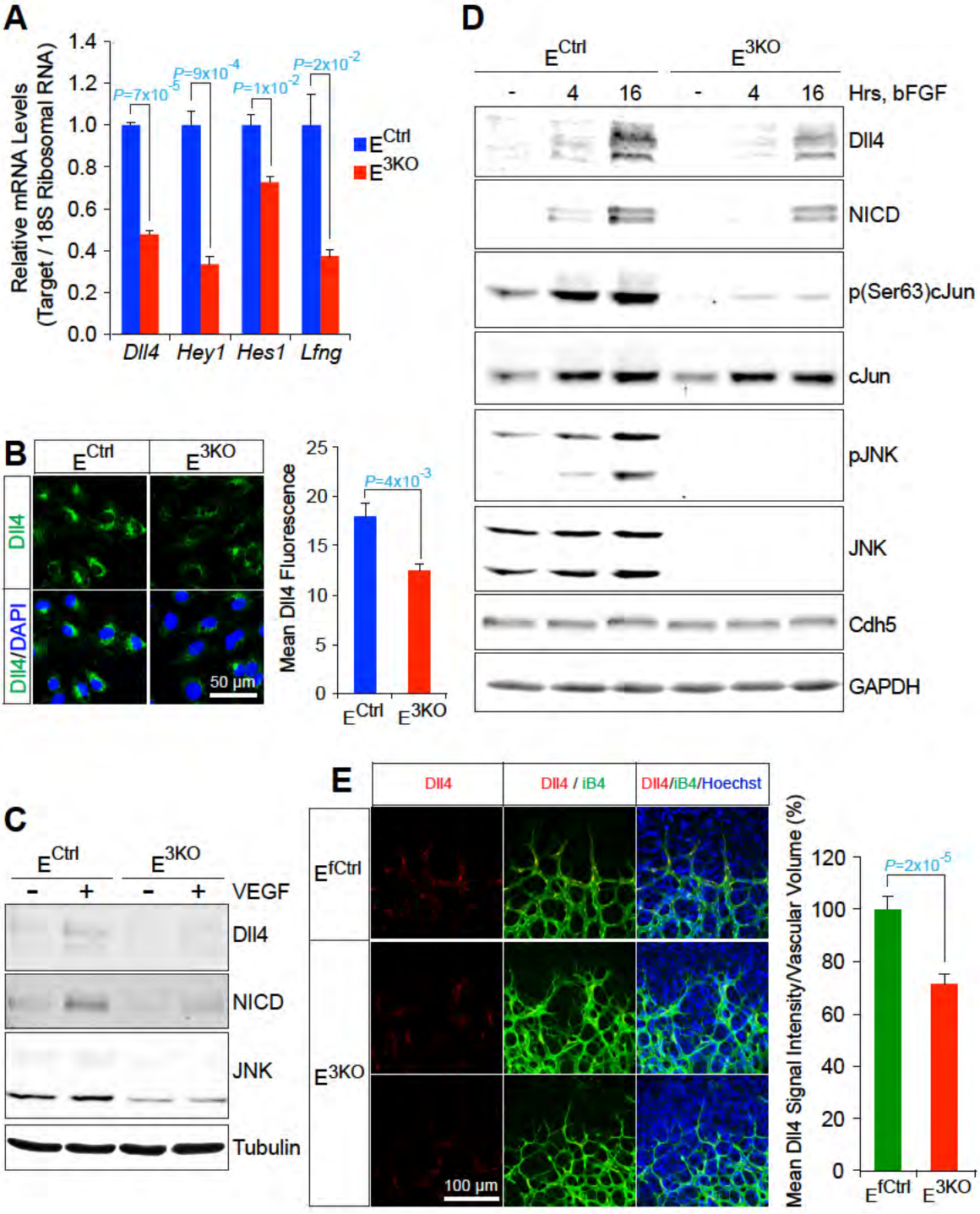

A
Relative mRNA Levels (Target / 18S Ribosomal RNA)
1.4
1.2
1.0
0.8
0.6
0.4
0.2
0.0
P=7x10-5
P=9x10-4
P=1x10-2
P=2x10-2
ECtrl
E3KO
Dll4
Hey1
Hes1
Lfng
B
ECtrl
E3KO
Dll4
Dll4/DAPI
50 μm
Mean Dll4 Fluorescence
25
20
15
10
5
0
P=4x10-3
ECtrl
E3KO
C
ECtrl
E3KO
- + - +
VEGF
Dll4
NICD
JNK
Tubulin
D
ECtrl
E3KO
- 4 16 - 4 16
Hrs, bFGF
Dll4
NICD
p(Ser63)cJun
cJun
pJNK
JNK
Cdh5
GAPDH
E
Dll4
Dll4 / iB4
Dll4/iB4/Hoechst
EfCtrl
E3KO
100 μm
Mean Dll4 Signal Intensity/Vascular Volume (%)
120
100
80
60
40
20
0
P=2x10-5
EfCtrl
E3KO

Figure II.10 Reduced Dll4 – Notch signaling in the JNK-deficient vascular endothelium

A) Quantitative RT-PCR analysis of Notch pathway genes revealing reduced expression in E^{3KO} endothelial cells compared to control cells (mean ± SEM; n = 4). Data shown represent one of three independent experiments with similar results. Each experiment was performed with independent endothelial cell preparations.

B) Immunofluorescence analysis on endothelial cells showing reduced Dll4 immunostaining in E^{3KO} cells compared to control cells. Quantification of Dll4 signal intensity demonstrates the difference is statistically significant (mean ± SEM; n = 10 images per group).

C) Endothelial cells were treated with VEGF for 16 hrs. Immunoblot analysis of cell lysates revealed reduced levels of Dll4 and Notch intracellular domain (NICD) in lysates from E^{3KO} endothelial cells compared to control cells. Lysates were also examined with antibodies to JNK and α-Tubulin. Data are representative of two experiments with independent endothelial cells preparations.

D) Endothelial cells were treated with bFGF for 4 or 16 hrs. Immunoblot analysis of cell lysates revealed reduced levels of Dll4 and NICD in lysates from E^{3KO} endothelial cells compared to control cells. Lysates were also examined with antibodies to phospho-cJun (pSer63), cJun, phospho-JNK (pJNK), JNK, Cdh5 and GAPDH. Data are representative of two experiments with independent endothelial cell preparations.

E) Confocal immunofluorescence analysis of P6 retina wholemounts immunostained for Dll4 (red), and isolectinB4 (iB4, green) reveals reduced Dll4 signal intensity at the angiogenic vascular front of retinas from E^{3KO} mice compared to retinas from littermate control mice. Hoechst labels cell nuclei. Quantification of Dll4 signal intensity shows this difference is statistically significant (mean ± SEM; n = 42-44 images per group, retinas from 6 mice per group were analyzed).

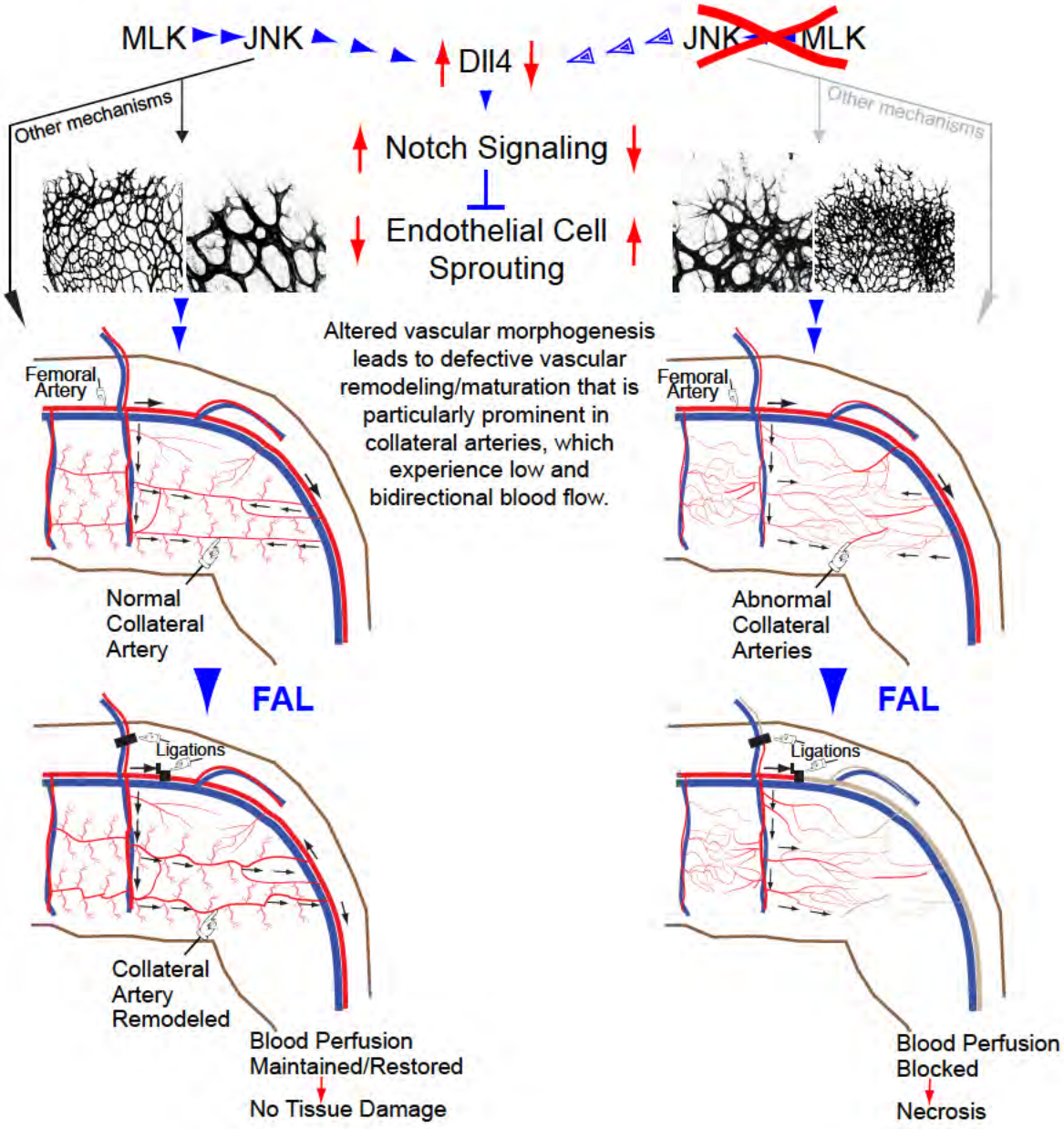

MLK
JNK
Dll4
JNK
MLK
Other mechanisms
Other mechanisms
Notch Signaling
Endothelial Cell Sprouting
Altered vascular morphogenesis leads to defective vascular remodeling/maturation that is particularly prominent in collateral arteries, which experience low and bidirectional blood flow.
Femoral Artery
Femoral Artery
Normal Collateral Artery
Abnormal Collateral Arteries
FAL
FAL
Ligations
Ligations
Collateral Artery Remodeled
Blood Perfusion Maintained/Restored
No Tissue Damage
Blood Perfusion Blocked
Necrosis

Figure II.11 Diagram illustrating the functional importance of collateral arteries during arterial occlusion, and the collateral artery patterning / maturation defects and functional impairment in mice with disrupted MLK – JNK signaling.

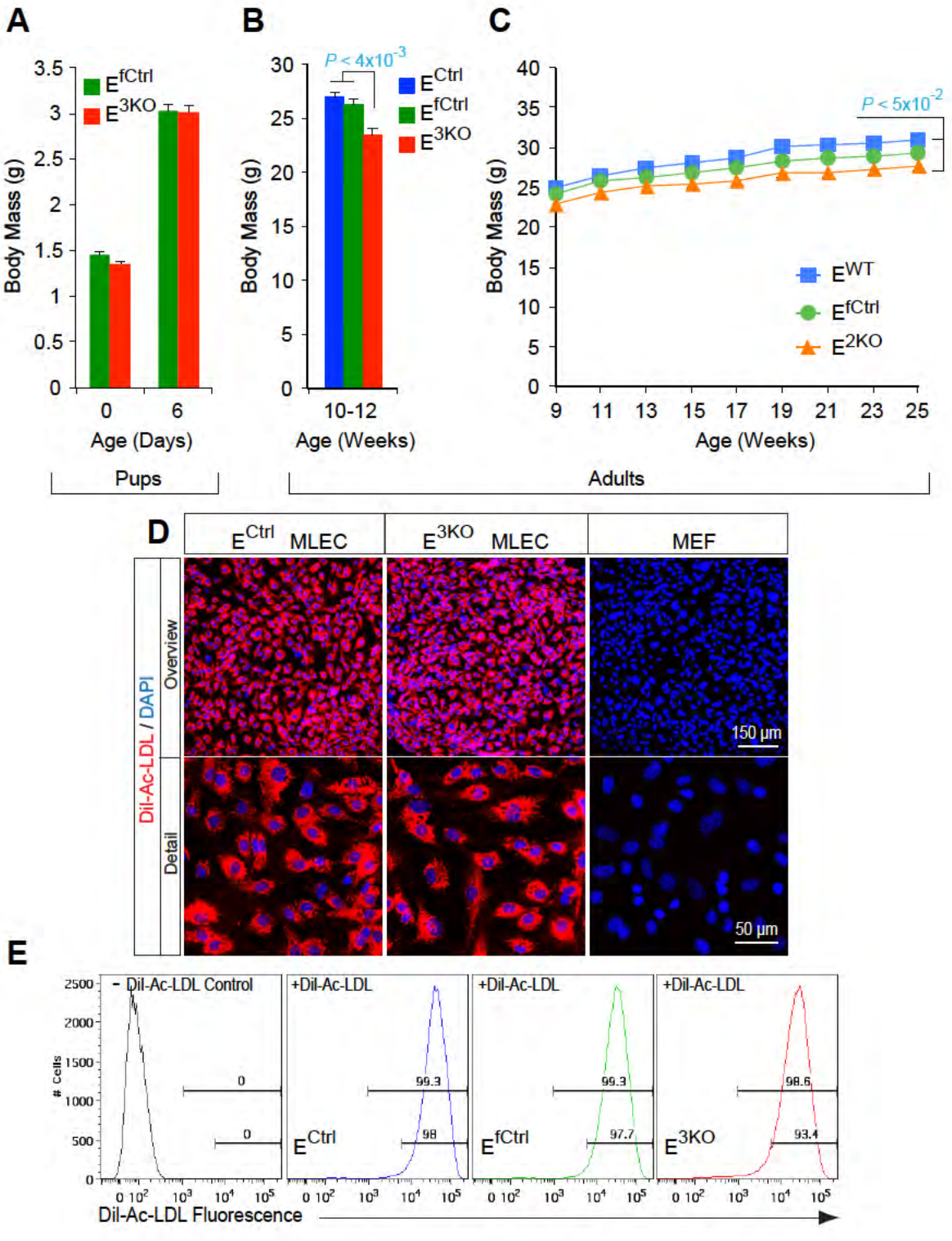
MLK-JNK signaling (left) contributes to high Dll4-Notch signaling in endothelial cells leading to formation of balanced vascular networks and formation of distinct collateral vessels that interconnect adjacent arteries.

Disrupted MLK-JNK signaling in the vascular endothelium (right) results in excessive sprouting angiogenesis, leading to hyperbranched vascular networks and defective formation of collateral arteries, which are smaller, display excessive branching and altered organization.

In addition to regulating Dll4-Notch signaling, the MLK-JNK pathway may also contribute to proper vascular morphogenesis and collateral artery formation via other mechanisms.

Following FAL blood flow (black arrows) through the femoral artery is blocked. Under these circumstances due to increased proximal and reduced distal pressure, more blood flow is diverted to the collateral circulation. Existing collateral arteries in the proximal adductor muscles are capable of restoring a significant amount of blood flow to the distal limb immediately following occlusion of the femoral artery. The increased pressure and flow stimulates the remodeling of existing collateral arteries, which increase in size and restore blood perfusion to the distal limb, limiting ischemic damage in control mice (left).

The abnormal collateral circulation in the absence of MLK-JNK signaling prevents sufficient blood flow restoration to distal limb tissues following FAL resulting in enhanced blood perfusion reduction. The ensuing hypoxia and ischemia leads to severe necrotic damage to the distal limb (right).

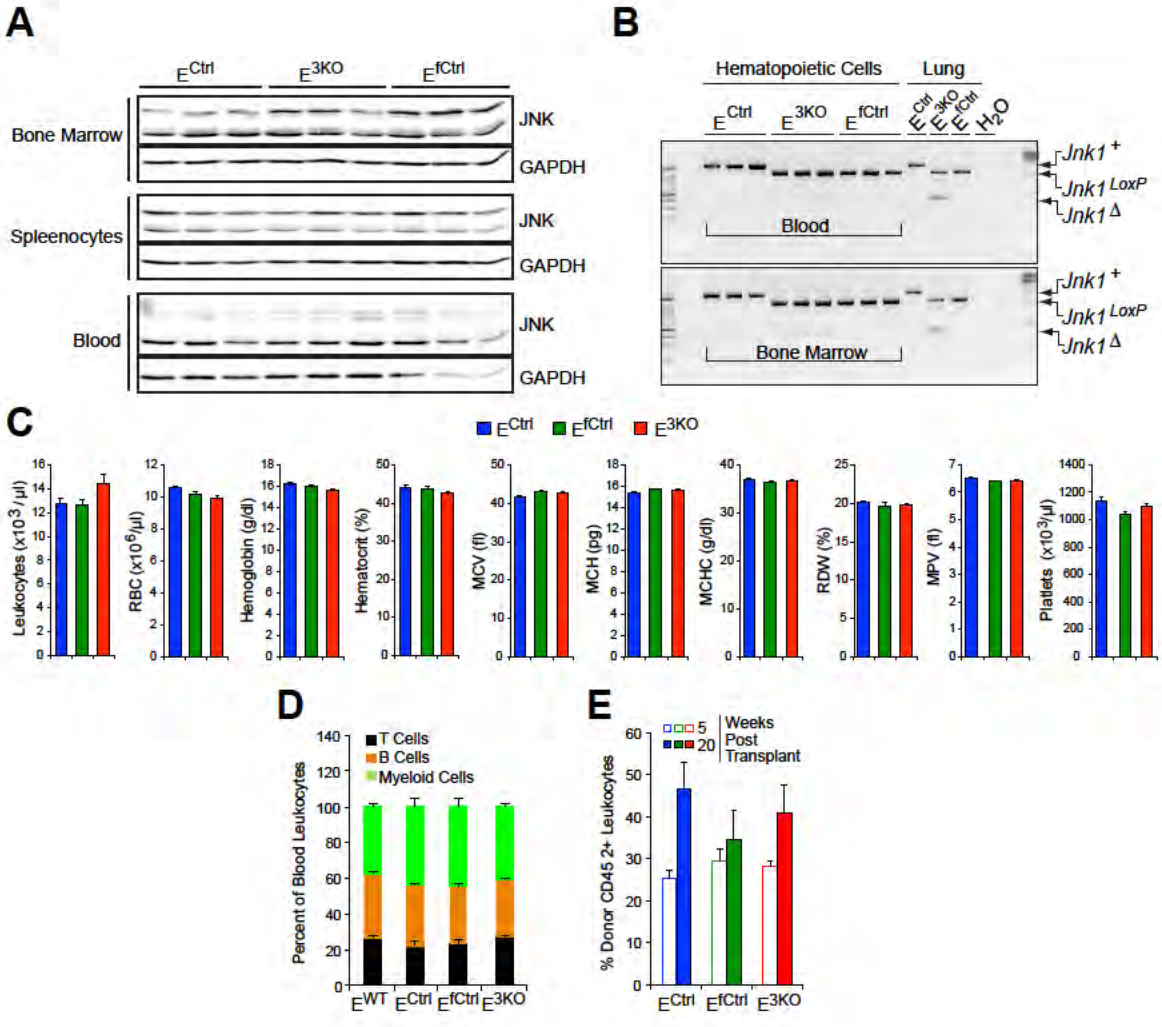

A
B
C
Body Mass (g)
E^fCtrl
E^3KO
Age (Days)
Pups
P < 4x10^-3
E^Ctrl
E^fCtrl
E^3KO
10-12
Age (Weeks)
P < 5x10^-2
E^WT
E^fCtrl
E^2KO
Age (Weeks)
Adults
D
E^Ctrl MLEC
E^3KO MLEC
MEF
Dil-Ac-LDL / DAPI
Overview
Detail
150 µm
50 µm
E
- Dil-Ac-LDL Control
+Dil-Ac-LDL
+Dil-Ac-LDL
+Dil-Ac-LDL
Cells
99.3
98
E^Ctrl
99.3
97.7
E^fCtrl
98.6
93.4
E^3KO
Dil-Ac-LDL Fluorescence

Supplementary Figure II.1 Characterization of endothelial JNK-deficient mice and lung endothelial cells.

A-C) Body mass measurements showing no significant differences between E^{3KO} and littermate control mice at postnatal day 0 and 6. Adult endothelial JNK-deficient mice are slightly smaller than control mice (**B**), but continue to maintain their body mass similar to control mice (**C**), (mean ± SEM; n = ~8-23).

D) Following two rounds of ICAM2 antibody-conjugated magnetic bead purification, endothelial cell monolayers show efficient and homogeneous uptake of Dil-labeled acetylated low density lipoprotein (Dil-Ac-LDL, red). Mouse embryonic fibroblasts (MEF) show no Dil-Ac-LDL uptake.

E) Flow cytometry analysis confirming that ~99% of cells in endothelial cell preparations stained for Dil-Ac-LDL.


A
E^Ctrl
E^3KO
E^fCtrl
Bone Marrow
Spleenocytes
Blood
JNK
GAPDH
B
Hematopoietic Cells
Lung
E^Ctrl
E^3KO
E^fCtrl
E^Ctrl
E^3KO
E^fCtrl
H2O
Blood
Bone Marrow
Jnk1 +
Jnk1 LoxP
Jnk1 Δ
C
E^Ctrl
E^fCtrl
E^3KO
Leukocytes (x10^3/μl)
RBC (x10^6/μl)
Hemoglobin (g/dl)
Hematocrit (%)
MCV (fl)
MCH (pg)
MCHC (g/dl)
RDW (%)
MPV (fl)
Platlets (x10^3/μl)
D
T Cells
B Cells
Myeloid Cells
Percent of Blood Leukocytes
E^WT
E^Ctrl
E^fCtrl
E^3KO
E
5
20
Weeks Post Transplant
% Donor CD45 2+ Leukocytes
E^Ctrl
E^fCtrl
E^3KO

Supplementary Figure II.2 Endothelial JNK-deficient mice have no major perturbations in the hematopoietic system.

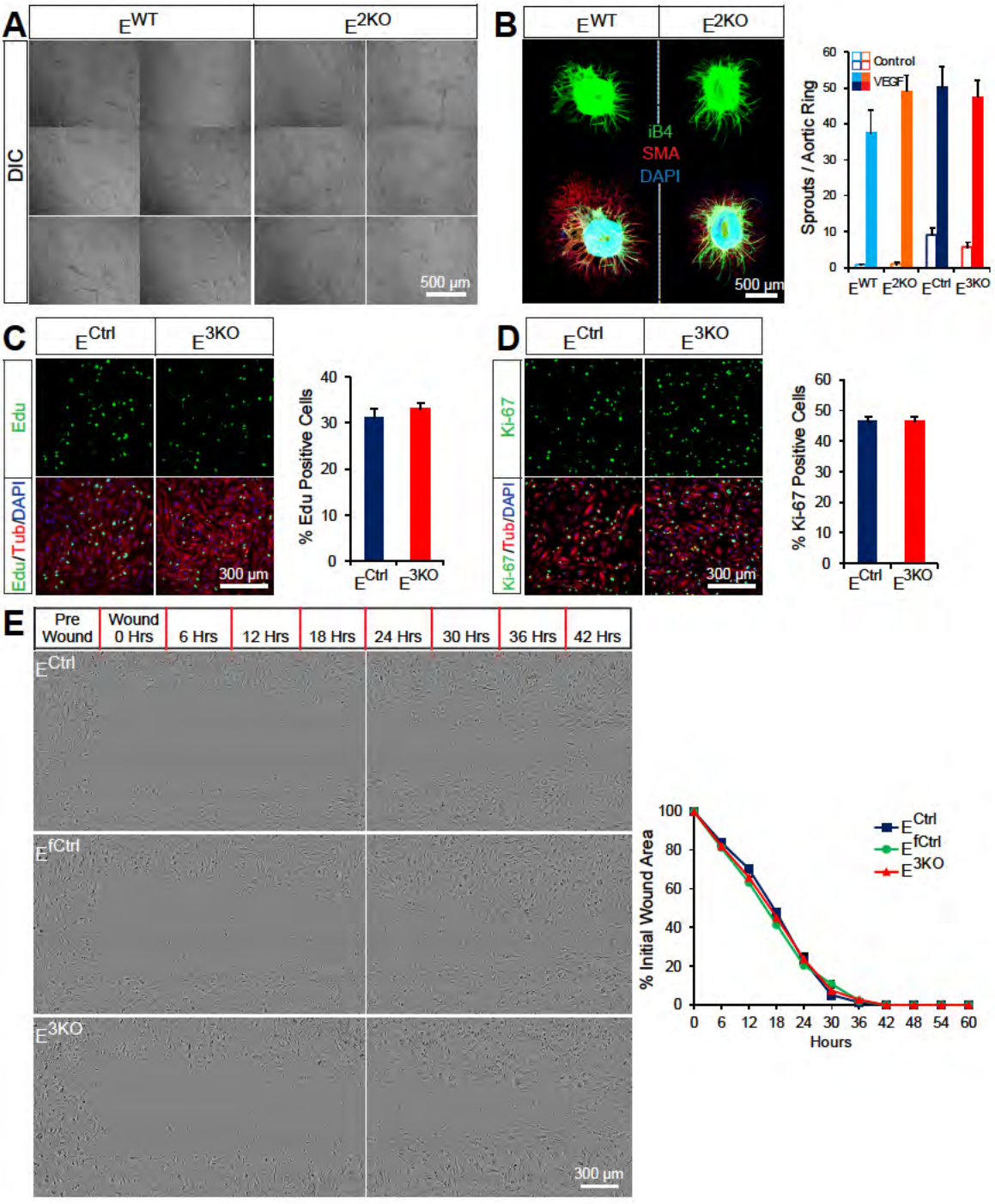
A) Immunoblot analysis demonstrating no major differences in JNK protein abundance in hematopoietic tissues. The data presented are representative of 2 independent experiments (n=5 mice)

B) Genomic DNA isolated from blood, bone marrow, and lung tissue was examined by PCR analysis to detect Cre-mediated recombination of the Jnk1 gene (n=3 mice).

C) Complete blood cell analysis showing no significant JNK-dependent differences in any of the measured indices (mean ± SEM; n = 15). RBC, red blood cells; MCV, mean corpuscular volume; MCH, mean corpuscular hemoglobin; MCHC, mean corpuscular hemoglobin concentration; RDW, red cell distribution width; MPV, mean platelet volume.

D) Flow cytometry analysis demonstrating no significant differences in the frequency of myeloid cells ($CD11b^+$), B cells ($CD19^+$) and T cells ($CD3e^+$) in the blood of E^{3KO} and control mice (mean ± SEM; n = ~8-10).

E) Flow cytometry analysis of peripheral blood showing no significant differences in chimerism at 5 and 20 weeks post-transplantation between mice transplanted with bone marrow cells from E^{3KO} or control mice (mean ± SEM; n = ~7-8).


A
E^WT
E^2KO
DIC
500 μm
B
E^WT
E^2KO
iB4
SMA
DAPI
500 μm
Control
VEGF
Sprouts / Aortic Ring
E^WT E^2KO E^Ctrl E^3KO
C
E^Ctrl
E^3KO
Edu
Edu/Tub/DAPI
300 μm
% Edu Positive Cells
E^Ctrl E^3KO
D
E^Ctrl
E^3KO
Ki-67
Ki-67/Tub/DAPI
300 μm
% Ki-67 Positive Cells
E^Ctrl E^3KO
E
Pre Wound
Wound 0 Hrs
6 Hrs
12 Hrs
18 Hrs
24 Hrs
30 Hrs
36 Hrs
42 Hrs
E^Ctrl
E^fCtrl
E^3KO
300 μm
% Initial Wound Area
Hours
E^Ctrl
E^fCtrl
E^3KO

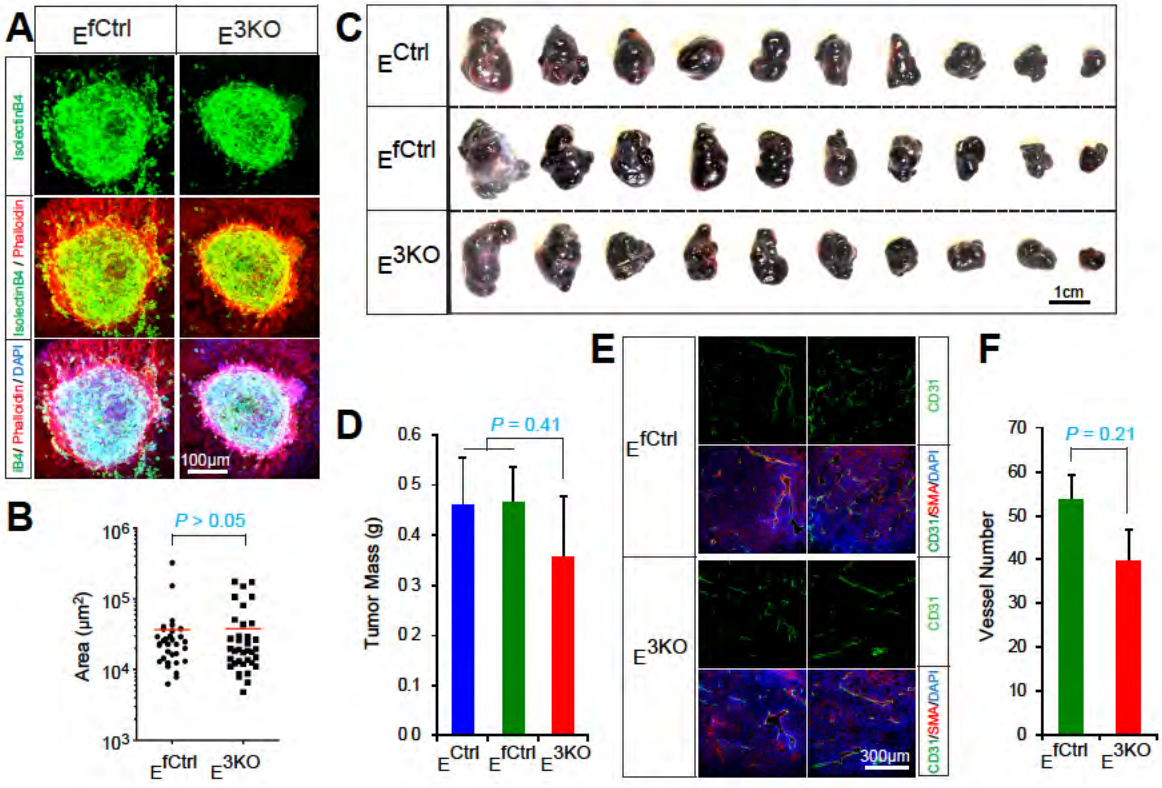
Supplementary Figure II.3 Endothelial JNK is dispensable for proliferation, migration and angiogenic responses *in vitro*.

A) JNK-deficient endothelial cells form tubular networks in matrigel similarly to control endothelial cells. Images are representative of two experiments performed in triplicate with independent endothelial cell preparations.

B) Representative maximum projection confocal images of collagen imbedded aortic ring explants showing similar numbers of VEGF-induced iB4 (green) positive microvessels sprouting from aortic rings from control and endothelial JNK-deficient mice. Smooth muscle actin (SMA) immunofluorescence (red) labels supporting cells. DAPI (blue) labels nuclei. Quantification of microvessel number per aortic ring demonstrated no significant differences between aortic rings from control and JNK-deficient mice (mean ± SEM; n = ~8-21 rings per group). Data presented are from one of three experiments with similar results. Aortas from 2-3 mice per group were used in each experiment.

C and **D**) Representative confocal images and quantification of the percentage of endothelial cells incorporating Edu (green, **C**) following a 6 hour Edu pulse or staining positive for the proliferation marker Ki-67 (green, **D**), (mean ± SEM; n = 10 images per group). Data presented are from one of three experiments with similar results. α-Tubulin (red) labels cell bodies. DAPI (blue) labels nuclei.

E) Endothelial monolayers were wounded using a Woundmaker and wound closure was monitored over time. Representative images showing similar migratory ability of JNK-deficient endothelial cells. Quantification of wound area closure over time demonstrated no statistically significant differences between JNK-deficient and control endothelial cells (mean ± SEM; n = 8). Data presented are from one of three experiments with similar results.

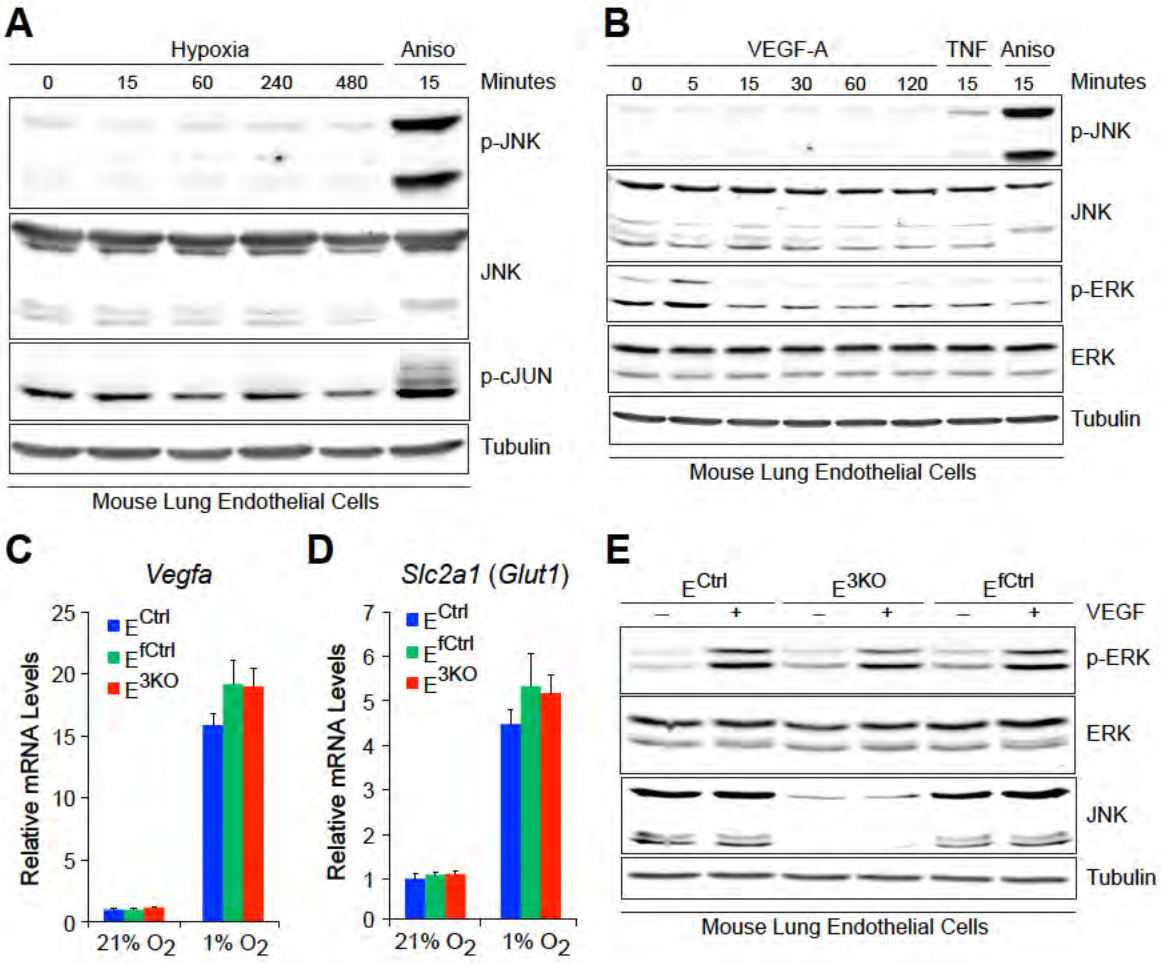

A
E^fCtrl
E^3KO
IsolectinB4
IsolectinB4 / Phalloidin
IB4/ Phalloidin/ DAPI
100μm
B
P > 0.05
Area (μm²)
10⁶
10⁵
10⁴
10³
E^fCtrl
E^3KO
C
E^Ctrl
E^fCtrl
E^3KO
1cm
D
P = 0.41
Tumor Mass (g)
0.6
0.5
0.4
0.3
0.2
0.1
0.0
E^Ctrl
E^fCtrl
E^3KO
E
E^fCtrl
E^3KO
CD31
CD31/SMA/DAPI
CD31
CD31/SMA/DAPI
300μm
F
P = 0.21
Vessel Number
70
60
50
40
30
20
10
0
E^fCtrl
E^3KO

Supplementary Figure II.4 Endothelial JNK is dispensable for *in vivo* pathologic angiogenesis.

A and **B**) Representative examples of iB4 positive laser-induced choroidal neovascular (CNV) tufts 7 days post-lasering in control and E^{3KO} mice (**A**). Quantification of CNV size (**B**) shows no statistically significant differences between the two groups (mean ± SEM; n = ~32-36 CNV tufts) from 5 mice per group.

C and **D**) Images of tumors grown in the flanks of E^{3KO} and control mice following subcutaneous transplantation of congenic B16F10 melanoma cells. (**D**) Quantification of tumor weight shows no statistically significant differences between E^{3KO} and control mice (mean ± SEM; n = 10 tumors). Data presented are from one of two experiments with 5 mice per group.

E and **F**) Examples of CD31 (green) immunofluorescence images of B16F10 melanoma tumor cryosections showing similar vascularization of tumors from E^{3KO} and control mice. Smooth muscle actin (SMA, red) labels supporting cells. DAPI (blue) labels nuclei. (**F**) Quantification of vessel number in tumor cryosections showing no significant differences between tumors from E^{3KO} and control mice (mean ± SEM; n = 5 mice, 5-6 images from tumors from each mouse were quantified and averaged per mouse).


A
Hypoxia
Aniso
0
15
60
240
480
15
Minutes
p-JNK
JNK
p-cJUN
Tubulin
Mouse Lung Endothelial Cells
B
VEGF-A
TNF
Aniso
0
5
15
30
60
120
15
15
Minutes
p-JNK
JNK
p-ERK
ERK
Tubulin
Mouse Lung Endothelial Cells
C
Vegfa
Relative mRNA Levels
E Ctrl
E fCtrl
E 3KO
21% O2
1% O2
D
Slc2a1 (Glut1)
Relative mRNA Levels
E Ctrl
E fCtrl
E 3KO
21% O2
1% O2
E
E Ctrl
E 3KO
E fCtrl
–
+
–
+
–
+
VEGF
p-ERK
ERK
JNK
Tubulin
Mouse Lung Endothelial Cells

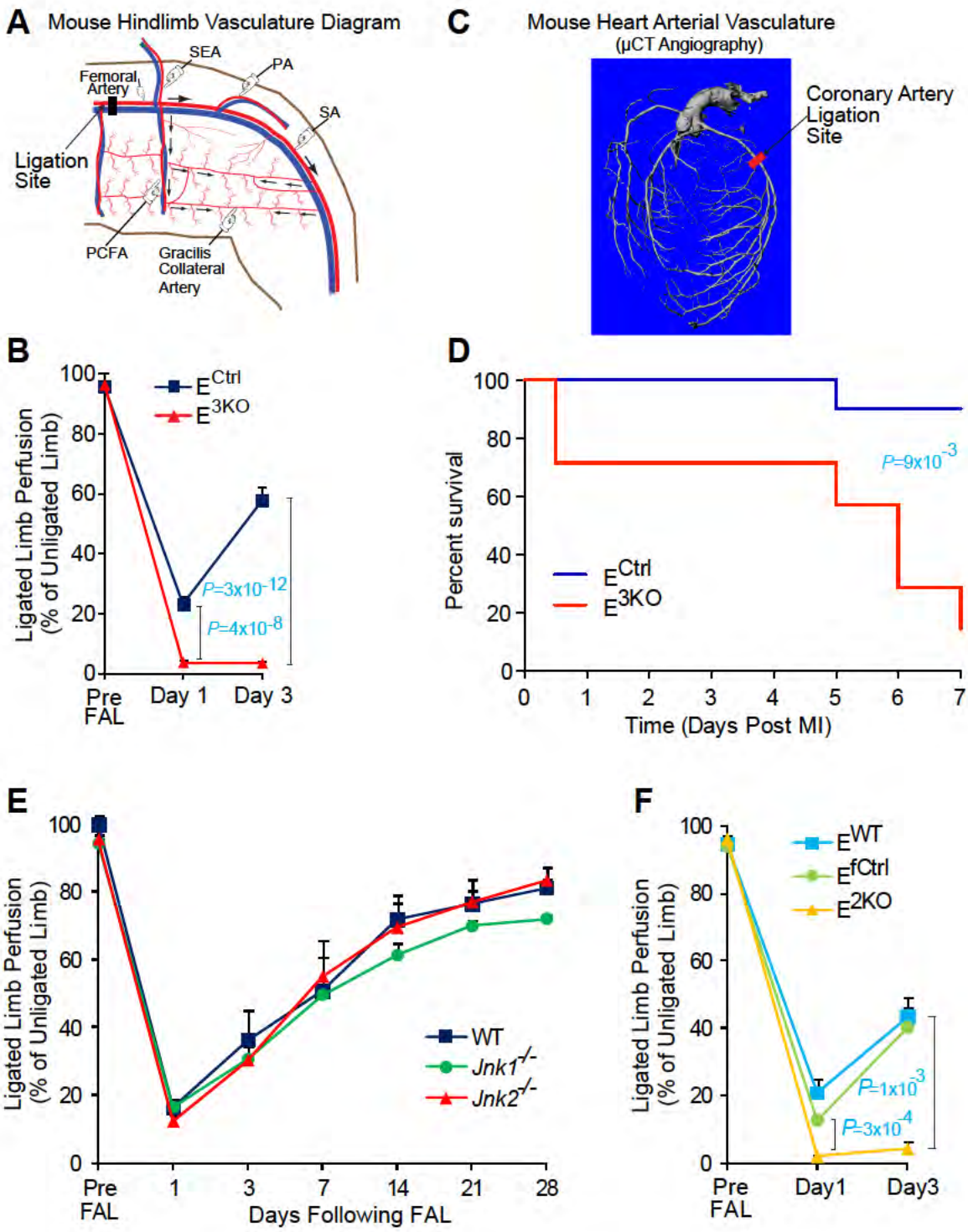
Supplementary Figure II.5 Normal hypoxia responses and VEGF signaling in JNK-deficient endothelial cells.

A) Endothelial cells incubated overnight in media containing only 1% FBS were placed under hypoxic (1% O_2) conditions for the indicated times and extracts were examined by immunoblot analysis with antibodies to p-JNK, JNK, p(S63)-cJun, and α-Tubulin. No change in the phosphorylation of JNK or its substrate cJun is detected. Anisomycin (Aniso, 1µg/ml) treatment causes robust JNK and cJun phosphorylation. Data presented are representative of two independent experiments.

B) Endothelial cells incubated overnight in media containing only 1% FBS were treated with VEGFa (100 ng/ml, added directly to existing media) for the indicated times and extracts were examined by immunoblot analysis with antibodies to p-JNK, JNK, p-ERK, ERK and α-Tubulin. VEGFa treatment leads to phosphorylation of ERK at 5 minutes, but not JNK. TNF (20 ng/ml) and Anisomycin (Aniso, 1 µg /ml) treatment leads to JNK phosphorylation. Data presented are representative of two independent experiments.

C and **D**) Endothelial cells in media containing only 1% FBS were incubated under normoxic (21% O_2) or hypoxic (1% O_2) conditions for 16 hours. The mRNA expression of the hypoxia responsive genes *Vegfa* (**C**) and *Slc2a1* (**D**) was examined by quantitative RT-PCR analysis (mean ± SEM; n = 4). Data presented are from one of at least 2 similar experiments with independent endothelial cell preparations.

E) Endothelial cells incubated overnight in media containing only 1% FBS were treated with VEGFa (100 ng/ml, added directly to existing media) for 5 minutes and extracts were examined by immunoblot analysis with antibodies to p-ERK, ERK, JNK and Tubulin. VEGFa-stimulated ERK phosphorylation was similar in JNK-deficient and control cells. Data presented are representative of two experiments with independent endothelial cell preparations.


A
Mouse Hindlimb Vasculature Diagram
SEA
PA
Femoral Artery
SA
Ligation Site
PCFA
Gracilis Collateral Artery
C
Mouse Heart Arterial Vasculature
(μCT Angiography)
Coronary Artery Ligation Site
B
Ligated Limb Perfusion (% of Unligated Limb)
E^Ctrl
E^3KO
P=3x10^-12
P=4x10^-8
Pre FAL
Day 1
Day 3
D
Percent survival
P=9x10^-3
E^Ctrl
E^3KO
Time (Days Post MI)
E
Ligated Limb Perfusion (% of Unligated Limb)
WT
Jnk1-/-
Jnk2-/-
Pre FAL
Days Following FAL
F
Ligated Limb Perfusion (% of Unligated Limb)
E^WT
E^fCtrl
E^2KO
P=1x10^-3
P=3x10^-4
Pre FAL
Day1
Day3

Supplementary Figure II.6 Compound endothelial deficiency of JNK1 plus JNK2 leads to enhanced blood perfusion blockade in models of arterial occlusion.

A) Simplified diagram of the medial aspect of the mouse hindlimb skeletal muscle vasculature indicating the location of the femoral artery ligation site for the experiment shown in panel **B**. Unlike experiments described in Figure I.1, the ligation site indicated here is proximal to the PCFA.

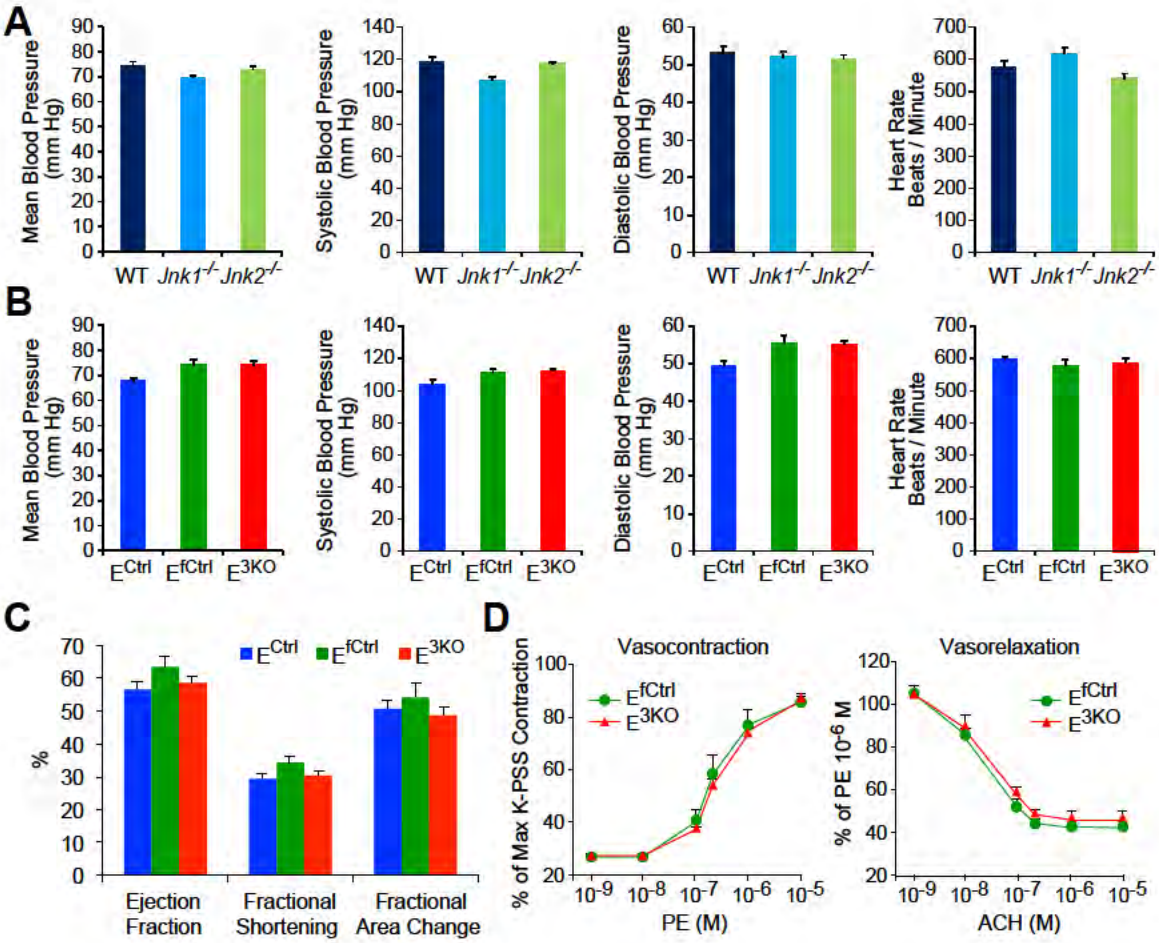
B) Following ligation of the femoral artery at its origin as shown in panel **A**, quantification of limb blood perfusion by laser Doppler imaging shows significantly enhanced blood perfusion blockade and no recovery 3 days after ligation in E^{3KO} mice (mean ± SEM; n = ~7-14).

C) Simplified diagram of the coronary artery circulation indicating the location of the coronary artery ligation site for the experiment shown in panel **D**.

D) Following coronary artery ligation as shown in panel **C**, E^{3KO} mice show significantly decreased survival (n = ~7-10).

E) Following FAL as shown in panel **A**, laser Doppler quantification of limb blood perfusion shows no significant differences in blood perfusion blockade and recovery over 28 days in single *Jnk1*$^{-/-}$ or *Jnk2*$^{-/-}$ mice compared to WT mice (mean ± SEM; n = 5).

F) Following FAL as shown in Figure I.B, quantification of limb blood perfusion by laser Doppler imaging shows significantly enhanced blood perfusion blockade and no recovery 3 days after ligation in E^{2KO} mice (mean ± SEM; n = 4).


A
Mean Blood Pressure (mm Hg)
Systolic Blood Pressure (mm Hg)
Diastolic Blood Pressure (mm Hg)
Heart Rate Beats / Minute
WT
Jnk1-/-
Jnk2-/-
B
ECtrl
EfCtrl
E3KO
C
%
Ejection Fraction
Fractional Shortening
Fractional Area Change
D
Vasocontraction
% of Max K-PSS Contraction
PE (M)
Vasorelaxation
% of PE 10-6 M
ACH (M)

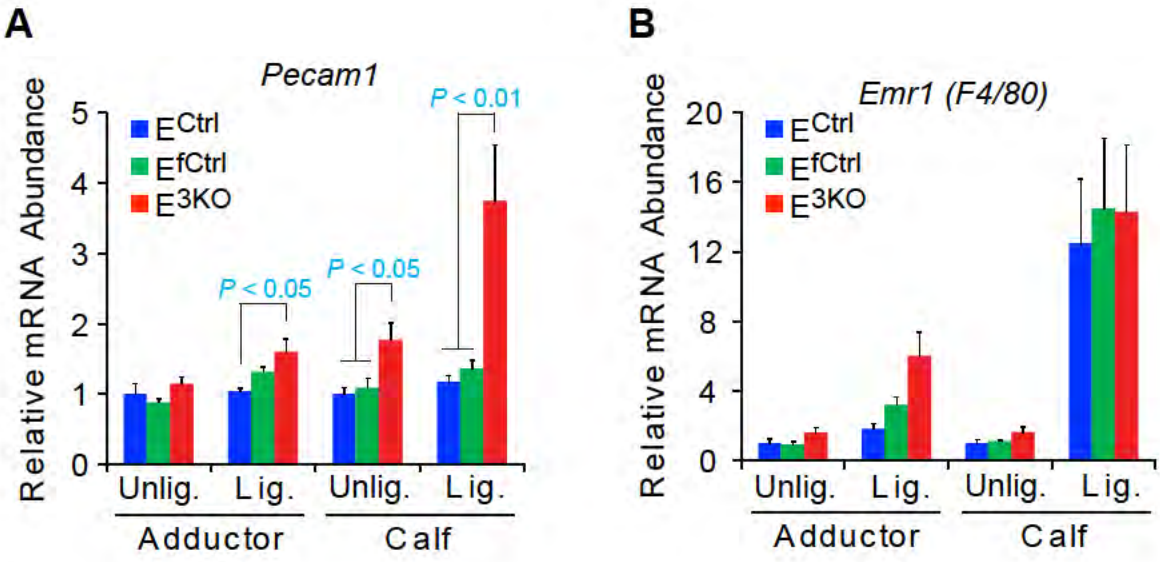
Supplementary Figure II.7 JNK deficient mice show no perturbations in overall cardiovascular function.

A) Analysis of blood pressure and heart rate in WT and single *Jnk1*$^{-/-}$ and *Jnk2*$^{-/-}$ mice showing no statistically significant differences (mean ± SEM; n = ~9-15).

B) Analysis of blood pressure and heart rate in E^{3KO} and control mice showing no JNK-dependent statistically significant differences between the groups (mean ± SEM; n = ~9-15).

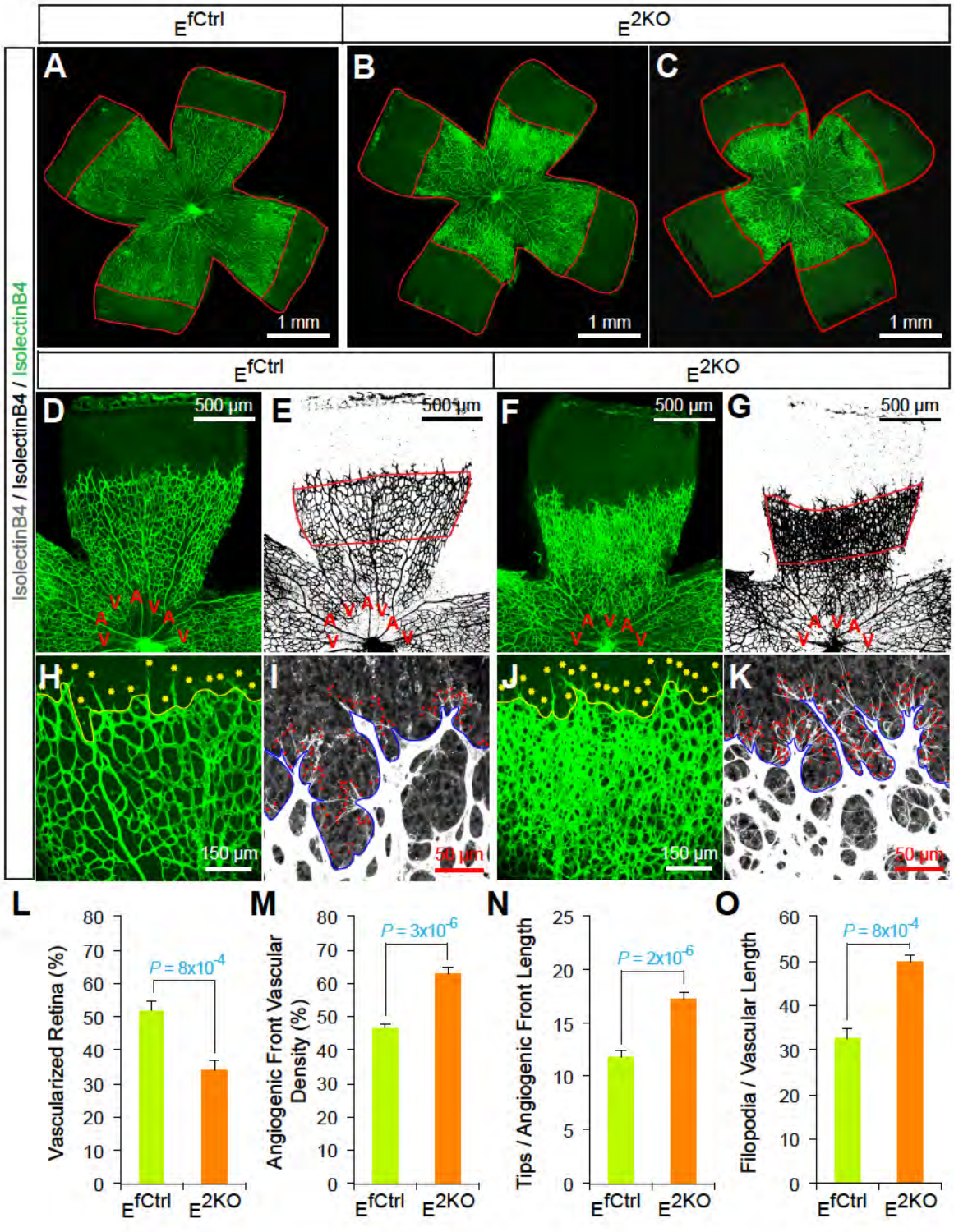
C) Echocardiographic analysis of heart function in E^{3KO} and control mice showing no statistically significant differences between the groups (mean ± SEM; n = ~12-15).

D) Segments from thoracic aortas from E^{3KO} and control mice were mounted on a myograph and vasocontraction and vasorelaxation in response to increasing doses of phenylephrine (PE) or acetylcholine (ACH) respectively were recorded. Contraction in response to PE is expressed as a percentage of maximum aortic contraction obtained in the presence of K^+ containing buffer (K-PSS). Vasorelaxation in response to ACH is expressed as a percentage of maximum contraction obtained in the presence of 10^{-3} µM PE (mean ± SEM; n =2 m). Data presented are from one of two experiments with similar results. Aortas from 2 mice per group were used in each experiment.


A
Pecam1
Relative mRNA Abundance
E^Ctrl
E^fCtrl
E^3KO
P < 0.05
P < 0.05
P < 0.01
0
1
2
3
4
5
Unlig.
Lig.
Unlig.
Lig.
Adductor
Calf
B
Emr1 (F4/80)
Relative mRNA Abundance
E^Ctrl
E^fCtrl
E^3KO
0
4
8
12
16
20
Unlig.
Lig.
Unlig.
Lig.
Adductor
Calf

Supplementary Figure II.8 Gene expression analysis in adductor and calf muscles of E^{3KO} and control mice.

A and **B**) Taqman gene expression analysis quantitating the mRNA abundance of the endothelial cell specific marker *Pecam1* (**A**) and the macrophage specific marker *Emr1* (**B**) on day 4 post FAL (mean ± SEM; n = ~7-8 mice per group).

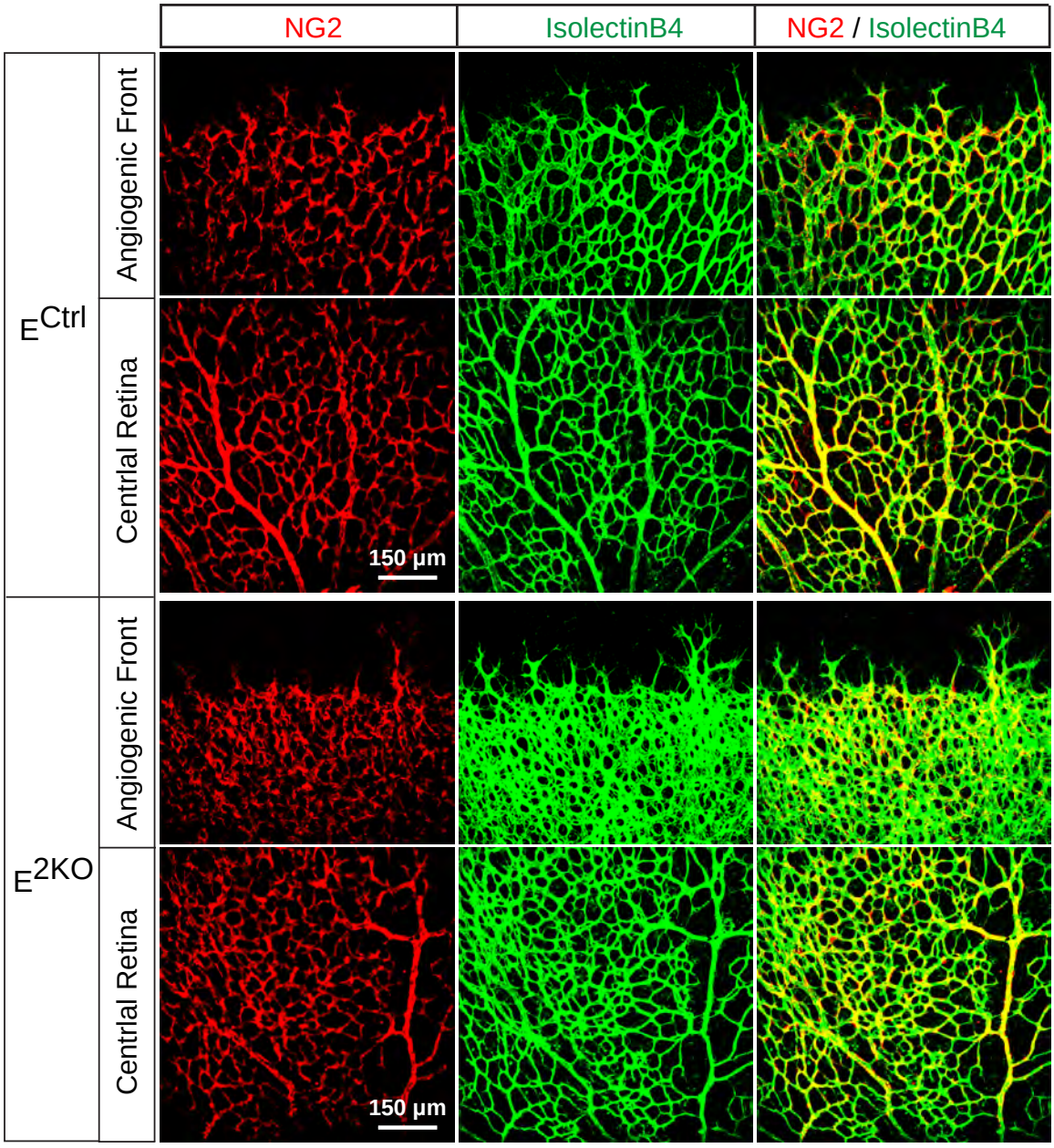

E^fCtrl
E^2KO
A
B
C
1 mm
IsolectinB4 / IsolectinB4 / IsolectinB4
D
E
F
G
500 µm
H
I
J
K
150 µm
50 µm
L
M
N
O
Vascularized Retina (%)
Angiogenic Front Vascular Density (%)
Tips / Angiogenic Front Length
Filopodia / Vascular Length
P = 8x10^-4
P = 3x10^-6
P = 2x10^-6
P = 8x10^-4
E^fCtrl
E^2KO

Supplementary Figure II.9 Abnormal retinal vascular development marked by excessive sprouting in E^{2KO} mice

A-**C**) Representative examples of whole mount retina iB4 immunofluorescence showing reduced vascular extension in P6 E^{2KO} retinas (**B** and **C**) compared to littermate control retinas (**A**).

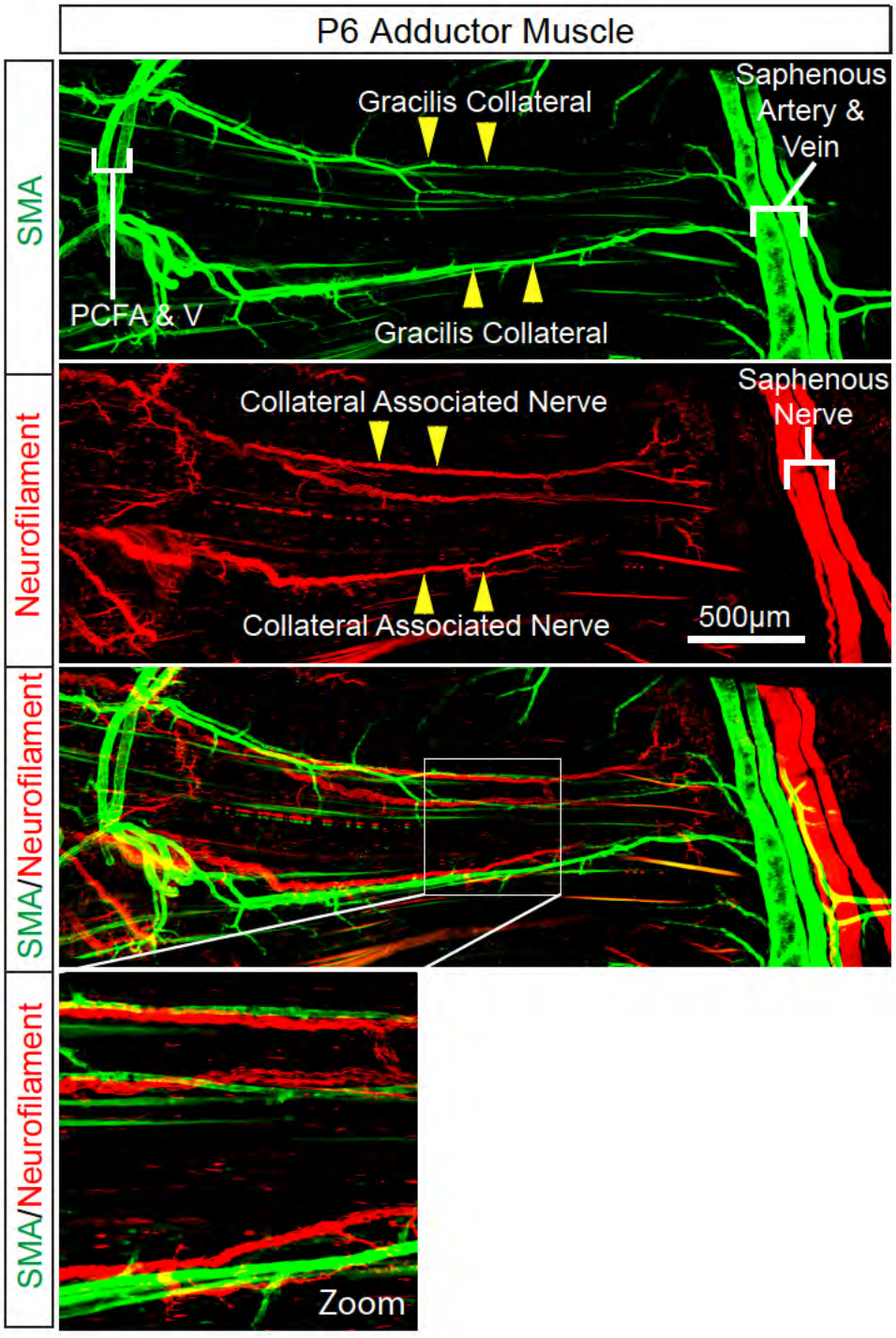
D-**K**) Closer examination reveals increased vascular density (**D**-**G** and **H** and **J**), increased tip cell numbers (yellow asterisks in **H** and **J**) and more filopodia (red dots in **I** and **K**) at the vascular front region of E^{2KO} retinas compared to littermate control retinas.

L-**O**) Quantitative analysis of vascularized retinal area (**L**), vascular density within angiogenic front regions indicated in **E** and **G** (**M**), tip cell number (**N**) and filopodia (**O**) demonstrates that differences between E^{2KO} and control mice are statistically significant (mean ± SEM; n = ~4-9 retinas from at least 4 mice per group - multiple confocal images per retina were quantified and averaged).


NG2
IsolectinB4
NG2 / IsolectinB4
E Ctrl
E 2KO
Angiogenic Front
Centrlal Retina
Angiogenic Front
Centrlal Retina
150 µm
150 µm

Supplementary Figure II.10 No major perturbations in NG2^{+} pericyte coverage in the E^{2KO} retinal vasculature at P6.

Confocal microscopy analysis of whole mount retinal vasculature immunostained for the pericyte marker NG2 and isolectinB4 showing no major differences in vessel pericyte coverage in retinas from E^{2KO} mice compared to retinas from littermate control mice. Data presented are representative of multiple images of retinas from 4 mice per group.


P6 Adductor Muscle
SMA
Gracilis Collateral
Saphenous Artery & Vein
PCFA & V
Gracilis Collateral
Neurofilament
Collateral Associated Nerve
Saphenous Nerve
Collateral Associated Nerve
500μm
SMA/Neurofilament
SMA/Neurofilament
Zoom

Supplementary Figure II.11 Intimate association of gracillis collaterals and peripheral nerves in adductor muscles.

Confocal microscopy of a whole mount adductor muscle immunostained for smooth muscle actin (green) and Neurofilament-M shows close association of gracillis collateral arteries with peripheral nerves.

Chapter III

JNK is cell-autonomously dispensable for hematopoietic development and hematopoietic stem cell self-renewal

Abstract

cJun NH_2-terminal kinases (JNK) exist in multiple isoforms with high functional redundancy. JNK mediates pleiotropic cellular responses to diverse environmental stimuli, including various types of stress as well as numerous growth factors and cytokines. JNK has been implicated in immune cell differentiation and function, however its role in hematopoiesis or hematopoietic stem cell (HSC) self-renewal has not been explored. Here, we employ mice with single or compound ablation of *Jnk* genes and serial competitive bone marrow or HSC transplantation assays to dissect the function of JNK in hematopoiesis and HSC self-renewal. Unexpectedly, we find that JNK is not required for normal hematopoiesis, HSC and progenitor cell homing and engraftment following transplantation, HSC self-renewal or 5-FU-induced stress hematopoiesis. These results may be medically relevant because JNK inhibitors have reached clinical trials.

Introduction

c-Jun NH_2-terminal kinase (JNK), a member of the stress and mitogen activated family of protein kinases, is encoded by three separate genes. JNK1 and JNK2 are ubiquitously expressed, whereas expression of JNK3 is confined to neurons, heart and testis.[1] Alternative splicing of the messenger RNA (mRNA) transcripts of the three JNK genes generates ten JNK isoforms.[3] Studies have demonstrated that some of these isoforms have differential substrate binding specificities; however, often JNK isoforms show significant functional redundancy.[1,200] JNK has been implicated in embryonic development, proliferation, apoptosis, inflammation and cytokine expression among other processes.[1,6] Indeed, JNK is required in embryonic development as compound *Jnk1*$^{-/-}$*Jnk2*$^{-/-}$ embryos die in utero and murine embryonic fibroblasts (MEFs) from *Jnk1*$^{-/-}$*Jnk2*$^{-/-}$ mice show major defects in proliferation.[20,183] In contrast, compound *Jnk1*$^{-/-}$*Jnk2*$^{-/-}$ murine embryonic stem cells display increased proliferation and self-renewal compared to *Jnk*$^{+/+}$ stem cells.[201]

Hematopoiesis is the process that gives rise to all blood cells from hematopoietic stem cells (HSCs). In addition to their ability to generate all hematopoietic cells, HSCs have the capacity to self-renew (i.e., proliferate without differentiating).[202-204] The processes of blood cell production and HSC self-renewal are regulated by a multitude of secreted growth factors and cytokines, cell-cell or cell-

extracellular matrix interactions as well as numerous signaling pathways, which collectively orchestrate hematopoietic cell survival, proliferation, differentiation or quiescence.[33,205,206]

JNK has been implicated in the regulation hematopoietic cell survival, cytokine expression, effector T cell differentiation and inflammation.[4,24,158,162] However, due to the early embryonic death of compound *Jnk1*$^{-/-}$*Jnk2*$^{-/-}$ mice, almost all studies have been confined to the examination of *Jnk1*$^{-/-}$ or *Jnk2*$^{-/-}$ mice. Furthermore, with the exception of one recent study that analyzed hematopoietic progenitor cell expansion using whole body single *Jnk1*$^{-/-}$ or *Jnk2*$^{-/-}$ mice,[170] no extensive studies on the role of JNK specifically in HSC self-renewal and function have been undertaken. Given the high functional redundancy of JNK isoforms, and their different roles in multiple tissues, hematopoietic cell specific compound ablation of all JNK isoforms is required to better understand the function of JNK in hematopoietic development and HSC self-renewal. In this study, we employ hematopoietic cell specific compound mutant mice with dual disruption of both *Jnk1* plus *Jnk2* genes, and surprisingly, find that absence of all JNK isoforms in hematopoietic cells does not perturb normal, transplant-induced or drug-induced stress hematopoiesis or HSC self-renewal.

Results

Normal HSC and progenitor cell development in single Jnk1$^{-/-}$ and Jnk2$^{-/-}$ mice

To assess if different JNK isoform subsets are important for normal development of HSCs or progenitor cells we performed immunophenotyping of bone marrow cells from adult WT, *Jnk1*$^{-/-}$ and *Jnk2*$^{-/-}$ mice using antibodies against established HSC and/or progenitor cell markers (Supplementary Figure III.1). Total bone marrow cellularity was not significantly different between WT and *Jnk1*$^{-/-}$ or *Jnk2*$^{-/-}$ mice (Figure III.1D), and multiparameter flow cytometry analysis revealed no significant differences in the frequency of HSCs or any of the progenitor cells examined (Figure III.1A-C). Thus, JNK1 or JNK2 isoforms in hematopoietic or non-hematopoietic cells are not required for normal development of HSCs or the progenitor cell populations that we examined.

HSCs and progenitors from single Jnk1$^{-/-}$ and Jnk2$^{-/-}$ mice have normal multilineage reconstitution potential and self-renewal

To examine the role of different JNK isoform subsets in HSC and progenitor cell function, we performed serial competitive bone marrow transplantation assays. WT or JNK knockout bone marrow cells expressing the pan-hematopoietic cell marker CD45.2 were mixed with competitor bone marrow cells expressing CD45.1 at two different ratios (20:80 and 50:50) and transplanted into lethally irradiated mice (Figure III.2A). Peripheral blood from recipient mice was

examined by flow cytometry analysis for donor cell chimerism and multilineage reconstitution as indicated in Figure III.2B. Analysis of peripheral blood chimerism in primary recipient mice at 5, 10, 15 and 20 weeks post-transplantation revealed no consistently significant differences in overall reconstitution between recipients that received WT and those that received *Jnk1*$^{-/-}$ or *Jnk2*$^{-/-}$ bone marrow cells (Figure III.2C, primary transplant). Furthermore, we found no consistently significant differences in reconstitution of individual myeloid, B and T cell subsets (Figure III.2D, primary transplant), or frequency of myeloid, B and T cell subsets (within the CD45.2+ donor population) in the blood of recipients that received WT, *Jnk1*$^{-/-}$ or *Jnk2*$^{-/-}$ bone marrow cells (Figure III.2E, primary transplant). This analysis indicates that HSC and progenitor multilineage reconstitution function as well as hematopoietic cell differentiation into myeloid, B and T cell lineages is preserved in the absence of JNK1 or JNK2. Twenty weeks post-transplantation, we analyzed bone marrow from recipient mice and found no significant differences in overall reconstitution as well as no significant differences in reconstitution or frequency of HSC and progenitor populations in the bone marrow of recipients that received WT, *Jnk1*$^{-/-}$ or *Jnk2*$^{-/-}$ bone marrow cells (Figure III.3A-C).

To test if absence of JNK1 or JNK2 affected HSC self-renewal potential, we pooled bone marrow from primary recipient mice and used it to transplant secondary recipients. Peripheral blood analysis over 20 weeks revealed no

consistently significant differences in overall CD45.2^{+} donor cell chimerism, as well as no consistently significant differences in reconstitution or frequency of myeloid, B and T cell subsets in the blood of secondary recipients that received WT, *Jnk1*$^{-/-}$ or *Jnk2*$^{-/-}$ bone marrow cells (Figure III.2C-E, secondary transplant). This analysis demonstrates that *Jnk1*$^{-/-}$ *and Jnk2*$^{-/-}$ bone marrow cells are able to maintain blood cell production for extended periods and upon serial transplantation, similarly to WT bone marrow cells, indicating that HSC self-renewal potential is not significantly altered in the absence of JNK1 or JNK2 isoforms.

Compound deficiency of Jnk1 plus Jnk2 in hematopoietic cells does not perturb hematopoiesis or homing of HSC and progenitor cells

JNK1 and JNK2 isoforms expressed in hematopoietic cells display significant functional redundancy. Therefore, the absence of significant perturbations in hematopoietic cell function in single JNK knockout mice may be due to functional compensation by remaining JNK isoforms. To test if JNK has a role in hematopoiesis would therefore require ablation of all JNK isoforms expressed in hematopoietic cells. To disrupt both JNK1 plus JNK2 genes simultaneously, we employed *Jnk1*$^{LoxP/LoxP}$*Jnk2*$^{LoxP/LoxP}$ mice in conjunction with a tamoxifen-inducible Cre recombinase system (*Rosa26-CreERT2 Jnk1*$^{LoxP/LoxP}$*Jnk2*$^{LoxP/LoxP}$), referred to as *J1*$^{f/f}$*J2*$^{f/f}$ *R-Cre* mice and control mice (*Rosa26-CreERT2 Jnk1*$^{+/+}$*Jnk2*$^{+/+}$), referred to as *J1*$^{+/+}$*J2*$^{+/+}$ *R-Cre* mice. We, then, assessed the effect of compound

disruption of both *Jnk1* plus *Jnk2* genes on HSC and progenitor function in competitive bone marrow transplantation assays. To avoid potentially confounding effects of JNK disruption in non-hematopoietic cells and also issues with homing of JNK-deficient HSC and progenitor cells following transplantation, we performed transplantations with bone marrow from $J1^{+/+}J2^{+/+}$ *R-Cre* and $J1^{f/f}J2^{f/f}$ *R-Cre* mice prior to induction of JNK ablation (Figure III.4A). Two groups of recipient mice received $J1^{+/+}J2^{+/+}$ *R-Cre* bone marrow cells, while two other groups received $J1^{f/f}J2^{f/f}$ *R-Cre* bone marrow cells. All four groups also received the same number of competitor $CD45.1^{+}$ bone marrow cells. Ten weeks following transplantation we confirmed equal levels of engraftment in all four groups of recipient mice by flow cytometry analysis of peripheral blood (Figure III.4C-E, 10 weeks post transplant timepoint) and then administered either tamoxifen to induce Cre activity in donor hematopoietic cells or oil as a control (Figure III.4A). Peripheral blood analysis, over 20 weeks following tamoxifen administration, revealed no significant alterations in overall $CD45.2^{+}$ donor cell chimerism, as well as no significant changes in reconstitution or frequency of myeloid, B and T cell subsets in the blood of recipients from any of the four groups (Figure III.4C-E). Efficient ablation of JNK in $J1^{f/f}J2^{f/f}$ *R-Cre* bone marrow cells ~20 weeks following tamoxifen administration was confirmed by immunoblot analysis of bone marrow from recipient mice that had received either $J1^{+/+}J2^{+/+}$ *R-Cre* alone or $J1^{f/f}J2^{f/f}$ *R-Cre* alone (i.e., in a non-competitive setting, Figure III.4A and B).

This analysis indicates that JNK in hematopoietic cells is not required for normal blood cell production in adult mice.

To test if compound JNK-deficiency might affect homing and initial engraftment of HSC and/or progenitor cells following transplantation, we administered tamoxifen to adult *J1*$^{+/+}$*J2*$^{+/+}$ *R-Cre* or *J1*$^{f/f}$*J2*$^{f/f}$ *R-Cre* (*J1*$^{\Delta/\Delta}$*J2*$^{\Delta/\Delta}$ *R-Cre*) mice and 5 weeks later harvested bone marrow from these mice and performed competitive bone marrow transplantations into lethally irradiated recipient mice (Figure III.4F). Peripheral blood analysis, over 20 weeks following transplantation, revealed no consistently significant differences in overall CD45.2^{+} donor cell chimerism, as well as no consistently significant changes in reconstitution or frequency of myeloid, B and T cell subsets in the blood of recipients (Figure III.4G-I), indicating that JNK in adult hematopoietic cells is also not required for homing or engraftment of HSC and/or progenitor cells following transplantation.

JNK in hematopoietic cells is dispensable for normal HSC and progenitor cell development

Although our data so far indicate that JNK is not required for normal HSC and/or progenitor cell function in adult mice, JNK in hematopoietic cells may be important for HSC and/or progenitor cell development and function at earlier developmental times. To test this possibility we crossed *Jnk1*$^{LoxP/LoxP}$*Jnk2*$^{LoxP/LoxP}$ or *Jnk1*$^{+/+}$*Jnk2*$^{+/+}$ mice to mice expressing a constituitive version of Cre

recombinase under the control of *Vav1* regulatory elements that drive *Cre* expression in all hematopoietic cells including HSCs.[185,207] Prior studies have reported *Vav1* expression in hematopoietic cells as early as embryonic day (E)11.5 in blood islands.[208] We generated *Vav1-Cre*$^{+}$ *Jnk1*$^{LoxP/LoxP}$*Jnk2*$^{LoxP/LoxP}$ (H^{2KO}) mice. *Cre*$^{-}$ littermate mice *Vav1-Cre*$^{-}$ *Jnk1*$^{LoxP/LoxP}$*Jnk2*$^{LoxP/LoxP}$ (H^{fCtrl}) and *Vav1-Cre*$^{+}$ *Jnk1*$^{+/+}$*Jnk2*$^{+/+}$ (H^{Ctrl}) mice served as controls. H^{2KO} mice developed normally, showed no obvious morphological defects and had normal body mass (Supplementary Figure III.2A). Immunoblot analysis confirmed the absence of detectable JNK protein in lysates from H^{2KO} bone marrow cells (Figure III.6F). Automated complete blood cell analysis showed no significant perturbations in any of the indices examined (Supplementary Figure III.2B). Furthermore, total bone marrow cellularity was not significantly different between adult H^{2KO}, H^{fCtrl} or H^{Ctrl} mice (Figure III.5D), and multiparameter flow cytometry analysis of bone marrow cells revealed no significant differences in the frequency of HSCs or any of the progenitor cells examined (Figure III.5A-C), indicating normal HSC and progenitor cell development in H^{2KO} mice.

JNK in hematopoietic cells is dispensable for normal HSC and progenitor cell engraftment, multilineage reconstitution and HSC self-renewal

To directly examine the role of JNK in HSC function, we sorted HSCs (Lineage$^{-/low}$, Sca1^{+}, cKit^{+}, CD150^{+}, CD48^{-}) and transplanted 100 H^{2KO}, H^{fCtrl} or H^{Ctrl} HSCs together with $2x10^{5}$ competitor CD45.1^{+} total bone marrow cells into lethally

irradiated recipient mice (Figure III.6A). Peripheral blood analysis, over 20 weeks following transplantation, revealed no significant differences in overall $CD45.2^+$ donor cell chimerism (Figure III.6B, 1^o Transplant), as well as no consistently significant JNK-dependent changes in reconstitution or frequency of myeloid, B and T cell subsets in the blood of recipients that received H^{2KO}, H^{fCtrl}, or H^{Ctrl} HSCs (Figure III.6C and D, 1^o Transplant), indicating that JNK is not required for normal HSC function following transplantation.

To test H^{2KO} HSC self-renewal potential, we pooled bone marrow from primary recipients and used it to transplant secondary recipient mice (Figure III.6A). Peripheral blood analysis, over 20 weeks following transplantation, revealed no consistently significant JNK-dependent differences in overall $CD45.2^+$ donor cell chimerism, as well as no consistently significant changes in reconstitution or frequency of myeloid, B and T cell subsets in the blood of secondary recipients that received H^{2KO}, H^{fCtrl}, or H^{Ctrl} bone marrow cells (Figure III.6B-D, 2^o Transplant).

We also performed competitive bone marrow transplantations with total bone marrow cells from H^{2KO}, H^{fCtrl}, and H^{Ctrl} mice and competitor mice at two different ratios (20:80 or 50:50) of test to competitor cells (Figure III.6E) and found no significant differences in overall $CD45.2^+$ donor cell chimerism, as well as no consistently significant JNK-dependent changes in reconstitution or frequency of

myeloid, B and T cell subsets in the blood of recipient mice that received H^{2KO}, H^{fCtrl}, or H^{Ctrl} bone marrow cells (Figure III.6G-I). Collectively, these data indicate that JNK in hematopoietic cells is not required for normal HSC and progenitor cell development, and function following transplantation or HSC self-renewal.

H^{2KO} mice show normal sensitivity to 5-fluorouracil (5-FU) treatment

Although JNK-deficiency in hematopoietic cells does not appear to affect normal hematopoiesis or hematopoiesis following transplantation, JNK may play a role during drug-induced stress hematopoiesis. We examined if hematopoietic stress induced by treatment of mice with 5-FU affected the survival of H^{2KO} mice differently from control mice. Weekly treatments of mice with 150 mg/Kg 5-FU resulted in similar mortality between H^{2KO}, H^{fCtrl} and H^{Ctrl} mice (Figure III.7), suggesting that JNK in hematopoietic cells is also not required for 5-FU-induced stress hematopoiesis.

Discussion

Hematopoiesis is a complex biological process that involves the integration of multiple signaling pathways.[33,205,206] Members of the mitogen activated family of protein kinases have been shown to play important roles in hematopoietic cell development and function.[24,167,170] In this study, we explored the role of JNK in hematopoiesis and HSC self-renewal. We employed hematopoietic cell specific mutant mice with dual disruption of *Jnk1* plus *Jnk2* genes and found that JNK is dispensable for normal and stress-induced hematopoiesis as well as HSC self-renewal. These findings are unexpected, because JNK has been shown to regulate numerous biological processes both in hematopoietic and non-hematopoietic cells that are important for hematopoietic development.

JNK has been shown to regulate the expression of various cytokines, such as TNF-α, TGF-β and INF-γ that regulate various aspects of hematopoiesis, including HSC self-renewal, differentiation and survival.[163,209-214] It is possible that JNK regulates cytokine expression only in specific contexts (e.g., during inflammatory responses) and that JNK may not be involved in cytokine expression during hematopoietic development in the bone marrow. Furthermore, JNK is activated by numerous cytokines, including erythropoietin (EPO), thrombopoietin (TPO), stem cell factor (SCF), IL-3, and GM-CSF that are major regulators of the hematopoietic process.[215,216] The activation of JNK by these

cytokines may be important for processes that are not essential for normal hematopoiesis or JNK activation by these cytokines may not be physiologically relevant.

A recent study reported that JNK in hematopoietic cells is activated by Wnt4 in vitro, and that *Jnk2*$^{-/-}$ mice show increased rates of progenitor cell apoptosis associated with decreased numbers of hematopoietic progenitors in the bone marrow.[170] This finding contrasts with ours, as we found no significant differences in the abundance of various progenitor populations in *Jnk1*$^{-/-}$ or *Jnk2*$^{-/-}$ mice or in compound mutants with disruption of both *Jnk1* and *Jnk2* genes in hematopoietic cells. This discrepancy may be due to mouse background differences between our mice, which were on a fully backcrossed C57BL/6J background, while the mice in that study were on mixed background.

JNK has also been implicated in embryonic stem cell proliferation, differentiation and self-renewal.[201] In contrast, here we find that JNK in hematopoietic cells is dispensable for HSC self-renewal and differentiation, suggesting that JNK has distinct roles in embryonic compared to somatic stem cells in general, or that JNK is dispensable in HSCs.

Despite the numerous lines of evidence suggesting a possible role for JNK in hematopoietic development and function, our study demonstrates that this is not

the case. Collectively, our study shows that JNK in hematopoietic cells is cell-autonomously dispensable for normal, transplantation-induced and 5-FU-induced hematopoiesis as well as for HSC self-renewal. These findings are medically relevant because JNK inhibitors are being used in clinical trials.[217]

Experimental Procedures

Mice

We have previously described *Jnk1*$^{LoxP/LoxP}$, *Jnk2*$^{LoxP/LoxP}$, *Jnk1*$^{-/-}$ *and Jnk2*$^{-/-}$.[161-163][183] B6.Cg-Tg(Vav1-cre)A2Kio/J mice[185] expressing an improved version of Cre recombinase (iCre) driven by *Vav1* regulatory elements, B6.129-*Gt(ROSA)26Sortm1(cre/ERT2)Tyj*/J[218] expressing a tamoxifen inducible version of Cre recombinase from the *Gt(ROSA)26Sor* promoter and *B6.SJL-Ptprc*^{a} *Pepc*^{b}*/BoyJ* mice expressing the CD45.1 allele were obtained from the Jackson Laboratories. Here we generated and analyzed the following mice:

J1$^{f/f}$*J2*$^{f/f}$ *R-Cre (Rosa26-CreERT2 Jnk1*$^{LoxP/LoxP}$*Jnk2*$^{LoxP/LoxP}$)

J1$^{+/+}$*J2*$^{+/+}$ *R-Cre (Rosa26-CreERT2 Jnk1*$^{+/+}$*Jnk2*$^{+/+}$)

H^{2KO} *(Vav1-Cre*$^{+}$ *Jnk1*$^{LoxP/LoxP}$*Jnk2*$^{LoxP/LoxP}$*)*

H^{LoxP} *(Vav1-Cre* $^{-}$ *Jnk1*$^{LoxP/LoxP}$*Jnk2*$^{LoxP/LoxP}$*)*

H^{WT} *(Vav1-Cre*$^{+}$*Jnk1*$^{+/+}$*Jnk2*$^{+/+}$*)*

All mice used in this study were backcrossed (≥ ten generations) to the C57BL/6J strain (The Jackson Laboratories). Mice were housed in a facility accredited by the American Association for Laboratory Animal Care. All animal studies were approved by the Institutional Animal Care and Use Committee of the University of Massachusetts Medical School.

Genotyping

PCR assays with genomic DNA and the amplimers 5'-GCGAAGAGTTTGTCCTCAACC-3', 5'-GGAGCGGGAGAAATGGATATG-3' and 5'-AAAGTCGCTCTGAGTTGTTAT-3' were used to detect the *Rosa26 Cre*$^{+}$ allele (250 bp) and the WT allele (550 bp). The amplimers 5'-CTAGGCCACAGAATTGAAAGATCT-3', 5'-GTAGGTGGAAATTCTAGCATCATCC-3', 5'-AGATGCCAGGACATCAGGAACCTG-3' and 5'- ATCAGCCACACCAGACACAGAGATC-3' were used to detect an internal positive control fragment (324 bp) and the *iCre*$^{+}$ allele (236 bp). The amplimers 5'-CCTCAGGAAGAAAGGGCTTATTTC-3' and 5'-GAACCACTGTTCCAATTTCCATCC-3' detected the *Jnk1*$^{+}$ allele (1,550 bp), the *Jnk1*^{LoxP} allele (1,095 bp), and the *Jnk1*$^{\Delta}$ allele (395 bp). The amplimers 5'-GTTTTGTAAAGGGAGCCGAC-3' and 5'-CCTGACTACTGAGCCTGGTTTCTC-3' were used to detect the *Jnk2*$^{+}$ allele (224 bp) and the *Jnk2*^{LoxP} allele (264 bp). The amplimers 5'-GGAATGTTTGGTCCTTTAG-3', 5'-GCTATTCAGAGTTAAGTG-3', and 5'-TTCATTCTAAGCTCAGACTC-3' were used to detect the *Jnk2*^{LoxP} allele (560 bp) and the *Jnk2*$^{\Delta}$ allele (400 bp).

Tamoxifen Treatments

Tamoxifen (Sigma) was dissolved in 2% ethanol 98% sunflower seed oil (Sigma)

and 1 mg/mouse was administered intraperitoneally (ip) 3 times on alternate days.

Transplantations

Bone marrow (BM) was harvested by flushing tibias and femurs from at least five 10-12 week old mice with ice cold PBS. Erythrocytes were lysed by incubating the BM in ACK lysing buffer (Life Technologies). BM cells were then resuspended in PBS and passed through a 100 µm filter. Cells were counted and mixtures of test BM cells from the indicated genotypes were prepared by mixing test BM cells expressing the CD45.2 allele with competitor BM cells expressing the CD45.1 allele at various test to competitor cell ratios. $1x10^6$ total BM cells were intravenously injected via the tail vein into lethally irradiated (11 Gy) 10-12 week old CD45.1/CD45.2 heterozygous or CD45.1 homozygous female mice. Transplanted mice were maintained on antibiotic water for the first two weeks post transplantation. Blood was harvested via the retroorbital sinus using heparinized capillary tubes and EDTA coated vials at 5, 10, 15 and 20 weeks post transplantation and subjected to flow cytometry analysis.

Flow Cytometry

Blood was washed in PBS, stained with live/dead fixable blue dead cell staining

kit (Invitrogen), washed in PBS and blocked in 2% FBS-PBS 0.02% sodium azide plus Fc-block (Anti-CD16/32 antibody 1:200, BD Biosciences). Surface antigens were detected by incubation for 30 min at 4^{o}C with conjugated antibodies including CD45.1-Pacific Blue, CD45.2-FITC, CD3e-APC, CD19-APC-H7, CD11b-PE (BD Biosciences), GR1-Alexa Fluor 700 (Biolegend). Following washing with 2% FBS-PBS 0.02% sodium azide, red cells were lysed and leukocytes fixed by incubating in lyse/fix solution (BD Biosciences) and then washed with PBS.

Bone marrow cells were stained with live/dead fixable blue dead cell staining kit (Invitrogen), washed in PBS and blocked in 2% FBS-PBS 0.02% sodium azide plus Fc-block (unconjugated anti-CD16/32 antibody 1:200, BD Biosciences). This Fc-block was not done on cells that were going to be stained for myeloid progenitors. Instead these cells were incubated with a CD16/32-AlexaFluor 700 antibody. Cells were incubated for 30 min at 4^{o}C with a lineage cocktail that included biotinylated antibodies against CD3e, CD4, CD8, B220, CD11b, GR-1 and Ter119. Cells were then washed, and surface antigens were detected by incubation with Streptavidin-PE-TexasRed and conjugated antibodies including CD45.2-APC, cKit-APC-Cy7, Sca-1-PacificBlue, CD150-PE-Cy7 and CD48-FITC (Panel 1) or Streptavidin-PE-TexasRed and conjugated antibodies including CD45.2-APC, cKit-APC-Cy7, Sca-1-PacificBlue, IL7R-PE-Cy7, CD34-FITC, and CD135-PE-Cy5.5 (Panel 2). A CD45.1-PE antibody was

included when bone marrow cells from chimeric mice were analyzed. Cells were washed, fixed with 4% PFA, washed with PBS and analyzed on an LSR-II cytometer (Becton Dickenson). Data were processed using FlowJo Software (Tree Star).

For HSC sorting, bone marrow cells were lineage depleted using a Lineage Cell Depletion kit (Miltenyi Biotec) and MACS columns (Miltenyi Biotec). Cells were stained with live/dead fixable blue dead cell staining kit (Invitrogen), washed in PBS and blocked in 2% FBS-PBS plus Fc-block. Cells were then stained with antibodies from Panel 1 above and HSCs were sorted on a BD FACSAria II Cell Sorter. Using the single cell mode live HSCs ($CD45.2^+$, Lin^-, $cKit^+$, $Sca\text{-}1^+$, $CD150^+$ and $CD48^-$) were collected directly into tubes containing competitor total bone marrow cells and cell mixtures were immediately transplanted into lethally irradiated mice.

Immunoblot Analysis

Cell extracts were prepared using Triton lysis buffer (20 mM Tris at pH 7.4, 1% Triton X-100, 10% glycerol, 137 mM NaCl, 2 mM EDTA, 25 mM β-glycerophosphate, 1 mM sodium orthovanadate, 1 mM phenylmethylsulfonylfluoride, 10 mg/mL of aprotinin and leupeptin). Extracts (20-50 µg of protein) were examined by protein immunoblot analysis by probing with antibodies to JNK (R&D Systems or Pharmigen), GAPDH (Santa Cruz)

and αTubulin (Sigma). Immune complexes were detected using the Odyssey infrared imaging system (LI-COR Biosciences).

Statistical Analysis

Differences between groups were examined for statistical significance with an unpaired Student's test with equal variance or a log-rank (Mantel-Cox) test for determining significance of Kaplan-Meier survival curves.

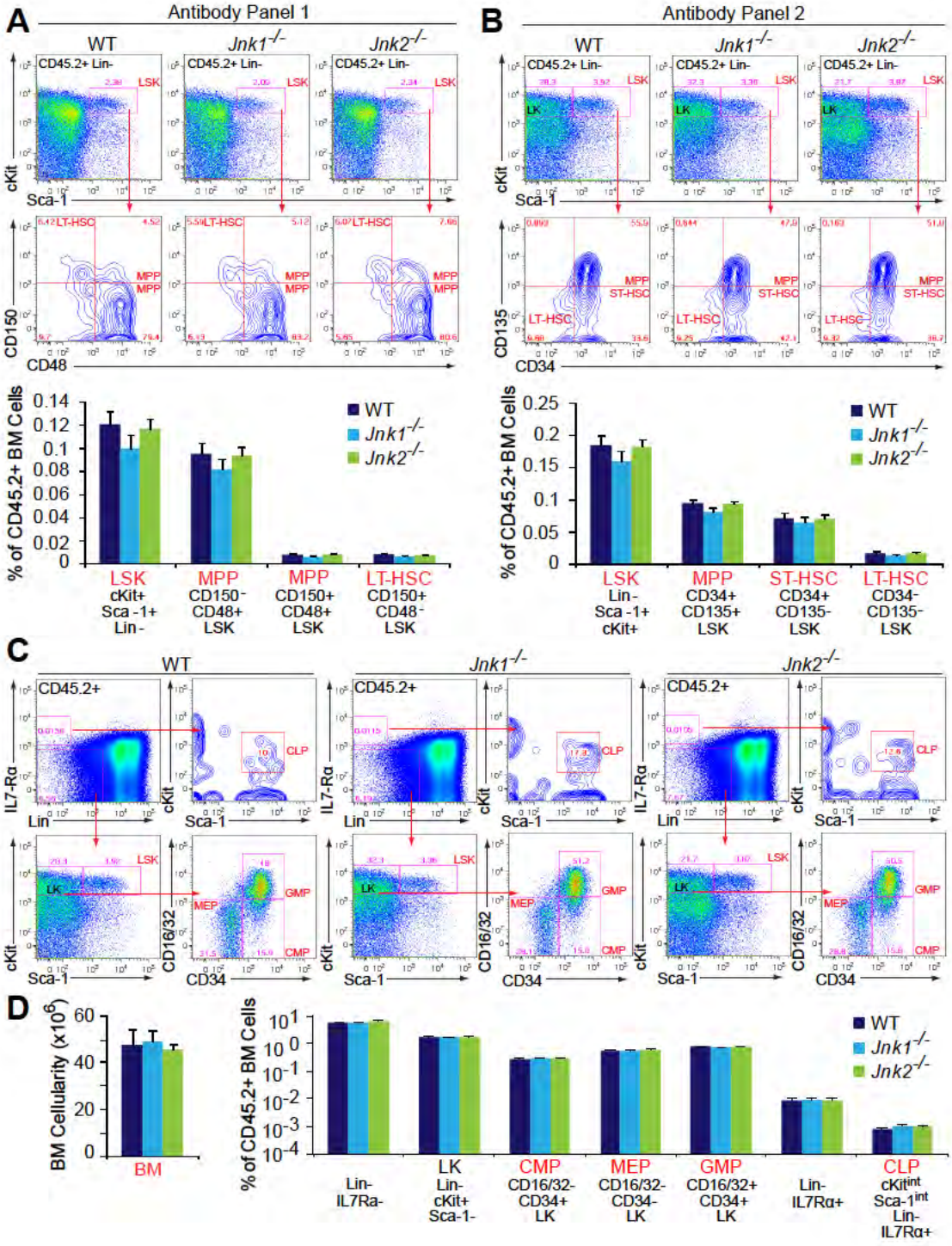

A
Antibody Panel 1
WT
Jnk1-/-
Jnk2-/-
CD45.2+ Lin-
LSK
cKit
Sca-1
LT-HSC
MPP
CD150
CD48
% of CD45.2+ BM Cells
WT
Jnk1-/-
Jnk2-/-
LSK cKit+ Sca-1+ Lin-
MPP CD150- CD48+ LSK
MPP CD150+ CD48+ LSK
LT-HSC CD150+ CD48- LSK
B
Antibody Panel 2
LK
ST-HSC
CD135
CD34
LSK Lin- Sca-1+ cKit+
MPP CD34+ CD135+ LSK
ST-HSC CD34+ CD135- LSK
LT-HSC CD34- CD135- LSK
C
CD45.2+
IL7-Rα
Lin-
CLP
GMP
MEP
CMP
CD16/32
D
BM Cellularity (x10^6)
BM
Lin- IL7Ra-
LK Lin- cKit+ Sca-1-
CMP CD16/32- CD34+ LK
MEP CD16/32- CD34- LK
GMP CD16/32+ CD34+ LK
Lin- IL7Rα+
CLP cKit^int Sca-1^int Lin- IL7Rα+

Figure III.1 *Jnk1*$^{-/-}$ and *Jnk2*$^{-/-}$ mice have normal HSC and progenitor cell composition in the bone marrow.

A) Bone marrow (BM) cells from WT, *Jnk1*$^{-/-}$ and *Jnk2*$^{-/-}$ mice were immunostained with fluorochrome-conjugated antibodies and analyzed by flow cytometry to identify bone marrow cell populations enriched in HSC and progenitor cells. The detailed step-by-step gating strategy is presented in Supplementary Figure II.1. Lineage negative (Lin-) cells staining positive for Sca-1 and cKit identify the LSK population that is enriched in long term HSCs (LT-HSC) and multipotent progenitors (MPP). Staining LSK cells with antibodies to CD150 and CD48 defines populations of LT-HSCs and MPPs more specifically. Quantitative flow cytometry analysis revealed no significant perturbations in the proportions of any of the of BM populations examined between WT and *Jnk1*$^{-/-}$ or *Jnk2*$^{-/-}$ mice (mean ± SEM; n = ~5-7 mice per group). Data presented are from one of two experiments with similar results.

B) A second panel of antibodies that includes antibodies to CD135 and CD34 also defines populations of LT-HSCs, short-term (ST)-HSCs and MPPs within the LSK population. Quantitative flow cytometry analysis using this panel of antibodies also revealed no significant perturbations in the proportions of the indicated HSC and MPP populations examined between WT and *Jnk1*$^{-/-}$ or *Jnk2*$^{-/-}$ mice (mean ± SEM; n = ~5-7 mice per group). Data presented are from one of two experiments with similar results.

C) Flow cytometry analysis of lymphoid and myeloid progenitors including the common lymphoid progenitors (CLP), common myeloid progenitors (CMP), granulocyte macrophage progenitors (GMP) and megakaryocyte erythrocyte progenitors (MEP) shows no significant differences in their proportion in the BM of *Jnk1*$^{-/-}$ or *Jnk2*$^{-/-}$ compared to WT BM (mean ± SEM; n = ~5-7 mice per group). Data presented are from one of two experiments with similar results.

D) No significant differences were detected in total BM cellularity between *Jnk1*$^{-/-}$ or *Jnk2*$^{-/-}$ and WT mice (mean ± SEM; n = ~5-7 mice per group). Data presented are from one of two experiments with similar results.

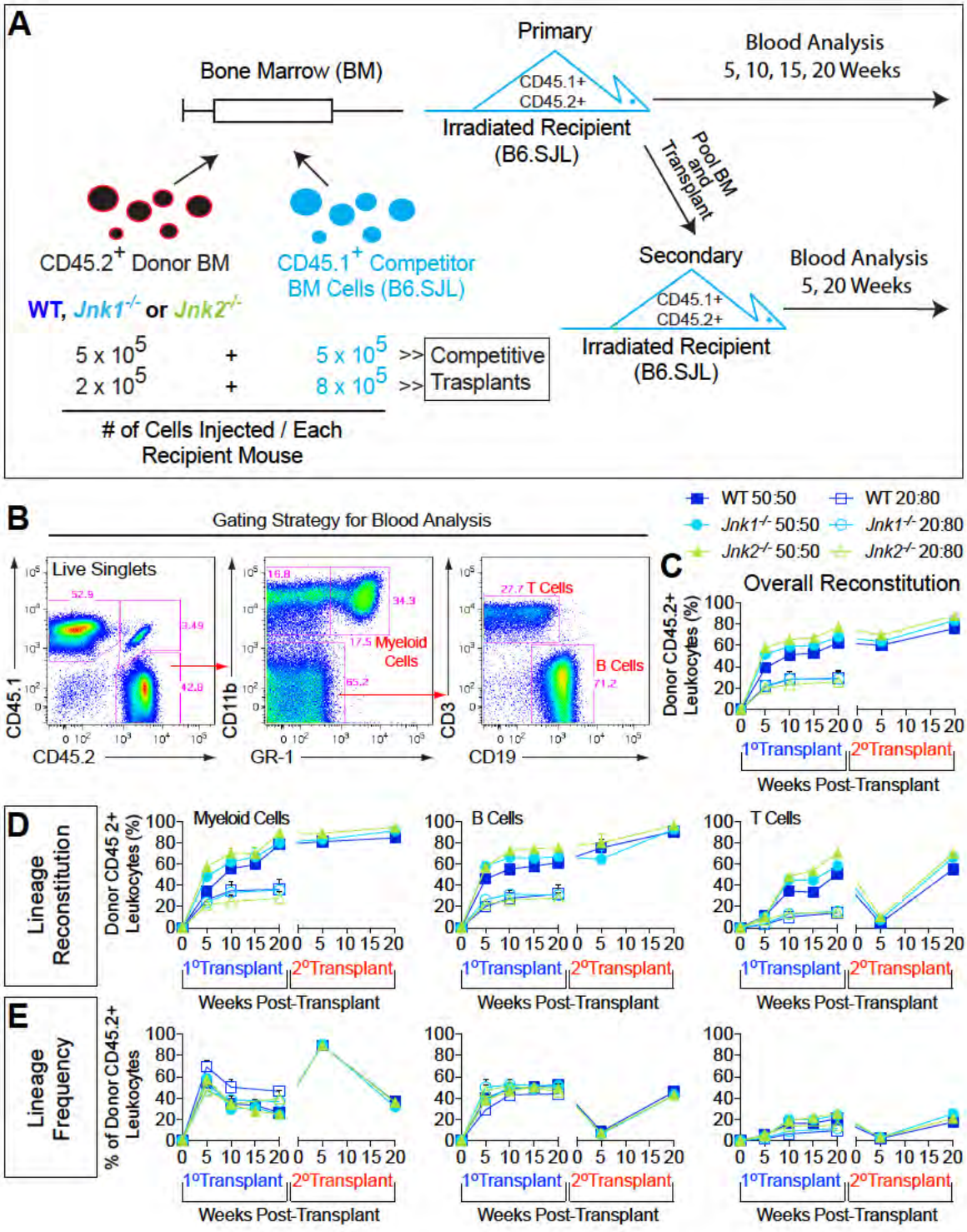

A
Primary
Bone Marrow (BM)
CD45.1+
CD45.2+
Irradiated Recipient
(B6.SJL)
Blood Analysis
5, 10, 15, 20 Weeks
Pool BM and Transplant
CD45.2+ Donor BM
WT, Jnk1-/- or Jnk2-/-
CD45.1+ Competitor BM Cells (B6.SJL)
Secondary
CD45.1+
CD45.2+
Irradiated Recipient
(B6.SJL)
Blood Analysis
5, 20 Weeks
5 x 10^5 + 5 x 10^5 >> Competitive Trasplants
2 x 10^5 + 8 x 10^5 >> Trasplants
# of Cells Injected / Each Recipient Mouse
B
Gating Strategy for Blood Analysis
Live Singlets
52.9
3.49
42.8
CD45.1
CD45.2
16.8
34.3
17.5 Myeloid Cells
65.2
CD11b
GR-1
27.7 T Cells
B Cells
71.2
CD3
CD19
C
WT 50:50
WT 20:80
Jnk1-/- 50:50
Jnk1-/- 20:80
Jnk2-/- 50:50
Jnk2-/- 20:80
Overall Reconstitution
Donor CD45.2+ Leukocytes (%)
1°Transplant
2°Transplant
Weeks Post-Transplant
D
Lineage Reconstitution
Myeloid Cells
B Cells
T Cells
Donor CD45 2+ Leukocytes (%)
E
Lineage Frequency
% of Donor CD45.2+ Leukocytes

Figure III.2 Bone marrow cells from *Jnk1*$^{-/-}$ and *Jnk2*$^{-/-}$ mice display normal multilineage reconstitution potential in serial competitive transplantation experiments

A) Serial competitive BM transplantation experimental set up. Test BM cells from WT, *Jnk1*$^{-/-}$ and *Jnk2*$^{-/-}$ mice expressing the CD45.2 allele were each mixed with competitor BM cells expressing the CD45.1 allele at two different ratios, as indicated, and transplanted via the tail vein into primary lethally irradiated recipient mice expressing both CD45.1 and CD45.2. Peripheral blood from primary recipient mice was analyzed at different times over 20 weeks for donor cell chimerism and multilineage reconstitution with antibodies to lineage markers. Twenty weeks post-transplantation BM from primary recipient mice transplanted with the 50:50 ratio of test to competitor BM cells was pooled and used to transplant secondary recipient mice that were analyzed similarly to primary recipients.

B) Flow cytometry gating strategy for donor cell chimerism and multilineage reconstitution analysis of peripheral blood from recipient mice.

C) Primary and secondary recipient mice transplanted with *Jnk1*$^{-/-}$ or *Jnk2*$^{-/-}$ BM cells show no consistently significant differences in overall peripheral blood leukocyte reconstitution compared to recipients transplanted with WT BM cells (mean ± SEM; n = ~7-9 recipient mice per group)

D) Primary and secondary recipient mice transplanted with *Jnk1*$^{-/-}$ or *Jnk2*$^{-/-}$ BM cells show no consistently significant differences in reconstitution of myeloid, B and T cells compared to recipients transplanted with WT BM cells (mean ± SEM; n = ~7-9 recipient mice per group)

E) Primary and secondary recipient mice transplanted with *Jnk1*$^{-/-}$ or *Jnk2*$^{-/-}$ BM cells show no consistently significant differences in the frequency of myeloid, B and T cells within the donor CD45.2^{+} leukocyte population compared to recipients transplanted with WT BM cells (mean ± SEM; n = ~7-9 recipient mice per group)

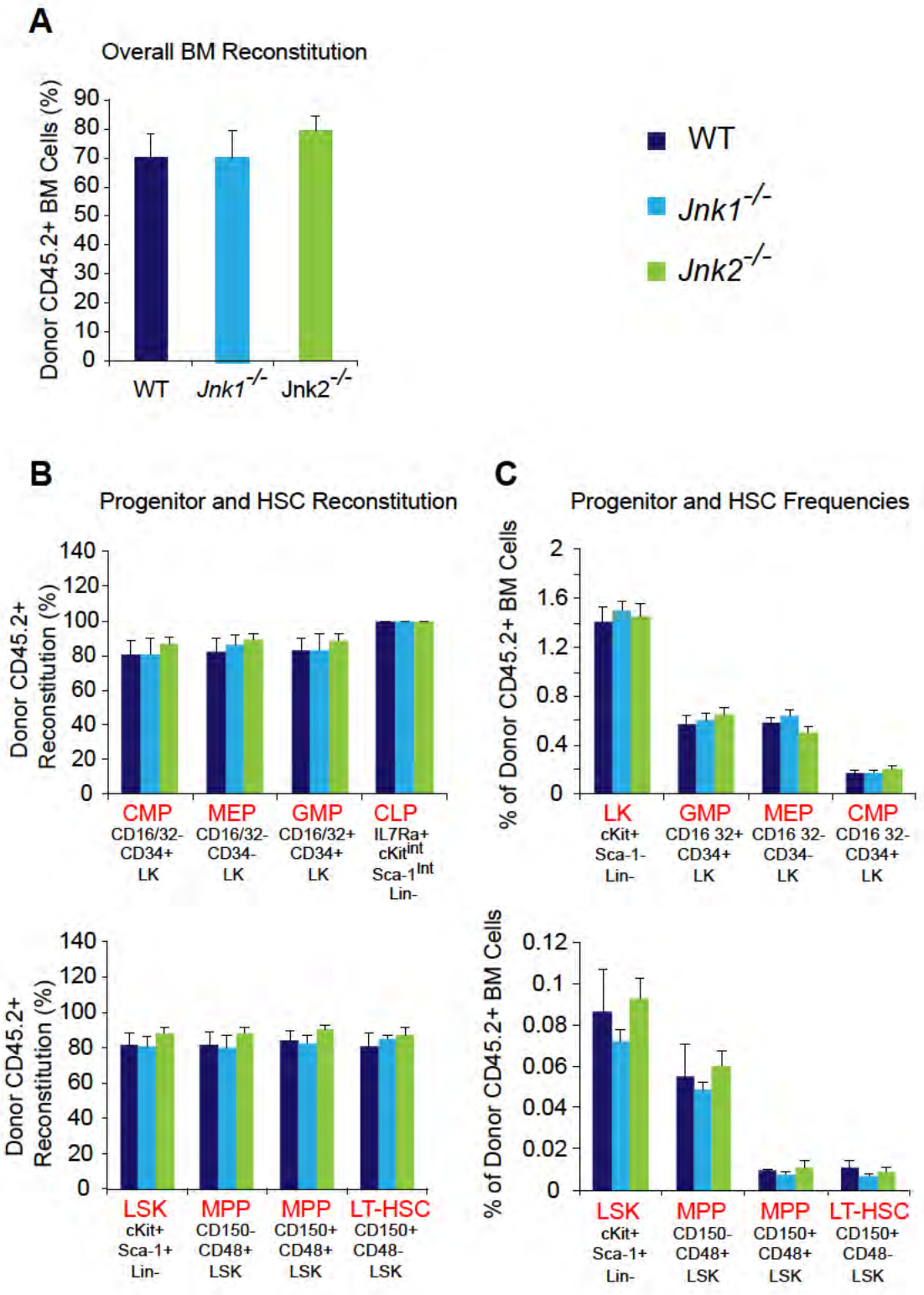

A
Overall BM Reconstitution
Donor CD45.2+ BM Cells (%)
90
80
70
60
50
40
30
20
10
0
WT
Jnk1-/-
Jnk2-/-
WT
Jnk1-/-
Jnk2-/-
B
Progenitor and HSC Reconstitution
Donor CD45.2+ Reconstitution (%)
140
120
100
80
60
40
20
0
CMP CD16/32- CD34+ LK
MEP CD16/32- CD34- LK
GMP CD16/32+ CD34+ LK
CLP IL7Ra+ cKitint Sca-1Int Lin-
LSK cKit+ Sca-1+ Lin-
MPP CD150- CD48+ LSK
MPP CD150+ CD48+ LSK
LT-HSC CD150+ CD48- LSK
C
Progenitor and HSC Frequencies
% of Donor CD45.2+ BM Cells
2
1.6
1.2
0.8
0.4
0
LK cKit+ Sca-1- Lin-
GMP CD16 32+ CD34+ LK
MEP CD16 32- CD34- LK
CMP CD16 32- CD34+ LK
0.12
0.1
0.08
0.06
0.04
0.02
0
LSK cKit+ Sca-1+ Lin-
MPP CD150- CD48+ LSK
MPP CD150+ CD48+ LSK
LT-HSC CD150+ CD48- LSK

Figure III.3 HSC and progenitor analysis 20 weeks post-transplantation in the bone marrow of primary recipients from the experiment in Figure III.2

A) Flow cytometry analysis of BM from primary recipient mice 20 weeks post transplantation shows no statistically significant differences in overall donor CD45.2^{+} cell reconstitution in mice that were transplanted with *Jnk1*$^{-/-}$ or *Jnk2*$^{-/-}$ BM cells compared to recipients that were transplanted with WT BM cells. (mean ± SEM; n = ~7-9 recipient mice per group)

B) No statistically significant differences in the reconstitution of various progenitors and HSCs were detected between primary recipient mice that were transplanted with *Jnk1*$^{-/-}$ or *Jnk2*$^{-/-}$ BM cells compared to recipients that were transplanted with WT BM cells. (mean ± SEM; n = ~7-9 recipient mice per group)

C) No statistically significant differences in the frequency of various progenitors and HSCs within the donor CD45.2^{+} population were detected between primary recipient mice that were transplanted with *Jnk1*$^{-/-}$ or *Jnk2*$^{-/-}$ BM cells compared to recipients that were transplanted with WT BM cells. (mean ± SEM; n = ~7-9 recipient mice per group)

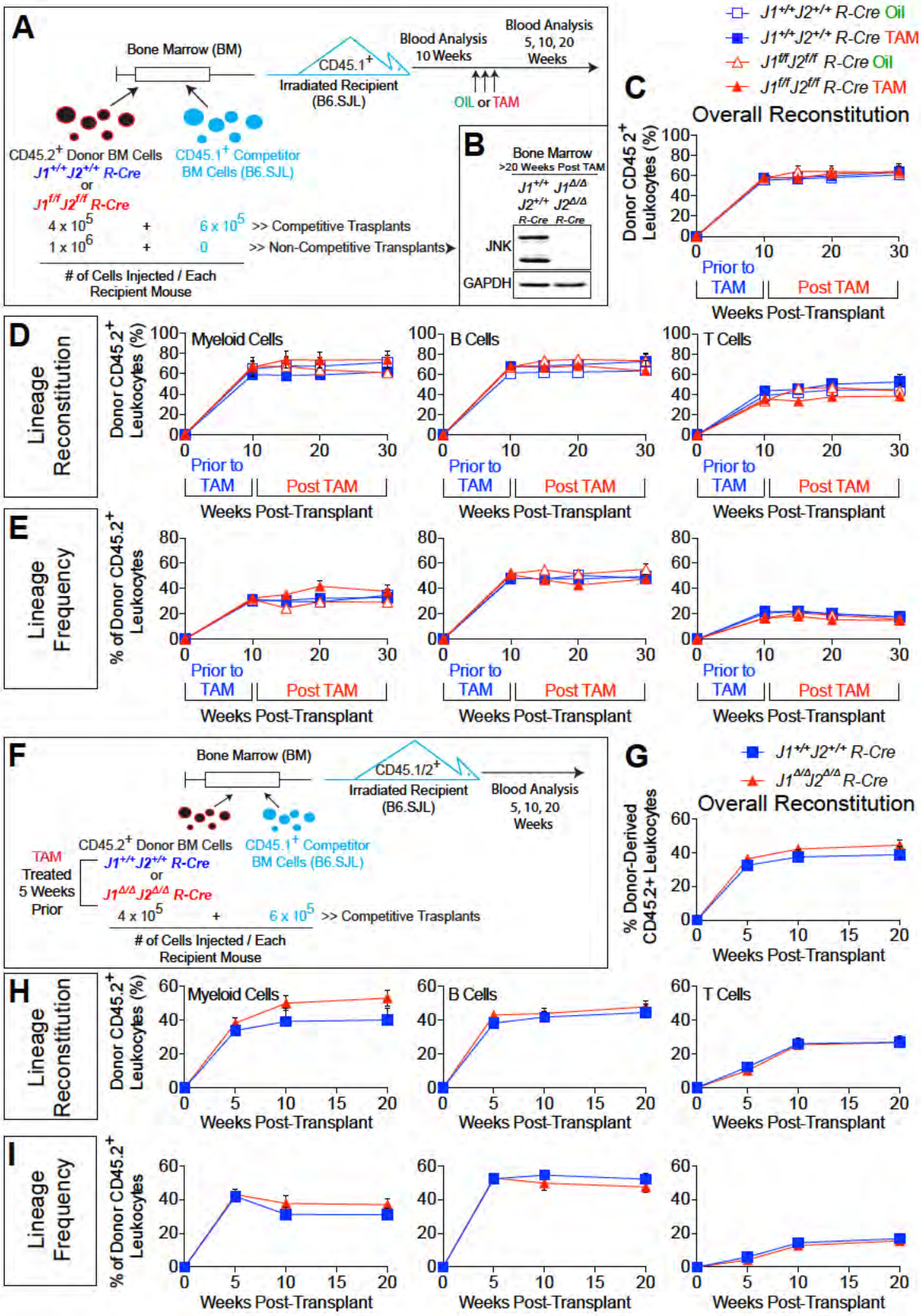

A
Bone Marrow (BM)
CD45.1+
Irradiated Recipient
(B6.SJL)
Blood Analysis
10 Weeks
Blood Analysis
5, 10, 20
Weeks
OIL or TAM
CD45.2+ Donor BM Cells
J1+/+J2+/+ R-Cre
or
J1f/fJ2f/f R-Cre
CD45.1+ Competitor
BM Cells (B6.SJL)
4 x 10^5 + 6 x 10^5 >> Competitive Trasplants
1 x 10^6 + 0 >> Non-Competitive Transplants
# of Cells Injected / Each
Recipient Mouse
B
Bone Marrow
>20 Weeks Post TAM
J1+/+ J1Δ/Δ
J2+/+ J2Δ/Δ
R-Cre R-Cre
JNK
GAPDH
C
J1+/+J2+/+ R-Cre Oil
J1+/+J2+/+ R-Cre TAM
J1f/fJ2f/f R-Cre Oil
J1f/fJ2f/f R-Cre TAM
Overall Reconstitution
Donor CD45.2+ Leukocytes (%)
Prior to TAM
Post TAM
Weeks Post-Transplant
D
Lineage Reconstitution
Myeloid Cells
B Cells
T Cells
E
Lineage Frequency
% of Donor CD45.2+ Leukocytes
F
Bone Marrow (BM)
CD45.1/2+
Irradiated Recipient
(B6.SJL)
Blood Analysis
5, 10, 20
Weeks
TAM
Treated
5 Weeks
Prior
CD45.2+ Donor BM Cells
J1+/+J2+/+ R-Cre
or
J1Δ/ΔJ2Δ/Δ R-Cre
CD45.1+ Competitor
BM Cells (B6.SJL)
4 x 10^5 + 6 x 10^5 >> Competitive Trasplants
# of Cells Injected / Each
Recipient Mouse
G
J1+/+J2+/+ R-Cre
J1Δ/ΔJ2Δ/Δ R-Cre
Overall Reconstitution
% Donor-Derived CD45.2+ Leukocytes
H
Lineage Reconstitution
Myeloid Cells
B Cells
T Cells
I
Lineage Frequency
% of Donor CD45.2+ Leukocytes

Figure III.4 Compound ablation of both *Jnk1* plus *Jnk2* genes in hematopoietic cells of adult mice does not perturb hematopoiesis or BM cell homing and engraftment following transplantation.

A) Competitive BM transplantation experimental set up involving *in situ* ablation of both *Jnk1* plus *Jnk2* genes after engraftment into recipient mice was completed. Test BM cells from $J1^{+/+}J2^{+/+}$ *R-Cre* or $J1^{f/f}J2^{f/f}$ *R-Cre* mice expressing the CD45.2 allele were each either transplanted alone (non-competitive transplants), or mixed with competitor BM cells expressing the CD45.1 allele, as indicated, and transplanted via the tail vein into lethally irradiated recipient mice. Two groups of recipient mice received $J1^{+/+}J2^{+/+}$ *R-Cre* and another two groups received $J1^{f/f}J2^{f/f}$ *R-Cre* BM cells in conjunction with competitor cells. Ten weeks post-transplantation, successful and similar engraftment in all 4 groups of competitively transplanted mice was confirmed by flow cytometry analysis of peripheral blood, and recipient mice received either tamoxifen (TAM) to induce Cre activity in donor-derived test hematopoietic cells or oil as control. Peripheral blood from recipient mice was then analyzed at different times over 20 weeks for alterations in donor cell chimerism and multilineage reconstitution.

B) Bone marrow cells from recipient mice that were transplanted with either $J1^{+/+}J2^{+/+}$ *R-Cre* or $J1^{f/f}J2^{f/f}$ *R-Cre* alone (i.e., in a non-competitive fashion) were harvested >20 weeks post-tamoxifen administration and examined by immunoblot analysis with antibodies to JNK and GAPDH. This analysis revealed successful deletion of JNK in BM cells from mice transplanted with $J1^{f/f}J2^{f/f}$ *R-Cre* BM.

C) Recipient mice transplanted with $J1^{+/+}J2^{+/+}$ *R-Cre* or $J1^{f/f}J2^{f/f}$ *R-Cre* BM cells showed no significant alterations in overall peripheral blood leukocyte reconstitution whether they were treated with oil or tamoxifen (mean ± SEM; n = 10 recipient mice per group).

D) Recipient mice transplanted with $J1^{+/+}J2^{+/+}$ *R-Cre* or $J1^{f/f}J2^{f/f}$ *R-Cre* BM cells showed no significant alterations in reconstitution of myeloid, B and T cells whether they were treated with oil or tamoxifen (mean ± SEM; n = 10 recipient mice per group).

E) Recipient mice transplanted with $J1^{+/+}J2^{+/+}$ *R-Cre* or $J1^{f/f}J2^{f/f}$ *R-Cre* BM cells showed no significant alterations in the frequency of myeloid, B and T cells within the donor $CD45.2^{+}$ leukocyte population whether they were treated with oil or tamoxifen (mean ± SEM; n = 10 recipient mice per group).

F) Competitive BM transplantation experimental set up involving ablation of both *Jnk1* plus *Jnk2* genes before transplantation into recipient mice. $J1^{+/+}J2^{+/+}$ *R-Cre* and $J1^{f/f}J2^{f/f}$ *R-Cre* mice were treated with tamoxifen to induce Cre activity and

disrupt *Jnk1* and *Jnk2* floxed alleles in $J1^{f/f}J2^{f/f}$ *R-Cre* mice, now refered to as $J1^{\Delta/\Delta}J2^{\Delta/\Delta}$ *R-Cre*. Successful deletion was confirmed by immunoblot analysis. Test BM cells from $J1^{+/+}J2^{+/+}$ *R-Cre* or $J1^{\Delta/\Delta}J2^{\Delta/\Delta}$ *R-Cre* mice expressing the CD45.2 allele were each mixed with competitor BM cells expressing the CD45.1 allele, as indicated, and transplanted via the tail vein into lethally irradiated recipient mice. Peripheral blood from recipient mice was analyzed at different times over 20 weeks for donor cell chimerism and multilineage reconstitution with antibodies to lineage markers.

G) Recipient mice transplanted with $J1^{+/+}J2^{+/+}$ *R-Cre* or $J1^{\Delta/\Delta}J2^{\Delta/\Delta}$ *R-Cre* BM cells showed no consistently significant differences in overall peripheral blood leukocyte reconstitution (mean ± SEM; n = ~8-10 recipient mice per group).

H) Recipient mice transplanted with $J1^{+/+}J2^{+/+}$ *R-Cre* or $J1^{\Delta/\Delta}J2^{\Delta/\Delta}$ *R-Cre* BM cells showed no consistently significant differences in reconstitution of myeloid, B and T cells (mean ± SEM; n = ~8-10 recipient mice per group).

I) Recipient mice transplanted with $J1^{+/+}J2^{+/+}$ *R-Cre* or $J1^{\Delta/\Delta}J2^{\Delta/\Delta}$ *R-Cre* BM cells showed no consistently significant differences in the frequency of myeloid, B and T cells within the donor $CD45.2^{+}$ leukocyte population (mean ± SEM; n = ~8-10 recipient mice per group).

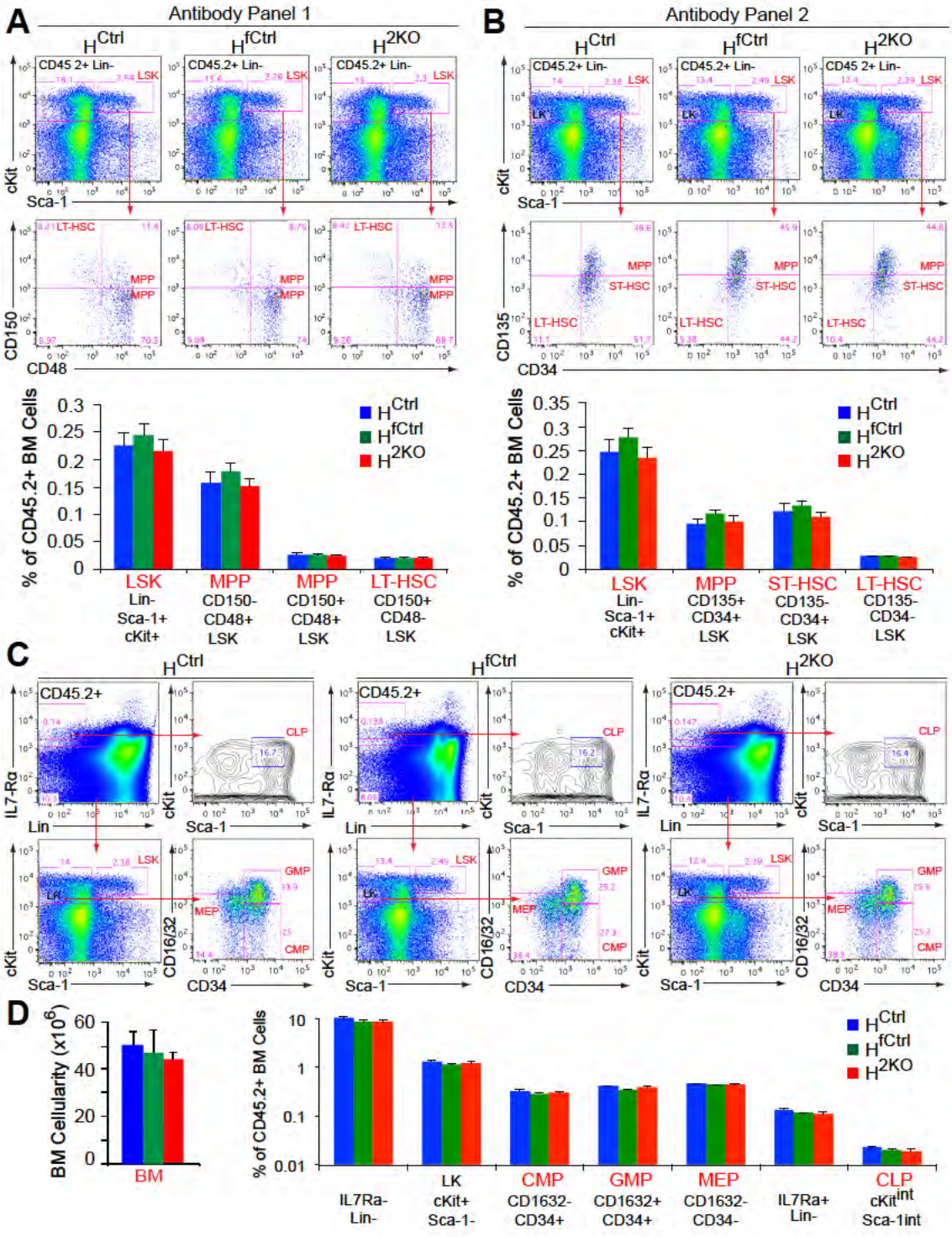

A
Antibody Panel 1
H^Ctrl
H^fCtrl
H^2KO
CD45 2+ Lin-
CD45.2+ Lin-
LSK
cKit
Sca-1
LT-HSC
MPP
CD150
CD48
% of CD45.2+ BM Cells
LSK Lin- Sca-1+ cKit+
MPP CD150- CD48+ LSK
MPP CD150+ CD48+ LSK
LT-HSC CD150+ CD48- LSK
B
Antibody Panel 2
LK
ST-HSC
CD135
CD34
LSK Lin- Sca-1+ cKit+
MPP CD135+ CD34+ LSK
ST-HSC CD135- CD34+ LSK
LT-HSC CD135- CD34- LSK
C
CD45.2+
CLP
IL7-Rα
Lin
GMP
MEP
CMP
CD16/32
D
BM Cellularity (x10^6)
BM
% of CD45.2+ BM Cells
IL7Ra- Lin-
LK cKit+ Sca-1-
CMP CD1632- CD34+
GMP CD1632+ CD34+
MEP CD1632- CD34-
IL7Ra+ Lin-
CLP cKit^int Sca-1int

Figure III.5 Compound ablation of both *Jnk1* plus *Jnk2* genes in hematopoietic cells starting in embryonic life does not perturb HSC and progenitor cell development.

A) Bone marrow (BM) cells from H^{2KO} and control mice were immunostained with fluorochrome-conjugated antibodies and analyzed by flow cytometry to identify bone marrow cell populations enriched in HSC and progenitor cells. Quantitative flow cytometry analysis revealed no significant perturbations in the proportions of the indicated HSC and MPP populations examined between H^{2KO} and control mice (mean ± SEM; n = 7 mice per group). Data presented are from one of two experiments with similar results.

B) Quantitative flow cytometry analysis using a second panel of antibodies also revealed no significant perturbations in the proportions of the indicated HSC and MPP populations examined between H^{2KO} and control mice (mean ± SEM; n = 7 mice per group). Data presented are from one of two experiments with similar results.

C) Flow cytometry analysis of lymphoid and myeloid progenitors including the common lymphoid progenitors (CLP), common myeloid progenitors (CMP), granulocyte macrophage progenitors (GMP) and megakaryocyte erythrocyte progenitors (MEP) shows no significant differences in their proportion in the BM of H^{2KO} and control mice (mean ± SEM; n = 7 mice per group). Data presented are from one of two experiments with similar results.

D) No significant differences were detected in total BM cellularity between H^{2KO} and control mice mice (mean ± SEM; n = 7 mice per group). Data presented are from one of two experiments with similar results.

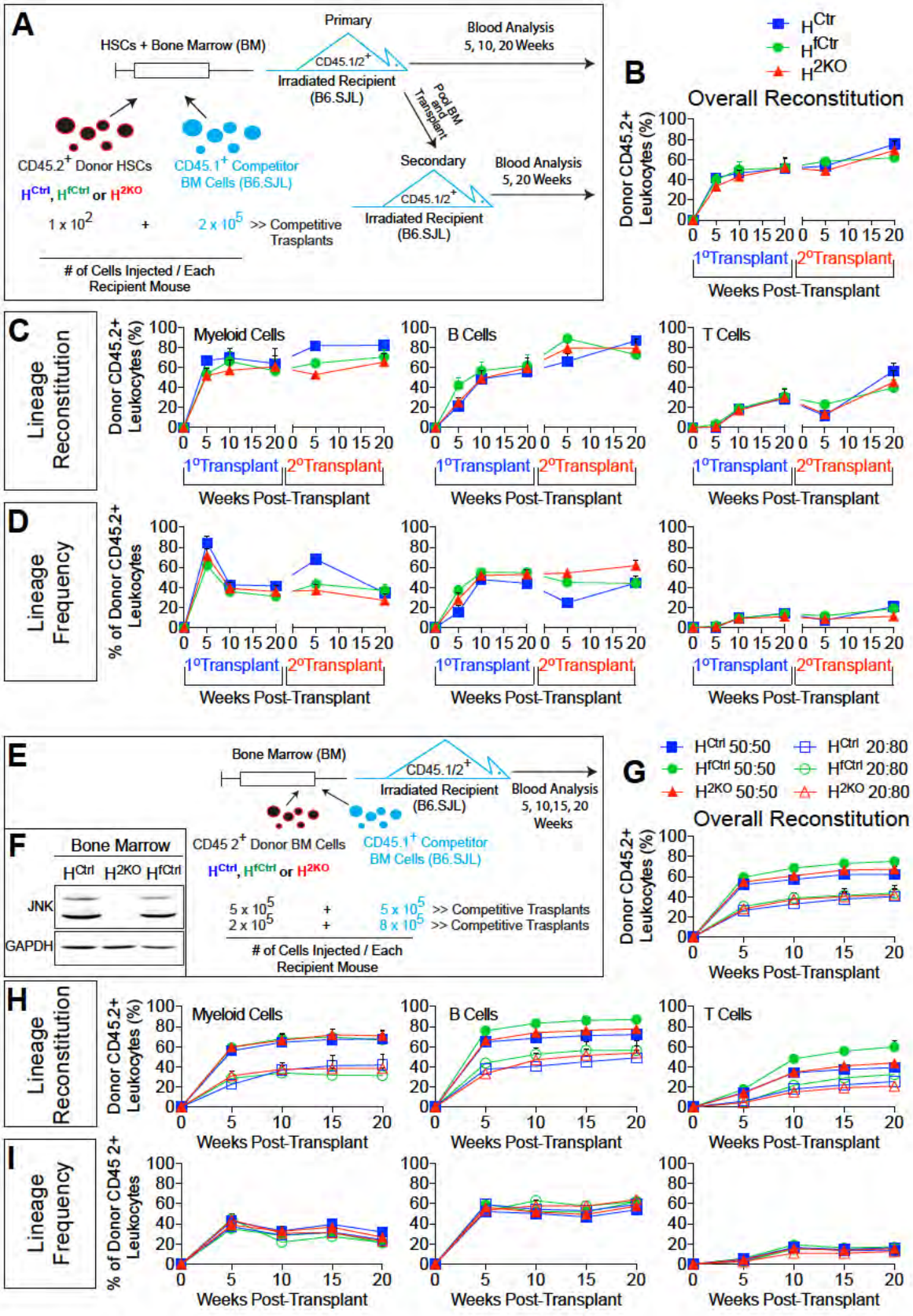

A
HSCs + Bone Marrow (BM)
Primary
CD45.1/2+
Irradiated Recipient (B6.SJL)
Blood Analysis 5, 10, 20 Weeks
Pool BM and Transplant
Secondary
CD45.1/2+
Irradiated Recipient (B6.SJL)
Blood Analysis 5, 20 Weeks
CD45.2+ Donor HSCs
HCtrl, HfCtrl or H2KO
1 x 10^2
+
CD45.1+ Competitor BM Cells (B6.SJL)
2 x 10^5 >> Competitive Trasplants
# of Cells Injected / Each Recipient Mouse
B
HCtr
HfCtr
H2KO
Overall Reconstitution
Donor CD45.2+ Leukocytes (%)
1°Transplant
2°Transplant
Weeks Post-Transplant
C
Lineage Reconstitution
Myeloid Cells
B Cells
T Cells
Donor CD45.2+ Leukocytes (%)
1°Transplant
2°Transplant
Weeks Post-Transplant
D
Lineage Frequency
% of Donor CD45.2+ Leukocytes
1°Transplant
2°Transplant
Weeks Post-Transplant
E
Bone Marrow (BM)
CD45.1/2+
Irradiated Recipient (B6.SJL)
Blood Analysis 5, 10,15, 20 Weeks
CD45 2+ Donor BM Cells
HCtrl, HfCtrl or H2KO
CD45.1+ Competitor BM Cells (B6.SJL)
5 x 10^5 + 5 x 10^5 >> Competitive Trasplants
2 x 10^5 + 8 x 10^5 >> Competitive Trasplants
# of Cells Injected / Each Recipient Mouse
F
Bone Marrow
HCtrl H2KO HfCtrl
JNK
GAPDH
G
HCtrl 50:50
HfCtrl 50:50
H2KO 50:50
HCtrl 20:80
HfCtrl 20:80
H2KO 20:80
Overall Reconstitution
Donor CD45.2+ Leukocytes (%)
Weeks Post-Transplant
H
Lineage Reconstitution
Myeloid Cells
B Cells
T Cells
Donor CD45.2+ Leukocytes (%)
Weeks Post-Transplant
I
Lineage Frequency
% of Donor CD45 2+ Leukocytes
Weeks Post-Transplant

Figure III.6 Compound ablation of both *Jnk1* plus *Jnk2* genes in hematopoietic cells starting in embryonic life does not perturb HSC and progenitor function upon transplantation

A) Serial competitive BM transplantation experimental set up using purified HSCs from H^{2KO} and control mice. Test HSCs (Lin^-, $Sca\text{-}1^+$, $cKit^+$, $CD150^+$, $CD44^-$) from H^{2KO} and control mice expressing the CD45.2 allele were sorted, mixed with competitor BM cells expressing the CD45.1 allele, as indicated, and transplanted via the tail vein into lethally irradiated recipient mice. Peripheral blood from primary recipient mice was analyzed at different times over 20 weeks for donor cell chimerism and multilineage reconstitution with antibodies to lineage markers. Twenty weeks post-transplantation BM from primary recipient mice was pooled and used to transplant secondary recipient mice that were analyzed similarly to primary recipients.

B) Primary and secondary recipient mice transplanted with H^{2KO} HSCs show no significant differences in overall peripheral blood leukocyte reconstitution compared to recipients transplanted with control HSCs. (mean ± SEM; n = ~5-8 recipient mice per group)

C) Primary and secondary recipient mice transplanted with H^{2KO} HSCs show no consistently significant JNK-dependent differences in reconstitution of myeloid, B and T cells compared to recipients transplanted with control HSCs. In some instances, significant differences between H^{2KO} recipients and one of the control recipient groups, but not the other were detected. These differences were not maintained over time. (mean ± SEM; n = ~5-8 recipient mice per group)

D) Primary and secondary recipient mice transplanted with H^{2KO} HSCs show no consistently significant JNK-dependent differences in the frequency of myeloid, B and T cells within the donor $CD45.2^+$ leukocyte population compared to recipients transplanted with control HSCs. In some instances, significant differences between H^{2KO} recipients and one of the control recipient groups, but not the other were detected. Furthermore, these differences were not maintained over time. (mean ± SEM; n = ~5-8 recipient mice per group)

E) Competitive BM transplantation experimental set up. Test BM cells from H^{2KO} and control mice expressing the CD45.2 allele were mixed with competitor BM cells expressing the CD45.1 allele at two different ratios, as indicated, and transplanted via the tail vein into lethally irradiated recipient mice. Peripheral blood from primary recipient mice was analyzed at different times over 20 weeks for donor cell chimerism and multilineage reconstitution with antibodies to lineage markers.

F) Immunoblot analysis of BM cell lysates from H^{2KO} and control mice with antibodies to JNK and GAPDH confirmed absence of JNK protein in BM cells from H^{2KO} mice.

G) Recipient mice transplanted with H^{2KO} BM cells show no significant differences in overall peripheral blood leukocyte reconstitution compared to recipients transplanted with control BM cells. (mean ± SEM; n = ~9-10 recipient mice per group)

H) Recipient mice transplanted with H^{2KO} BM cells show no consistently significant JNK-dependent differences in reconstitution of myeloid, B and T cells (mean ± SEM; n = ~9-10 recipient mice per group).

I) Recipient mice transplanted with H^{2KO} BM cells show no consistently significant JNK-dependent differences in the frequency of myeloid, B and T cells within the donor $CD45.2^+$ leukocyte population (mean ± SEM; n = ~9-10 recipient mice per group).

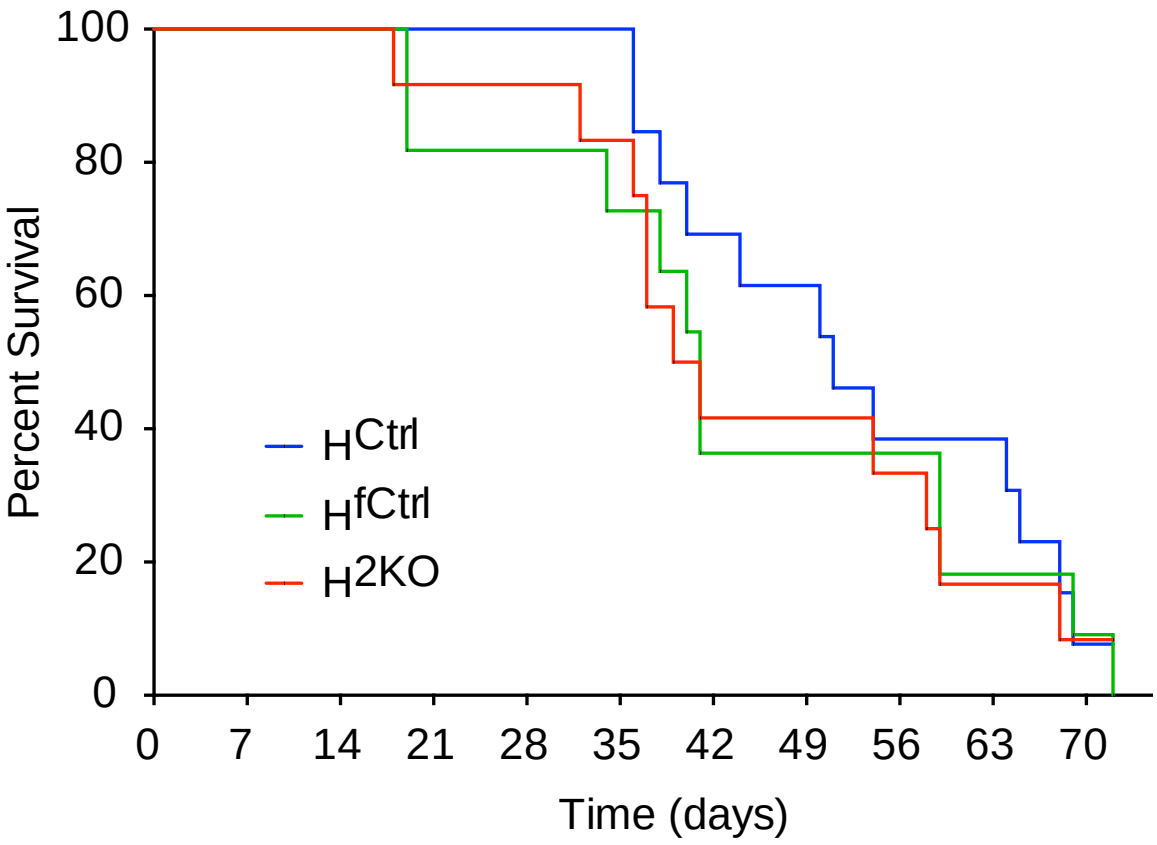
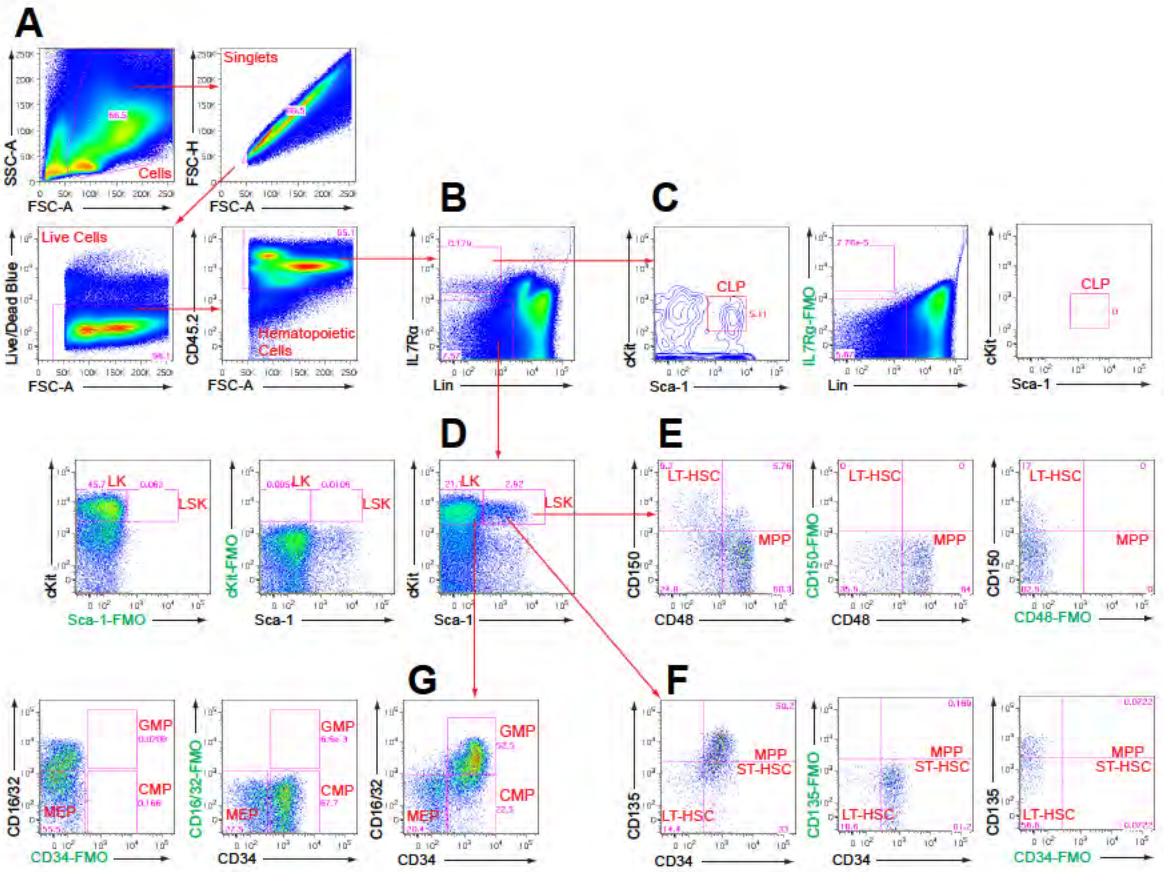

100
80
60
40
20
0
Percent Survival
0
7
14
21
28
35
42
49
56
63
70
Time (days)
HCtrl
HfCtrl
H2KO

Figure III.7 Sensitivity to 5-fluorouracil (5-FU) is not altered in H^{2KO} mice.

H^{2KO} and control mice received weakly intraperitoneal injections of 5-FU (150 mg/Kg) and were monitored over time. H^{2KO} mice showed similar survival kinetics compared to control mice (n = ~11-13 mice per group).


A
SSC-A
FSC-A
Cells
Singlets
FSC-H
FSC-A
Live Cells
Live/Dead Blue
FSC-A
CD45.2
FSC-A
Hematopoietic Cells
B
IL7Rα
Lin
C
cKit
Sca-1
CLP
IL7Rα-FMO
Lin
cKit
Sca-1
CLP
D
cKit
Sca-1-FMO
LK
LSK
cKit-FMO
Sca-1
LK
LSK
cKit
Sca-1
LK
LSK
E
CD150
CD48
LT-HSC
MPP
CD150-FMO
CD48
LT-HSC
MPP
CD150
CD48-FMO
LT-HSC
MPP
F
CD135
CD34
MPP
ST-HSC
LT-HSC
CD135-FMO
CD34
MPP
ST-HSC
LT-HSC
CD135
CD34-FMO
MPP
ST-HSC
LT-HSC
G
CD16/32
CD34-FMO
GMP
CMP
MEP
CD16/32-FMO
CD34
GMP
CMP
MEP
CD16/32
CD34
GMP
CMP
MEP

Supplementary Figure III.1 Gating strategy and fluorescence minus one (FMO) controls used for the identification of HSC and progenitor cell populations.

A) Bone marrow cell singlets were selected based on forward scatter (FSC-A, and FSC-H) and side scatter (SSC-A) properties. Live cells staining negative for Live/Dead Blue and positive for the pan-hematopoietic cell marker CD45 were then selected and displayed as shown in (**B**).

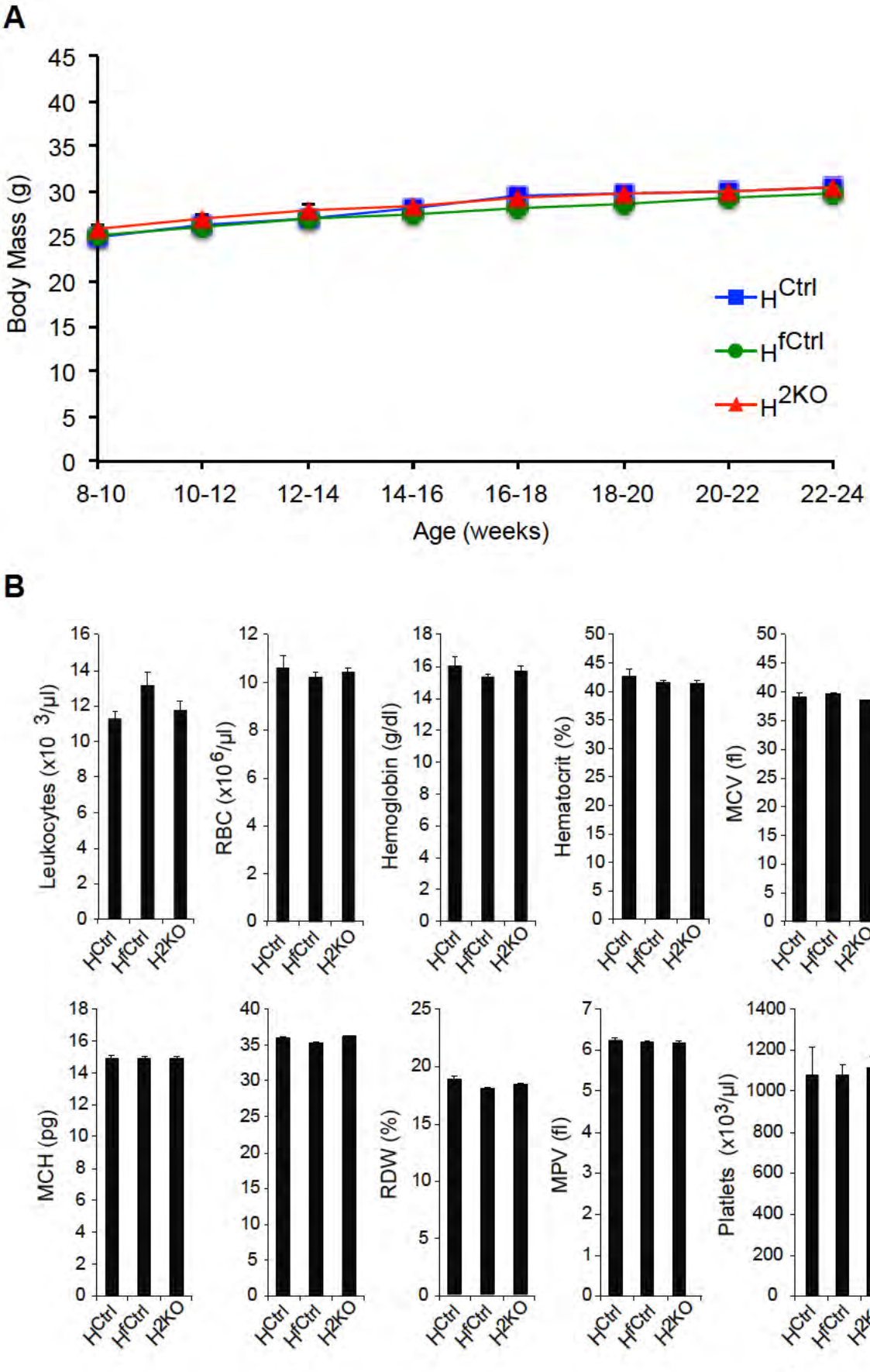
C) Lineage (Lin^-), $IL7R\alpha^+$ cells gated in panel **B** with intermediate cKit and Sca-1 staining identified common lymphoid progenitors (CLP). IL7Rα FMO antibody control that includes all antibodies in the panel except for the IL7Rα antibody is shown (right).

D) Lin^-, $IL7R\alpha^-$ cells gated in panel (**B**) were displayed as shown. cKit and Sca-1 FMO controls are shown (left).

E) Lin^-, $Sca\text{-}1^+$, $cKit^+$ (LSK) cells gated in panel (**D**) that stained positive for CD150 and negative for CD48 were identified as long-term HSCs (LT-HSC). LSK cells staining positive for CD48 were identified as multipotent progenitors (MPP). CD150 and CD48 FMO controls are shown (right).

F) LSK cells gated in panel (**D**) that stained negative for CD135 and CD34 were also identified as LT-HSC. LSK cells staining negative for CD135, but positive for CD34 were identified as short-term HSCs (ST-HSC). LSK cells staining positive for CD135 and CD34 were identified as MPP. CD135 and CD34 FMO controls are shown (right).

G) Lin^-, $Sca\text{-}1^-$, $cKit^+$ (LK) cells gated in panel (**D**) that stained positive for CD16/32 and CD34 were identified as granulocyte/macrophage progenitors (GMP). LK cells staining negative for CD16/32, but positive for CD34 were identified as common myeloid progenitors (CMP). LK cells staining negative for both CD16/32 and CD34 were identified as megakaryocyte/erythrocyte progenitors (MEP). CD16/32 and CD34 FMO controls are shown (left).


A
Body Mass (g)
45
40
35
30
25
20
15
10
5
0
8-10
10-12
12-14
14-16
16-18
18-20
20-22
22-24
Age (weeks)
H Ctrl
H fCtrl
H 2KO
B
Leukocytes (x10 3/µl)
RBC (x10 6/µl)
Hemoglobin (g/dl)
Hematocrit (%)
MCV (fl)
MCH (pg)
RDW (%)
MPV (fl)
Platlets (x10 3/µl)
HCtrl
HfCtrl
H2KO

Supplementary Figure III.2 Normal body mass and blood cell indices in H^{2KO} mice.

A) Body mass measurements showing no significant differences between adult H^{2KO} and control mice (mean ± SEM; n =~9-10).

B) Complete blood cell analysis showing no significant JNK-dependent differences in any of the measured indices (mean ± SEM; n =~4-6 mice per group). RBC, red blood cells; MCV, mean corpuscular volume; MCH, mean corpuscular hemoglobin; MCHC, mean corpuscular hemoglobin concentration; RDW, red cell distribution width; MPV, mean platelet volume.

Chapter IV

Discussion & Future Directions

Discussion

JNK has pleiotropic roles in many areas of biology. Studies have revealed important physiologic and pathologic functions of JNK in embryonic development, inflammation, metabolism and cancer.[1,12,158] The work presented in this dissertation uncovers new functions of JNK and expands the repertoire of knowledge on the role of JNK in vascular biology and the hematopoietic system.

Prior to our study the role of JNK in endothelial cells and vascular biology was limited to *in vitro* investigations or a few studies that employed *Jnk1*$^{-/-}$ mice. Thus, the role of JNK in endothelial cell-mediated vascular development and function was unknown. In Chapter II of this dissertation I have presented a body of data that adds considerable insight into the role of JNK in the endothelium, but also vascular biology in general. In this study, we generated endothelial-specific constitutive and inducible compound mutant mice that lack all JNK isoforms in the vascular endothelium. These mice were instrumental in our investigations and allowed us to identify critical roles for JNK in retinal and muscle vascular morphogenesis as well as native collateral artery development. In contrast to the essential function of JNK during the embryonic and early postnatal development of the vasculature, our study of mice in which we ablated JNK only after mice had reached adulthood demonstrated that endothelial JNK does not play a major role in the process of arteriogenesis in the setting of vascular occlusion.

Our study of *Mlk2*$^{-/-}$*Mlk3*$^{-/-}$ mice reveals an important role for these kinases in vascular morphogenesis and native collateral artery development that in many respects mirrors the role of endothelial JNK indicating that MLK mediate JNK activation important for vascular development. Although, MLK are known to activate JNK, our study demonstrates for the first time that they play a major role in vascular development.

In addition to the identification of a MLK – JNK signaling axis that is critical for vascular morphogenesis and native collateral artery formation, our study makes a significant advance in the understanding of how muscle collateral arteries form during ontogeny. Our detailed tracing of gracilis muscle collaterals at different times during development have lead us to propose a model in which gracilis collaterals form via a plexus intermediate from which vessels within the plexus get selected to become collateral arteries due to their proximity to peripheral nerves. This model is different from that proposed for pial collateral artery formation, which appear to form as distinct sprouts from existing arterioles.[61] Both models may be correct and may reflect the differences in tissue composition and architecture between brain and skeletal muscle.

By combining our morphological observations and functional data with information from the literature and our RNA Seq results from JNK-deficient and control endothelial cells, we were able to identify perturbations in Dll4 – Notch

signaling in JNK-deficient endothelial cells and the JNK-deficient retinal vasculature that provide a likely mechanism that may contribute to the retinal vascular and native collateral artery defects in mice that lack JNK in the endothelium. Our RNA Seq data also provides a wealth of gene expression information that may fuel many future investigations.

We have identified perturbations in the expression of several guidance molecules including downregulation of several class 3 semaphorins as well as upregulation of Slit2 and smaller perturbations in Netrin 1 and the semaphorin receptor, Nrp1. Semaphorins were originally described as axon guidance factors, but have now also been shown to act as attractive or repulsive regulators of angiogenesis.[219-221] Although the role of the alterations in expression of particular semaphorins in JNK-deficient endothelial cells and the role of the endothelium as a source of semaphorins remains unclear, it is possible that the perturbations in semaphorin expression in JNK-deficient endothelial cells may contribute to the dysfunctional vascular morphogenesis in E^{3KO} mice. The strong upregulation of the guidance molecule Slit2 is also interesting. Slits bind to several Robo receptors that are expressed in endothelial cells and mediate cellular motility.[222] Indeed, a recent study reported a critical role for Slit2 signaling in promoting retinal vascularization through endothelial Robo1 and Robo2.[223] Although, again, the role of the endothelium as a source of Slit2 is unclear, the increased Slit2 expression in the JNK-deficient endothelial cells may contribute to the excessive sprouting

angiogenesis observed in E^{3KO} mice.

The downregulation of several gap junction proteins including connexin37 (Cx37, encoded by *Gja4*) and connexin40 (Cx40, encoded by *Gja5*) in JNK-deficient endothelial cells may also play a role in the defective formation of native collateral arteries in E^{3KO} mice. *Cx40*$^{-/-}$ mice have been reported to modulate arterial identity in response to shear stress and show markedly reduced blood perfusion restoration in the FAL model.[80,92] The role of Cx40 specifically in the formation of native collateral arteries has not been demonstrated. In contrast to *Cx40*$^{-/-}$ mice, *Cx37*$^{-/-}$ mice[81] show significantly enhanced blood perfusion immediately after FAL, suggesting that they have improved collateral artery function. Connexins are known to form homo or heteromeric hemichannels (or connexons). Gap junctions are composed of two hemichannels from neighboring cells that provide intercellular communication by facilitating the diffusion of ions, small metabolites and second messengers.[224] Thus, the phenotype in the absence of a particular connexin may reflect altered composition of hemichannels. Therefore, the improved bood perfusion recovery following FAL in *Cx37*$^{-/-}$ mice may be due to hemichannels that contain more Cx40 molecules. Hence, the reduction in both Cx37 and Cx40 expression in JNK-deficient endothelial cells may result in altered hemichannel composition and gap junction function and may contribute to the native collateral artery defects in E^{3KO} mice.

Another gene whose expression is increased in JNK-deficient endothelial cells and may contribute to abnormal vascular morphogenesis in E^{3KO} mice is endothelial cell-specific molecule 1 (*Esm1*). Esm1 is a secreted glycoprotein that binds to fibronectin in the extracellular matrix and can displace fibronectin-bound VEGF-A165, thus, enhancing regional VEGF-A165 bioavailability.[225] Increased Esm1 expression by JNK-deficient endothelial cells may result in increased regional VEGF-A165 bioavailability that may mediate excessive sprouting angiogenesis and altered vascular morphogeneis in E^{3KO} mice.

Other gene expression alterations in JNK-deficient endothelial cells that are displayed in the heatmap in Figure II.9D are potentially interesting and open the door for much future exploration into the mechanism of JNK-mediated regulation of vascular morphogenesis and native collateral artery formation.

Our study points to an important role for JNK-mediated regulation of Dll4 – Notch signaling and vascular morphogenesis, and identifies a MLK – JNK signaling axis that is critical for native collateral artery formation. Genetically modified mice with disruption in this pathway display defective collateral artery patterning and undergo severe blood perfusion blockade and severe tissue injury following arterial occlusion (Figure II.11).

Endothelial and hematopoietic cells are thought to arise from a common precursor.[33] Although JNK has major roles in endothelial cell biology and vascular development, our studies presented in Chapter III demonstrate that JNK in hematopoietic cells is dispensable for normal hematopoiesis and HSC self-renewal. However, JNK in hematopoietic cells may be important in certain conditions such as in inflammatory responses to infection or during hematopoietic cell transformation.

Future Directions

Future research into the role of JNK in the vasculature could include the following:

A synthetic Jag1 peptide has been previously reported to induce Dll4 expression and Notch signaling resulting in suppression of endothelial cell sprouting activity.[46,47,175] To test if the decreased Dll4 expression in the retinal vasculature of E^{3KO} mice is biologically relevant, E^{3KO} pups can be treated with Jag1 peptide or a scrambled peptide. Analysis of the retinal vasculature should reveal whether treatment with Jag1 peptide restores Dll4 levels in the vascualture of E^{3KO} pups and whether this normalizes endothelial cell sprouting activity. Suppression of excessive endothelial cell sprouting by Jag1 peptide treatment of E^{3KO} mice would strongly support the hypothesis that the endothelial cell hypersprouting in the E^{3KO} vasculature is mediated by decreased Dll4-Notch signaling. It is unclear how Jag1 peptide treatment enhances Dll4 levels and Notch signaling. It is possible that Jag1 peptide treatment may not restore Dll4 levels in the E^{3KO} retinal vasculature. This would indicate that JNK may regulate Dll4 expression and Notch signaling via mechanism(s) that are distinct from those that mediate the effects of Jag1 peptide treatment.

A detailed analysis of muscle collateral arteries in *Dll4*$^{+/-}$ mice via methods employed in our study would reveal whether these mice display similar defects to

those observed in E^{3KO} mice. This analysis would clarify the role of Dll4-Notch signaling in native collateral artery formation.

In addition to perturbations in Dll4-Notch signaling other mechanisms are likely to contribute to the vascular defects in JNK-deficient mice. Direct investigation of the possible role of other genes that were shown to be differentially expressed in JNK-deficient endothelial cells may reveal additional mechanisms through which the JNK pathway may contribute to vascular morphogenesis and native collateral artery formation.

We found that gracilis collateral arteries form in close apposition to peripheral nerves. These data suggest that factors secreted by peripheral nerves may be important for formation and maturation of collateral arteries. Investigation of the role of peripheral nerves in collateral artery formation would, therefore, be an exciting area for future investigations. It is also possible that the vasculature may influence peripheral nerve morphogenesis and/or function. Thus the vasculature and the peripheral nervous system may have important interdependent functions, and perturbations in either system may lead to defects in both systems.

We found that the JNK pathway plays an essential role in endothelial cells, however, JNK in hematopoietic or skeletal muscle does not appear to play a role in vascular development and function as suggested by the absence of defects in

the response to arterial occlusion in mice that lack JNK in these tissues. We did not investigate the role of JNK in smooth muscle cells. It is possible that JNK in smooth muscle cells may be important for vascular development and collateral artery formation and thus analysis of mice with smooth muscle cell-specific ablation of JNK may be warranted.

JNK in liver, adipose tissue, pituitary and hematopoietic cells has essential roles in the metabolic response to high fat diet consumption.[13,163,226,227] The endothelium also participates in metabolic homeostasis.[228,229] Investigation of the role of endothelial JNK in metabolism may reveal important functions of the JNK pathway in these cells. We have initiated these studies.

Investigation of the effect of endothelial JNK disruption in experimental tumor cell metastasis models also represents an area of research that deserves further exploration. We have initiated these studies.

Some E^{2KO} and E^{3KO} mice display defects in tooth development. We have initiated studies that indicate that bone development may also be affected. Investigation of the role of endothelial JNK in bone and tooth development represents an exciting area of future research particularly because recent studies have demonstrated an important role for endothelial cells in osteogenesis.[230-232]

Future research into the role of JNK in the hematopoietic system could include the following:

Although an unlikely scenario, low levels of JNK3 expression in hematopoietic cells may have compensated for the loss of JNK1 and JNK2 in our mice. We have not been able to detect *Jnk3* expression in bone marrow cells from WT or hematopoietic cell JNK-deficient mice by quantitative RT-PCR analysis. Nevertheless, we have now generated mice with hematopoietic cell specific compound deficiency of JNK1 plus JNK2 plus JNK3. These mice appear morphologically normal. Future experiments will analyze if hematopoiesis is perturbed in these mice.

Although we have not found a required role for JNK in normal hematopoietic cell development and bone marrow cell function in transplantation assays, assessing the role of compound ablation of JNK genes in hematopoietic cell transformation induced by BCR-ABL, Pten deletion or other methods may reveal if the JNK pathway is important during hematopoietic cell transformation. We have generated *Vav1-Cre* $Jnk1^{LoxP/LoxP}Jnk2^{LoxP/LoxP}Pten^{LoxP/LoxP}$ and have initiated their analysis.

Assessing the role of compound ablation of JNK genes in infection or autoinflammatory disease models may also potentially reveal a role for JNK in these processes.

References

1. Davis, R.J. Signal transduction by the JNK group of MAP kinases. *Cell* **103**, 239-252 (2000).
2. Karin, M. & Gallagher, E. From JNK to pay dirt: jun kinases, their biochemistry, physiology and clinical importance. *IUBMB Life* **57**, 283-295 (2005).
3. Manning, A.M. & Davis, R.J. Targeting JNK for therapeutic benefit: from junk to gold? *Nat Rev Drug Discov* **2**, 554-565 (2003).
4. Rincon, M., Flavell, R.A. & Davis, R.J. Signal transduction by MAP kinases in T lymphocytes. *Oncogene* **20**, 2490-2497 (2001).
5. Kant, S., Swat, W., Zhang, S., Zhang, Z.Y., Neel, B.G., Flavell, R.A. & Davis, R.J. TNF-stimulated MAP kinase activation mediated by a Rho family GTPase signaling pathway. *Genes Dev* **25**, 2069-2078 (2011).
6. Jaeschke, A. & Davis, R.J. Metabolic stress signaling mediated by mixed-lineage kinases. *Mol Cell* **27**, 498-508 (2007).
7. Brancho, D., Ventura, J.J., Jaeschke, A., Doran, B., Flavell, R.A. & Davis, R.J. Role of MLK3 in the regulation of mitogen-activated protein kinase signaling cascades. *Mol Cell Biol* **25**, 3670-3681 (2005).
8. Kuan, C.Y., Yang, D.D., Samanta Roy, D.R., Davis, R.J., Rakic, P. & Flavell, R.A. The Jnk1 and Jnk2 protein kinases are required for regional specific apoptosis during early brain development. *Neuron* **22**, 667-676 (1999).
9. Barnat, M., Enslen, H., Propst, F., Davis, R.J., Soares, S. & Nothias, F. Distinct roles of c-Jun N-terminal kinase isoforms in neurite initiation and elongation during axonal regeneration. *J Neurosci* **30**, 7804-7816 (2010).
10. Tournier, C., Dong, C., Turner, T.K., Jones, S.N., Flavell, R.A. & Davis, R.J. MKK7 is an essential component of the JNK signal transduction pathway activated by proinflammatory cytokines. *Genes Dev* **15**, 1419-1426 (2001).
11. Derijard, B., Hibi, M., Wu, I.H., Barrett, T., Su, B., Deng, T., Karin, M. & Davis, R.J. JNK1: a protein kinase stimulated by UV light and Ha-Ras that binds and phosphorylates the c-Jun activation domain. *Cell* **76**, 1025-1037 (1994).
12. Weston, C.R. & Davis, R.J. The JNK signal transduction pathway. *Curr Opin Cell Biol* **19**, 142-149 (2007).
13. Vernia, S., Cavanagh-Kyros, J., Garcia-Haro, L., Sabio, G., Barrett, T., Jung, D.Y., Kim, J.K., Xu, J., Shulha, H.P., Garber, M., Gao, G. & Davis, R.J. The PPARalpha-FGF21 hormone axis contributes to metabolic regulation by the hepatic JNK signaling pathway. *Cell Metab* **20**, 512-525 (2014).

14. Ventura, J.J., Hubner, A., Zhang, C., Flavell, R.A., Shokat, K.M. & Davis, R.J. Chemical genetic analysis of the time course of signal transduction by JNK. *Mol Cell* **21**, 701-710 (2006).
15. Lamb, J.A., Ventura, J.J., Hess, P., Flavell, R.A. & Davis, R.J. JunD mediates survival signaling by the JNK signal transduction pathway. *Mol Cell* **11**, 1479-1489 (2003).
16. Varfolomeev, E.E. & Ashkenazi, A. Tumor necrosis factor: an apoptosis JuNKie? *Cell* **116**, 491-497 (2004).
17. Sakon, S., Xue, X., Takekawa, M., Sasazuki, T., Okazaki, T., Kojima, Y., Piao, J.H., Yagita, H., Okumura, K., Doi, T. & Nakano, H. NF-kappaB inhibits TNF-induced accumulation of ROS that mediate prolonged MAPK activation and necrotic cell death. *EMBO J* **22**, 3898-3909 (2003).
18. Ventura, J.J., Cogswell, P., Flavell, R.A., Baldwin, A.S., Jr. & Davis, R.J. JNK potentiates TNF-stimulated necrosis by increasing the production of cytotoxic reactive oxygen species. *Genes Dev* **18**, 2905-2915 (2004).
19. Chang, L., Kamata, H., Solinas, G., Luo, J.L., Maeda, S., Venuprasad, K., Liu, Y.C. & Karin, M. The E3 ubiquitin ligase itch couples JNK activation to TNFalpha-induced cell death by inducing c-FLIP(L) turnover. *Cell* **124**, 601-613 (2006).
20. Tournier, C., Hess, P., Yang, D.D., Xu, J., Turner, T.K., Nimnual, A., Bar-Sagi, D., Jones, S.N., Flavell, R.A. & Davis, R.J. Requirement of JNK for stress-induced activation of the cytochrome c-mediated death pathway. *Science* **288**, 870-874 (2000).
21. Gelinas, C. & White, E. BH3-only proteins in control: specificity regulates MCL-1 and BAK-mediated apoptosis. *Genes Dev* **19**, 1263-1268 (2005).
22. Morel, C., Carlson, S.M., White, F.M. & Davis, R.J. Mcl-1 integrates the opposing actions of signaling pathways that mediate survival and apoptosis. *Mol Cell Biol* **29**, 3845-3852 (2009).
23. Almeida, E.A., Ilic, D., Han, Q., Hauck, C.R., Jin, F., Kawakatsu, H., Schlaepfer, D.D. & Damsky, C.H. Matrix survival signaling: from fibronectin via focal adhesion kinase to c-Jun NH(2)-terminal kinase. *J Cell Biol* **149**, 741-754 (2000).
24. Hess, P., Pihan, G., Sawyers, C.L., Flavell, R.A. & Davis, R.J. Survival signaling mediated by c-Jun NH(2)-terminal kinase in transformed B lymphoblasts. *Nat Genet* **32**, 201-205 (2002).
25. Jacinto, A., Woolner, S. & Martin, P. Dynamic analysis of dorsal closure in Drosophila: from genetics to cell biology. *Dev Cell* **3**, 9-19 (2002).
26. Tada, M., Concha, M.L. & Heisenberg, C.P. Non-canonical Wnt signalling and regulation of gastrulation movements. *Semin Cell Dev Biol* **13**, 251-260 (2002).
27. Yamanaka, H., Moriguchi, T., Masuyama, N., Kusakabe, M., Hanafusa, H., Takada, R., Takada, S. & Nishida, E. JNK functions in the non-canonical Wnt pathway to regulate convergent extension movements in vertebrates. *EMBO Rep* **3**, 69-75 (2002).

28. Weston, C.R., Wong, A., Hall, J.P., Goad, M.E., Flavell, R.A. & Davis, R.J. The c-Jun NH2-terminal kinase is essential for epidermal growth factor expression during epidermal morphogenesis. *Proc Natl Acad Sci U S A* **101**, 14114-14119 (2004).
29. Weston, C.R., Wong, A., Hall, J.P., Goad, M.E., Flavell, R.A. & Davis, R.J. JNK initiates a cytokine cascade that causes Pax2 expression and closure of the optic fissure. *Genes Dev* **17**, 1271-1280 (2003).
30. Monahan-Earley, R., Dvorak, A.M. & Aird, W.C. Evolutionary origins of the blood vascular system and endothelium. *J Thromb Haemost* **11 Suppl 1**, 46-66 (2013).
31. Fish, J.E. & Wythe, J.D. The molecular regulation of arteriovenous specification and maintenance. *Dev Dyn* **244**, 391-409 (2015).
32. Coultas, L., Chawengsaksophak, K. & Rossant, J. Endothelial cells and VEGF in vascular development. *Nature* **438**, 937-945 (2005).
33. Orkin, S.H. & Zon, L.I. Hematopoiesis: an evolving paradigm for stem cell biology. *Cell* **132**, 631-644 (2008).
34. Potente, M., Gerhardt, H. & Carmeliet, P. Basic and therapeutic aspects of angiogenesis. *Cell* **146**, 873-887 (2011).
35. Stahl, A., Connor, K.M., Sapieha, P., Chen, J., Dennison, R.J., Krah, N.M., Seaward, M.R., Willett, K.L., Aderman, C.M., Guerin, K.I., Hua, J., Lofqvist, C., Hellstrom, A. & Smith, L.E. The mouse retina as an angiogenesis model. *Invest Ophthalmol Vis Sci* **51**, 2813-2826 (2010).
36. Pitulescu, M.E., Schmidt, I., Benedito, R. & Adams, R.H. Inducible gene targeting in the neonatal vasculature and analysis of retinal angiogenesis in mice. *Nat Protoc* **5**, 1518-1534 (2010).
37. Roca, C. & Adams, R.H. Regulation of vascular morphogenesis by Notch signaling. *Genes Dev* **21**, 2511-2524 (2007).
38. Eilken, H.M. & Adams, R.H. Dynamics of endothelial cell behavior in sprouting angiogenesis. *Curr Opin Cell Biol* **22**, 617-625 (2010).
39. Phng, L.K. & Gerhardt, H. Angiogenesis: a team effort coordinated by notch. *Dev Cell* **16**, 196-208 (2009).
40. Olsson, A.K., Dimberg, A., Kreuger, J. & Claesson-Welsh, L. VEGF receptor signalling - in control of vascular function. *Nat Rev Mol Cell Biol* **7**, 359-371 (2006).
41. Gerhardt, H., Golding, M., Fruttiger, M., Ruhrberg, C., Lundkvist, A., Abramsson, A., Jeltsch, M., Mitchell, C., Alitalo, K., Shima, D. & Betsholtz, C. VEGF guides angiogenic sprouting utilizing endothelial tip cell filopodia. *J Cell Biol* **161**, 1163-1177 (2003).
42. Taylor, K.L., Henderson, A.M. & Hughes, C.C. Notch activation during endothelial cell network formation in vitro targets the basic HLH transcription factor HESR-1 and downregulates VEGFR-2/KDR expression. *Microvasc Res* **64**, 372-383 (2002).
43. Suchting, S., Freitas, C., le Noble, F., Benedito, R., Breant, C., Duarte, A. & Eichmann, A. The Notch ligand Delta-like 4 negatively regulates

endothelial tip cell formation and vessel branching. *Proc Natl Acad Sci U S A* **104**, 3225-3230 (2007).

44. Benedito, R., Rocha, S.F., Woeste, M., Zamykal, M., Radtke, F., Casanovas, O., Duarte, A., Pytowski, B. & Adams, R.H. Notch-dependent VEGFR3 upregulation allows angiogenesis without VEGF-VEGFR2 signalling. *Nature* **484**, 110-114 (2012).
45. Jakobsson, L., Franco, C.A., Bentley, K., Collins, R.T., Ponsioen, B., Aspalter, I.M., Rosewell, I., Busse, M., Thurston, G., Medvinsky, A., Schulte-Merker, S. & Gerhardt, H. Endothelial cells dynamically compete for the tip cell position during angiogenic sprouting. *Nat Cell Biol* **12**, 943-953 (2010).
46. Hellstrom, M., Phng, L.K., Hofmann, J.J., Wallgard, E., Coultas, L., Lindblom, P., Alva, J., Nilsson, A.K., Karlsson, L., Gaiano, N., Yoon, K., Rossant, J., Iruela-Arispe, M.L., Kalen, M., Gerhardt, H. & Betsholtz, C. Dll4 signalling through Notch1 regulates formation of tip cells during angiogenesis. *Nature* **445**, 776-780 (2007).
47. Benedito, R., Roca, C., Sorensen, I., Adams, S., Gossler, A., Fruttiger, M. & Adams, R.H. The notch ligands Dll4 and Jagged1 have opposing effects on angiogenesis. *Cell* **137**, 1124-1135 (2009).
48. Dou, G.R., Wang, Y.C., Hu, X.B., Hou, L.H., Wang, C.M., Xu, J.F., Wang, Y.S., Liang, Y.M., Yao, L.B., Yang, A.G. & Han, H. RBP-J, the transcription factor downstream of Notch receptors, is essential for the maintenance of vascular homeostasis in adult mice. *FASEB J* **22**, 1606-1617 (2008).
49. Izumi, N., Helker, C., Ehling, M., Behrens, A., Herzog, W. & Adams, R.H. Fbxw7 controls angiogenesis by regulating endothelial Notch activity. *PLoS One* **7**, e41116 (2012).
50. Corada, M., Orsenigo, F., Morini, M.F., Pitulescu, M.E., Bhat, G., Nyqvist, D., Breviario, F., Conti, V., Briot, A., Iruela-Arispe, M.L., Adams, R.H. & Dejana, E. Sox17 is indispensable for acquisition and maintenance of arterial identity. *Nat Commun* **4**, 2609 (2013).
51. Folkman, J. & D'Amore, P.A. Blood vessel formation: what is its molecular basis? *Cell* **87**, 1153-1155 (1996).
52. Hanahan, D. Signaling vascular morphogenesis and maintenance. *Science* **277**, 48-50 (1997).
53. Gale, N.W. & Yancopoulos, G.D. Growth factors acting via endothelial cell-specific receptor tyrosine kinases: VEGFs, angiopoietins, and ephrins in vascular development. *Genes Dev* **13**, 1055-1066 (1999).
54. Carmeliet, P. & Collen, D. Role of vascular endothelial growth factor and vascular endothelial growth factor receptors in vascular development. *Curr Top Microbiol Immunol* **237**, 133-158 (1999).
55. Rossant, J. & Hirashima, M. Vascular development and patterning: making the right choices. *Curr Opin Genet Dev* **13**, 408-412 (2003).

56. Bicknell, R. & Harris, A.L. Novel angiogenic signaling pathways and vascular targets. *Annu Rev Pharmacol Toxicol* **44**, 219-238 (2004).
57. Faber, J.E., Chilian, W.M., Deindl, E., van Royen, N. & Simons, M. A brief etymology of the collateral circulation. *Arterioscler Thromb Vasc Biol* **34**, 1854-1859 (2014).
58. Schaper, W. Collateral circulation: past and present. *Basic Res Cardiol* **104**, 5-21 (2009).
59. van Royen, N., Piek, J.J., Schaper, W. & Fulton, W.F. A critical review of clinical arteriogenesis research. *J Am Coll Cardiol* **55**, 17-25 (2009).
60. Faber, J.E., Zhang, H., Lassance-Soares, R.M., Prabhakar, P., Najafi, A.H., Burnett, M.S. & Epstein, S.E. Aging causes collateral rarefaction and increased severity of ischemic injury in multiple tissues. *Arterioscler Thromb Vasc Biol* **31**, 1748-1756 (2011).
61. Lucitti, J.L., Mackey, J.K., Morrison, J.C., Haigh, J.J., Adams, R.H. & Faber, J.E. Formation of the collateral circulation is regulated by vascular endothelial growth factor-A and a disintegrin and metalloprotease family members 10 and 17. *Circ Res* **111**, 1539-1550 (2012).
62. Dai, X. & Faber, J.E. Endothelial nitric oxide synthase deficiency causes collateral vessel rarefaction and impairs activation of a cell cycle gene network during arteriogenesis. *Circ Res* **106**, 1870-1881 (2010).
63. Heil, M., Ziegelhoeffer, T., Wagner, S., Fernandez, B., Helisch, A., Martin, S., Tribulova, S., Kuziel, W.A., Bachmann, G. & Schaper, W. Collateral artery growth (arteriogenesis) after experimental arterial occlusion is impaired in mice lacking CC-chemokine receptor-2. *Circ Res* **94**, 671-677 (2004).
64. Chalothorn, D. & Faber, J.E. Formation and maturation of the native cerebral collateral circulation. *J Mol Cell Cardiol* **49**, 251-259 (2010).
65. Chalothorn, D., Zhang, H., Smith, J.E., Edwards, J.C. & Faber, J.E. Chloride intracellular channel-4 is a determinant of native collateral formation in skeletal muscle and brain. *Circ Res* **105**, 89-98 (2009).
66. Pohl, T., Seiler, C., Billinger, M., Herren, E., Wustmann, K., Mehta, H., Windecker, S., Eberli, F.R. & Meier, B. Frequency distribution of collateral flow and factors influencing collateral channel development. Functional collateral channel measurement in 450 patients with coronary artery disease. *J Am Coll Cardiol* **38**, 1872-1878 (2001).
67. Meier, P., Gloekler, S., Zbinden, R., Beckh, S., de Marchi, S.F., Zbinden, S., Wustmann, K., Billinger, M., Vogel, R., Cook, S., Wenaweser, P., Togni, M., Windecker, S., Meier, B. & Seiler, C. Beneficial effect of recruitable collaterals: a 10-year follow-up study in patients with stable coronary artery disease undergoing quantitative collateral measurements. *Circulation* **116**, 975-983 (2007).
68. Bang, O.Y., Saver, J.L., Buck, B.H., Alger, J.R., Starkman, S., Ovbiagele, B., Kim, D., Jahan, R., Duckwiler, G.R., Yoon, S.R., Vinuela, F., Liebeskind, D.S. & Investigators, U.C. Impact of collateral flow on tissue

fate in acute ischaemic stroke. *J Neurol Neurosurg Psychiatry* **79**, 625-629 (2008).

69. Christoforidis, G.A., Karakasis, C., Mohammad, Y., Caragine, L.P., Yang, M. & Slivka, A.P. Predictors of hemorrhage following intra-arterial thrombolysis for acute ischemic stroke: the role of pial collateral formation. *AJNR Am J Neuroradiol* **30**, 165-170 (2009).
70. Miteff, F., Levi, C.R., Bateman, G.A., Spratt, N., McElduff, P. & Parsons, M.W. The independent predictive utility of computed tomography angiographic collateral status in acute ischaemic stroke. *Brain* **132**, 2231-2238 (2009).
71. Maas, M.B., Lev, M.H., Ay, H., Singhal, A.B., Greer, D.M., Smith, W.S., Harris, G.J., Halpern, E., Kemmling, A., Koroshetz, W.J. & Furie, K.L. Collateral vessels on CT angiography predict outcome in acute ischemic stroke. *Stroke* **40**, 3001-3005 (2009).
72. Abul-Khoudoud, O. Diagnosis and risk assessment of lower extremity peripheral arterial disease. *J Endovasc Ther* **13 Suppl 2**, II10-18 (2006).
73. Bobek, V., Taltynov, O., Pinterova, D. & Kolostova, K. Gene therapy of the ischemic lower limb--Therapeutic angiogenesis. *Vascul Pharmacol* **44**, 395-405 (2006).
74. Chalothorn, D., Clayton, J.A., Zhang, H., Pomp, D. & Faber, J.E. Collateral density, remodeling, and VEGF-A expression differ widely between mouse strains. *Physiol Genomics* **30**, 179-191 (2007).
75. Chalothorn, D. & Faber, J.E. Strain-dependent variation in collateral circulatory function in mouse hindlimb. *Physiol Genomics* **42**, 469-479 (2010).
76. Zhang, H., Prabhakar, P., Sealock, R. & Faber, J.E. Wide genetic variation in the native pial collateral circulation is a major determinant of variation in severity of stroke. *J Cereb Blood Flow Metab* **30**, 923-934 (2010).
77. Clayton, J.A., Chalothorn, D. & Faber, J.E. Vascular endothelial growth factor-A specifies formation of native collaterals and regulates collateral growth in ischemia. *Circ Res* **103**, 1027-1036 (2008).
78. Takeda, Y., Costa, S., Delamarre, E., Roncal, C., Leite de Oliveira, R., Squadrito, M.L., Finisguerra, V., Deschoemaeker, S., Bruyere, F., Wenes, M., Hamm, A., Serneels, J., Magat, J., Bhattacharyya, T., Anisimov, A., Jordan, B.F., Alitalo, K., Maxwell, P., Gallez, B., Zhuang, Z.W., Saito, Y., Simons, M., De Palma, M. & Mazzone, M. Macrophage skewing by Phd2 haplodeficiency prevents ischaemia by inducing arteriogenesis. *Nature* **479**, 122-126 (2011).
79. Chen, Z., Rubin, J. & Tzima, E. Role of PECAM-1 in arteriogenesis and specification of preexisting collaterals. *Circ Res* **107**, 1355-1363 (2010).
80. Fang, J.S., Angelov, S.N., Simon, A.M. & Burt, J.M. Cx40 is required for, and cx37 limits, postischemic hindlimb perfusion, survival and recovery. *J Vasc Res* **49**, 2-12 (2012).

81. Fang, J.S., Angelov, S.N., Simon, A.M. & Burt, J.M. Cx37 deletion enhances vascular growth and facilitates ischemic limb recovery. *Am J Physiol Heart Circ Physiol* **301**, H1872-1881 (2011).
82. Cristofaro, B., Shi, Y., Faria, M., Suchting, S., Leroyer, A.S., Trindade, A., Duarte, A., Zovein, A.C., Iruela-Arispe, M.L., Nih, L.R., Kubis, N., Henrion, D., Loufrani, L., Todiras, M., Schleifenbaum, J., Gollasch, M., Zhuang, Z.W., Simons, M., Eichmann, A. & le Noble, F. Dll4-Notch signaling determines the formation of native arterial collateral networks and arterial function in mouse ischemia models. *Development* **140**, 1720-1729 (2013).
83. Wang, S., Zhang, H., Dai, X., Sealock, R. & Faber, J.E. Genetic architecture underlying variation in extent and remodeling of the collateral circulation. *Circ Res* **107**, 558-568 (2010).
84. Wang, S., Zhang, H., Wiltshire, T., Sealock, R. & Faber, J.E. Genetic dissection of the Canq1 locus governing variation in extent of the collateral circulation. *PLoS One* **7**, e31910 (2012).
85. Sealock, R., Zhang, H., Lucitti, J.L., Moore, S.M. & Faber, J.E. Congenic fine-mapping identifies a major causal locus for variation in the native collateral circulation and ischemic injury in brain and lower extremity. *Circ Res* **114**, 660-671 (2014).
86. Baklanov, D. & Simons, M. Arteriogenesis: lessons learned from clinical trials. *Endothelium* **10**, 217-223 (2003).
87. Fraisl, P., Mazzone, M., Schmidt, T. & Carmeliet, P. Regulation of angiogenesis by oxygen and metabolism. *Dev Cell* **16**, 167-179 (2009).
88. Troidl, K. & Schaper, W. Arteriogenesis versus angiogenesis in peripheral artery disease. *Diabetes Metab Res Rev* **28 Suppl 1**, 27-29 (2012).
89. Deindl, E. & Schaper, W. The art of arteriogenesis. *Cell Biochem Biophys* **43**, 1-15 (2005).
90. Deindl, E., Buschmann, I., Hoefer, I.E., Podzuweit, T., Boengler, K., Vogel, S., van Royen, N., Fernandez, B. & Schaper, W. Role of ischemia and of hypoxia-inducible genes in arteriogenesis after femoral artery occlusion in the rabbit. *Circ Res* **89**, 779-786 (2001).
91. Heil, M., Eitenmuller, I., Schmitz-Rixen, T. & Schaper, W. Arteriogenesis versus angiogenesis: similarities and differences. *J Cell Mol Med* **10**, 45-55 (2006).
92. Buschmann, I., Pries, A., Styp-Rekowska, B., Hillmeister, P., Loufrani, L., Henrion, D., Shi, Y., Duelsner, A., Hoefer, I., Gatzke, N., Wang, H., Lehmann, K., Ulm, L., Ritter, Z., Hauff, P., Hlushchuk, R., Djonov, V., van Veen, T. & le Noble, F. Pulsatile shear and Gja5 modulate arterial identity and remodeling events during flow-driven arteriogenesis. *Development* **137**, 2187-2196 (2010).
93. Hoefer, I.E., den Adel, B. & Daemen, M.J. Biomechanical factors as triggers of vascular growth. *Cardiovasc Res* **99**, 276-283 (2013).
94. Simons, M. & Eichmann, A. Molecular Controls of Arterial Morphogenesis. *Circ Res* **116**, 1712-1724 (2015).

95. Moraes, F., Paye, J., Mac Gabhann, F., Zhuang, Z.W., Zhang, J., Lanahan, A.A. & Simons, M. Endothelial cell-dependent regulation of arteriogenesis. *Circ Res* **113**, 1076-1086 (2013).
96. Pipp, F., Boehm, S., Cai, W.J., Adili, F., Ziegler, B., Karanovic, G., Ritter, R., Balzer, J., Scheler, C., Schaper, W. & Schmitz-Rixen, T. Elevated fluid shear stress enhances postocclusive collateral artery growth and gene expression in the pig hind limb. *Arterioscler Thromb Vasc Biol* **24**, 1664-1668 (2004).
97. Yu, J., deMuinck, E.D., Zhuang, Z., Drinane, M., Kauser, K., Rubanyi, G.M., Qian, H.S., Murata, T., Escalante, B. & Sessa, W.C. Endothelial nitric oxide synthase is critical for ischemic remodeling, mural cell recruitment, and blood flow reserve. *Proc Natl Acad Sci U S A* **102**, 10999-11004 (2005).
98. Troidl, K., Tribulova, S., Cai, W.J., Ruding, I., Apfelbeck, H., Schierling, W., Troidl, C., Schmitz-Rixen, T. & Schaper, W. Effects of endogenous nitric oxide and of DETA NONOate in arteriogenesis. *J Cardiovasc Pharmacol* **55**, 153-160 (2010).
99. Le Clerc, V., Bazante, F., Baril, C., Guiard, J. & Zhang, D. Assessing temporal changes in genetic diversity of maize varieties using microsatellite markers. *Theor Appl Genet* **110**, 294-302 (2005).
100. Ito, W.D., Arras, M., Winkler, B., Scholz, D., Schaper, J. & Schaper, W. Monocyte chemotactic protein-1 increases collateral and peripheral conductance after femoral artery occlusion. *Circ Res* **80**, 829-837 (1997).
101. Voskuil, M., van Royen, N., Hoefer, I.E., Seidler, R., Guth, B.D., Bode, C., Schaper, W., Piek, J.J. & Buschmann, I.R. Modulation of collateral artery growth in a porcine hindlimb ligation model using MCP-1. *Am J Physiol Heart Circ Physiol* **284**, H1422-1428 (2003).
102. Scholz, D., Ito, W., Fleming, I., Deindl, E., Sauer, A., Wiesnet, M., Busse, R., Schaper, J. & Schaper, W. Ultrastructure and molecular histology of rabbit hind-limb collateral artery growth (arteriogenesis). *Virchows Arch* **436**, 257-270 (2000).
103. Heil, M., Ziegelhoeffer, T., Pipp, F., Kostin, S., Martin, S., Clauss, M. & Schaper, W. Blood monocyte concentration is critical for enhancement of collateral artery growth. *Am J Physiol Heart Circ Physiol* **283**, H2411-2419 (2002).
104. van Royen, N., Hoefer, I., Buschmann, I., Kostin, S., Voskuil, M., Bode, C., Schaper, W. & Piek, J.J. Effects of local MCP-1 protein therapy on the development of the collateral circulation and atherosclerosis in Watanabe hyperlipidemic rabbits. *Cardiovasc Res* **57**, 178-185 (2003).
105. Hamm, A., Veschini, L., Takeda, Y., Costa, S., Delamarre, E., Squadrito, M.L., Henze, A.T., Wenes, M., Serneels, J., Pucci, F., Roncal, C., Anisimov, A., Alitalo, K., De Palma, M. & Mazzone, M. PHD2 regulates arteriogenic macrophages through TIE2 signalling. *EMBO Mol Med* **5**, 843-857 (2013).

106. Patel, A.S., Smith, A., Nucera, S., Biziato, D., Saha, P., Attia, R.Q., Humphries, J., Mattock, K., Grover, S.P., Lyons, O.T., Guidotti, L.G., Siow, R., Ivetic, A., Egginton, S., Waltham, M., Naldini, L., De Palma, M. & Modarai, B. TIE2-expressing monocytes/macrophages regulate revascularization of the ischemic limb. *EMBO Mol Med* **5**, 858-869 (2013).
107. Buschmann, I.R., Hoefer, I.E., van Royen, N., Katzer, E., Braun-Dulleaus, R., Heil, M., Kostin, S., Bode, C. & Schaper, W. GM-CSF: a strong arteriogenic factor acting by amplification of monocyte function. *Atherosclerosis* **159**, 343-356 (2001).
108. Deindl, E., Zaruba, M.M., Brunner, S., Huber, B., Mehl, U., Assmann, G., Hoefer, I.E., Mueller-Hoecker, J. & Franz, W.M. G-CSF administration after myocardial infarction in mice attenuates late ischemic cardiomyopathy by enhanced arteriogenesis. *FASEB J* **20**, 956-958 (2006).
109. Seiler, C., Pohl, T., Wustmann, K., Hutter, D., Nicolet, P.A., Windecker, S., Eberli, F.R. & Meier, B. Promotion of collateral growth by granulocyte-macrophage colony-stimulating factor in patients with coronary artery disease: a randomized, double-blind, placebo-controlled study. *Circulation* **104**, 2012-2017 (2001).
110. Arai, M., Misao, Y., Nagai, H., Kawasaki, M., Nagashima, K., Suzuki, K., Tsuchiya, K., Otsuka, S., Uno, Y., Takemura, G., Nishigaki, K., Minatoguchi, S. & Fujiwara, H. Granulocyte colony-stimulating factor: a noninvasive regeneration therapy for treating atherosclerotic peripheral artery disease. *Circ J* **70**, 1093-1098 (2006).
111. van Royen, N., Schirmer, S.H., Atasever, B., Behrens, C.Y., Ubbink, D., Buschmann, E.E., Voskuil, M., Bot, P., Hoefer, I., Schlingemann, R.O., Biemond, B.J., Tijssen, J.G., Bode, C., Schaper, W., Oskam, J., Legemate, D.A., Piek, J.J. & Buschmann, I. START Trial: a pilot study on STimulation of ARTeriogenesis using subcutaneous application of granulocyte-macrophage colony-stimulating factor as a new treatment for peripheral vascular disease. *Circulation* **112**, 1040-1046 (2005).
112. Schierling, W., Troidl, K., Troidl, C., Schmitz-Rixen, T., Schaper, W. & Eitenmuller, I.K. The role of angiogenic growth factors in arteriogenesis. *J Vasc Res* **46**, 365-374 (2009).
113. Murakami, M. & Simons, M. Fibroblast growth factor regulation of neovascularization. *Curr Opin Hematol* **15**, 215-220 (2008).
114. Unger, E.F., Banai, S., Shou, M., Lazarous, D.F., Jaklitsch, M.T., Scheinowitz, M., Correa, R., Klingbeil, C. & Epstein, S.E. Basic fibroblast growth factor enhances myocardial collateral flow in a canine model. *Am J Physiol* **266**, H1588-1595 (1994).
115. Yanagisawa-Miwa, A., Uchida, Y., Nakamura, F., Tomaru, T., Kido, H., Kamijo, T., Sugimoto, T., Kaji, K., Utsuyama, M., Kurashima, C. & et al. Salvage of infarcted myocardium by angiogenic action of basic fibroblast growth factor. *Science* **257**, 1401-1403 (1992).

116. Deindl, E., Hoefer, I.E., Fernandez, B., Barancik, M., Heil, M., Strniskova, M. & Schaper, W. Involvement of the fibroblast growth factor system in adaptive and chemokine-induced arteriogenesis. *Circ Res* **92**, 561-568 (2003).
117. Yang, X., Liaw, L., Prudovsky, I., Brooks, P.C., Vary, C., Oxburgh, L. & Friesel, R. Fibroblast growth factor signaling in the vasculature. *Curr Atheroscler Rep* **17**, 509 (2015).
118. Ortega, S., Ittmann, M., Tsang, S.H., Ehrlich, M. & Basilico, C. Neuronal defects and delayed wound healing in mice lacking fibroblast growth factor 2. *Proc Natl Acad Sci U S A* **95**, 5672-5677 (1998).
119. Zhou, M., Sutliff, R.L., Paul, R.J., Lorenz, J.N., Hoying, J.B., Haudenschild, C.C., Yin, M., Coffin, J.D., Kong, L., Kranias, E.G., Luo, W., Boivin, G.P., Duffy, J.J., Pawlowski, S.A. & Doetschman, T. Fibroblast growth factor 2 control of vascular tone. *Nat Med* **4**, 201-207 (1998).
120. Miller, D.L., Ortega, S., Bashayan, O., Basch, R. & Basilico, C. Compensation by fibroblast growth factor 1 (FGF1) does not account for the mild phenotypic defects observed in FGF2 null mice. *Mol Cell Biol* **20**, 2260-2268 (2000).
121. Molin, D. & Post, M.J. Therapeutic angiogenesis in the heart: protect and serve. *Curr Opin Pharmacol* **7**, 158-163 (2007).
122. Henry, T.D., Annex, B.H., McKendall, G.R., Azrin, M.A., Lopez, J.J., Giordano, F.J., Shah, P.K., Willerson, J.T., Benza, R.L., Berman, D.S., Gibson, C.M., Bajamonde, A., Rundle, A.C., Fine, J., McCluskey, E.R. & Investigators, V. The VIVA trial: Vascular endothelial growth factor in Ischemia for Vascular Angiogenesis. *Circulation* **107**, 1359-1365 (2003).
123. Morrison, A.R., Yarovinsky, T.O., Young, B.D., Moraes, F., Ross, T.D., Ceneri, N., Zhang, J., Zhuang, Z.W., Sinusas, A.J., Pardi, R., Schwartz, M.A., Simons, M. & Bender, J.R. Chemokine-coupled beta2 integrin-induced macrophage Rac2-Myosin IIA interaction regulates VEGF-A mRNA stability and arteriogenesis. *J Exp Med* **211**, 1957-1968 (2014).
124. Lanahan, A., Zhang, X., Fantin, A., Zhuang, Z., Rivera-Molina, F., Speichinger, K., Prahst, C., Zhang, J., Wang, Y., Davis, G., Toomre, D., Ruhrberg, C. & Simons, M. The neuropilin 1 cytoplasmic domain is required for VEGF-A-dependent arteriogenesis. *Dev Cell* **25**, 156-168 (2013).
125. Carmeliet, P. Mechanisms of angiogenesis and arteriogenesis. *Nat Med* **6**, 389-395 (2000).
126. Lanahan, A.A., Hermans, K., Claes, F., Kerley-Hamilton, J.S., Zhuang, Z.W., Giordano, F.J., Carmeliet, P. & Simons, M. VEGF receptor 2 endocytic trafficking regulates arterial morphogenesis. *Dev Cell* **18**, 713-724 (2010).
127. Lampugnani, M.G., Orsenigo, F., Gagliani, M.C., Tacchetti, C. & Dejana, E. Vascular endothelial cadherin controls VEGFR-2 internalization and signaling from intracellular compartments. *J Cell Biol* **174**, 593-604 (2006).

128. Sakurai, Y., Ohgimoto, K., Kataoka, Y., Yoshida, N. & Shibuya, M. Essential role of Flk-1 (VEGF receptor 2) tyrosine residue 1173 in vasculogenesis in mice. *Proc Natl Acad Sci U S A* **102**, 1076-1081 (2005).
129. Kofler, N.M. & Simons, M. Angiogenesis versus arteriogenesis: neuropilin 1 modulation of VEGF signaling. *F1000Prime Rep* **7**, 26 (2015).
130. Lanahan, A.A., Lech, D., Dubrac, A., Zhang, J., Zhuang, Z.W., Eichmann, A. & Simons, M. PTP1b is a physiologic regulator of vascular endothelial growth factor signaling in endothelial cells. *Circulation* **130**, 902-909 (2014).
131. Koch, S. & Claesson-Welsh, L. Signal transduction by vascular endothelial growth factor receptors. *Cold Spring Harb Perspect Med* **2**, a006502 (2012).
132. Tam, S.J., Richmond, D.L., Kaminker, J.S., Modrusan, Z., Martin-McNulty, B., Cao, T.C., Weimer, R.M., Carano, R.A., van Bruggen, N. & Watts, R.J. Death receptors DR6 and TROY regulate brain vascular development. *Dev Cell* **22**, 403-417 (2012).
133. Murata, Y., Fujiwara, N., Seo, J.H., Yan, F., Liu, X., Terasaki, Y., Luo, Y., Arai, K., Ji, X. & Lo, E.H. Delayed inhibition of c-Jun N-terminal kinase worsens outcomes after focal cerebral ischemia. *J Neurosci* **32**, 8112-8115 (2012).
134. Pi, X., Wu, Y., Ferguson, J.E., 3rd, Portbury, A.L. & Patterson, C. SDF-1alpha stimulates JNK3 activity via eNOS-dependent nitrosylation of MKP7 to enhance endothelial migration. *Proc Natl Acad Sci U S A* **106**, 5675-5680 (2009).
135. Guma, M., Rius, J., Duong-Polk, K.X., Haddad, G.G., Lindsey, J.D. & Karin, M. Genetic and pharmacological inhibition of JNK ameliorates hypoxia-induced retinopathy through interference with VEGF expression. *Proc Natl Acad Sci U S A* **106**, 8760-8765 (2009).
136. Du, H., Sun, X., Guma, M., Luo, J., Ouyang, H., Zhang, X., Zeng, J., Quach, J., Nguyen, D.H., Shaw, P.X., Karin, M. & Zhang, K. JNK inhibition reduces apoptosis and neovascularization in a murine model of age-related macular degeneration. *Proc Natl Acad Sci U S A* **110**, 2377-2382 (2013).
137. Jimenez, B., Volpert, O.V., Reiher, F., Chang, L., Munoz, A., Karin, M. & Bouck, N. c-Jun N-terminal kinase activation is required for the inhibition of neovascularization by thrombospondin-1. *Oncogene* **20**, 3443-3448 (2001).
138. Salvucci, O., Ohnuki, H., Maric, D., Hou, X., Li, X., Yoon, S.O., Segarra, M., Eberhart, C.G., Acker-Palmer, A. & Tosato, G. EphrinB2 controls vessel pruning through STAT1-JNK3 signalling. *Nat Commun* **6**, 6576 (2015).
139. Bryan, M.T., Duckles, H., Feng, S., Hsiao, S.T., Kim, H.R., Serbanovic-Canic, J. & Evans, P.C. Mechanoresponsive networks controlling vascular inflammation. *Arterioscler Thromb Vasc Biol* **34**, 2199-2205 (2014).

140. Cuhlmann, S., Van der Heiden, K., Saliba, D., Tremoleda, J.L., Khalil, M., Zakkar, M., Chaudhury, H., Luong le, A., Mason, J.C., Udalova, I., Gsell, W., Jones, H., Haskard, D.O., Krams, R. & Evans, P.C. Disturbed blood flow induces RelA expression via c-Jun N-terminal kinase 1: a novel mode of NF-kappaB regulation that promotes arterial inflammation. *Circ Res* **108**, 950-959 (2011).
141. Boon, R.A., Leyen, T.A., Fontijn, R.D., Fledderus, J.O., Baggen, J.M., Volger, O.L., van Nieuw Amerongen, G.P. & Horrevoets, A.J. KLF2-induced actin shear fibers control both alignment to flow and JNK signaling in vascular endothelium. *Blood* **115**, 2533-2542 (2010).
142. Hahn, C., Wang, C., Orr, A.W., Coon, B.G. & Schwartz, M.A. JNK2 promotes endothelial cell alignment under flow. *PLoS One* **6**, e24338 (2011).
143. Hahn, C., Orr, A.W., Sanders, J.M., Jhaveri, K.A. & Schwartz, M.A. The subendothelial extracellular matrix modulates JNK activation by flow. *Circ Res* **104**, 995-1003 (2009).
144. Yamawaki, H., Pan, S., Lee, R.T. & Berk, B.C. Fluid shear stress inhibits vascular inflammation by decreasing thioredoxin-interacting protein in endothelial cells. *J Clin Invest* **115**, 733-738 (2005).
145. Blank, U., Karlsson, G. & Karlsson, S. Signaling pathways governing stem-cell fate. *Blood* **111**, 492-503 (2008).
146. Shalaby, F., Ho, J., Stanford, W.L., Fischer, K.D., Schuh, A.C., Schwartz, L., Bernstein, A. & Rossant, J. A requirement for Flk1 in primitive and definitive hematopoiesis and vasculogenesis. *Cell* **89**, 981-990 (1997).
147. Gomez Perdiguero, E., Klapproth, K., Schulz, C., Busch, K., Azzoni, E., Crozet, L., Garner, H., Trouillet, C., de Bruijn, M.F., Geissmann, F. & Rodewald, H.R. Tissue-resident macrophages originate from yolk-sac-derived erythro-myeloid progenitors. *Nature* **518**, 547-551 (2015).
148. Cumano, A. & Godin, I. Ontogeny of the hematopoietic system. *Annu Rev Immunol* **25**, 745-785 (2007).
149. Bertrand, J.Y., Chi, N.C., Santoso, B., Teng, S., Stainier, D.Y. & Traver, D. Haematopoietic stem cells derive directly from aortic endothelium during development. *Nature* **464**, 108-111 (2010).
150. Ottersbach, K. & Dzierzak, E. The murine placenta contains hematopoietic stem cells within the vascular labyrinth region. *Dev Cell* **8**, 377-387 (2005).
151. Gekas, C., Dieterlen-Lievre, F., Orkin, S.H. & Mikkola, H.K. The placenta is a niche for hematopoietic stem cells. *Dev Cell* **8**, 365-375 (2005).
152. Kohli, L. & Passegue, E. Surviving change: the metabolic journey of hematopoietic stem cells. *Trends Cell Biol* **24**, 479-487 (2014).
153. Lin, K.K. & Goodell, M.A. Detection of hematopoietic stem cells by flow cytometry. *Methods Cell Biol* **103**, 21-30 (2011).
154. Kiel, M.J., Yilmaz, O.H., Iwashita, T., Yilmaz, O.H., Terhorst, C. & Morrison, S.J. SLAM family receptors distinguish hematopoietic stem and

progenitor cells and reveal endothelial niches for stem cells. *Cell* **121**, 1109-1121 (2005).
155. Avagyan, S., Amrani, Y.M. & Snoeck, H.W. Identification and in vivo analysis of murine hematopoietic stem cells. *Methods Enzymol* **476**, 429-447 (2010).
156. Szilvassy, S.J., Nicolini, F.E., Eaves, C.J. & Miller, C.L. Quantitation of murine and human hematopoietic stem cells by limiting-dilution analysis in competitively repopulated hosts. *Methods Mol Med* **63**, 167-187 (2002).
157. Kent, D., Dykstra, B. & Eaves, C. Isolation and assessment of long-term reconstituting hematopoietic stem cells from adult mouse bone marrow. *Curr Protoc Stem Cell Biol* **Chapter 2**, Unit 2A 4 (2007).
158. Rincon, M. & Davis, R.J. Regulation of the immune response by stress-activated protein kinases. *Immunol Rev* **228**, 212-224 (2009).
159. Rincon, M., Whitmarsh, A., Yang, D.D., Weiss, L., Derijard, B., Jayaraj, P., Davis, R.J. & Flavell, R.A. The JNK pathway regulates the In vivo deletion of immature CD4(+)CD8(+) thymocytes. *J Exp Med* **188**, 1817-1830 (1998).
160. Sabapathy, K., Kallunki, T., David, J.P., Graef, I., Karin, M. & Wagner, E.F. c-Jun NH2-terminal kinase (JNK)1 and JNK2 have similar and stage-dependent roles in regulating T cell apoptosis and proliferation. *J Exp Med* **193**, 317-328 (2001).
161. Dong, C., Yang, D.D., Wysk, M., Whitmarsh, A.J., Davis, R.J. & Flavell, R.A. Defective T cell differentiation in the absence of Jnk1. *Science* **282**, 2092-2095 (1998).
162. Yang, D.D., Conze, D., Whitmarsh, A.J., Barrett, T., Davis, R.J., Rincon, M. & Flavell, R.A. Differentiation of CD4+ T cells to Th1 cells requires MAP kinase JNK2. *Immunity* **9**, 575-585 (1998).
163. Han, M.S., Jung, D.Y., Morel, C., Lakhani, S.A., Kim, J.K., Flavell, R.A. & Davis, R.J. JNK expression by macrophages promotes obesity-induced insulin resistance and inflammation. *Science* **339**, 218-222 (2013).
164. Humphreys, B.D., Rice, J., Kertesy, S.B. & Dubyak, G.R. Stress-activated protein kinase/JNK activation and apoptotic induction by the macrophage P2X7 nucleotide receptor. *J Biol Chem* **275**, 26792-26798 (2000).
165. Ricci, R., Sumara, G., Sumara, I., Rozenberg, I., Kurrer, M., Akhmedov, A., Hersberger, M., Eriksson, U., Eberli, F.R., Becher, B., Boren, J., Chen, M., Cybulsky, M.I., Moore, K.J., Freeman, M.W., Wagner, E.F., Matter, C.M. & Luscher, T.F. Requirement of JNK2 for scavenger receptor A-mediated foam cell formation in atherogenesis. *Science* **306**, 1558-1561 (2004).
166. Libby, P. Inflammation in atherosclerosis. *Nature* **420**, 868-874 (2002).
167. Tang, M., Wei, X., Guo, Y., Breslin, P., Zhang, S., Zhang, S., Wei, W., Xia, Z., Diaz, M., Akira, S. & Zhang, J. TAK1 is required for the survival of hematopoietic cells and hepatocytes in mice. *J Exp Med* **205**, 1611-1619 (2008).

168. Shim, J.H., Xiao, C., Paschal, A.E., Bailey, S.T., Rao, P., Hayden, M.S., Lee, K.Y., Bussey, C., Steckel, M., Tanaka, N., Yamada, G., Akira, S., Matsumoto, K. & Ghosh, S. TAK1, but not TAB1 or TAB2, plays an essential role in multiple signaling pathways in vivo. *Genes Dev* **19**, 2668-2681 (2005).
169. Sato, S., Sanjo, H., Takeda, K., Ninomiya-Tsuji, J., Yamamoto, M., Kawai, T., Matsumoto, K., Takeuchi, O. & Akira, S. Essential function for the kinase TAK1 in innate and adaptive immune responses. *Nat Immunol* **6**, 1087-1095 (2005).
170. Heinonen, K.M., Vanegas, J.R., Lew, D., Krosl, J. & Perreault, C. Wnt4 enhances murine hematopoietic progenitor cell expansion through a planar cell polarity-like pathway. *PLoS One* **6**, e19279 (2011).
171. Antoniucci, D., Valenti, R., Migliorini, A., Moschi, G., Trapani, M., Buonamici, P., Cerisano, G., Bolognese, L. & Santoro, G.M. Relation of time to treatment and mortality in patients with acute myocardial infarction undergoing primary coronary angioplasty. *Am J Cardiol* **89**, 1248-1252 (2002).
172. Antoniucci, D., Valenti, R., Moschi, G., Migliorini, A., Trapani, M., Santoro, G.M., Bolognese, L., Cerisano, G., Buonamici, P. & Dovellini, E.V. Relation between preintervention angiographic evidence of coronary collateral circulation and clinical and angiographic outcomes after primary angioplasty or stenting for acute myocardial infarction. *Am J Cardiol* **89**, 121-125 (2002).
173. Wang, J., Peng, X., Lassance-Soares, R.M., Najafi, A.H., Alderman, L.O., Sood, S., Xue, Z., Chan, R., Faber, J.E., Epstein, S.E. & Burnett, M.S. Aging-induced collateral dysfunction: impaired responsiveness of collaterals and susceptibility to apoptosis via dysfunctional eNOS signaling. *J Cardiovasc Transl Res* **4**, 779-789 (2011).
174. Faber, J.E. Reprogrammed endothelial cells: cell therapy for coronary collateral growth? *Circ Res* **110**, 192-194 (2012).
175. Tirziu, D., Jaba, I.M., Yu, P., Larrivee, B., Coon, B.G., Cristofaro, B., Zhuang, Z.W., Lanahan, A.A., Schwartz, M.A., Eichmann, A. & Simons, M. Endothelial nuclear factor-kappaB-dependent regulation of arteriogenesis and branching. *Circulation* **126**, 2589-2600 (2012).
176. Alva, J.A., Zovein, A.C., Monvoisin, A., Murphy, T., Salazar, A., Harvey, N.L., Carmeliet, P. & Iruela-Arispe, M.L. VE-Cadherin-Cre-recombinase transgenic mouse: a tool for lineage analysis and gene deletion in endothelial cells. *Dev Dyn* **235**, 759-767 (2006).
177. Kochi, T., Imai, Y., Takeda, A., Watanabe, Y., Mori, S., Tachi, M. & Kodama, T. Characterization of the arterial anatomy of the murine hindlimb: functional role in the design and understanding of ischemia models. *PLoS One* **8**, e84047 (2013).

178. Kant, S., Barrett, T., Vertii, A., Noh, Y.H., Jung, D.Y., Kim, J.K. & Davis, R.J. Role of the mixed-lineage protein kinase pathway in the metabolic stress response to obesity. *Cell Rep* **4**, 681-688 (2013).
179. Gallo, K.A. & Johnson, G.L. Mixed-lineage kinase control of JNK and p38 MAPK pathways. *Nat Rev Mol Cell Biol* **3**, 663-672 (2002).
180. Wang, Y., Nakayama, M., Pitulescu, M.E., Schmidt, T.S., Bochenek, M.L., Sakakibara, A., Adams, S., Davy, A., Deutsch, U., Luthi, U., Barberis, A., Benjamin, L.E., Makinen, T., Nobes, C.D. & Adams, R.H. Ephrin-B2 controls VEGF-induced angiogenesis and lymphangiogenesis. *Nature* **465**, 483-486 (2010).
181. Takeshita, K., Satoh, M., Ii, M., Silver, M., Limbourg, F.P., Mukai, Y., Rikitake, Y., Radtke, F., Gridley, T., Losordo, D.W. & Liao, J.K. Critical role of endothelial Notch1 signaling in postnatal angiogenesis. *Circ Res* **100**, 70-78 (2007).
182. Meisner, J.K., Niu, J., Sumer, S. & Price, R.J. Trans-illuminated laser speckle imaging of collateral artery blood flow in ischemic mouse hindlimb. *J Biomed Opt* **18**, 096011 (2013).
183. Das, M., Jiang, F., Sluss, H.K., Zhang, C., Shokat, K.M., Flavell, R.A. & Davis, R.J. Suppression of p53-dependent senescence by the JNK signal transduction pathway. *Proc Natl Acad Sci U S A* **104**, 15759-15764 (2007).
184. Kuan, C.Y., Whitmarsh, A.J., Yang, D.D., Liao, G., Schloemer, A.J., Dong, C., Bao, J., Banasiak, K.J., Haddad, G.G., Flavell, R.A., Davis, R.J. & Rakic, P. A critical role of neural-specific JNK3 for ischemic apoptosis. *Proc Natl Acad Sci U S A* **100**, 15184-15189 (2003).
185. de Boer, J., Williams, A., Skavdis, G., Harker, N., Coles, M., Tolaini, M., Norton, T., Williams, K., Roderick, K., Potocnik, A.J. & Kioussis, D. Transgenic mice with hematopoietic and lymphoid specific expression of Cre. *Eur J Immunol* **33**, 314-325 (2003).
186. Bruning, J.C., Michael, M.D., Winnay, J.N., Hayashi, T., Horsch, D., Accili, D., Goodyear, L.J. & Kahn, C.R. A muscle-specific insulin receptor knockout exhibits features of the metabolic syndrome of NIDDM without altering glucose tolerance. *Mol Cell* **2**, 559-569 (1998).
187. Muzumdar, M.D., Tasic, B., Miyamichi, K., Li, L. & Luo, L. A global double-fluorescent Cre reporter mouse. *Genesis* **45**, 593-605 (2007).
188. Craige, S.M., Chen, K., Pei, Y., Li, C., Huang, X., Chen, C., Shibata, R., Sato, K., Walsh, K. & Keaney, J.F., Jr. NADPH oxidase 4 promotes endothelial angiogenesis through endothelial nitric oxide synthase activation. *Circulation* **124**, 731-740 (2011).
189. Limbourg, A., Korff, T., Napp, L.C., Schaper, W., Drexler, H. & Limbourg, F.P. Evaluation of postnatal arteriogenesis and angiogenesis in a mouse model of hind-limb ischemia. *Nat Protoc* **4**, 1737-1746 (2009).

190. Cashman, S.M., Ramo, K. & Kumar-Singh, R. A non membrane-targeted human soluble CD59 attenuates choroidal neovascularization in a model of age related macular degeneration. *PLoS One* **6**, e19078 (2011).
191. Baker, M., Robinson, S.D., Lechertier, T., Barber, P.R., Tavora, B., D'Amico, G., Jones, D.T., Vojnovic, B. & Hodivala-Dilke, K. Use of the mouse aortic ring assay to study angiogenesis. *Nat Protoc* **7**, 89-104 (2012).
192. Li, Y., Hiroi, Y., Ngoy, S., Okamoto, R., Noma, K., Wang, C.Y., Wang, H.W., Zhou, Q., Radtke, F., Liao, R. & Liao, J.K. Notch1 in bone marrow-derived cells mediates cardiac repair after myocardial infarction. *Circulation* **123**, 866-876 (2011).
193. Bauer, M., Cheng, S., Jain, M., Ngoy, S., Theodoropoulos, C., Trujillo, A., Lin, F.C. & Liao, R. Echocardiographic speckle-tracking based strain imaging for rapid cardiovascular phenotyping in mice. *Circ Res* **108**, 908-916 (2011).
194. Simons, M. Chapter 14. Assessment of arteriogenesis. *Methods Enzymol* **445**, 331-342 (2008).
195. Li, Y., Song, Y., Zhao, L., Gaidosh, G., Laties, A.M. & Wen, R. Direct labeling and visualization of blood vessels with lipophilic carbocyanine dye DiI. *Nat Protoc* **3**, 1703-1708 (2008).
196. Kim, D., Pertea, G., Trapnell, C., Pimentel, H., Kelley, R. & Salzberg, S.L. TopHat2: accurate alignment of transcriptomes in the presence of insertions, deletions and gene fusions. *Genome Biol* **14**, R36 (2013).
197. Trapnell, C., Williams, B.A., Pertea, G., Mortazavi, A., Kwan, G., van Baren, M.J., Salzberg, S.L., Wold, B.J. & Pachter, L. Transcript assembly and quantification by RNA-Seq reveals unannotated transcripts and isoform switching during cell differentiation. *Nat Biotechnol* **28**, 511-515 (2010).
198. Kanehisa, M., Goto, S., Sato, Y., Furumichi, M. & Tanabe, M. KEGG for integration and interpretation of large-scale molecular data sets. *Nucleic Acids Res* **40**, D109-114 (2012).
199. Huang da, W., Sherman, B.T. & Lempicki, R.A. Systematic and integrative analysis of large gene lists using DAVID bioinformatics resources. *Nat Protoc* **4**, 44-57 (2009).
200. Gupta, S., Barrett, T., Whitmarsh, A.J., Cavanagh, J., Sluss, H.K., Derijard, B. & Davis, R.J. Selective interaction of JNK protein kinase isoforms with transcription factors. *EMBO J* **15**, 2760-2770 (1996).
201. Xu, P. & Davis, R.J. c-Jun NH2-terminal kinase is required for lineage-specific differentiation but not stem cell self-renewal. *Mol Cell Biol* **30**, 1329-1340 (2010).
202. Seita, J. & Weissman, I.L. Hematopoietic stem cell: self-renewal versus differentiation. *Wiley Interdiscip Rev Syst Biol Med* **2**, 640-653 (2010).
203. Pazianos, G., Uqoezwa, M. & Reya, T. The elements of stem cell self-renewal: a genetic perspective. *Biotechniques* **35**, 1240-1247 (2003).

204. Reya, T. Regulation of hematopoietic stem cell self-renewal. *Recent Prog Horm Res* **58**, 283-295 (2003).
205. Clements, W.K. & Traver, D. Signalling pathways that control vertebrate haematopoietic stem cell specification. *Nat Rev Immunol* **13**, 336-348 (2013).
206. Loose, M., Swiers, G. & Patient, R. Transcriptional networks regulating hematopoietic cell fate decisions. *Curr Opin Hematol* **14**, 307-314 (2007).
207. Ding, L., Saunders, T.L., Enikolopov, G. & Morrison, S.J. Endothelial and perivascular cells maintain haematopoietic stem cells. *Nature* **481**, 457-462 (2012).
208. Bustelo, X.R., Rubin, S.D., Suen, K.L., Carrasco, D. & Barbacid, M. Developmental expression of the vav protooncogene. *Cell Growth Differ* **4**, 297-308 (1993).
209. Ventura, J.J., Kennedy, N.J., Flavell, R.A. & Davis, R.J. JNK regulates autocrine expression of TGF-beta1. *Mol Cell* **15**, 269-278 (2004).
210. Das, M., Sabio, G., Jiang, F., Rincon, M., Flavell, R.A. & Davis, R.J. Induction of hepatitis by JNK-mediated expression of TNF-alpha. *Cell* **136**, 249-260 (2009).
211. Challen, G.A., Boles, N.C., Chambers, S.M. & Goodell, M.A. Distinct hematopoietic stem cell subtypes are differentially regulated by TGF-beta1. *Cell Stem Cell* **6**, 265-278 (2010).
212. King, K.Y. & Goodell, M.A. Inflammatory modulation of HSCs: viewing the HSC as a foundation for the immune response. *Nat Rev Immunol* **11**, 685-692 (2011).
213. King, K.Y., Baldridge, M.T., Weksberg, D.C., Chambers, S.M., Lukov, G.L., Wu, S., Boles, N.C., Jung, S.Y., Qin, J., Liu, D., Songyang, Z., Eissa, N.T., Taylor, G.A. & Goodell, M.A. Irgm1 protects hematopoietic stem cells by negative regulation of IFN signaling. *Blood* **118**, 1525-1533 (2011).
214. Baldridge, M.T., King, K.Y. & Goodell, M.A. Inflammatory signals regulate hematopoietic stem cells. *Trends Immunol* **32**, 57-65 (2011).
215. Nagata, Y., Nishida, E. & Todokoro, K. Activation of JNK signaling pathway by erythropoietin, thrombopoietin, and interleukin-3. *Blood* **89**, 2664-2669 (1997).
216. McLeish, K.R., Knall, C., Ward, R.A., Gerwins, P., Coxon, P.Y., Klein, J.B. & Johnson, G.L. Activation of mitogen-activated protein kinase cascades during priming of human neutrophils by TNF-alpha and GM-CSF. *J Leukoc Biol* **64**, 537-545 (1998).
217. https://www.clinicaltrials.gov/ct2/show/NCT01630252?term=jnk+inhibitor&rank=1
218. Ventura, A., Kirsch, D.G., McLaughlin, M.E., Tuveson, D.A., Grimm, J., Lintault, L., Newman, J., Reczek, E.E., Weissleder, R. & Jacks, T. Restoration of p53 function leads to tumour regression in vivo. *Nature* **445**, 661-665 (2007).

219. Sakurai, A., Doci, C.L. & Gutkind, J.S. Semaphorin signaling in angiogenesis, lymphangiogenesis and cancer. *Cell Res* **22**, 23-32 (2012).
220. Torres-Vazquez, J., Gitler, A.D., Fraser, S.D., Berk, J.D., Van, N.P., Fishman, M.C., Childs, S., Epstein, J.A. & Weinstein, B.M. Semaphorin-plexin signaling guides patterning of the developing vasculature. *Dev Cell* **7**, 117-123 (2004).
221. Adams, R.H. & Eichmann, A. Axon guidance molecules in vascular patterning. *Cold Spring Harb Perspect Biol* **2**, a001875 (2010).
222. Fujiwara, M., Ghazizadeh, M. & Kawanami, O. Potential role of the Slit/Robo signal pathway in angiogenesis. *Vasc Med* **11**, 115-121 (2006).
223. Rama, N., Dubrac, A., Mathivet, T., Ni Charthaigh, R.A., Genet, G., Cristofaro, B., Pibouin-Fragner, L., Ma, L., Eichmann, A. & Chedotal, A. Slit2 signaling through Robo1 and Robo2 is required for retinal neovascularization. *Nat Med* **21**, 483-491 (2015).
224. Simon, A.M. & Goodenough, D.A. Diverse functions of vertebrate gap junctions. *Trends Cell Biol* **8**, 477-483 (1998).
225. Rocha, S.F., Schiller, M., Jing, D., Li, H., Butz, S., Vestweber, D., Biljes, D., Drexler, H.C., Nieminen-Kelha, M., Vajkoczy, P., Adams, S., Benedito, R. & Adams, R.H. Esm1 modulates endothelial tip cell behavior and vascular permeability by enhancing VEGF bioavailability. *Circ Res* **115**, 581-590 (2014).
226. Sabio, G., Das, M., Mora, A., Zhang, Z., Jun, J.Y., Ko, H.J., Barrett, T., Kim, J.K. & Davis, R.J. A stress signaling pathway in adipose tissue regulates hepatic insulin resistance. *Science* **322**, 1539-1543 (2008).
227. Vernia, S., Cavanagh-Kyros, J., Barrett, T., Jung, D.Y., Kim, J.K. & Davis, R.J. Diet-induced obesity mediated by the JNK/DIO2 signal transduction pathway. *Genes Dev* **27**, 2345-2355 (2013).
228. Sung, H.K., Doh, K.O., Son, J.E., Park, J.G., Bae, Y., Choi, S., Nelson, S.M., Cowling, R., Nagy, K., Michael, I.P., Koh, G.Y., Adamson, S.L., Pawson, T. & Nagy, A. Adipose vascular endothelial growth factor regulates metabolic homeostasis through angiogenesis. *Cell Metab* **17**, 61-72 (2013).
229. Kubota, T., Kubota, N., Kumagai, H., Yamaguchi, S., Kozono, H., Takahashi, T., Inoue, M., Itoh, S., Takamoto, I., Sasako, T., Kumagai, K., Kawai, T., Hashimoto, S., Kobayashi, T., Sato, M., Tokuyama, K., Nishimura, S., Tsunoda, M., Ide, T., Murakami, K., Yamazaki, T., Ezaki, O., Kawamura, K., Masuda, H., Moroi, M., Sugi, K., Oike, Y., Shimokawa, H., Yanagihara, N., Tsutsui, M., Terauchi, Y., Tobe, K., Nagai, R., Kamata, K., Inoue, K., Kodama, T., Ueki, K. & Kadowaki, T. Impaired insulin signaling in endothelial cells reduces insulin-induced glucose uptake by skeletal muscle. *Cell Metab* **13**, 294-307 (2011).
230. Kusumbe, A.P. & Adams, R.H. Osteoclast progenitors promote bone vascularization and osteogenesis. *Nat Med* **20**, 1238-1240 (2014).

231. Ramasamy, S.K., Kusumbe, A.P., Wang, L. & Adams, R.H. Endothelial Notch activity promotes angiogenesis and osteogenesis in bone. *Nature* **507**, 376-380 (2014).
232. Kusumbe, A.P., Ramasamy, S.K. & Adams, R.H. Coupling of angiogenesis and osteogenesis by a specific vessel subtype in bone. *Nature* **507**, 323-328 (2014).